PNEUMATIC TYRES

OF FABRICLESS CONSTRUCTION

by

P.S.OUBRIDGE

A Doctoral Thesis.

Submitted in partial fulfilment of the requirements for the award of Doctor of Philosophy of the Loughborough University of Technology.

Institute of Polymer Technology, 1984.

To Maureen

ORIGINALITY

The research described in this thesis was carried out in Technology Division, Dunlop Ltd., Kingsbury Road, Birmingham B24 9QU.

The author was responsible for tyre design, the associated theory, overall planning of the experiments and analysis of the results. Much of the experimental work was undertaken by members of Design and Performance Engineering Department under his supervision.

ACKNOWLEDGEMENTS

This thesis was submitted with the permission of:

Dr B.C. Lindley, Director of Technology, Dunlop Ltd.;

Mr S. van der Burg, Director, Tyre Technical Division, Dunlop Ltd.

I am indebted to my colleagues in Dunlop Technology Division who carried out much of the experimental work, particularly Mr M.H. Walters whose co-operation is acknowledged.

I am also grateful for the encouragement given to me by Prof. A.W. Birley and Mr G.F. Morton.

Finally, I wish to thank my secretary Mrs Christina Lunn whose help in typing and assembling the thesis has been invaluable.

ABSTRACT

The aim of the research described in this thesis is to assess the technical feasibility of pneumatic tyres for passenger cars which have no directional reinforcement in their carcasses. Conventional tyres are constructed from composites of twisted textile or steel cords in a rubber matrix, a process which is both labour intensive and costly. If it were possible to injection mould or cast tyre carcasses in a single operation, and if the performance of the resulting tyres matched that of modern radial ply tyres, then the implications for the tyre industry would be of major proportions.

After reviewing the history of pneumatic tyres and summarising their principal attributes, the design of unreinforced or fabricless tyres is investigated and methods developed for defining their meridional profiles. Materials suitable for their carcasses and treads are then considered, prior to describing the manufacture of two series of tyres designed to have section height to width ratios, or aspect ratios, of 0.9 and 0.7 respectively.

To facilitate experimental work, two sizes of tyres were employed: half scale models for which testing procedures had been developed previously; and a size suitable for small saloon cars. The results obtained on a range of tyre properties are presented and analysed to give a number of empirical relationships between the properties and the design variables: carcass material Young's modulus, carcass wall thickness and the inflation pressure. For the important property of radial stiffness which affects other tyre characteristics, an improved method of analysis is developed to allow the structural and pneumatic components to be quantified.

Using the relationships established experimentally, consideration is given to optimising the design of a fabricless tyre. It is concluded that to approach the performance of a conventional tyre, a design with a low aspect ratio is preferred but, to restrict growth with inflation pressure, limited directional reinforcement must be included as a circumferential belt beneath the tread. Nevertheless, the discussion concludes that there are fundamental reasons why even the optimised tyre would be unacceptable for use on modern passenger cars, although less demanding applications may be identified.

CONTENTS

LIST OF TABLES

LIST OF TABLES (CONT.)

LIST OF FIGURES

LIST OF FIGURES (CONT.)

LIST OF FIGURES (CONT.)

CHAPTER I : INTRODUCTION

I.1 History of the Pneumatic Tyre

Since its invention in 1846, the pneumatic tyre has been a composite of rubber and some form of directional reinforcement. The original inventor, Robert William Thomson who was a trained engineer, a Scotsman and a contemporary of Robert Stevenson, was quite clear on the purposes of his innovation:

> "(it) consists in the application of elastic bearings round the tyres of wheels of carriages, for the purpose of lessening the power required to draw the carriages, - - - - and diminishing the noise they make when in motion."

If one interprets his use of the word noise liberally, it may be seen that Thomson appreciated two of the most important characteristics of pneumatic tyres: their low drag and low radial stiffness.

The construction of the tyre invented by Thomson was the opposite to that which has evolved over the years. He placed the reinforcement, square woven fabric, in the rubberised inner tube; while the carcass consisted of a single material, leather, which was chosen for its general toughness in resisting cutting when run over rough roads. A representation of Thomson's tyre is shown in figure 1.1.

This first pneumatic tyre was tested in Regents Park, London, in 1849 using a horse drawn carriage and the claims made for it were demonstrated. However, Thomson then became involved in other work and his tyre, which was probably conceived in advance of its time, was forgotten.

It was in 1886 that the pneumatic tyre was re-invented by John Boyd Dunlop, who trained as a veterinary in Scotland before moving to Northern Ireland. In response to his son's request for wheels which reduced the effort required to pedal his bicycle, he built a pneumatic tyre around the periphery of an existing wooden rimmed wheel. His construction was the direct forerunner of the modern tyre because he employed a rubber inner tube contained within a rubberised, fabric reinforced carcass which was tacked to the wooden rim, as illustrated in figure 1.2. The techniques used by Dunlop were those he had developed previously when making devices needed

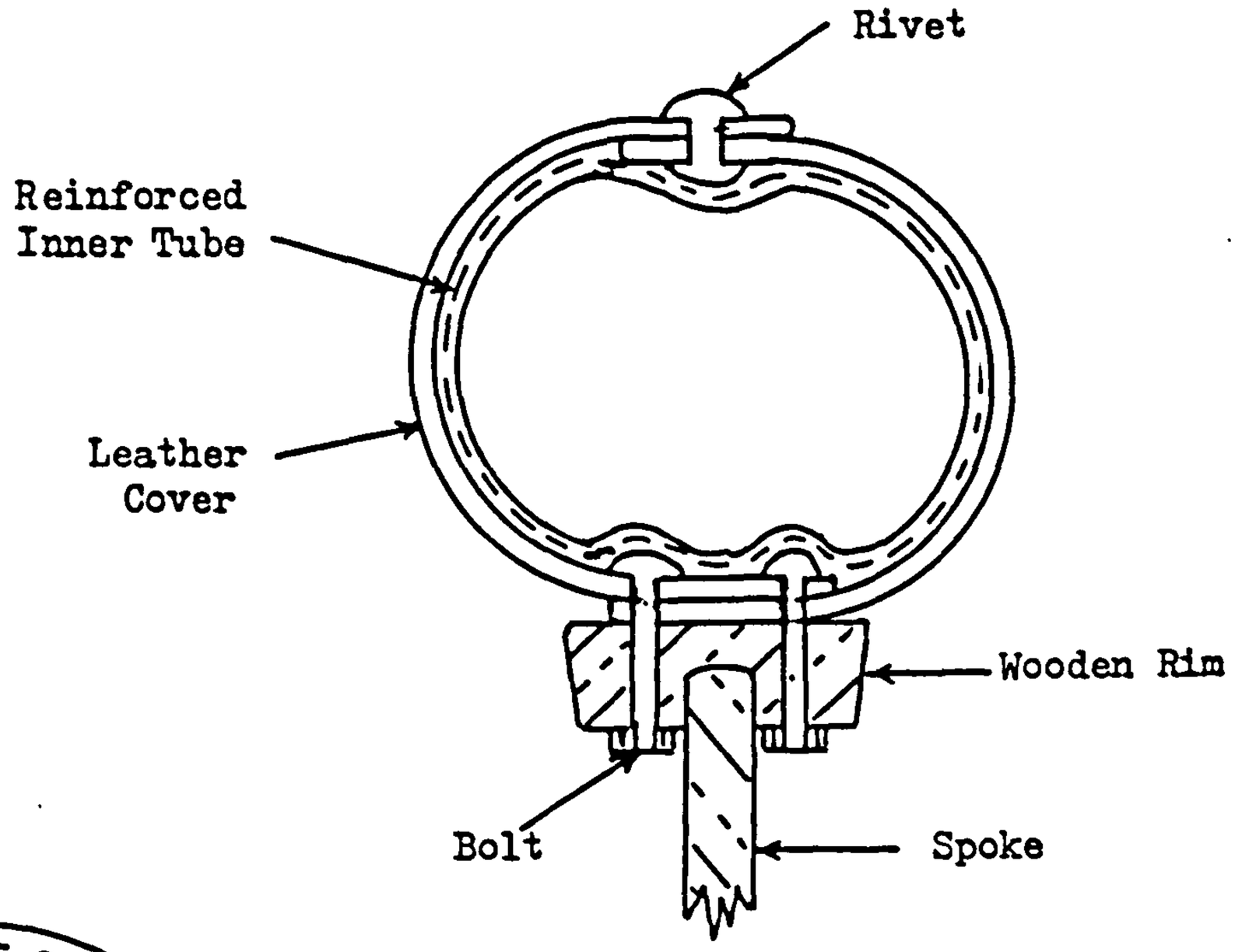

Fig 1.1

THOMSON'S

TYRE

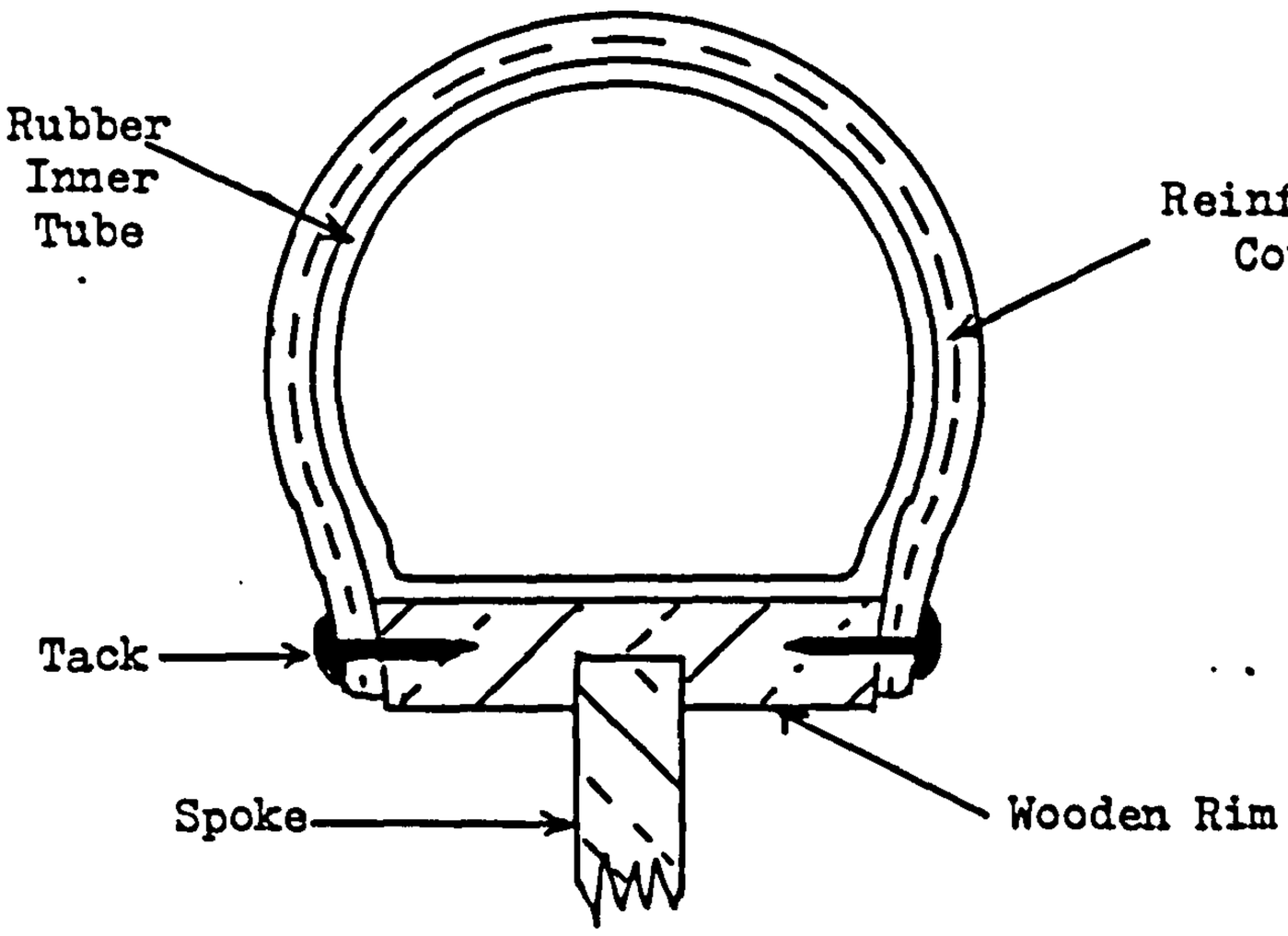

Fig 1.2

DUNLOP'S

ORIGINAL TYRE

Fig 1.3

DUNLOP'S

BICYCLE TYRE

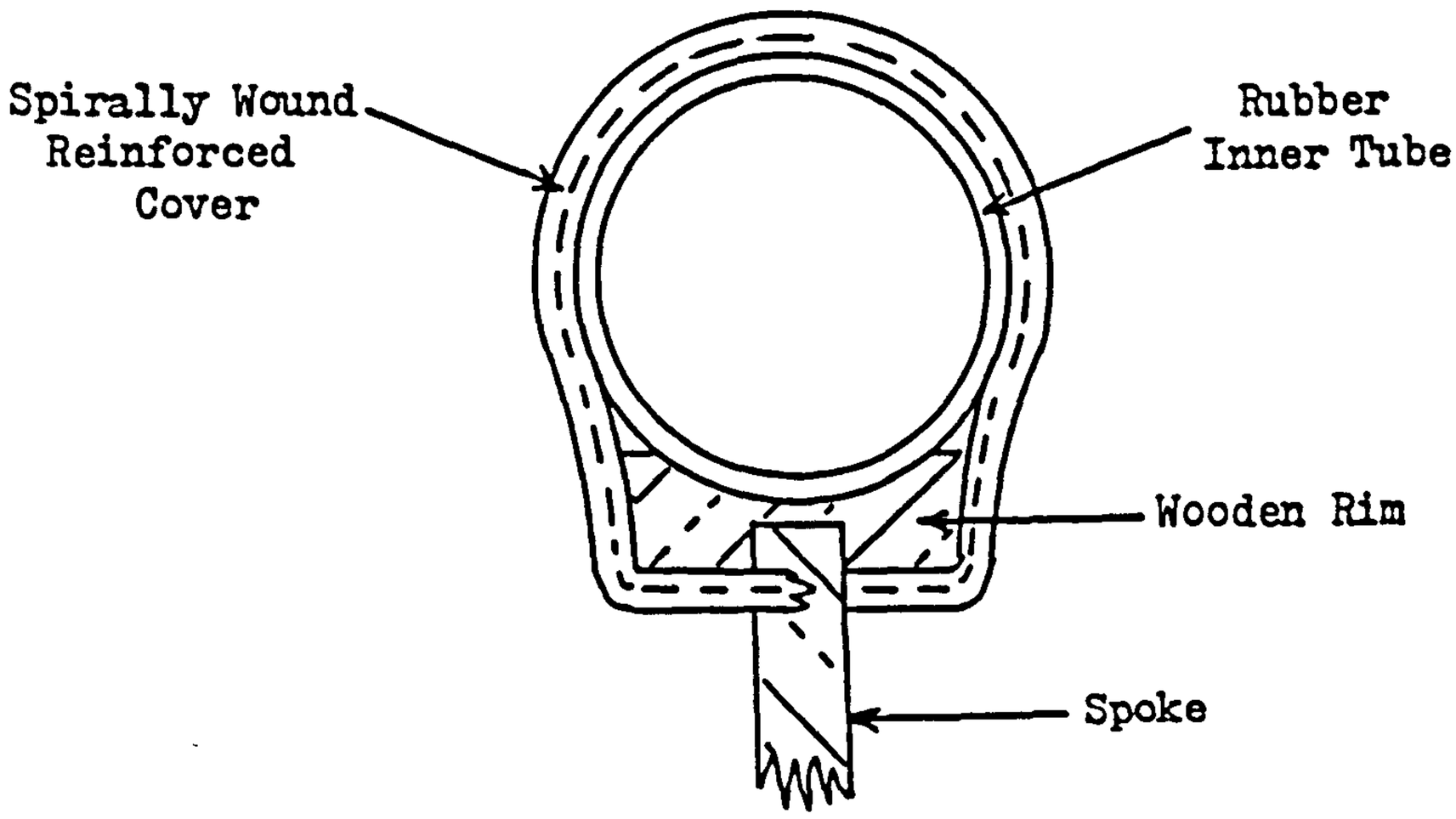

in his veterinary practice. Thus his approach contrasted to that of Thomson. The latter utilised his engineering understanding, while Dunlop called upon his experience, coupled with intuitive thinking. However he did conduct the equivalent of a laboratory experiment before proving his tyre when fitted to a bicycle. He bowled the modified and original wheels along the yard adjacent to his house and showed that the one fitted with a pneumatic tyre ran much further before losing its kinetic energy and falling sideways.

The tyres built by Dunlop for bicycles following his initial experiments were impracticable because, to avoid tacking them to the wooden rims, he constructed the carcass from a long strip of rubberised canvas wound in the form of a toroid. To anchor it to the rim, the strip passed under the rim and between the spokes, figure 1.3. In the event of a puncture, the wraps of canvas had to be released with solvent, the carcass unwound and then rebuilt after mending the inner tube. Nevertheless, the advantages of Dunlop's invention were clearly demonstrated in bicycle races organised by Queen's College, Belfast, when an unknown rider beat more experienced competitors using machines fitted with the standard wooden rimmed wheels.

The next stage in the history of the pneumatic tyre was concerned with the problem of removing the carcass from the rim in order to mend a puncture, a regular occurrence. Charles Kingston Welch from Middlesex invented the wire-on tyre; while William Erskine Bartlett from the USA but working in Scotland, developed the beaded edge tyre. As it happened, the work of Welch was the more important and represented an evolutionary step in the development of the pneumatic tyre. He introduced the concept of the bead wire, to be used in conjunction with a rim well to allow fitment of the tyre, figure 1.4. However, at the time patent complications meant that the beaded edge concept was taken further than otherwise might have been the case. This method requires the portion of the tyre sidewall adjacent to the rim to be thickened, shaped and strengthened so that it could be locked in place within the turned-over edge of the rim, figure 1.5. This technique was acceptable for bicycle tyres but problems of location ultimately resulted in its demise for car tyres.

In retrospect, the next important development came from the realisation that the structural life of pneumatic tyres was limited when square woven fabric was used for reinforcing the carcass. However well the rubberisation

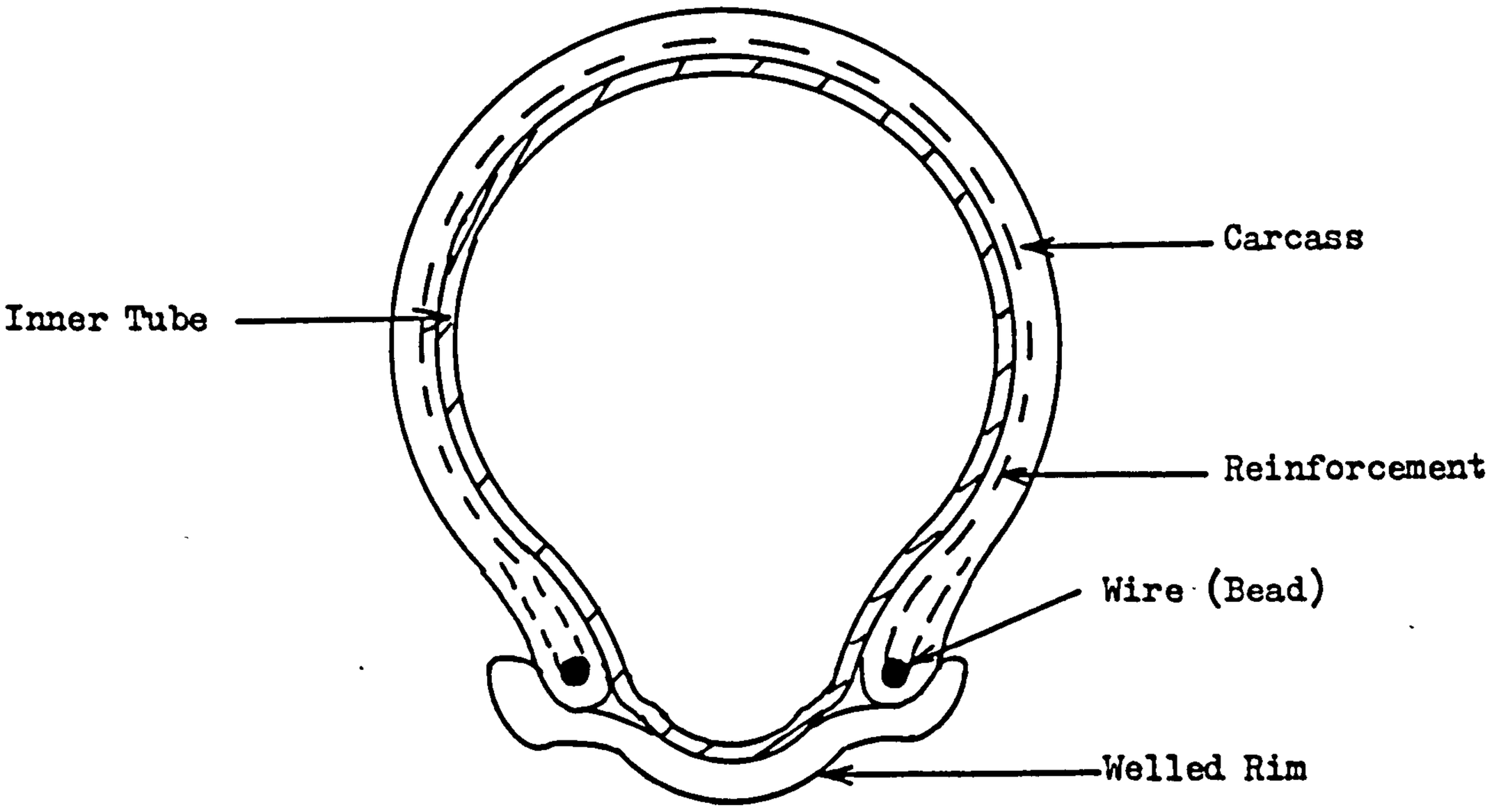

Fig 1.4 WELCH'S WIRED-ON TYRE

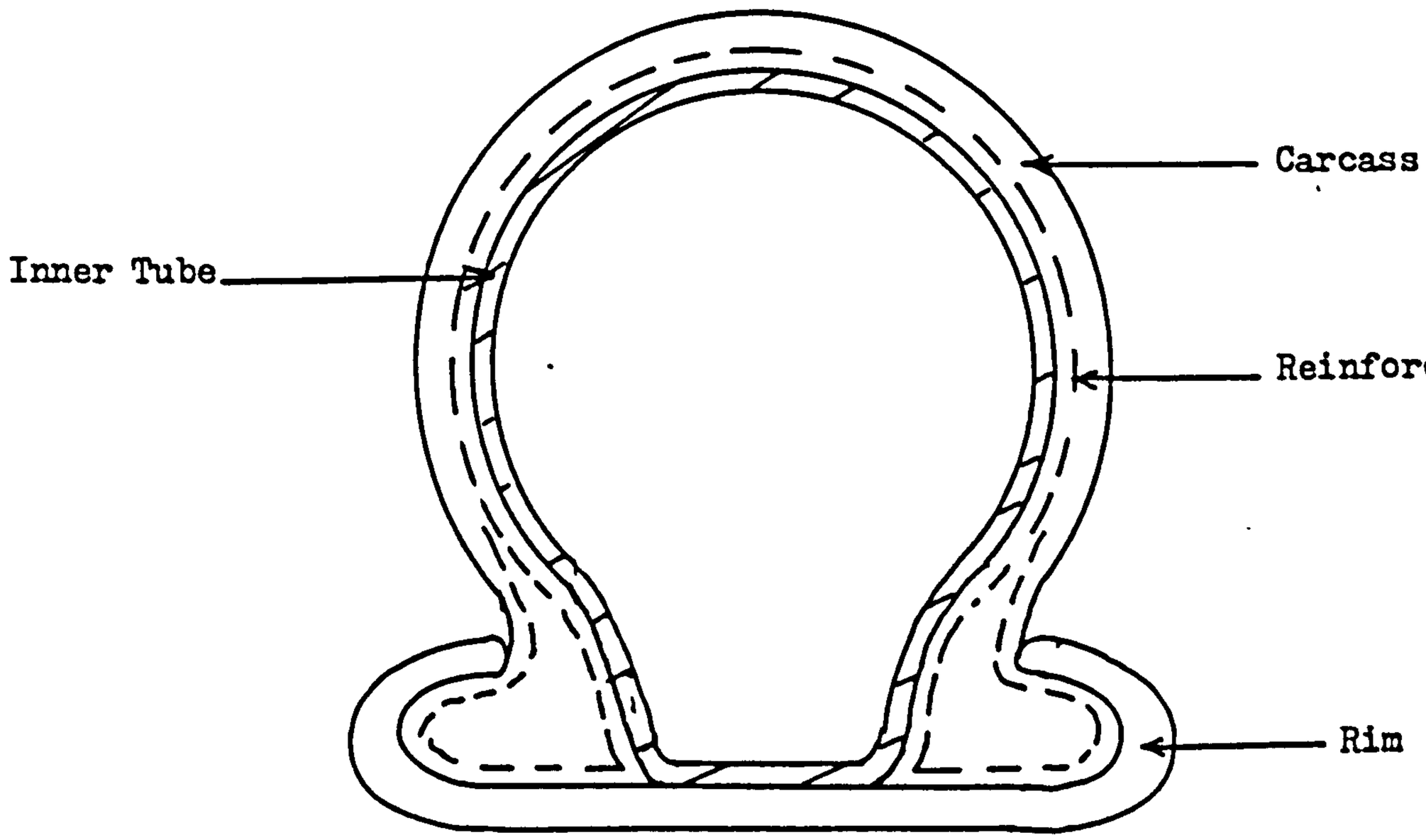

Fig 1.5 BARTLETT'S BEADED-EDGE TYRE

was performed, the warp and weft were in direct contact and during flexing of the tyre fretting was inevitable. John Fullerton Palmer patented a weftless fabric in 1892 in the USA but his innovation was predated by that of David Moseley of Manchester who filed a similar patent in 1888. Entirely weftless fabric was, of course, difficult to handle in manufacture, consequently thin wefts at about 25 mm intervals were introduced to give stability and this method is still employed today.

Over the next 50 years, the pneumatic tyre based on a cross-biassed, weftless ply carcass construction gradually developed. In general, section widths increased and inflation pressures decreased to enhance performance. Also tread patterns progressed from circumferential grooves, through block designs, to the complex configurations common to all current car tyres. Moreover the range of vehicles to which pneumatic tyres were fitted was extended from bicycles to cars and motor cycles, trucks and buses and, finally, earthmoving equipment. They were fitted to aeroplanes early in their development, primarily to save weight.

Since 1946, the history of car and truck tyres in particular has been dominated by the change from the cross-biassed to the radial construction. Although the latter was suggested in 1913 by Gray and Sloper of England, they did not appreciate its significance nor was the idea exploited. It was the patent filed by the French company Michelin and their "X" tyre which had the profound effect upon the tyre industry; an effect which is still having its repercussions today owing to the greatly improved tread life which a radial construction provides.

To conclude this brief history of the pneumatic tyre, figures 1.6 and 1.7 show the detailed constructions of cross-biassed and radial tyres respectively. Apart from the principal components : tread, casing plies, bead wires and, in the case of the radial tyre, the tread bracing layers or belt; there are a number of auxilliary parts, such as chafers and the apex strips, which provide additional reinforcement or distribute the stresses more favourably. It should be noted that the bias of cords in the casing of the cross-biassed tyre relative to the circumferential direction is typically about 35^{o} at the crown, increasing to 55^{o} at the bead. The bias in the casing of the radial tyre is 90^{o} but in the belt it is less than 20^{o}.

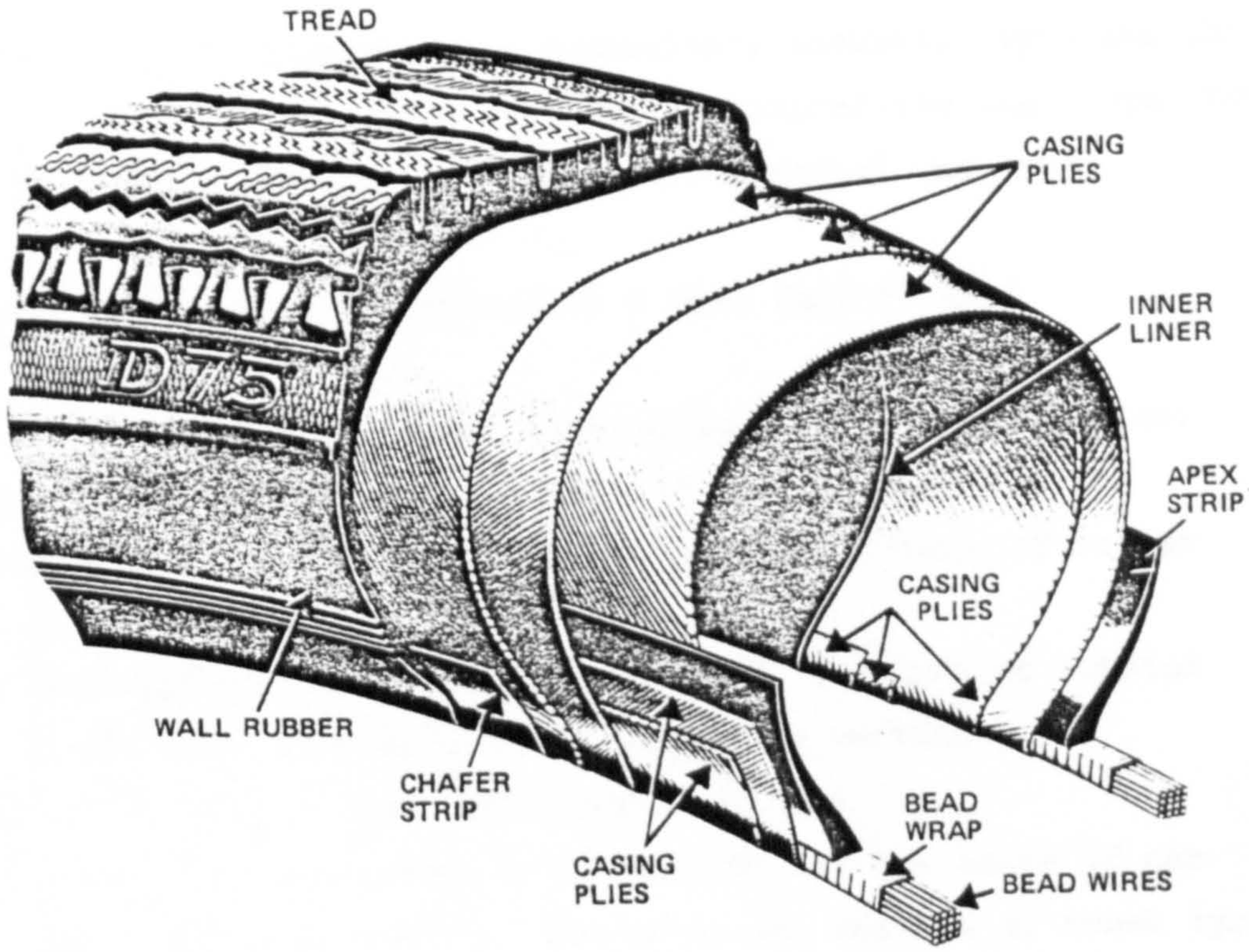
TREAD
CASING PLIES
INNER LINER
APEX STRIP
CASING PLIES
WALL RUBBER
CHAFER STRIP
CASING PLIES
BEAD WRAP
BEAD WIRES

Fig. 1.6

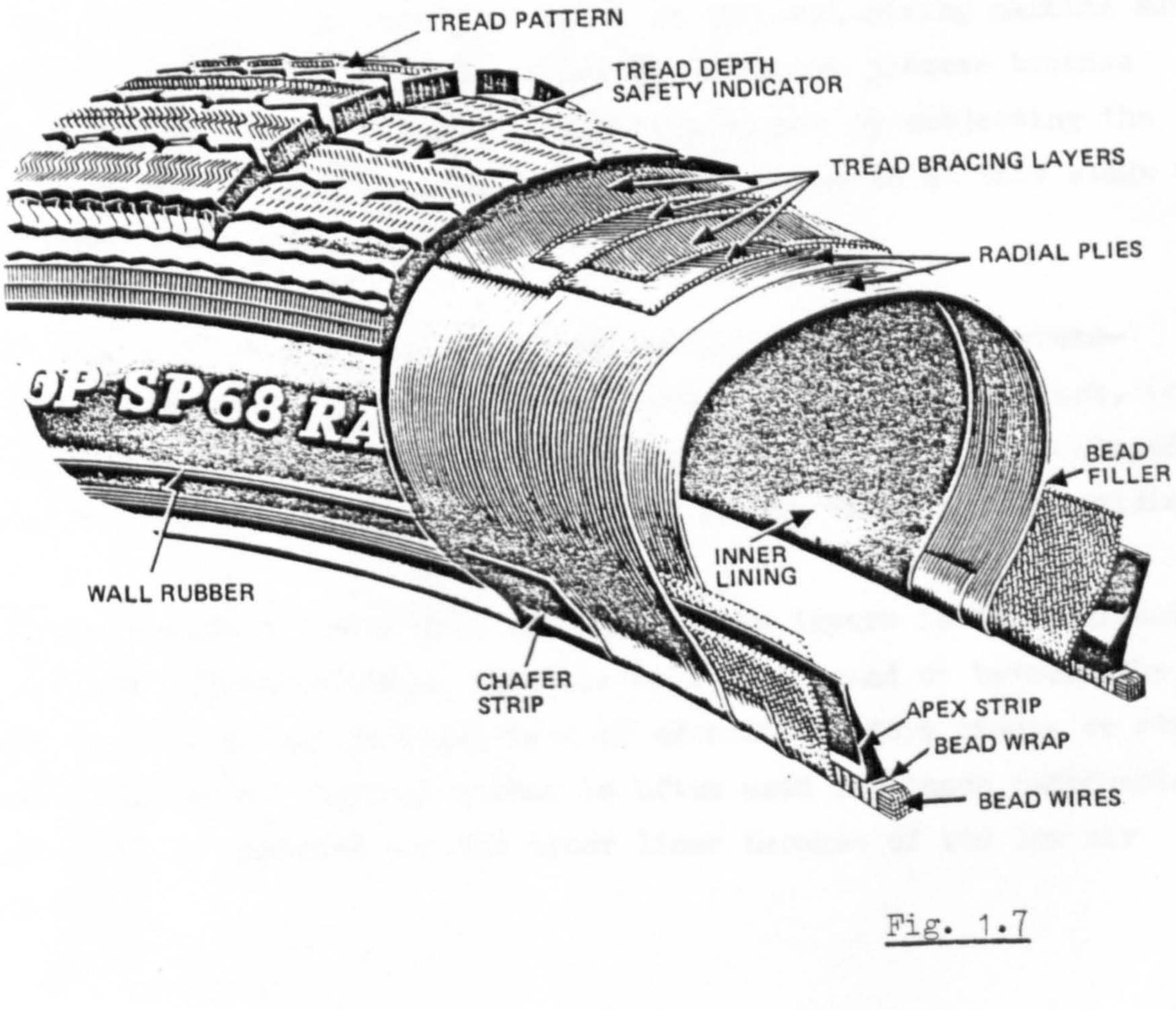
TREAD PATTERN
TREAD DEPTH SAFETY INDICATOR
TREAD BRACING LAYERS
RADIAL PLIES
BEAD FILLER
INNER LINING
WALL RUBBER
CHAFER STRIP
APEX STRIP
BEAD WRAP
BEAD WIRES

Fig. 1.7

I.2 Manufacturing Process

Before introducing the concept of a fabricless, pneumatic tyre and the advantages it would bring, it is important to appreciate the steps involved in the manufacture of modern cross-biassed and radial car tyres.

The principal raw materials received by a tyre factory are:

polymers, natural and synthetic usually in the form of bales;
carbon blacks, pellitised for ease of handling;
curatives and antidegradents, the minor ingredients of rubber compounds;
textiles, particularly rayon and nylon in the form of twisted cords in widths which are essentially weftless;
steel wire, used to make multi-strand beads;
steel cords, multifilament constructions for the belts of car tyres and also used for the belts and casings of truck tyres.

The manufacturing route may be simplified and illustrated with a flow diagram, shown in figure 1.8.

a) The polymers and carbon black, with or without curatives and other minor ingredients, are intimately mixed in an internal mixing machine such as a Banbury or Intermix. This is an energy intensive process because adequate dispersion of the black can only be achieved by subjecting the polymer to high shear forces. The curatives may be added at this stage or they can require a second mixing cycle.

b) Compound intended for the tread, usually based on a styrene-butadiene copolymer, oil extended and containing a fine carbon black, is then extruded to form what is known as a "camelback". This is so shaped to ensure the correct distribution of rubber in the tread during moulding.

c) The compounds which will form protective layers in the finished tyre : for the sidewalls and as cushions below the tread or between the belt and the casing; may be calendered or extruded to form sheets or strips of uniform thickness. Natural rubber is often used for these components, although butyl is employed for the inner liner because of its low air permeability.

Fig 1.8

TYRE MANUFACTURE

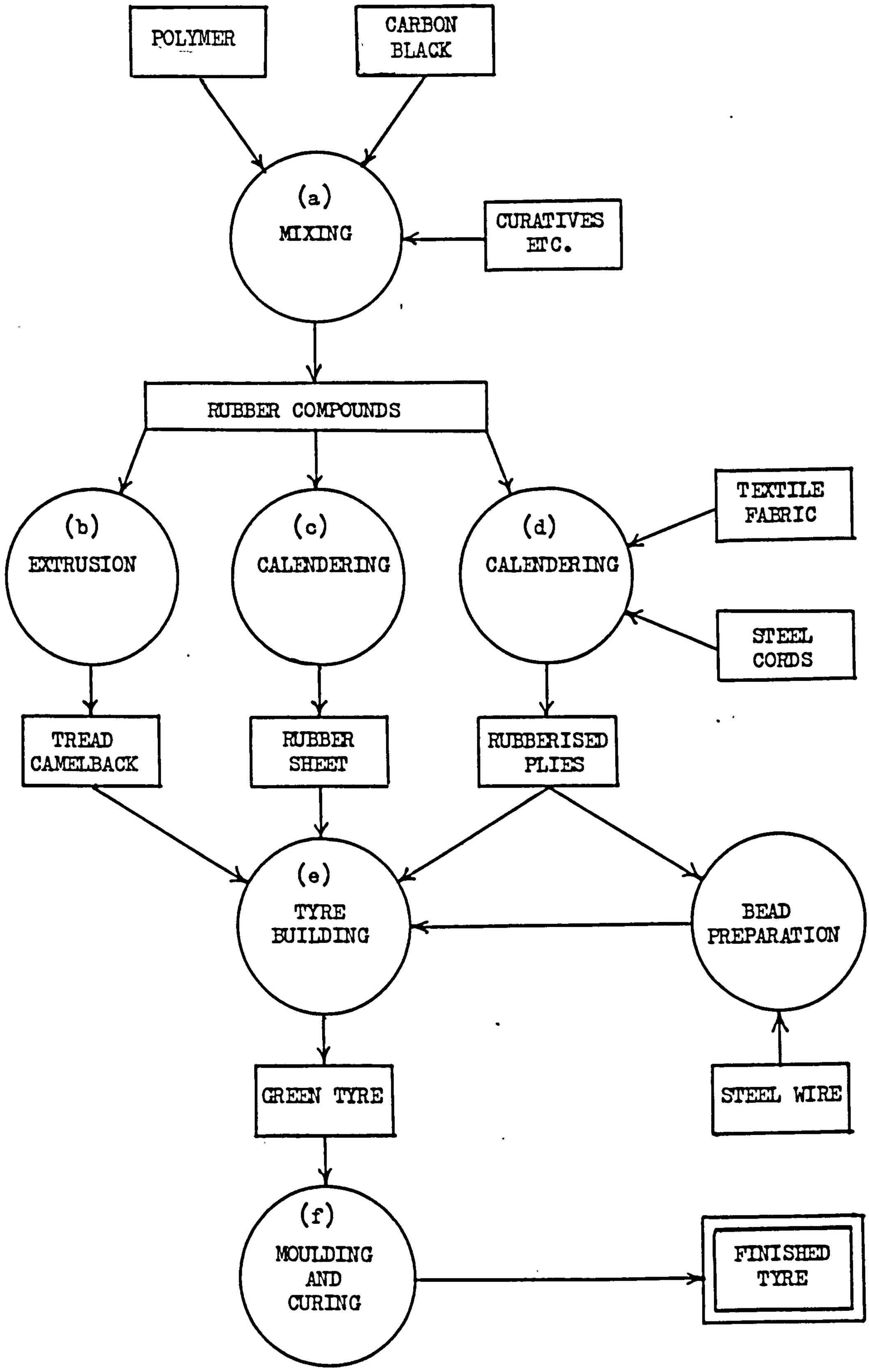

d) Calendering is also used to prepare the rubberised ply material when either textile or steel cord reinforcement is introduced. This composite material is then cut to the required dimensions and bias angle ready for incorporation in tyres.

e) Tyre building is essentially a skilled manual operation, although many mechanical aids are incorporated in the equipment used.

(i) When making a cross-biassed tyre, the various components : the liner, casing plies, sidewall protection strips and tread camelback; are wrapped in turn around a cylindrical former, care being taken to ensure close contact between successive layers to avoid air trapping. The prepared bead wires are fitted after the casing plies, which are then turned back to anchor the beads. The tyre is removed from the former without shaping it into a toroid so that the green tyre, as it is known before vulcanisation, is still cylindrical in shape.

(ii) Radial tyres demand a modified procedure because the plies of the belt are cut at a bias angle somewhat less than 20° to the circumference of the tyre and are, therefore, virtually inextensible. The liner, casing plies, bead wires and sidewall protection strips are built on to a cylindrical former in the same way as the components of a cross-biassed tyre. However, before the plies of the belt and the tread camelback are added, the casing is expanded by an inflatable diaphragm incorporated in the former until it attains the radius of the belt in the finished tyre. Thus, when the green tyre is removed from the former, its profile is that of an open toroid with the beads well separated compared to their positions after moulding.

f) The final shaping of the tyre, moulding the tread pattern and vulcanisation all take place in one, fairly automated, operation. Because the temperature required for vulcanisation is high, coupled with the low thermal conductivity of rubber compounds, this stage is the second energy intensive process in tyre production, comparable with mixing.

I.3 The Potential of Fabricless Tyres

It is clear from section I.2 that the manufacture of conventional cross-biassed and radial tyres is both complex and labour intensive. Moreover the preparation of the many components and the tyre building and moulding procedures themselves can be prone to errors of precision or integrity.

Lack of precision will lead to tyres which are unbalanced mechanically, while the introduction of flaws can result in premature failures.

It should be appreciated that advances in vehicle design have placed far more emphasis on tyre uniformity, because tyre induced shake and other vibrations are more readily detected in a modern car. Also consumer assurance legislation, existing or proposed, demands tyres whose structural performance consistently exceeds their tread life. The latter has probably quadrupled since the introduction of radial constructions with steel cord reinforced belts.

With these observations on the increasingly stringent specification for conventional tyres and the complexity of their manufacture, the potential of fabricless tyres can be introduced.

A fabricless tyre is, by definition, no longer a composite of reinforcing fibres and a rubber matrix. In the ultimate, it may be constructed from only one homogeneous material and, consequently, the manufacturing route would be radically different. Thus the stages in conventional tyre production concerned with preparing the many components : rubberised plies, tread camelbacks and others; would not be required and complete fabricless tyres could be produced by techniques well known in the plastics industry. Of these, injection moulding and casting are obvious contenders, depending upon the melt viscosity of the material chosen, while rotational or even blow moulding can be considered. Whichever method were chosen, labour costs would be reduced very significantly - the first advantage offered by fabricless tyres.

The second advantage comes from the precision offered by injection moulding or centrifugal casting; if the latter, like the former, is carried out in a closed mould which defines both the inner and outer surfaces of the tyre. When a conventional tyre is moulded, only the outer surface is defined by the mould, the tyre being consolidated and shaped by an internal rubber diaphragm. Any irregularities present in the green, unvulcanised cover are reproduced to some extent in the final, vulcanised tyre. Thus it can be expected that the uniformity of fabricless tyres will be greater and less variable compared to conventional tyres.

To summarise, a fabricless tyre offers the potential of a less complex manufacturing route and lower labour costs, together with less geometrical variability. However it must, at least, be able to match the mechanical

performance of a conventional cross-biassed tyre, preferably that of a modern radial tyre.

I.4 Known Previous Work on Fabricless Tyres

A literature survey reveals a number of articles which discuss, in general terms, the possibility of fabricless or cast tyres, as they are often known. For example, references (1) and (2) have the titles : "Will cast auto tyres roll over the tyre cord market?" and "Will future tyres be cast polyurethane?" respectively; which summarise succinctly the worries felt to a lesser or greater extent by the tyre industry and its suppliers.

On the technology of fabricless tyres, the first papers to arouse interest emanated from the Firestone Tire and Rubber Company in the early 1970's. Of these, reference (3) contains data on the mechanical performance of tyres centrifugally cast in closed moulds from polyurethane. It was shown that:

(i) growth with inflation was small and, even after 11,000 miles running, only amounted to 3.5%;

(ii) radial stiffness was significantly higher than equivalent cross-ply and radial tyres, by 32% and 65% respectively;

(iii) when run to failure at the inflation pressure recommended for conventional tyres, the requirements of the US Department of Transportation were met;

(iv) the cornering power was high;

(v) the strength of the carcass, when measured by plunger tests, was more than adequate;

(vi) uniformity was excellent.

These results, however, only cover some aspects of tyre performance, for example no data are given on wear resistance or road-grip. Moreover, recognising that the radial stiffnesses of the fabricless tyres were high, the suggestion is made that the inflation pressure could be reduced to restore compliance. When testing for fatigue no such reduction was made. Altogether, then, the information published by Firestone is incomplete

and no mention is made of the principles guiding the design of fabricless tyres.

The next papers worth considering resulted from the US Air Force's interest in cast tyres for aircraft. It initiated a programme with Zedron Inc. to establish the potential of such tyres and the first target was to screen and select suitable materials, reference (4). In this publication, key physical properties are identified : tear strength, Young's modulus, cracking resistance, hysteresis, friction and wear resistance; for a material to be used both in the carcass and tread of a 7.00–8 tyre, a small tyre chosen, presumably, to ease the problems of manufacture and testing in the early stages of the programme.

Candidate materials were based upon polyesters, polyurethanes and low molecular weight polybutadiene. The last was soon eliminated because of its poor properties, and from the first two the following were chosen for extensive laboratory examination:

A – a polyester with 20 p.h.p. of milled glass fibre;

B – an unfilled polyester;

C – a thermosetting polyurethane with 20 p.h.p. of milled glass fibre.

Of these, A was considered the most promising, although it was soon realised its performance as a tread material was inadequate, primarily due to its high hardness affecting road friction and wear resistance detrimentally. Thus a two part tyre was envisaged, using a conventional natural rubber compound for the tread.

Using the filled polyester for the carcass, the proposed method of manufacture was rotational moulding, followed by strip winding for the tread. However it was recognised that the chosen carcass material could be inadequate in terms of its strain to yield, only 7%, and its high hysteresis, 50%. Nevertheless, it was concluded that tyre tests should be undertaken.

A second report on the collaboration between the US Air Force and Zedron, reference (5), describes experiments carried out on rotationally moulded tyres, although the sizes examined were 6.00–6, 6.50–8 and 8.50–8, compared to the 7.00–8 originally chosen. The methods employed were fairly conventional static tests of radial stiffness and contact patch size, while the dynamic tests were related to the performance required in aircraft taxi-takeoff manoeuvres. It was concluded that fabricless tyre technology had been advanced but fundamental design changes were necessary to both the tyres and their rims to reduce the stress levels in the lower sidewalls, where failures were most numerous. As noted when reviewing the work published by Firestone, the Air Force/Zedron exercise seemed to pay little attention to design.

In the late 1970's and early 80's, a company not part of the established tyre industry created considerable interest. Polyair Maschinenbrau of Austria has a good reputation as a machinery manufacturer for the plastics industry and it proposed an extension of its technology to the production of car and tractor tyres by liquid injection moulding. It embarked on a development programme to improve the chemistry of polyurethanes and to automate tyre production.

References (6) and (7) summarise Polyair's work and there is no doubt that the manufacturing route established is excellent. By injecting reacting, liquid polyurethane into a closed mould whose toroidal form has replaceable crown segments, the carcass of a fabricless tyre can be made first. Then, crown segments containing a tread pattern can be substituted for the smooth segments used for the carcass and the tread injected in a second operation. Moreover, it is possible to introduce reinforcement into selected parts of the carcass as pre-prepared components, such as bead wires or a rudimentary belt, with the confidence that the liquid polyurethane will encapsulate them. The completed tyre is removed after the mould has been opened and a solid, segmented core extracted automatically.

As with the performance data given by Firestone, those from Polyair are sparse. A single size of car tyres, 165–13, was compared to equivalent cross-ply and radial tyres with the inference that every measured property was very nearly equal or superior. However the design of the fabricless tyre is not described apart from the facts that it had bead wires and a single ply 0^{o}, or circumferential, belt of steel or Kevlar cords called a restrictor.

Certainly such dimensions as carcass wall thickness and profile shape are not mentioned, nor are the elastic properties of the polyurethanes used for the carcass and the tread. Moreover, there is no record of any assessment of the tyre by an independent organisation.

To summarise the published information from previous workers in the field of fabricless tyres: the data are incomplete and can be questioned because tests were either limited or not sufficiently described. Also, no attempt has been made to show how tyre design and performance interact, an essential stage in the development of such a radically different tyre product. Overall, one cannot assess with any confidence whether or not fabricless tyres are technically viable.

CHAPTER II : AIMS OF THE RESEARCH

Before stating the principal objective of the research, it is worth discussing briefly and in general terms the mechanical performance required from a pneumatic tyre.

Tyres constitute the only connection between a vehicle and the road upon which it is running. They must therefore : carry the weight of the vehicle and its contents; and transmit or generate the forces necessary for accelerating, overcoming wind resistance, cornering and braking. Moreover, because a tyre only makes rolling contact with the road, all the forces other than those normal to the road are frictional in nature within the contact patch. Consequently, whether the road is dry or wet, the tyre must exhibit a high coefficient of friction.

The tyres also act in conjunction with the primary suspension of a vehicle to isolate it from road irregularities. A tyre, therefore, is required to act as a spring, particularly at frequencies above 10 to 15 Hz when, in the direction normal to the road surface, the primary spring is inoperative owing to its associated damper. Parallel to the road surface, any irregularities are isolated almost entirely by the tyres because, in this direction, the only other compliance is that provided by the rubber bushes used to anchor the suspension components.

The generation and transmission of forces, and its behaviour as a spring, may be regarded as the positive functions of a tyre. However, it also has a negative function because it is required to perform in these ways without failure and over a distance which has increased significantly since the introduction of the steel belted radial ply tyre. Now the useful life of a tyre can be terminated in two ways : when its tread has worn to the extent that the pattern depth has reached the legal minimum, currently 1 mm in the UK; or when it suffers some form of catastrophic failure owing to fatigue of its carcass. The latter will be aggravated if the tyre runs at too high a temperature. Heat is generated by the flexing of a tyre because the materials : rubber compounds and textiles; from which it is made exhibit hysteresis. Thus the materials must be chosen and the tyre designed to ensure that the temperature rise is not excessive.

The energy loss, due to hysteresis, within a tyre causes it to exhibit drag or rolling resistance which, like wind resistance, must be overcome by the engine of the vehicle. To minimise petrol consumption, the drag of a tyre should be kept as low as possible. However, one of the conflicts experienced in the design of tyres now becomes apparent. The rubber compounds chosen for the treads of tyres to enhance friction and resistance to wear, tend to have relatively high hysteresis, although the correlation is not absolute. Consequently a careful balance of the various properties must be sought.

It is against this general background of the performance requirements of pneumatic tyres that the aims of the research may be stated :

> "To establish whether a pneumatic tyre constructed with no directional reinforcement in its carcass is a technically viable alternative to conventional tyres on modern passenger cars".

The approach to be taken in achieving this aim is governed to some extent by the decision that, during the course of the research, demonstration tyres should be produced for vehicle trials. This dictates a largely experimental approach.

The first stage, however, is to establish criteria for the design of fabricless tyres. These are likely to be significantly different to those for conventional tyres, whose meridional profiles are dominated by the disposition of the reinforcing cords. A range of tyres will then be designed and manufactured using materials selected by virtue of their known physical properties.

The manufacturing route will depend upon the nature of the chosen materials; for example, whether they are thermoplastics and can be injection moulded, or liquid processing when casting can be considered. Once the tyres have been produced, a systematic examination of their performance may be undertaken, comparing the data obtained with the known or measured performance of equivalent conventional tyres, both cross-biassed and radial.

This approach alone, however, is limited because comparative data may not be sufficient to assess the viability of fabricless tyres. It is quite possible that the designs chosen are not optima, leading to incorrect conclusions. An analysis must be attempted whereby the key design parameters may be related to performance. In this way, the optimum may be identified without a contimuing demand for the manufacture of additional, modified tyres.

CHAPTER III : THE MECHANICS OF PNEUMATIC TYRES

III.1 The Tyre as a Spring

When outlining the performance requirements of pneumatic tyres in Chapter II, it was stated that they must act as springs in conjunction with the primary suspension of a vehicle. In fact, a tyre may be likened to a triaxial spring system with interactions between the three modes : radial (x), lateral (y) and longitudinal (z), figure 3.1.

If, for the purpose of describing a tyre's behaviour, one assumes it is linear in response, then the force developed in one mode, say x, is related to the deflections (d) in all three modes by an equation of the form :

$$F_x = K_x d_x \left(1 + k_{xy}\, d_y + k_{xz}\, d_z\right) \qquad (1)$$

where K_x is the principal stiffness in mode x,
and k_{xy}, k_{xz} are interaction stiffnesses.

In practice, however, it is the forces rather than the deflections which are defined, by the weight of the vehicle and its kinematics. Thus, in preference to equations with coefficients of stiffness, those involving compliance are more instructive. Moreover, because the longitudinal compliance of tyres in general is comparatively low, the mechanical behaviour of a tyre may be described by equations (2):

$$d_x = C_x F_x \left(1 + c_{xy}\, F_y\right) \qquad \text{- radial (2.1)}$$

$$d_y = C_y F_y \left(1 + c_{yx}\, F_x\right) \qquad \text{- lateral (2.2)}$$

where C and c are the principal and
interaction compliances respectively.

From equations (2) it may be seen that when a tyre is running straight ahead and not generating a cornering force ($F_y = 0$), the radial deflection is only a function of the radial force, F_x, which opposes the load on the tyre. However when cornering, the radial deflection increases, while the lateral deflection depends upon both the lateral and radial forces.

Fig. 3.1

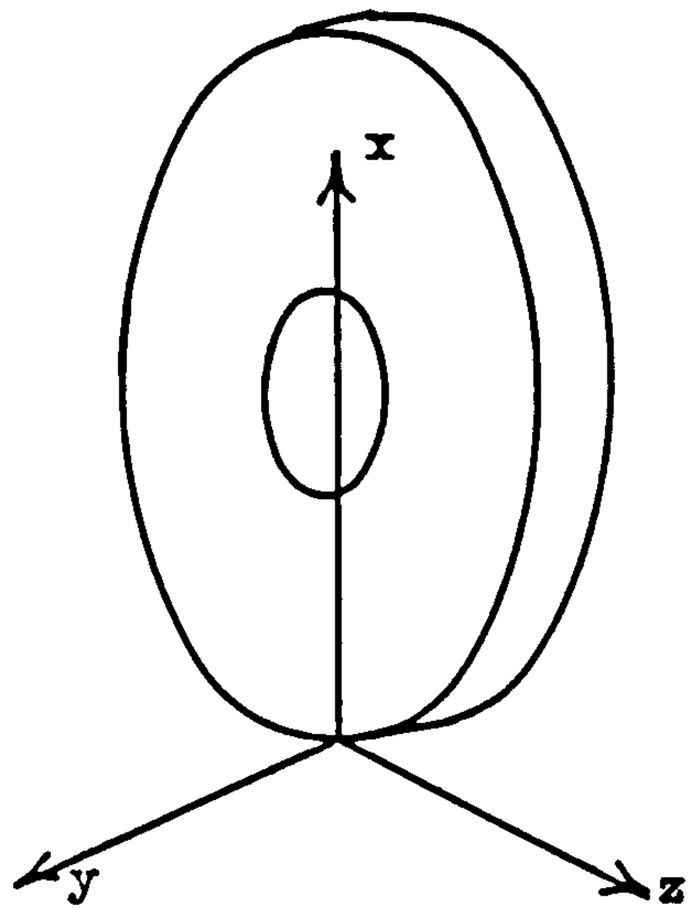

Fig. 3.3

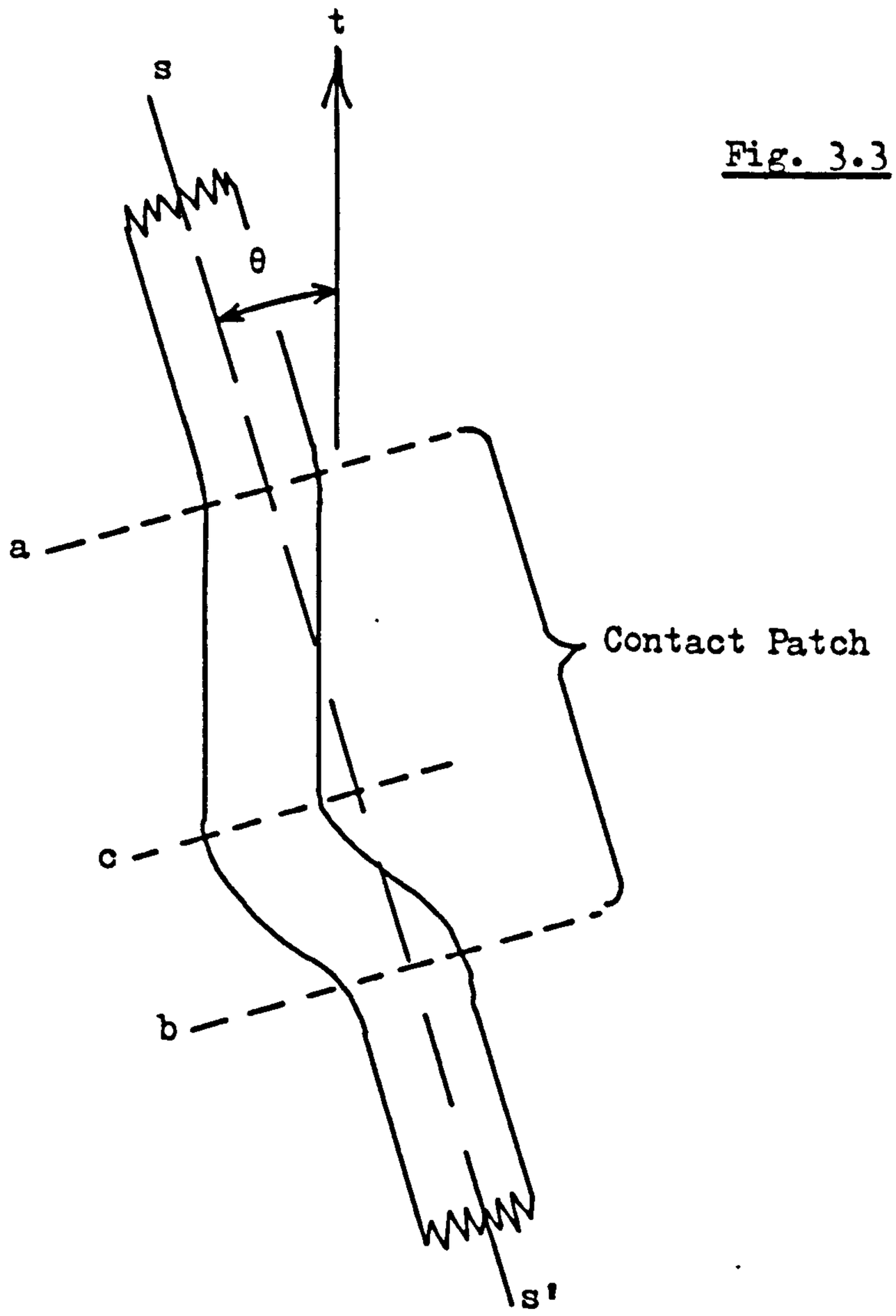

There is another factor which must be introduced and discussed when considering the pneumatic tyre as a spring : the inflation pressure, upon which the stiffnesses or compliances depend. Maintaining the assumption that the response of a tyre is linear and referring back to equation (1), the principal radial and lateral stiffnesses are related to the pressure, p, by:

$$K_{x,y} = A_{x,y} + B_{x,y}p \qquad (3)$$

In this equation, $A_{x,y}$ represents the structural component of stiffness and is due to the stresses induced in the materials of the tyre by its distortion; and $B_{x,y}$ is the additional component of stiffness caused by unit inflation pressure. The fundamental importance of these structural and pneumatic components to the performance of pneumatic tyres is explored in the next section.

III.2 The Pneumatic Component

Although a tyre is required to carry load, generate forces and act as a spring, these functions per se do not dictate a pneumatic construction. A solid rubber tyre is also able to act in these ways and, for many applications, it is preferred. Among other reasons, there is no need to check and maintain the inflation pressure. Thus, if the technical viability of fabricless, pneumatic tyres is to be assessed, it is vital to understand the importance of the pneumatic component.

Consider, first, the load (W_s) carried by the structure of a tyre when the inflation pressure is zero. From equations (1) and (3):

$$W_s = F_x = A_x d_x$$

where d_x is the radial deflection.

Confining the argument to the radial mode, the subscripts $_x$ may be omitted and the energy, E, stored in the tyre is:

$$E = \tfrac{1}{2} W_s\, d = \tfrac{1}{2} A d^2$$

and, if the overall hysteresis of the materials of the tyre is H and is defined as the ratio of energy lost in a cycle of deformation to the

energy input, then the energy appearing as heat, Q, per revolution of the tyre is:

$$Q = \tfrac{1}{2}fHAd^2 \qquad (4)$$

where f is a geometrical factor related to the proportion of the tyre distorted at any instant in the revolution.

Now introduce the pneumatic stiffness of the tyre so that its total radial stiffness becomes A + Bp, equation (3), and the total load carried is:

$$W = (A + Bp)d$$

or

$$d = \frac{W}{A + Bp} \qquad (5)$$

Assuming that the mechanism of pneumatic stiffness is lossless, the deflection given by equation (5) may be substituted into equation (4) to give:

$$Q = \frac{fHAW^2}{2\,(A + Bp)^2} \qquad (6)$$

Equation (6) may be interpreted in terms of three hypothetical tyre constructions:

1) a non-pneumatic tyre, when B = 0, giving:

$$Q \propto \frac{1}{A} \qquad (6.1)$$

2) a totally pneumatic tyre, A = 0, when:

$$Q = 0 \qquad (6.2)$$

3) a partially pneumatic tyre, for which:

$$Q \propto \frac{A}{(A + Bp)^2} \qquad (6.3)$$

Before examining the consequences of equations (6) in more detail, it is worth restating the importance of limiting the energy loss in a tyre. This must be done for two reasons: it results in drag or rolling resistance; and, of greater significance, the heat generated causes the temperature of the tyre to rise, thus leading to polymer degradation and fatigue. When running at constant speed, an equilibrium temperature distribution will be reached when the rate of heat generation is balanced by the rate of heat loss by forced convection and conduction through the wheel and the road. Clearly, the greater the speed, the higher is the temperature.

With these comments, the effects on energy loss of various combinations of the structural and pneumatic stiffnesses may be calculated using equation (6.3). In table I, the pneumatic stiffness, Bp, for the pneumatic tyre is maintained constant and put equal to 1.0; while the structural stiffness, A is varied to give total stiffnesses between 1.0 and 10.0.

Table I

Radial Stiffness and Energy Loss

Non-pneumatic Tyre		Pneumatic Tyre (Bp = 1)	
Radial Stiffness (A)	Energy Loss ($\propto 1/A$)	Radial Stiffness (A + Bp)	Energy Loss (Equ. 6.3)
1.0	1.00	1.0	0.00
-	-	1.1	0.08
1.2	0.83	1.2	0.14
-	-	1.3	0.18
1.4	0.71	1.4	0.20
1.6	0.63	1.6	0.23
1.8	0.56	1.8	0.25
2.0	0.50	2.0	0.25
2.5	0.40	2.5	0.24
3.0	0.33	3.0	0.22
4.0	0.25	4.0	0.19
10.0	0.1	10.0	0.09

With these data, energy loss may be plotted against radial stiffness for the non-pneumatic and pneumatic tyres, the latter with the range of structural stiffnesses, figure 3.2. For conventional pneumatic tyres, car, truck and aero, the structural component lies between 15% and 35% of the pneumatic stiffness component and in figure 3.2 this range is marked.

Figure 3.2 clearly demonstrates the advantage of pneumatic tyres. At the radial stiffness required for passenger cars and trucks, between 1.1 and 1.5 in these arbitrary units, their energy loss is less than one fifth of that of equivalent non-pneumatic tyres. Consequently they are able to run at much higher speeds without over-heating. Non-pneumatic tyres, as exemplified by solid tyres, can only be used for low speed applications, such as forklift trucks, and even then they have radial stiffnesses perhaps four times those of equivalent pneumatic tyres to limit the deflection and thus energy loss.

As the structural stiffness of pneumatic tyres is increased so that they become less dependent upon inflation, their energy loss approaches that of non-pneumatic tyres but, as seen in table I, the total stiffness is then about ten times that of conventional pneumatic tyres.

III.3 The Generation of Forces

To examine the mechanical behaviour of a pneumatic tyre further in order to define other aspects of its mechanics and performance, the nature of the forces transmitted or generated in the three modes must be considered. First, the force in the radial mode is simply the load applied by the vehicle, although, owing to load transfer during braking and cornering, this force will exhibit transient variations. In chapter V, the method by which a tyre carries load will be discussed in more detail but here it is sufficient to note that the radial force is directed vertically through the axis of the tyre and has no frictional component in the contact patch.

The second force to be considered is in the longitudinal direction and is responsible for accelerating a vehicle and overcoming wind resistance. It is most apparent during braking when it can result in decelerations similar in magnitude to 'g'. This means that, in an emergency stop,

Fig. 3.2

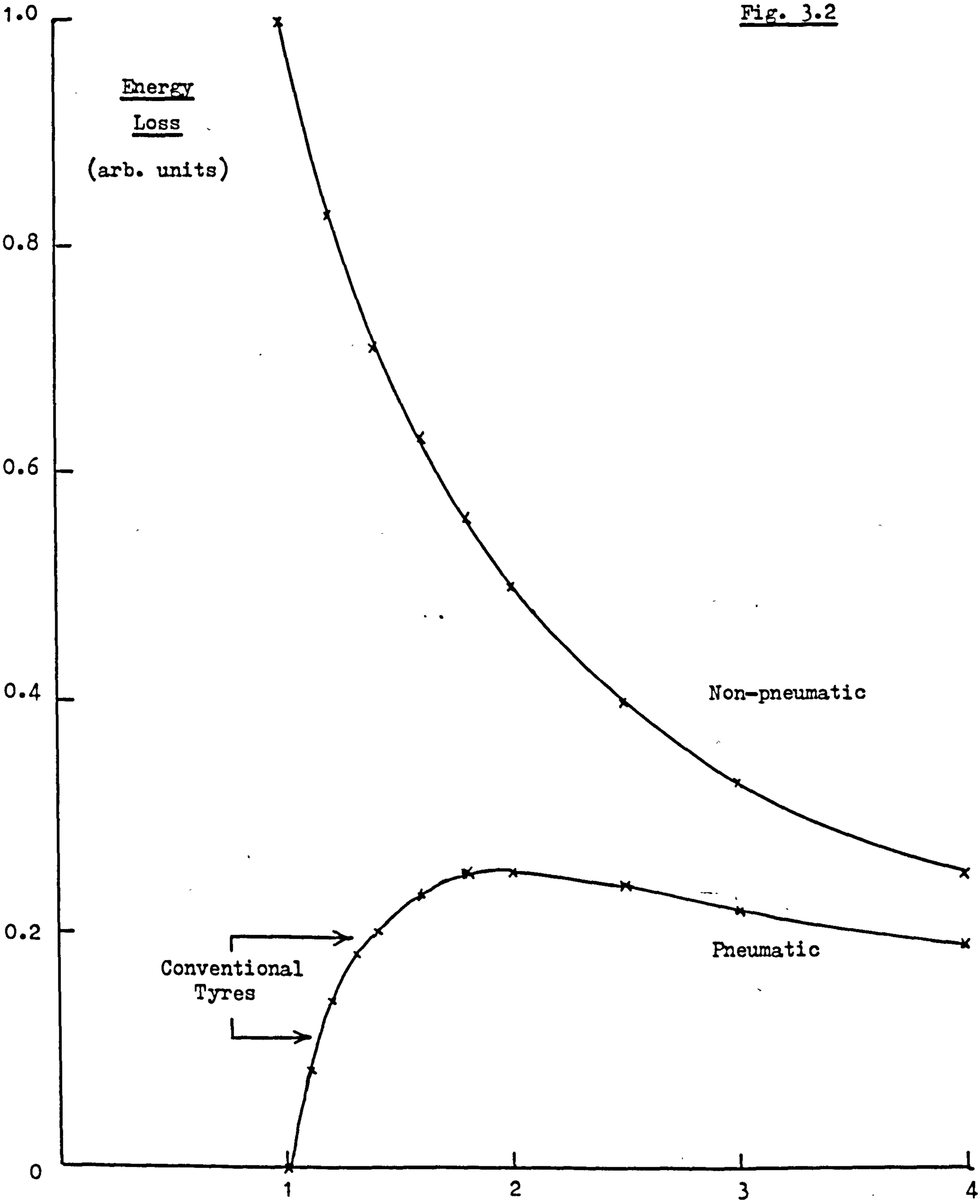
1.0
0.8
0.6
0.4
0.2
0
Energy
Loss
(arb. units)
Non-pneumatic
Pneumatic
Conventional
Tyres
1
2
3
4
Radial Stiffness (arb. units)

a tyre is required to generate a frictional force comparable to the load it is carrying. In other words, the coefficient of friction between the tread rubber of a tyre and a dry road surface must approach or even exceed unity. When the road is wet, an additional complication arises: the removal of water from between the tyre tread and the road in the contact patch. It is only when dry contact has been created that frictional forces can be generated. To remove the bulk of the water, a tread pattern of drainage grooves is used; whilst the elimination of the final film of water and the maximisation of friction in the dry contact zone are achieved by employing a rubber compound with a preferred balance of viscoelastic properties. In terms of the tyre as a whole, a longitudinal force is transmitted to or from the axle as a couple but, as stated before, the compliance of a tyre in this mode is relatively small and so need not be considered further.

The third and final force, in the lateral direction, is more complex because its development depends upon turning the wheel on which the tyre is fitted relative to the direction the vehicle is travelling, reference 8. Figure 3.3 shows, in schematic form, the plan view of a cornering tyre with the plane of the wheel, ss', inclined at a small angle θ to the direction of travel, t. The region defined by the broken lines 'a' and 'b' represents the contact patch, so that beyond 'a' and 'b' the tread of the tyre is not in contact with the road. As the tyre rotates, an element of the tread makes contact with the road at 'a' and friction causes it to adhere to the road, so distorting the tyre laterally. However, as the element moves further into the contact patch, the distortion increases until it reaches the point 'c' where the restoring force developed in the tyre overcomes the frictional force. Slip between the tread and the road then occurs in the zone 'cb' as the tyre recovers from the lateral distortion.

The relationship between the radial and lateral force intensity distributions in the contact patch of a cornering tyre may be represented by figure 3.4. Let the broken curve show the radial component, f_x, plotted against distance through the contact patch, 'ab', the integral of which gives the total radial force F_x. If scaled by the coefficient of friction ($\mu < 1$ as illustrated), the similar continuous curve results and defines the maximum lateral force intensity, μf_x, which may be developed. However, at the steering angles involved in normal vehicle

manoeuvres, this maximum is not utilised, rather the lateral force intensity develops progressively through the contact patch until limited by the coefficient of friction. This behaviour is represented by the solid line f_y in figure 3.4, which increases linearly to the point when it meets the curve μf_x. Slip then occurs and f_y returns to zero.

Clearly, as the steering angle is increased, the lateral force intensity develops at a greater rate but slip is induced earlier in the contact patch. Thus, when the lateral force intensity is integrated, it is found that the total lateral or cornering force increases with steering angle but at a reducing rate, figure 3.5. Eventually the maximum force available is reached and the vehicle can no longer be manoeuvred in a controlled manner and either a front or rear wheel lateral skid occurs. If the tyre is also being braked and is thus developing a longitudinal force F_z, a proportion of the available force intensity μf_x is not available for cornering so that control is lost at a lower steering angle.

It will be appreciated, then, that the radial force intensity through the contact patch, the coefficient of friction between the tread rubber and the road surface, and the radial and lateral stiffnesses of the tyre all affect the tyre's cornering characteristics. However they are also important in determining its wear rate because it is the slip at the rear of the contact patch which is the prime cause of abrasion or, to be more precise, the integral of lateral force intensity with respect to slip distance, reference 9. Thus if the lateral distortion occurring while the lateral force intensity distribution is developing could be lessened, zone 'ac' in figure 3.3, so would the amount of slip during recovery, zone 'cb', together with the resulting wear. A tyre with high lateral stiffness, therefore, wears at a lower rate under given driving conditions, where these are defined by the cornering forces demanded by the kinematics of the vehicle. The latter are, of course, chosen by the driver.

The modern radial-ply tyre with a steel cord reinforced belt illustrates the move to high lateral stiffness to reduce wear. However its casing, which often has a single ply radial construction, is relatively flexible compared to the four ply biassed construction used in an equivalent cross-ply tyre. To explain this apparent anomaly, it is necessary to consider the belt and the casing separately. To do this, the analogy

Fig. 3.4

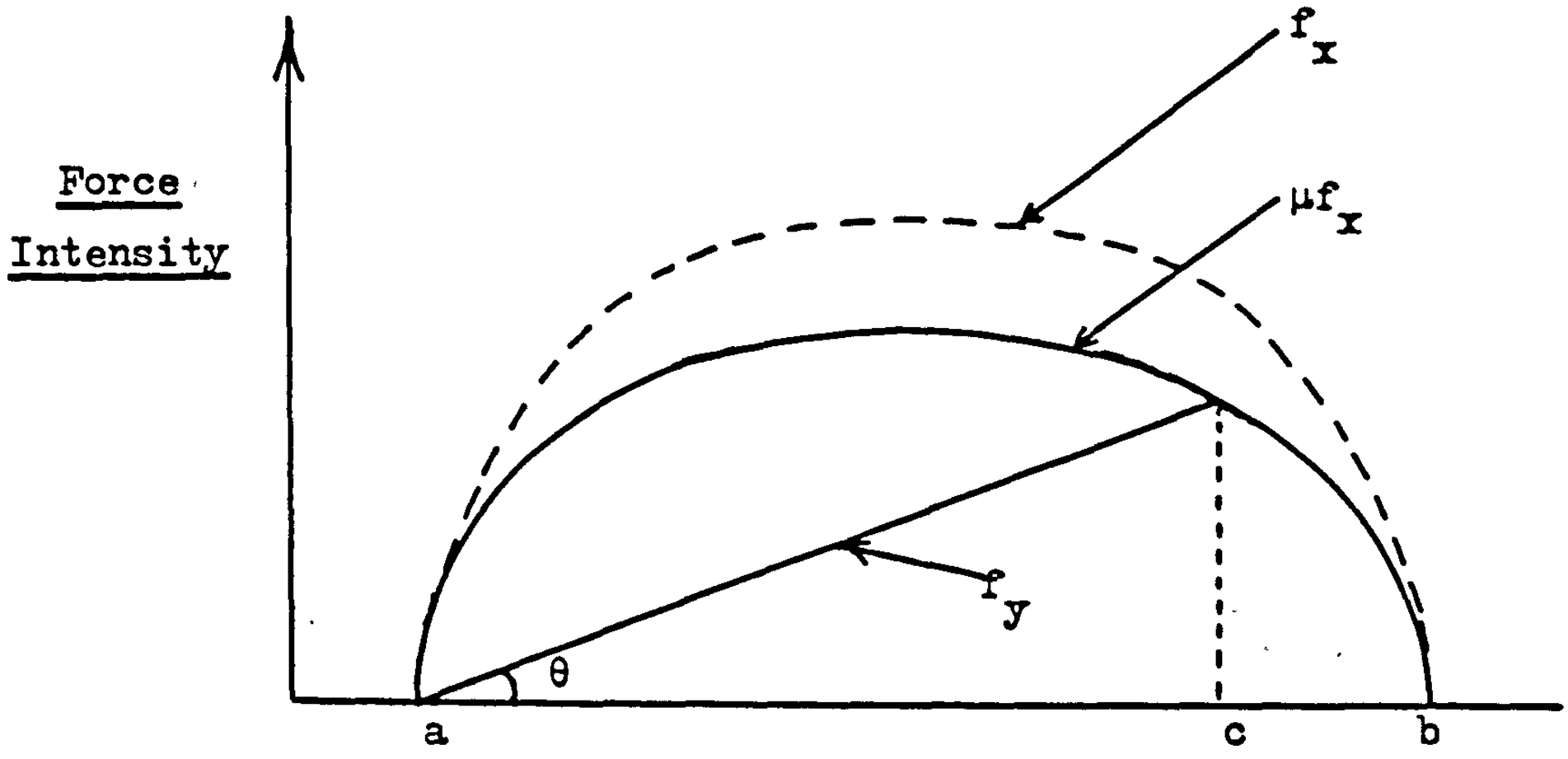
Force
Intensity
f_x
μf_x
f_y
θ
a
c
b

Fig. 3.5

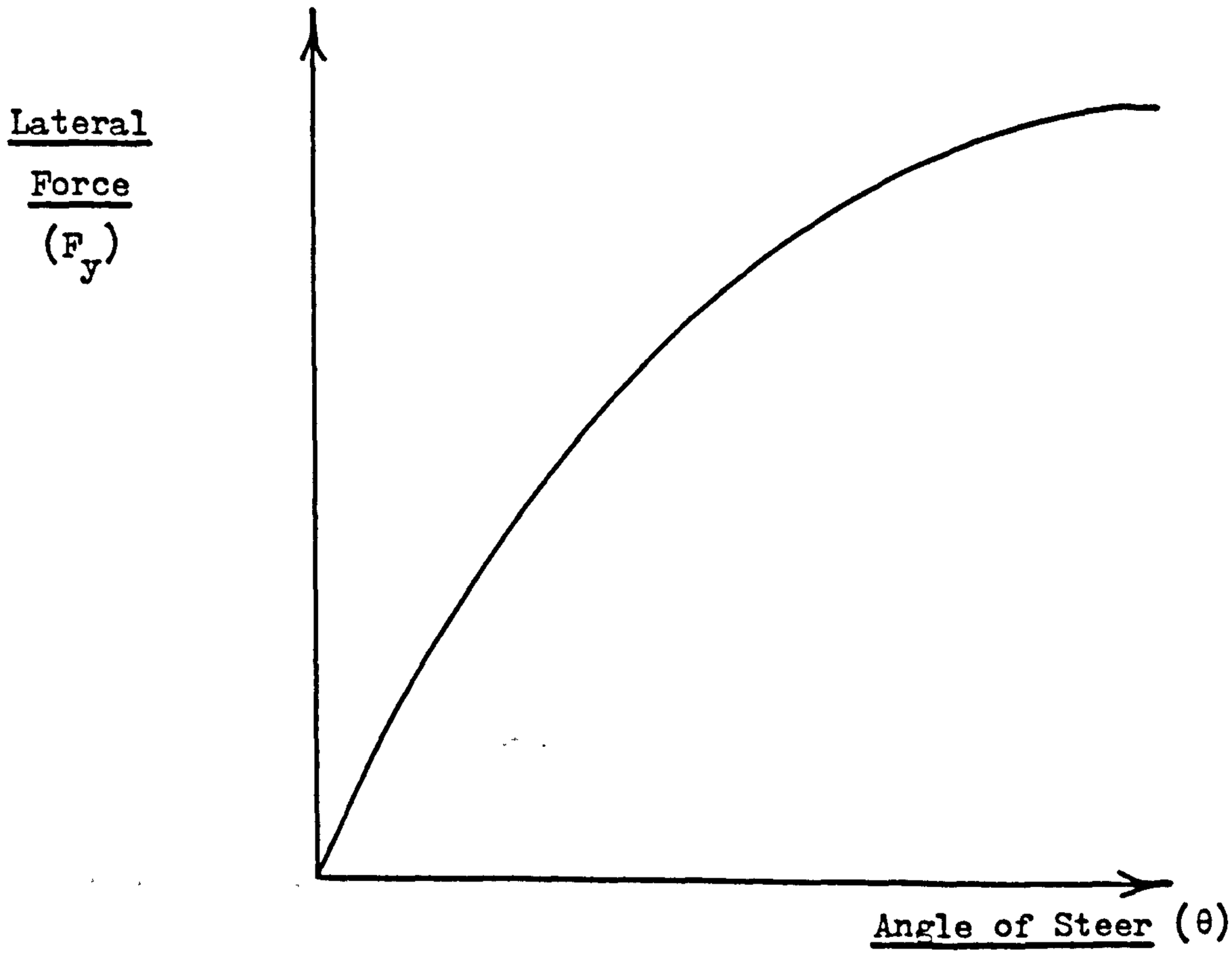
Lateral
Force
(F_y)
Angle of Steer (θ)

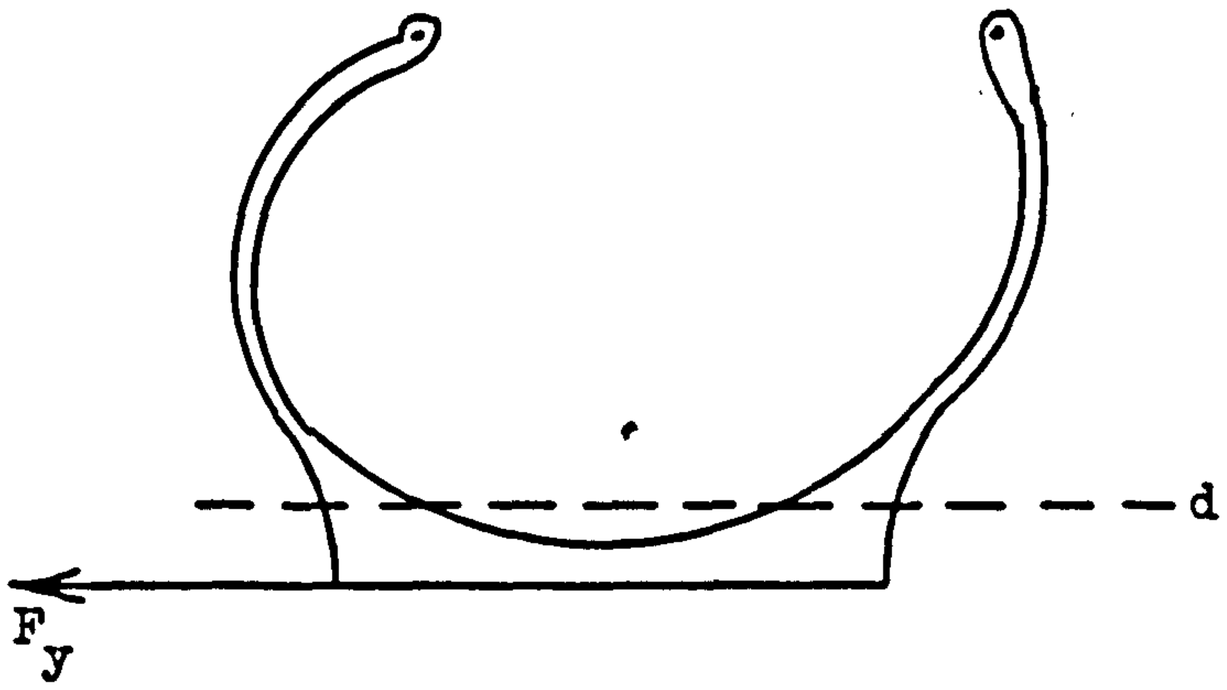

Fig. 3.6

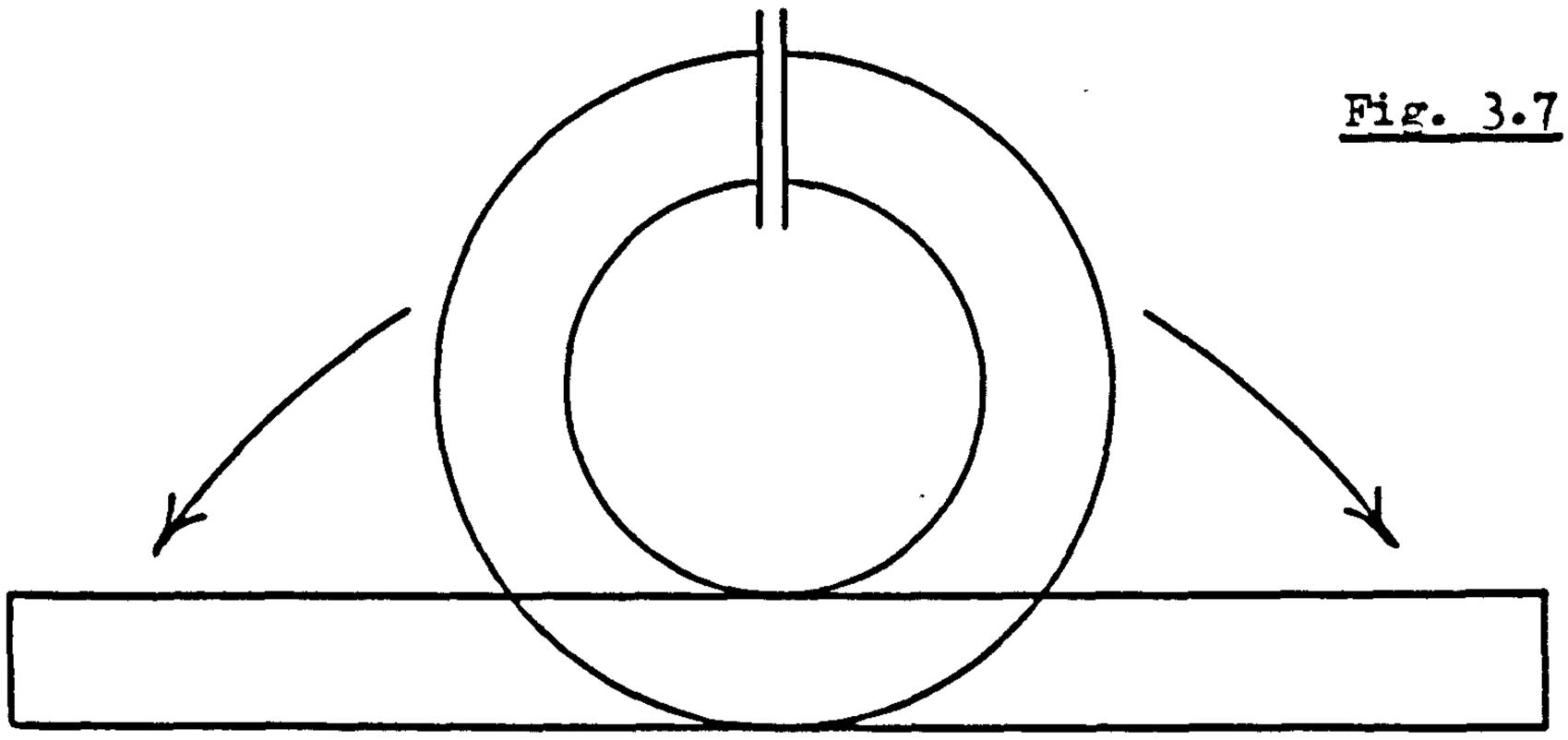

Fig. 3.7

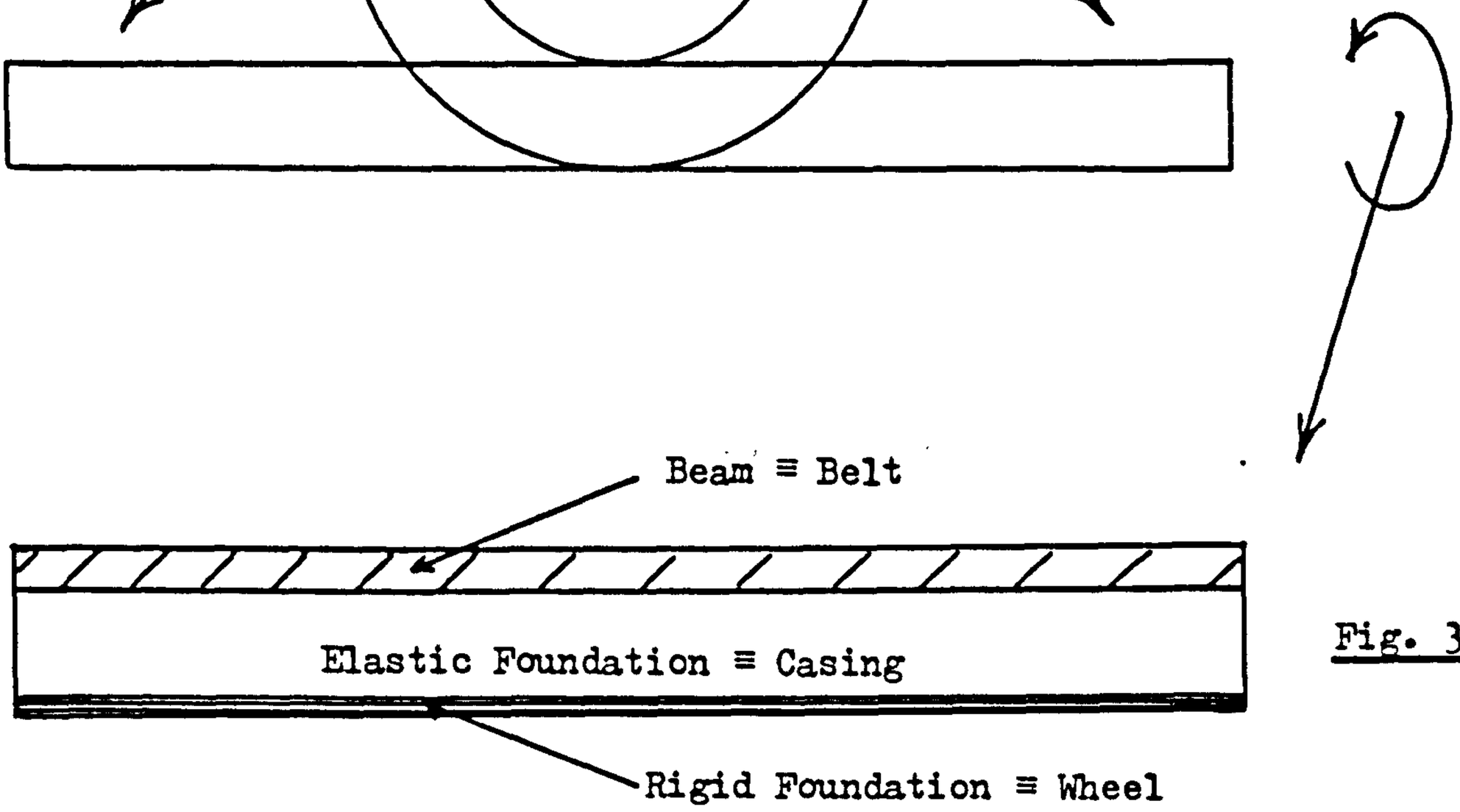

Fig. 3.8

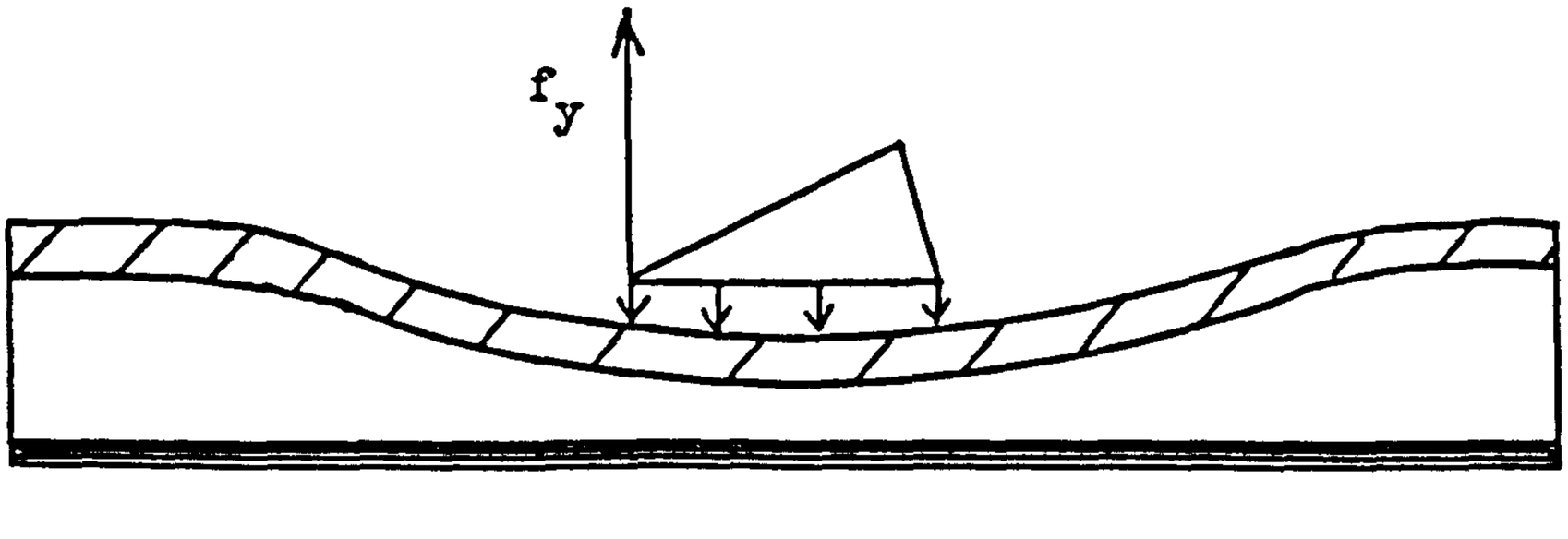

Fig. 3.9

of a beam on an elastic foundation is helpful, references 9 and 10.

To develop this analogy, consider the cross-section of a cornering tyre, as shown in figure 3.6. Two zones may be identified, separated by the broken line labelled 'd'. Above 'd' in the sidewalls, the tyre's mechanical behaviour is dominated by the radial construction of the casing, with only minimal coupling circumferentially around the tyre. However below 'd', the belt which has considerable circumferential reinforcement is dominant and may be likened to a bending beam when under the action of a lateral force. It is restrained by the sidewalls which act as the elastic foundation. Consequently, if one imagines a tyre cut radially at its highest point and then unrolled figure 3.7, it may be represented by the system shown in figure 3.8, where the rigid foundation models the rim of the wheel on which the tyre is mounted. With the application of a lateral force intensity distribution, the distortions shown in figure 3.9 result.

In mechanical terms, the elastic properties of the beam may be defined by a Young's modulus (E) and a second moment of area (I) to give an effective EI. The elastic foundation only requires a stiffness per unit length, K, because each element along its length can be deflected independently of adjacent elements. A complex function of EI and K determines the cornering and wear properties of a tyre. Thus a radial ply tyre has a high value of EI compared to a cross-ply tyre but a lower value of K. On balance this combination gives it superior performance.

From the resumé of the principal features of the mechanics of a pneumatic tyre in this and previous sections of the chapter, it may be appreciated that a tyre is a complex mechanical device. It is against this background that fabricless, pneumatic tyres must be assessed.

CHAPTER IV : DESIGN METHODS

IV.1 Introduction

In any structure, it is not the overall stress distribution which leads to failure in service but localised stress concentrations. When using, for example, ductile materials which exhibit linear elasticity over their working strain range, such as steel, the designer ensures that nowhere is the yield stress approached, usually employing a safety factor of at least 2. With elastomeric materials whose elasticity is non-linear, it is not stresses per se which are used in the theory of fatigue but the stored energy density. In the presence of a flaw in the polymer network, often made more likely by reinforcing, particulate fillers, this energy is available for propagating the flaw. As the flaw grows in size, more energy is often concentrated around it, leading to an accelerating growth rate and catastrophic failure. However, the stored energy density (W) is a function of the stress (σ) but also of the strain (ϵ):

$$W = \tfrac{1}{2}\sigma\epsilon$$

$$\text{or} \quad W = \tfrac{1}{2}E\epsilon^2 = \tfrac{1}{2}\frac{\sigma^2}{E}$$

where E is Young's modulus which, for elastomers, is defined as the initial slope of the stress-strain characteristic.

Any design method, therefore, must take into account as far as possible the stresses to be induced in a structure. Moreover, stress concentrations must be avoided.

Stresses are induced in pneumatic tyres, conventional or fabricless, in two stages. First, the tyre is fitted to the rim and inflated and, second, it is subjected to the radial and lateral forces described in III.3. Ideally, a tyre should be designed to minimise the stress concentrations arising from both these causes but this would involve calculating the stresses in an axisymmetrical body, the toroidal tyre, with both axisymmetrical and asymmetrical boundary conditions of pressure and force.

One method capable, in principle, of such a complex stress calculation is finite element analysis, whereby the geometry of a candidate fabricless tyre is subdivided into brick-like elements of defined, simple geometry. The behaviour of the individual elements, and their interactions with each other and the imposed boundary conditions, are expressed as a series of simultaneous equations. When solved, the required information on the overall deformation and detailed stress distribution is obtained. However, at present, available finite element methods capable of dealing with elastomers can only examine the section of an axisymmetrical body with axisymmetrical boundary conditions, such as a toroidal tyre freely inflated. This special case is explored in appendix I.

Recognising that, if finite element analysis were used, it would not be possible to take into account the stresses caused by the external radial and lateral forces on the tyre but only those induced by internal inflation, it was decided to employ the more simple shell theory as the basis for design. It was argued that, because the stresses due to the external forces, albeit unknown, were superimposed upon those due to inflation, the latter should be as low and uniform as possible. Moreover, a second criterion was also introduced, which was that the volume of material used in the carcass of a tyre to restrict dimensional growth due to inflation should be minimised for any given size of tyre. Finally, the problem of fitting the tyre to the rim was overcome by stipulating that the positions of the bead regions when a tyre was moulded should be identical to those when fitted to the rim. In other words, the axial separation of the beads would be unchanged, thus avoiding the imposition of further stresses.

It is important at this stage to introduce the concept of an equilibrium tyre profile, because upon this rest the design methods to be described. If the carcass of a tyre were composed of an inextensible but perfectly flexible material, it is said to have been moulded to its equilibrium profile if, on inflation, its profile does not change. In this hypothetical case, only stresses to oppose the inflation pressure are induced in the tyre; whereas, if a shape change occurs, bending strains would be superimposed. This definition does not limit the material to one with isotropic elastic properties but any anisotropy would need to be orientated and matched exactly to the chosen profile.

IV.2 Calculation of Stresses owing to Inflation

IV.2.1 Choice of theory

The carcass of a pneumatic tyre is a toroid, which means it is a shell of revolution and thus has an axis of symmetry and a surface of double but varying curvature. However before developing a method to calculate the stresses induced by inflation, it is instructive to consider the simpler case of a cylinder to determine whether the analysis should be based upon thick-walled or thin-walled theory, the latter being better known as membrane theory.

Consider a section of the cylinder with unit length shown in figure 4.1, whose inner radius is a and outer radius is b. If the radial stress is σ_r and the hoop stress is σ_m, then it may be shown, reference 11, that at any radius, r, within the wall:

$$\sigma_r = \frac{a^2 p}{b^2 - a^2} \left(1 - b^2/r^2\right) \tag{3}$$

$$\sigma_m = \frac{a^2 p}{b^2 - a^2} \left(1 + b^2/r^2\right)$$

To complete the analysis, it is necessary to calculate the axial stress. If it is assumed this is constant through the thickness, the product of the stress, σ_a, and cross-sectional area balances the pressure force, ie:

$$p \pi a^2 = \pi(b^2 - a^2)\, \sigma_a \tag{4}$$

$$\text{or } \sigma_a = \frac{a^2 p}{b^2 - a^2}$$

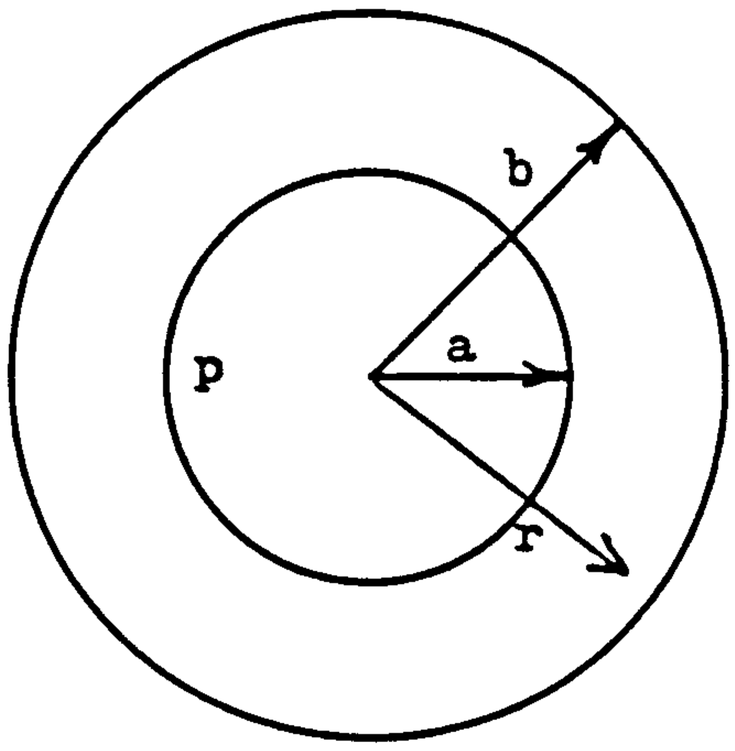

Figure 4.1

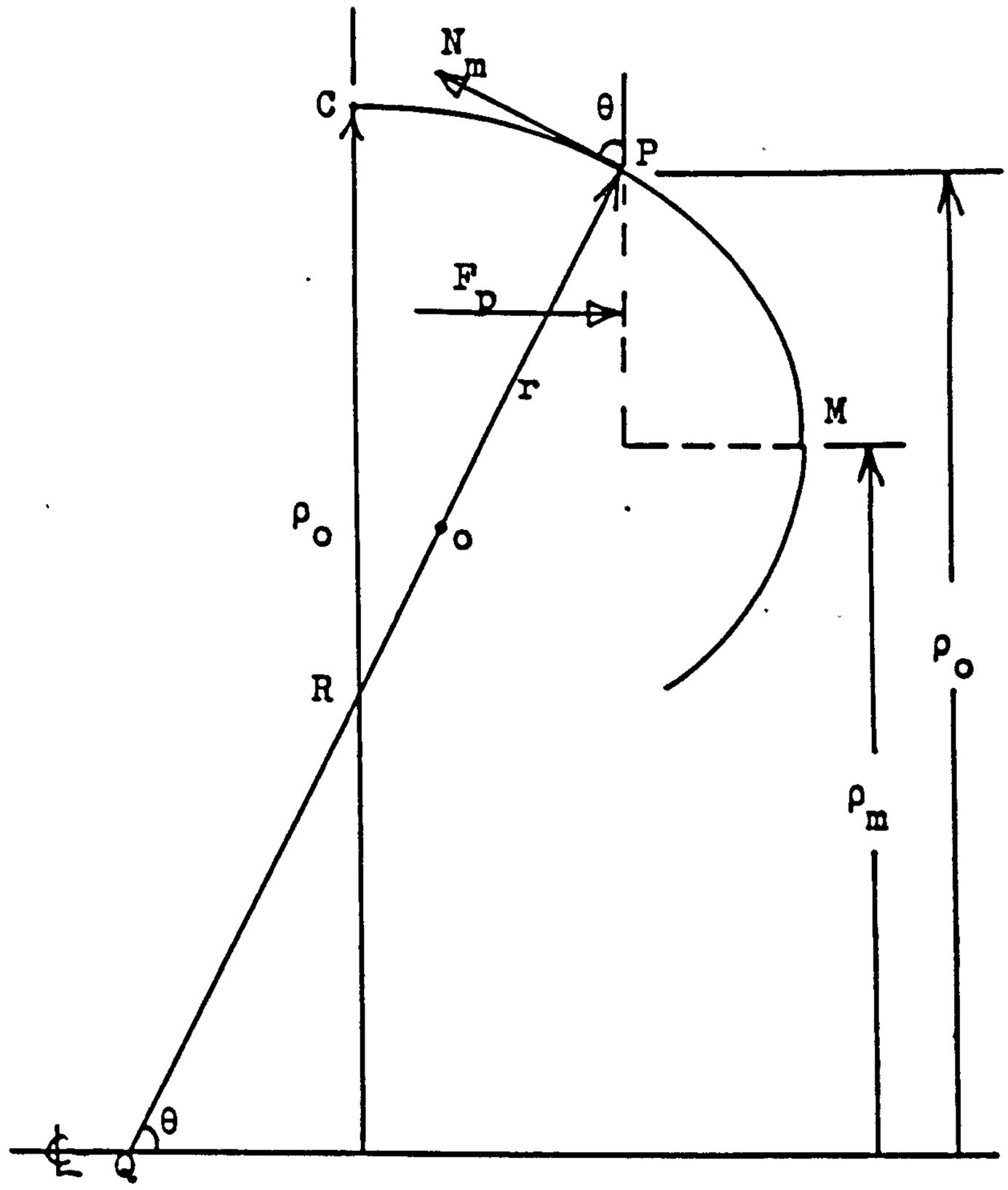

Figure 4.2

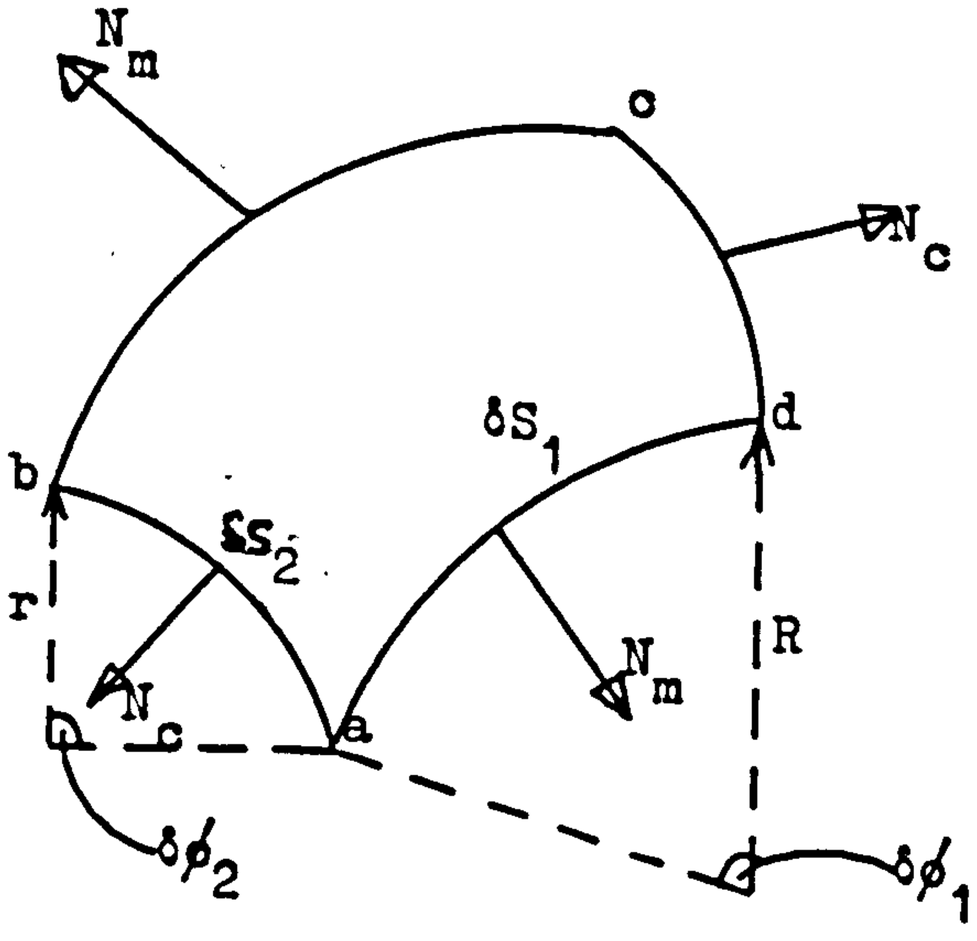

Figure 4.3

The meridional or hoop stress, σ_m from equations (3), and the axial stress may now be compared to those from the well known membrane theory for a cylinder:

$$\sigma_m = \frac{rp}{t}$$

$$\sigma_a = \frac{rp}{2t} \qquad (5)$$

where r is the mean radius of the cylinder,
and t is its wall thickness.

It may be seen that the equations for the stresses in the thick walled cylinder reduce to those from the membrane theory as:

$$a \rightarrow b = r$$

To determine whether it is necessary to use thick-walled theory for examining the stresses due to inflation in the carcass of a tyre, or whether membrane theory will suffice, some approximate dimensions must be introduced into the discussion of the cylinder.

A small cross-biassed tyre, such as a 5.20–10, has an approximately circular section of mean radius 60mm and a carcass wall thickness of about 5mm. Using the former dimension for the cylinder, the meridional and axial stresses were calculated for a range of wall thicknesses by the two theories. They are listed in table II for an inflation pressure of 200 kPa.

Table II

Comparison of Thin and Thick-wall Theories

Membrane Theory				Thick-Walled Theory				
Radius (r, mm)	Thickness (t, mm)	σ_m (MPa)	σ_a (MPa)	Radius (b, mm)	Radius (a, mm)	Max. σ_m (MPa)	Min. σ_m (MPa)	σ_a (MPa)
60	5	2.4	1.2	62.5	57.5	2.40	2.20	1.10
60	10	1.2	0.6	65.0	55.0	1.21	1.00	0.50
60	15	0.8	0.4	67.5	52.5	0.81	0.61	0.31
60	20	0.6	0.3	70.0	50.0	0.62	0.42	0.21

From the thick-walled theory, two values for the meridional stress are given : max. σ_m which occurs at the inner surface when r = a; and min. σ_m at r = b. Membrane theory only diverges by more than 10% from the greater of these two stresses when the wall thickness, t = b - a, exceeds about 12mm. Agreement between the axial stresses is less good, the difference being greater than 10% above a wall thickness of 5mm. However the membrane theory always results in the larger value and therefore errs on the side of safety.

It may be concluded that membrane theory is sufficiently accurate for wall thicknesses up to 12mm and that it is unnecessary to introduce the complications of thick-walled theory.

IV.2.2 Inflation Stresses in a Toroid

Having established that membrane theory may be used to calculate the stresses due to internal pressure in a shell of revolution whose wall thickness relative to its radius of curvature is comparable or somewhat greater than that of a conventional pneumatic tyre, the special case of a toroid may be considered.

In general, the two principal radii of curvature around the cross-section of a toroid will not be constant but will vary from point to point. How they vary will depend upon the exact shape of the meridian which defines the profile of the toroid. In IV.2.3, means for defining the profile will be developed but, initially, consider a single point, P, on some toroid as shown in figure 4.2.

If the radius to P from the axis is ρ and the meridional angle at P is θ, where this is defined as the angle between the tangent at P and the radial direction, then the circumferential radius of curvature (R) is PQ normal to the profile, that is:

$$R = \rho/\sin\theta$$

Clearly, when P coincides with the crown, C, of the toroid: $R = \rho_o$.

The meridional radius of curvature (r) cannot be evaluated without knowing the detailed meridional shape of the toroid, however it is normal to the profile and is represented by OP in figure 4.2.

Consider now a small element of the toroid at P with the principal radii of curvature R and r, figure 4.3. It has the dimensions δs_1 along circumferential lines and δs_2 along meridians. Let the principal tensions per unit length, equivalent to $\sigma.t$, be N_c and N_m.

The component of the forces on ab and cd normal to δs_1

$$= 2\left(N_m\ \delta s_1 \sin\frac{\delta\phi_2}{2}\right) = N_m\ \delta s_1 \frac{\delta s_2}{r}$$

and the component of the forces on ad and bc normal to δs_2

$$= 2\left(N_c\ \delta s_2 \sin\frac{\delta\phi_1}{2}\right) = N_c\ \delta s_2 \frac{\delta s_1}{R}$$

Summing these two components and equating them to the pressure force on the element:

$$N_m \, \delta s_1 \frac{\delta s_2}{r} + N_c \, \delta s_2 \frac{\delta s_1}{R} = p \, \delta s_1 \, \delta s_2$$

or

$$p = \frac{N_m}{r} + \frac{N_c}{R} \qquad (6)$$

This is the relationship between the direct tensions per unit length in a doubly curved membrane subject to a pressure. Alone, it is not sufficient for calculating N_m and N_c, knowing p, r and R.

To provide the additional information required, use must be made of another important and fundamental dimension of a toroid : the radius to the point of maximum width, M, shown as ρ_m in figure 4.2.

Consider the ring of the toroid bounded by the circumferential lines passing through M with radius ρ_m, and through P with radius ρ. The force on this ring in the axial direction, F_p, is given by:

$$F_p = \pi p \, (\rho^2 - \rho_m{}^2)$$

and it is balanced by the meridional tension around the boundary through P because the tension at M acts in the radial direction and has no component to oppose F_p. Thus:

$$F_p = 2\pi p \, N_m \sin \theta = \pi p \, (\rho^2 - \rho_m{}^2)$$

or

$$p = \frac{2\rho \, N_m \sin \theta}{\rho^2 - \rho_m{}^2} \qquad (7)$$

Given the geometry of a toroid, equations (6) and (7) allow the determination of the principal tensions per unit length at all points on its surface.

IV.2.3 Definition of Meridional Profiles

A number of approaches to defining, mathematically, the meridian of a fabricless, pneumatic tyre were developed in order to investigate the suitability of various profiles for containing the inflation pressure and meeting other mechanical requirements. The first two are based upon geometrical considerations, while the third and fourth use the analogy of a conventional cord-reinforced cross-biassed tyre and related constructions. However in all cases, it was stipulated that there should be no step changes in either slope or curvature around the meridians. The first of these criteria is self evident, while the second is the direct consequence of equation (6) and precludes the use of adjacent circular arcs, a common engineering practice for representing complex curves. Equation (6) relates the membrane tensions to the inflation pressure and if, at some point, there is an abrupt change in curvature, there will be a likewise change in tension. This would cause the carcass of the tyre to change shape until the tensions at the point were equalised and this would introduce additional, unnecessary strains into the structure.

IV.2.3.1 Circular meridional profile

The most simple meridional profile for a toroid is circular with radius r as shown in figure 4.4. If the toroid is positioned relative to its axis so that its centre and point of maximum width (M) are distance ρ_m, then the radius to some point P with meridional angle θ is:

$$\rho = \rho_m + r.\sin\theta$$

Equating the forces in the axial direction on the ring of the toroid bounded by circumferential lines through P and M, as explained in IV.2.2.

$$\pi p \left((\rho_m + r.\sin\theta)^2 - \rho_m^2\right) = 2\pi \left(\rho_m + r.\sin\theta\right) N_m \sin\theta$$

which gives the meridional tension per unit length at P:

$$N_m = \frac{pr\left(2\rho_m + r.\sin\theta\right)}{2\left(\rho_m + r.\sin\theta\right)} \qquad (8)$$

where p is the inflation pressure.

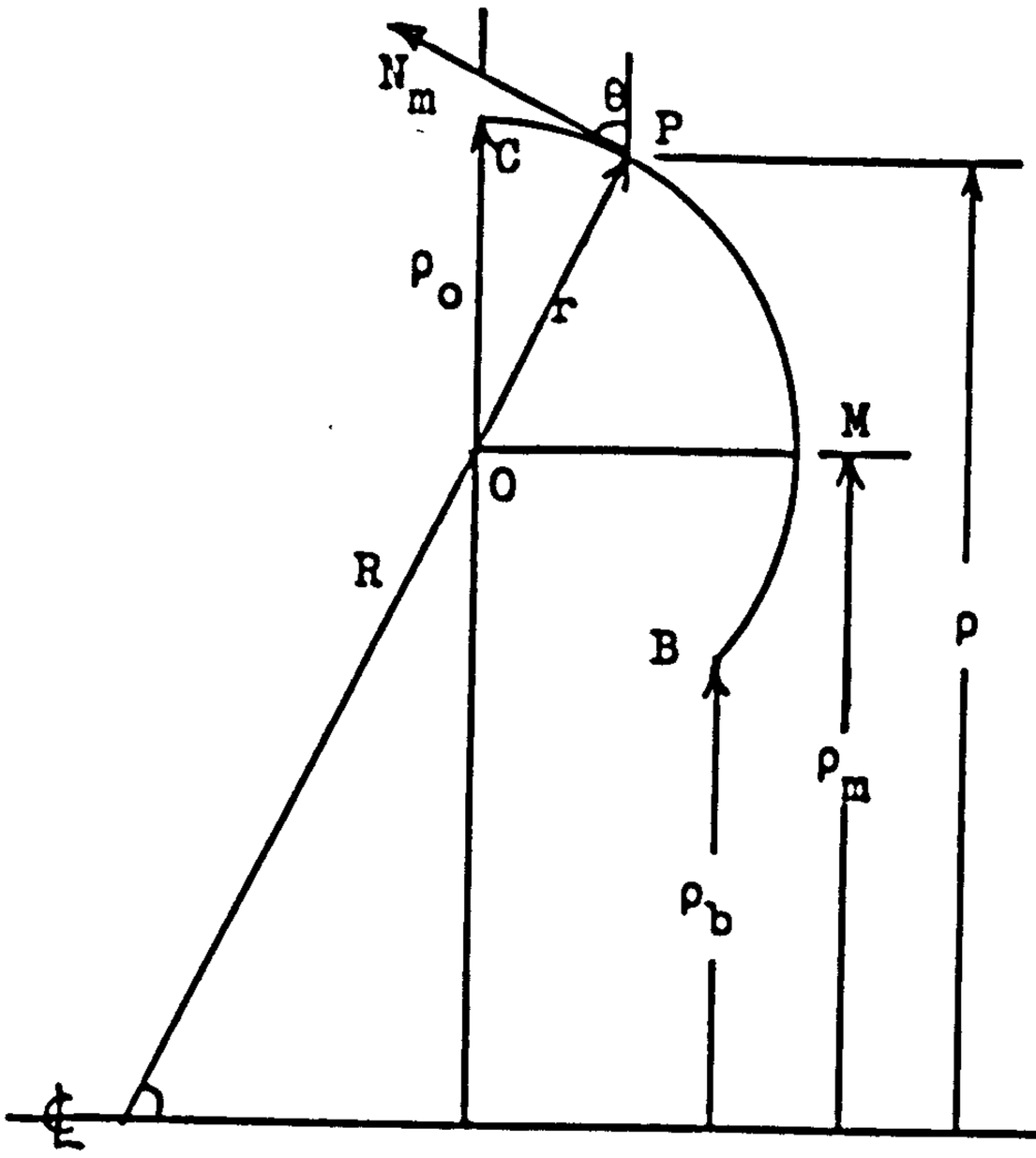

Figure 4.4

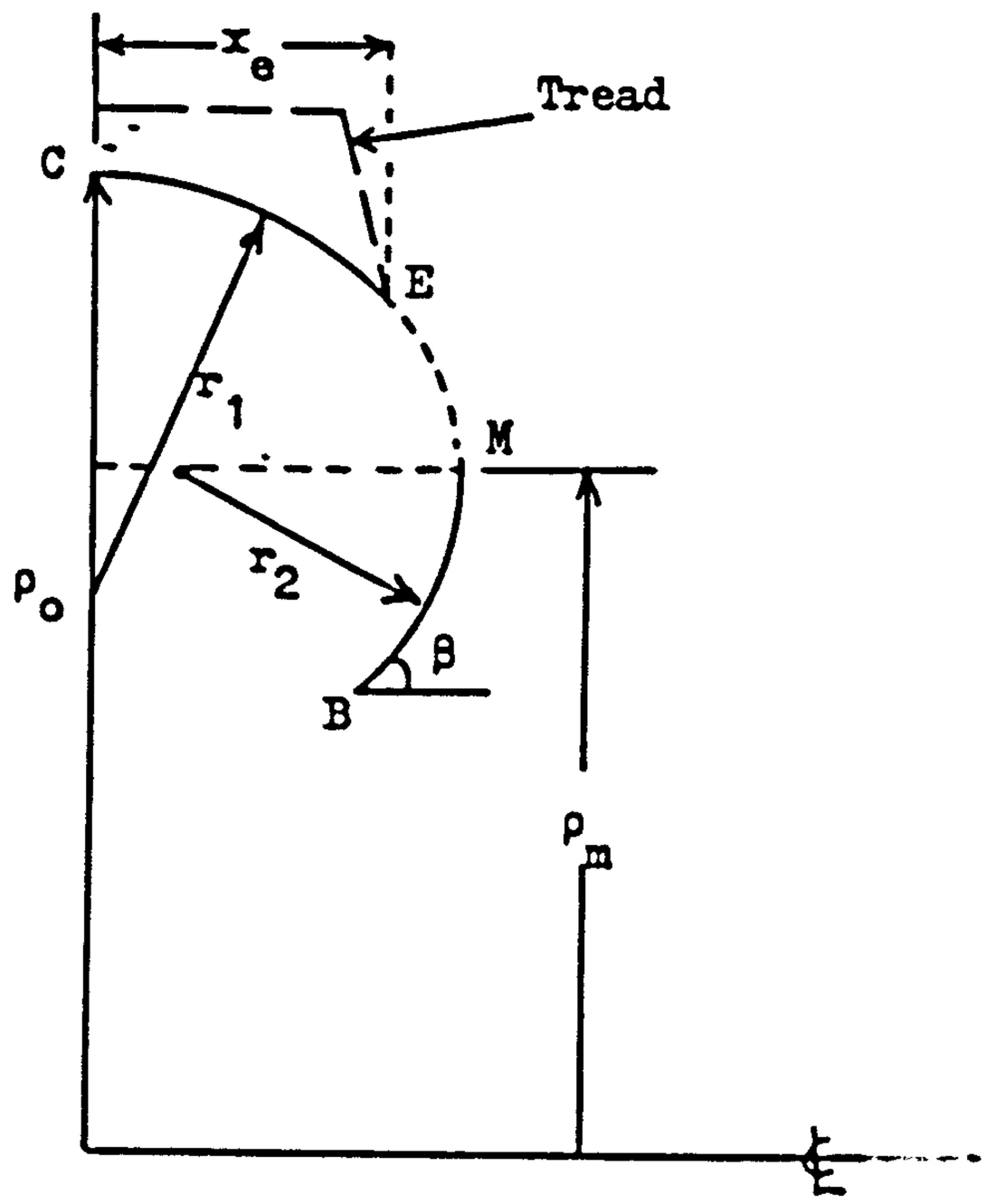

Figure 4.5

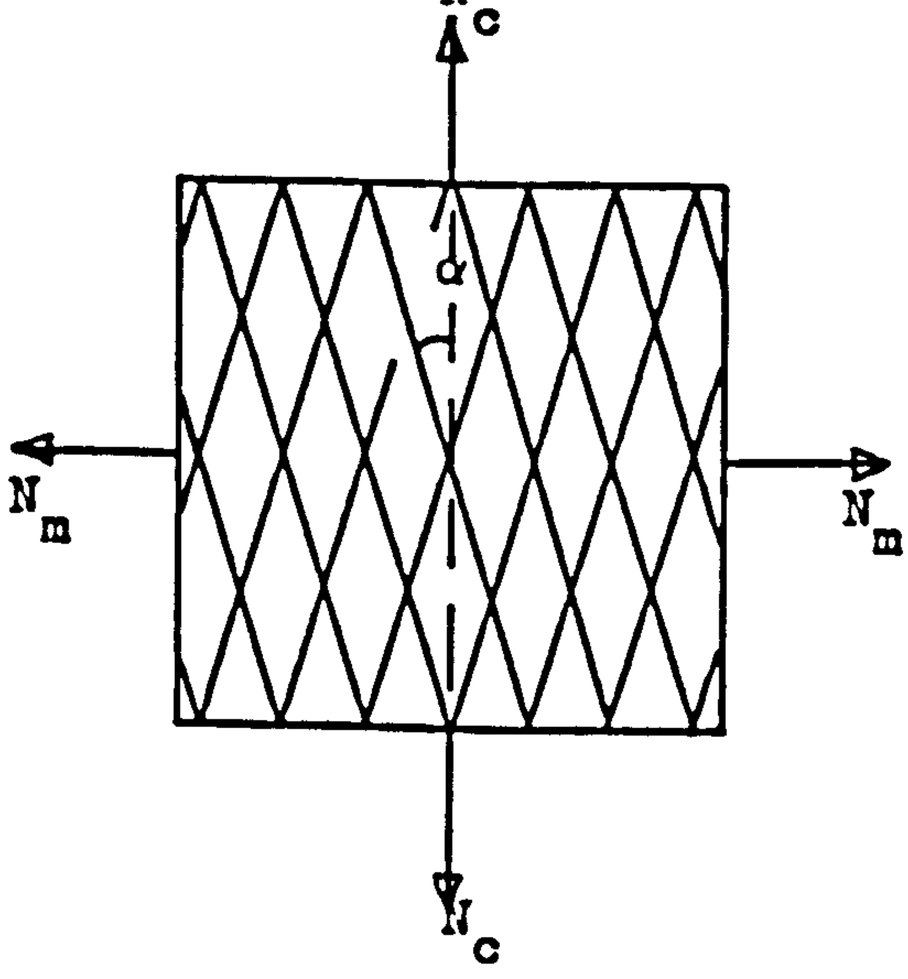

Figure 4.8

Now the circumferential radius of curvature at P is:

$$R = r + \rho_m / \sin \theta \qquad (8)$$

and substituting for N_m and R in equation (6) gives the circumferential tension per unit length:

$$N_c = \frac{pr}{2} \qquad (9)$$

Equation (9) shows that N_c is constant around the profile and therefore constant over the entire surface of the toroid because of its axisymmetry. The meridional tension, however, is a function of the meridional angle, equation (8), and to indicate the variation to be found, approximate mid-wall dimensions based upon those of the small cross-biassed tyre, size 5.10-10, were used:

radius to crown 240 mm;
section width 130 mm;
radius to bead 130 mm.

With reference to figure 4.4, these data give:

$r = 65$ mm; $\rho_m = 175$ mm; $\rho_b = 130$ mm; ($\rho_o = 240$ mm)

where ρ_b is the radius to the terminating point of the toroid which, for a conventional tyre, would be just outward of the bead wire.

At $\rho = \rho_b$, the meridional angle (θ) is approximately -45°.

For an inflation pressure of 200 kPa, table III lists the meridional and circumferential tensions per unit length from the crown, where $\theta = 90^\circ$, to beyond the terminating radius, $\theta = -50^\circ$.

Table III

Tensions/Unit Length in Circular Section Toroid

Meridional Angle (θ, °)	Meridional Tension (N_m, kN/m)	Circumferential Tension (N_c, kN/m)
90	11.24	6.5
70	11.32	6.5
50	11.56	6.5
30	11.98	6.5
10	12.61	6.5
-10	13.45	6.5
-30	14.48	6.5
-50	15.59	6.5

Now to limit the growth of a tyre due to the inflation pressure, and thus limit the strains, the product of the Young's modulus of the carcass material and the wall thickness must be sufficiently high at all points around the section. From table III, it may be seen that for a homogeneous construction the wall thickness should be a minimum at the crown and a maximum at the bead, the difference being about 28%. If a uniform wall thickness were employed, it would need to be sufficient for the bead region and therefore excessive at the crown, thus using unnecessary material. Moreover, as explained in chapter III, a tyre's carcass should be relatively stiff below the tread to enhance cornering power but flexible in the sidewalls. The fabricless tyre with a circular section reverses these conditions. Also it should be noted from table III that the tensions N_m and N_c are in the ratio of about 2 to 1 and this has implications to be discussed later in the chapter.

IV.2.3.2 Meridional profile from combined arcs

From the examination of the consequences of a circular meridional profile, it may be inferred that it could be advantageous to use arcs of different radii for the region of the carcass below the tread and for the sidewalls, the former being greater than the latter to give relative stiffness and flexibility respectively. However, as stated in IV.2.3, there must be no abrupt change in curvature when passing from one region to the other. Consequently the following geometrical construction was developed.

With reference to figure 4.5, the radii to the crown (C), ρ_o, and to the point of maximum width (M), ρ_m, are first chosen. The meridional radius of curvature of the carcass below the tread, r_1, is then defined and an arc CE constructed to a point E where the half width is x_e. An elliptical arc is then fitted between E and M such that it has the same slope and curvature as the circular arc at E and a tangent normal to the axis at M. By this means, the half width of the profile at M is calculated, together with the meridional radius of curvature at this point, r_2. Finally, a second circular arc with radius r_2 is drawn from M to the terminating point B. The latter may be defined by its radial distance from the axis, ρ_b as shown in figure 4.4, or by the angle β in figure 4.5. The second definition was used.

Altogether, this method of defining the meridional profile of a fabricless tyre requires five parameters:

ρ_o, the radius to the crown;
ρ_m, the radius to the point of maximum width;
r_1, the meridional radius of curvature at the crown;
x_e, the half width of the carcass below the tread;
and β , the terminating angle adjacent to the bead.

The derivation of the equation for the elliptical arc EM is given in appendix II.

To determine the geometry of a profile defined by combined arcs and the tensions induced in it by some inflation pressure, a simple computer program (FTGPR) was written and is listed in appendix III. The calculations

are divided into four parts:

(i) the profile of the tread region, a circular arc represented by 8 equally separated points;

(ii) the upper sidewall, which is elliptical and calls the subroutine CONIC (and SOLV) to fit the arc and to calculate the co-ordinates of 15 points arranged at equal increments of radius from the tyre's axis;

(iii) the lower sidewall, which is circular and represented by 7 equally spaced points;

and (iv) the determination of the meridional and circumferential tensions/unit length.

To illustrate this program, four tyre profiles were examined using the following data:

radius to crown	(ρ_o)	= 240 mm
width of tread region	(x_e)	= 50 mm
radius to maximum width	(ρ_m)	= 175 mm
terminating angle	(β)	= 40 ^{o}
meridional radius of tread region	(r_1)	= 65, 75, 85 and 95 mm
inflation pressure	(p)	= 200 kPa

Thus only one of the five defining parameters was varied.

The profiles of the four tyres are shown in figure 4.6, where it may be seen that the section width increases with the meridional radius of curvature below the tread. There is also a small increase in the terminating radius. The aspect ratios of the tyres, defined as the section height divided by the section width and expressed as a percentage, are:

profile no. 1 (r_1 = 65 mm)	88 %
2 (r_1 = 75 mm)	75 %
3 (r_1 = 85 mm)	67 %
4 (r_1 = 95 mm)	61 %

Thus the method allows tyres of any desired overall dimensions to be

Figure 4.6

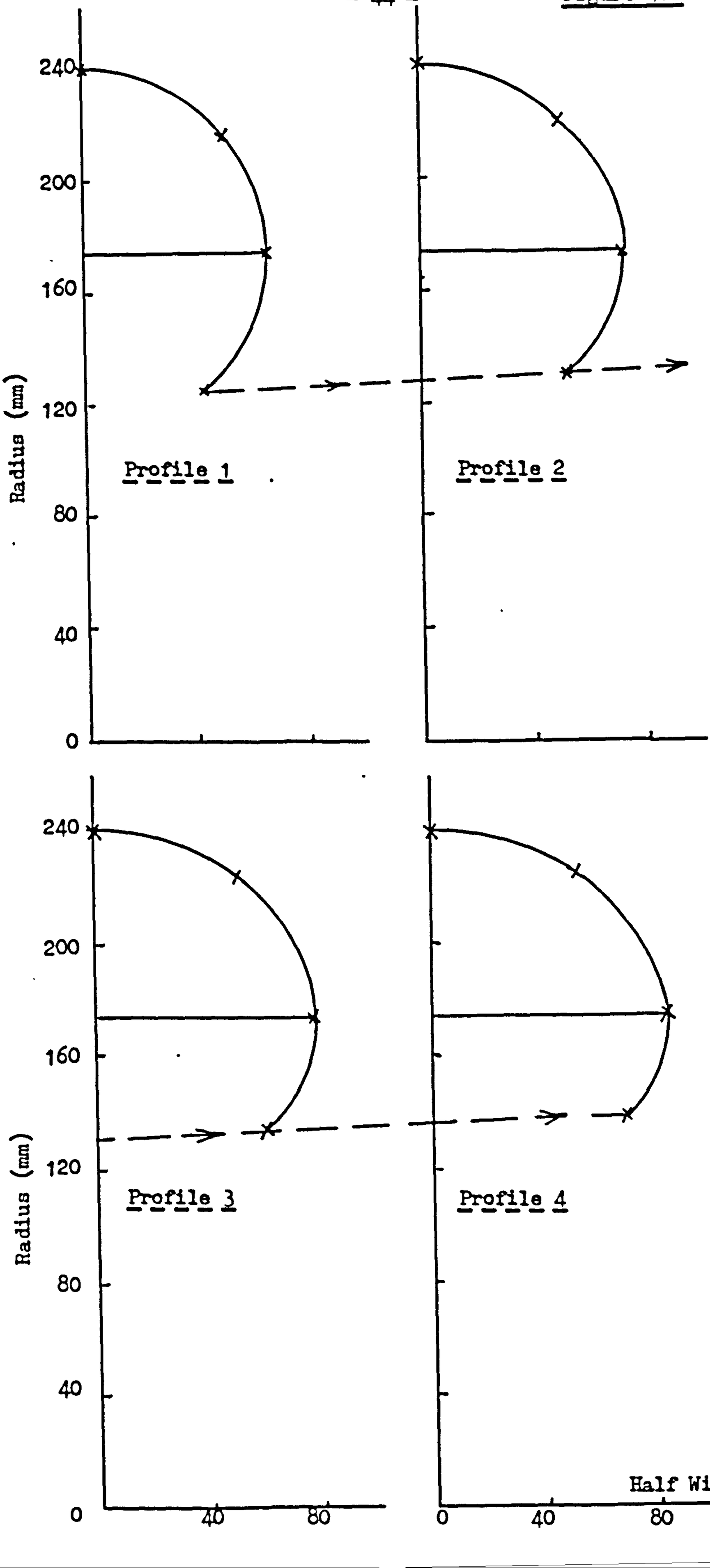
240
200
160
120
80
40
0
Radius (mm)
Profile 1
Profile 2
Profile 3
Profile 4
40
80
Half Width (mm)

defined, from the circular section of profile number 1 (noting that $\rho_o - \rho_m = 65$ mm $= r_1$) to the low profile of number 4. However, as emphasised before, a profile must be judged by the tensions induced in it by the inflation pressure.

Typical output from the computer program FTGPR is included in appendix III (for profile no. 2). In addition to the geometrical data: x, y co-ordinates (X, Y), meridional angle (A = θ) and the principal radii of curvature (RCM = r, RCC = R); the tensions per unit length in kN/m are listed (SM = N_m, SC = N_c). These are plotted against meridional angle in figure 4.7, where 90^o corresponds to the crown and -50^o to the terminating point.

As discussed before, the circular profile, number 1, has fairly uniform levels of N_m and N_c which are in the ratio of about 2 : 1, the circumferential tension being the lesser. As the aspect ratio is reduced, profiles 2 to 4, a clear pattern emerges for this tension, although the meridional tension remains fairly uniform and with approximately the same magnitude. At the crown, N_c exceeds N_m by an amount which increases as the aspect ratio decreases. It then rises to a peak at the edge of the tread region (x_e) before falling to reach a fairly constant level of about 5 kN/m, half the magnitude of the meridional tension, in the lower sidewall regions of the tyres.

In terms of inducing fairly uniform tensions throughout the carcass of a fabricless tyre, it may be concluded that none of those defined by combined arcs is acceptable. Moreover, the lower the profile, the greater is the variation and the higher is the ratio of the two principal stresses in the crown region of the tyres. However, compared to the circular profile, any thickness variations introduced to cope with the tensions can be arranged to place greater stiffness in the crown region where it is required.

Tension/
Unit Length
(kN/m)

Profile 1

Profile 2

Profile 3

Profile 4

N_m

N_o

Meridional Angle (°)

Figure 4.7

IV.2.3.3 Profile based on the analogue of a cross-biassed construction

The third design method considered for fabricless tyres is based upon the well established theory for the equilibrium shape of cross-biassed tyres (refs.12 and 13). In this it is assumed the tensions induced in the carcass by the inflation pressure are entirely taken by the reinforcing cords. Consequently there is a unique relationship between the principal tensions per unit length and the bias angle.

Let figure 4.8 represent a pair of cross-biassed plies at some point in a tyre. Each ply consists of parallel equi-spaced cords in a rubber matrix and the bias angle, α, is measured relative to the circumferential direction. If the element shown is a unit square, T is the cord tension and n is the end count (number of cords per unit length normal to the cords), then the principal tensions per unit length are given by:

$$N_c = T \cos \alpha . n \cos \alpha = nT \cos^2 \alpha$$

$$\text{and } N_m = T \sin \alpha . n \sin \alpha = nT \sin^2 \alpha$$

$$\text{thus } \frac{N_m}{N_c} = \tan^2 \alpha \qquad (10)$$

Now it has already been established that the relationship between the inflation pressure, p, and the principal tensions/unit length is:

$$p = \frac{N_m}{r} + \frac{N_c}{R} \qquad (6)$$

where r and R are the principal radii of curvature; and that the meridional angle, θ, may be introduced through equation (7):

$$p = \frac{2\rho N_m \sin \theta}{\rho^2 - \rho_m^2} \qquad (7)$$

However, to complete the information to develop the theory, it is necessary to define how the bias angle varies around the meridian.

In chapter I, it was explained that a cross-biassed tyre is built in the form of a cylinder or drum before being shaped into a toroid. In the theory, it is assumed that, during this shaping process, the cords do not

slip over one another but trellis. Figure 4.9 shows an axial view of a shaped tyre with representative cords drawn within a sector.

Now the number of cord intersections in a complete circumference at any radius ρ is constant and equal to N, where N is the total number of cords in a ply. Thus, with reference to figure 4.9:

$$ab = 2\pi\rho_1/N$$

$$cd = 2\pi\rho_2/N \quad \text{etc.} \tag{11}$$

Consequently, the angle subtended by any pair of adjacent intersections is given by:

$$\beta = \frac{2\pi\rho}{N\rho} = \frac{2\pi}{N}$$

so that intersections at different radii lie on radial lines, such as Oh and Oj in figure 4.9.

If α_1 and α_2 are the bias angles at radii ρ_1 and ρ_2, and if trellising occurs so that the meshes of the net formed by the biassed plies have sides of length s, then:

$$ab = 2s.\cos\alpha_1$$

$$cd = 2s.\cos\alpha_2 \tag{12}$$

Combining equations (11) and (12):

$$\frac{\cos\alpha_1}{\rho_1} = \frac{2\pi}{2Ns} \quad \text{and} \quad \frac{\cos\alpha_2}{\rho_2} = \frac{2\pi}{2Ns}$$

$$\text{Thus} \quad \frac{\cos\alpha_1}{\rho_1} = \frac{\cos\alpha_2}{\rho_2} = \text{etc.} \tag{13}$$

This is the well known cosine rule.

Equations (10), (6) and (7) form the basis of the theory developed, particularly in reference (13). It is shown that the meridional radius

Figure 4.9

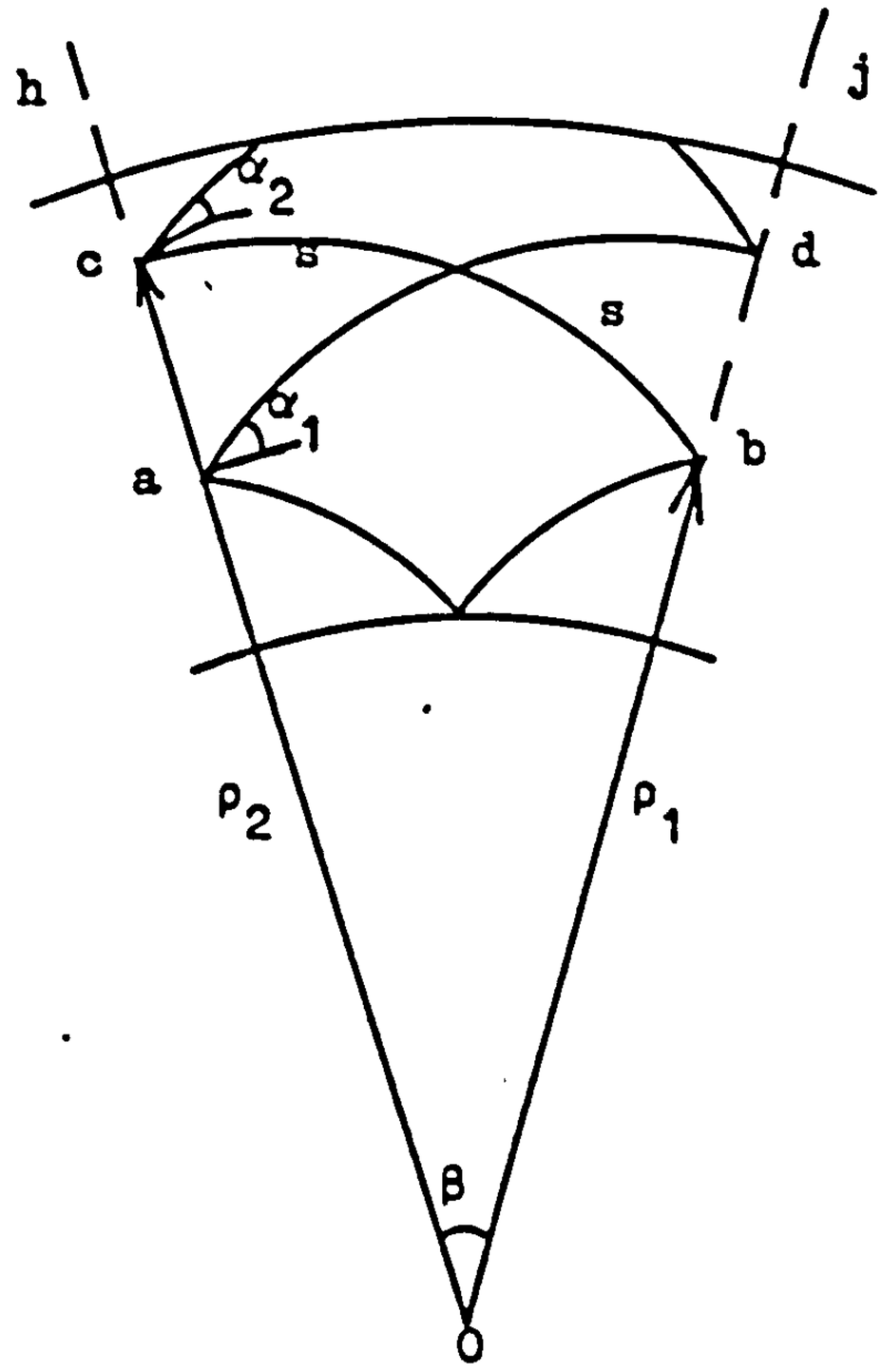

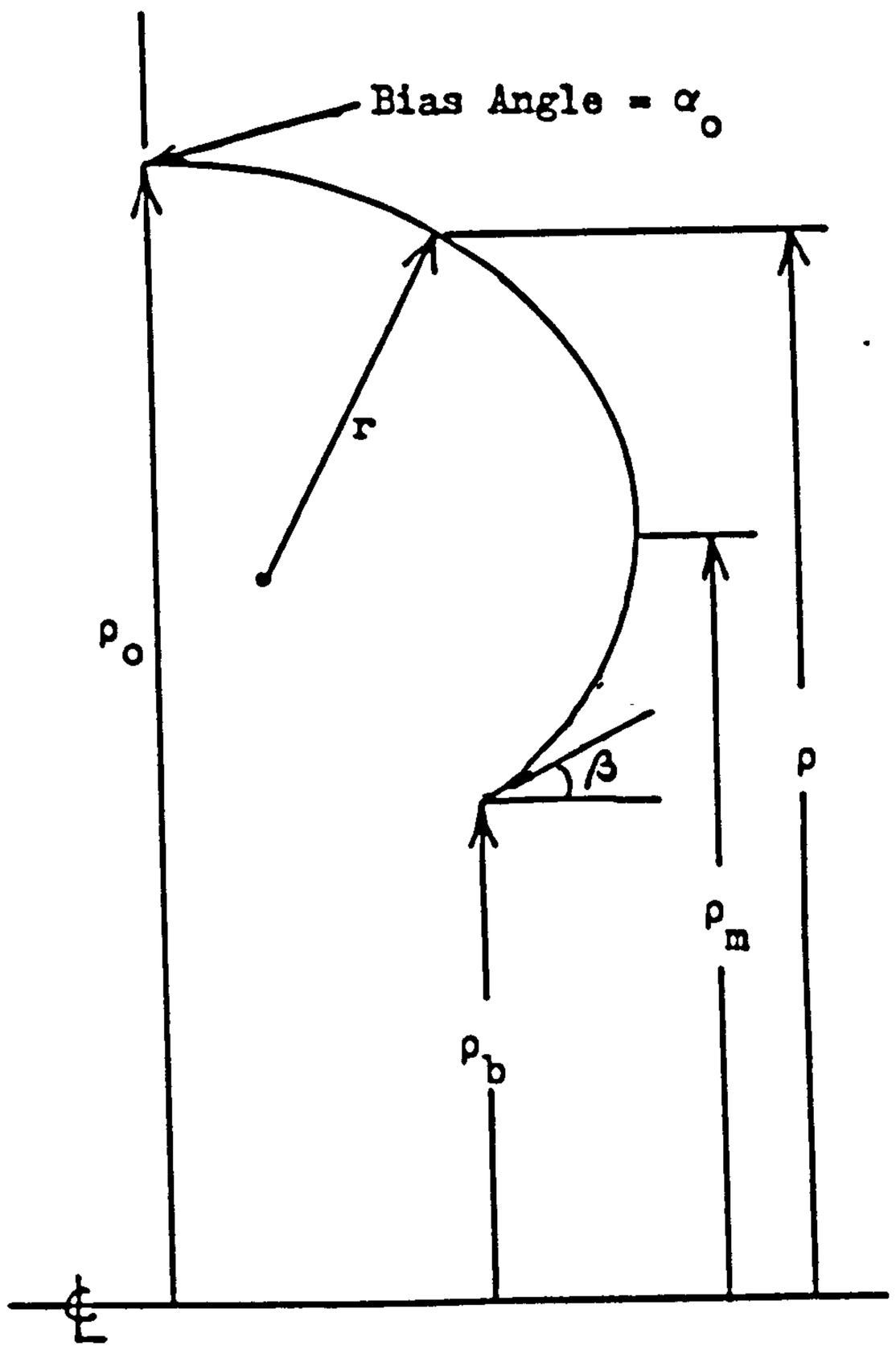

Figure 4.10

of curvature, r, is:

$$r = \frac{B}{dA/d\rho} \qquad (14)$$

where $B = \rho_m^2 - \rho_o^2$

and $A = (\rho_m^2 - \rho^2) \exp \int_{\rho}^{\rho_o} \frac{\cot^2 \alpha}{\rho} d\rho$

For drum built cross-biassed tyres, the integral may be evaluated using equation (13) to give:

$$r = \frac{\rho_o \sin \alpha_o (\rho_o^2 - \rho_m^2) (\rho_o^2 - \rho^2 \cos^2 \alpha_o)^{\frac{1}{2}}}{\rho[2\rho_o^2 - \cos^2 \alpha_o (3\rho^2 - \rho_m^2)]} \qquad (15)$$

Equation (15) expresses the meridional radius of curvature, r, for any value of the radius from the axis, ρ in figure 4.10, in terms of:

ρ_o - the radius to the crown

ρ_m - the radius to the point of maximum width

and α_o - the bias angle at the crown.

Unfortunately, it is not possible to derive a similar expression for tyre width at any radius because an integral which cannot be solved analytically results. Nevertheless, equation (15) may be used for the same purpose by utilising a geometrical construction. This is the basis of the computer program BTPR, listed in appendix IV.

If for some chosen profile, ρ_o, ρ_m and α_o are defined, the construction starts at the crown point where $\rho = \rho_o$. From equation (15), the meridional radius of curvature at that point (r_o) may be calculated. With reference to figure 4.11, a short arc CC_1 may then be drawn whose included angle decreases the meridional angle by δ. With axes x and y whose origin is at C, the co-ordinate of point C_1 are:

$$x_1 = r_o \sin \delta$$

$$y_1 = r_o - r_o \cos \delta \qquad (16a)$$

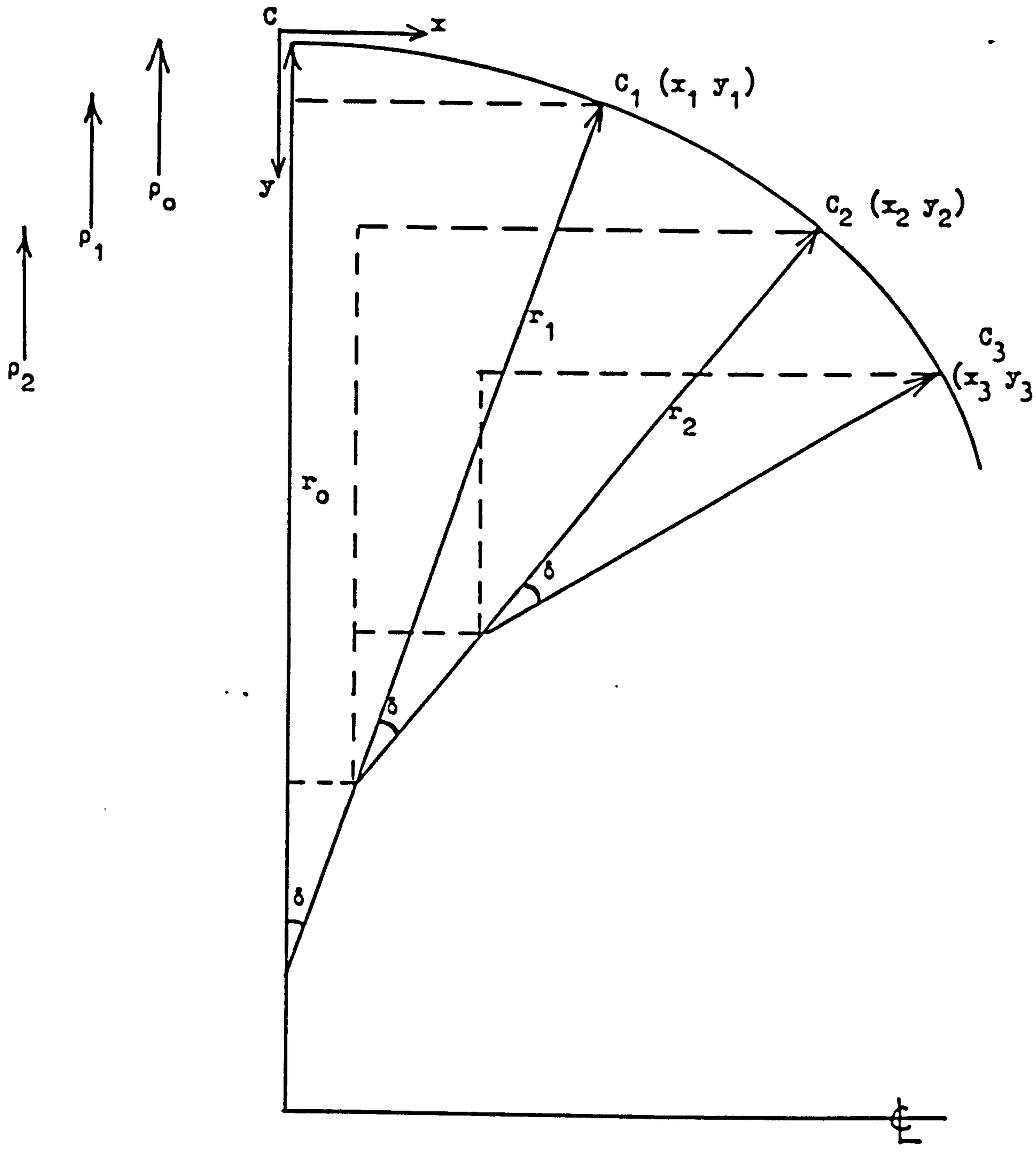
C
x
y
C_1 (x_1 y_1)
C_2 (x_2 y_2)
C_3
(x_3 y_3)
r_1
r_2
r_o
ρ_o
ρ_1
ρ_2
δ
δ
δ
$\mathcal{E}$

Figure 4.11

The radius to point C_1 is now known:

$$\rho_1 = \rho_o - y_1$$

so that, using equation (15), a new meridional radius of curvature may be calculated, r_1. A second arc is then drawn to C_2 with included angle δ, to give:

$$x_2 = r_1 \sin 2\delta + (r_o - r_1) \sin \delta$$

$$y_2 = r_o - [r_1 \cos 2\delta + (r_o - r_1) \cos \delta] \qquad (16b)$$

and $\rho_2 = \rho_o - y_2$

Following this procedure, the co-ordinates of the third point C_3 are:

$$x_3 = r_2 \sin 3\delta + (r_1 - r_2) \sin 2\delta + (r_o - r_1) \sin \delta$$

$$y_3 = r_o - [r_2 \cos 3\delta + (r_1 - r_2) \cos 2\delta + (r_o - r_1) \cos \delta] \qquad (16c)$$

with $\rho_3 = \rho_o - y_3$

It can be seen from equations (16) that a sequence of calculations is made which, for some point C_n, are:

$$x_{n+1} = r_n \sin n\delta + \sum_{m=n}^{o} (r_{m-1} - r_m) \sin (m - 1)\,\delta$$

$$y_{n+1} = r_o - [r_n \cos n\delta + \sum_{m=n}^{o} (r_{m-1} - r_m) \cos (m - 1)\,\delta] \qquad (17)$$

Expressions of this form are ideal for a computer program and are implemented in the subroutine PROF, called by program BTPR (appendix IV).

To determine a suitable value for the included angle (δ), trials were run with an earlier version of BTPR. With $\delta = 5^o$ and 2.5^o, the differences between the calculated co-ordinates, x and y, were less than 0.5%. Consequently, $\delta = 5^o$ was used for the final program.

The theory and its implementation so far may be summarised as follows. A cross-biassed tyre profile is defined by three parameters: ρ_o, the radius to the crown; ρ_m, the radius to the point of maximum width; and α_o, the bias angle at the crown. In addition, the terminating point must be specified by either ρ_b or β, figure 4.10. However, these four parameters are not ideal because, when designing a fabricless tyre, a particular section width will be required. Moreover, there is no guarantee that the meridional angle at the specified terminating radius will be acceptable, or vice versa. Consequently, it was decided to replace the four parameters:

$$\rho_o,\ \rho_m,\ \alpha_o \text{ and } \rho_b/\beta$$

by: ρ_o, w, ρ_b and β, where w is the profile width.

These specify a profile in a way which is more useful for the purpose. Otherwise, design would be very much more one of trial and error.

The method by which program BTPR arrives at a required profile uses the following algorithm.

(i) In addition to the parameters: ρ_o, w, ρ_b and w; an estimate or guess for ρ_m is input together with upper and lower limits of the crown bias angle.

(ii) Using the two extreme values of bias angle in turn, the tyre profile from the crown to the point of maximum width is determined. If the width is not within 0.1 mm of the required value, w, ρ_m is adjusted by simple proportion:

$$\rho_m' = \rho_o - \frac{w\ (\rho_o - \rho_m)}{w'}$$

where w' is the calculated width and ρ_m' is the new value for ρ_m. The calculations are then repeated.

(iii) Having obtained upper profiles with the required width, the lower profiles are determined to the point where the terminating angle is β. Using the two bias angles, two values for the terminating radius, ρ_b, are obtained.

(iv) The values of ρ_b are compared to the required value and a third bias angle calculated from:

$$\alpha_3 = \alpha_1 + \frac{(\rho_b - \rho_b')\ (\alpha_2 - \alpha_1)}{(\rho_b'' - \rho_b)}$$

where $\alpha_{1,\ 2,\ 3}$ are the values of α_o and ρ_b', ρ_b'' are the two calculated values of the terminating radius.

(v) The complete profile is now redetermined using the new bias angle and the calculated value of ρ_b compared to the required value. If it is within 0.1 mm the program is terminated. Otherwise α_3 is substituted for α_1 or α_2, depending upon the value of ρ_b.

This procedure, using a double iteration, works successfully when the initial values for the crown bias angle encompass the final value. However, if this is not the case, a solution cannot be found and a simple test using ρ_b' and ρ_b'' terminates the program and outputs a message to the effect that the bias angle range is unacceptable.

Having calculated the required meridional profile, program BTPR then determines the principal tensions per unit length for each pair of co-ordinates. For this, equations (7) and (6) are used.

To illustrate program BTPR, the following data were input:

radius to crown	(ρ_o)	=	240 mm
section width	(w)	=	130, 150 and 170 mm
radius to terminating point	(ρ_b)	=	130 mm
terminating angle	(β)*	=	40 ^{o}
inflation pressure	(p)	=	200 kPa

(* the program requires the absolute value of the meridional angle at the terminating point, ie. 90 - β).

Thus three profiles were sought, differing only in section width, and their principal dimensions are listed in table IV. Section drawings are shown in figure 4.12, while a typical output from the program is included in appendix IV (profile 1B).

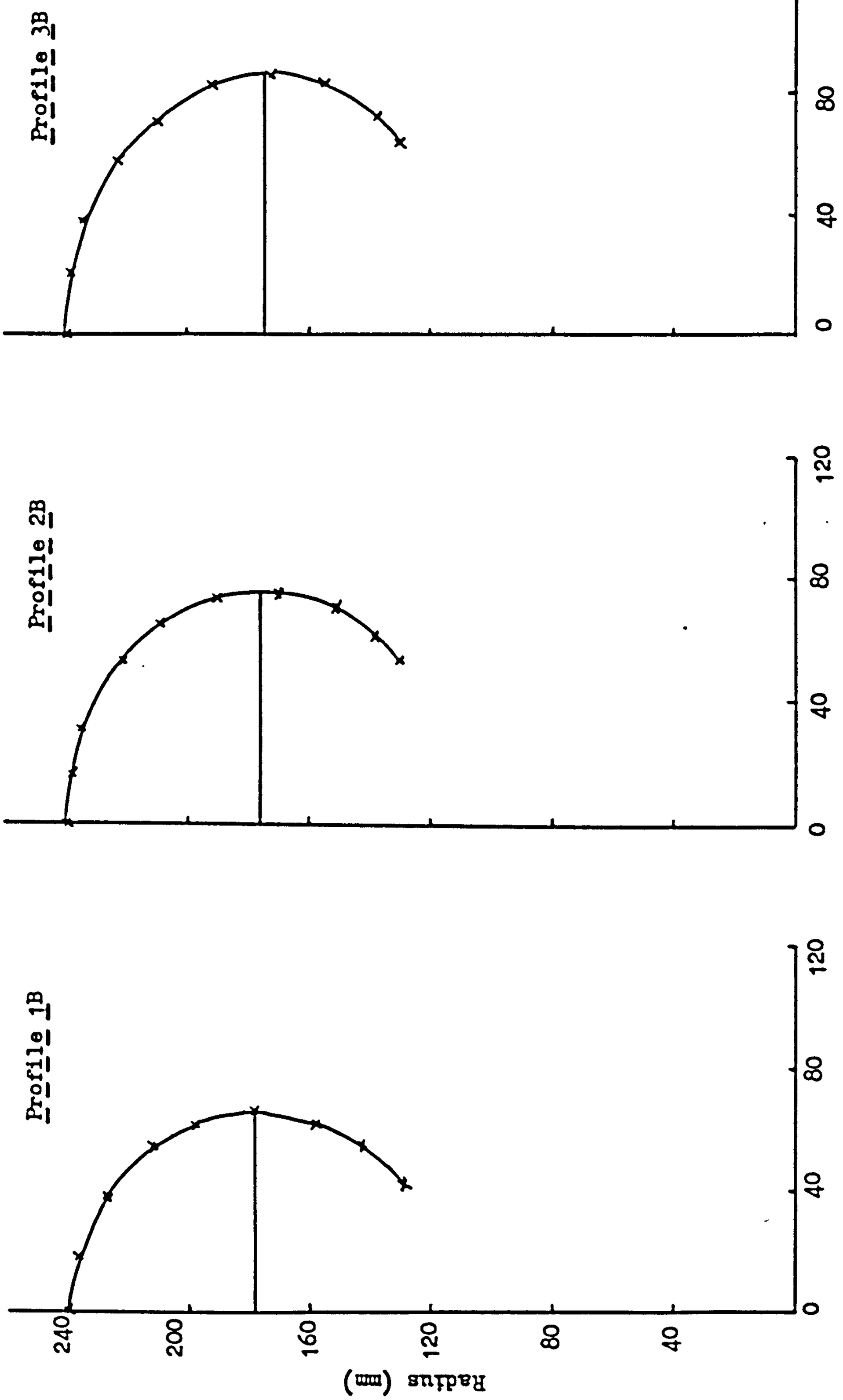
Profile 3B
Profile 2B
Profile 1B
Radius (mm)
Half Width (mm)
240
200
160
120
80
40
0
120
80
40
0
120
80
40
0

Figure 4.12

Table IV

Principal Dimensions of Cross-biassed Analogues

		Profile 1B	Profile 2B	Profile 3B
Bias angle at crown	(°)	45.01	38.35	34.67
Radius to crown	(mm)	240.0	240.0	240.0
Radius to max. width	(mm)	178.5	175.6	173.7
Section width	(mm)	130.0	150.2	170.1
Radius to term. point	(mm)	130.0	129.9	130.0
Width at term. point	(mm)	83.4	106.6	128.6
Aspect ratio	(%)	85	73	65

As the section width is increased, so that the aspect ratio decreases for these profiles of equal height, the required crown bias angle of the cross-biassed analogue decreases. The radius to the point of maximum width decreases slightly, by about 5 mm, while the width at the terminating point increases more than the section width (45.2 mm cf. 40 mm). The last dimension determines the size of wheel on which a tyre is mounted.

The principal tensions per unit length for the three profiles are shown in figure 4.13. It may be seen that there is a similar pattern to that exhibited by the profiles constructed from combined arcs. Thus, as the aspect ratio is decreased, the circumferential tension (N_c) at the crown increases rapidly but, in the lower sidewall, this tension is only a fraction of that in the meridional direction (N_m). However the changes in both tensions with meridional angle are smoother than those from the combined arcs (figure 4.13 cf. figure 4.7).

Text cut off in original

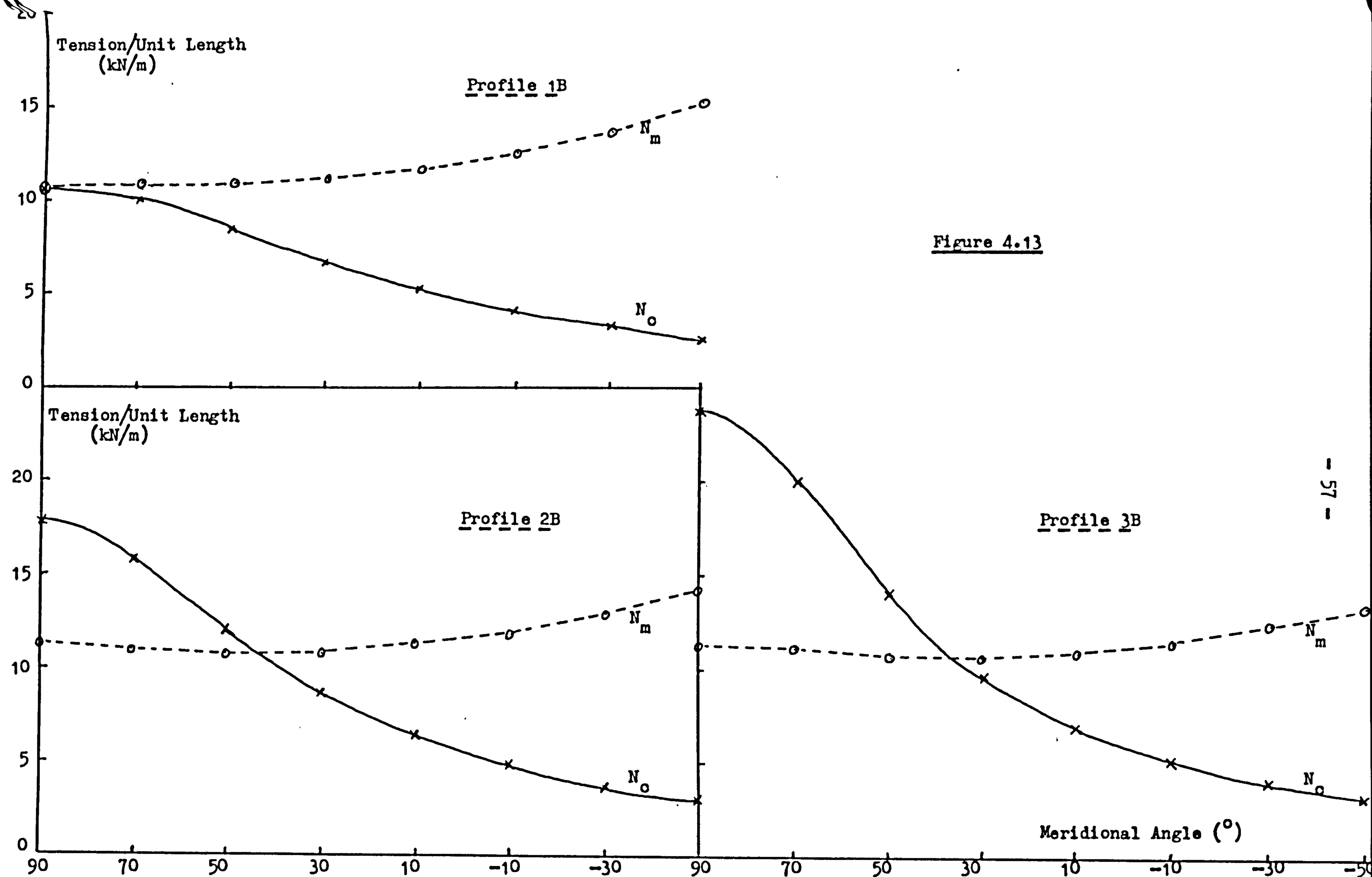
Tension/Unit Length
(kN/m)
Profile 1B
N_m
N_o
Tension/Unit Length
(kN/m)
Profile 2B
N_m
N_o
Profile 3B
N_m
N_o
Meridional Angle (°)
90
70
50
30
10
-10
-30
-50
0
5
10
15
20

Figure 4.13

IV.2.3.4 The constant bias angle analogue

In the preceeding section, the analogue of a cross-biassed construction was used to define meridional profiles and the cord path selected was that of a drum built tyre, the cosine rule. However, any cord path could have been chosen because the reinforced tyre is not going to be manufactured, it is only a mathematical convenience.

Another cord path of interest for designing fabricless tyres is one where the bias angle (α) is constant along all meridional and circumferential lines, in particular when $\alpha = 45^{\circ}$. For this case, from equation (6):

$$N_m = N_c$$

that is, the principal tensions per unit length are constant and equibiaxial over the entire surface of the toroid.

As noted in reference (3), $\alpha = 45^{\circ}$ corresponds to a surface of minimum stored energy and gives the shape of a toroidal soap bubble. Also stated is the possibility of obtaining an expression for the toroidal width as a function of the distance from the axis using elliptic functions, thus avoiding the geometrical construction method necessary for drum built tyres. However the latter method is equally applicable and, for ease of computer programming, was utilised in the research for any value of α.

Now, from equation (14), the meridional radius of curvature for any cord path is:

$$r = \frac{B}{dA/d\rho} \qquad (14)$$

$$\text{with } B = \rho_m^{\,2} - \rho_o^{\,2}$$

$$\text{and } A = (\rho_m - \rho^2)\ \exp \int_{p}^{p_o} \frac{\cot^2 \alpha}{\rho}\, d\rho$$

In fact, B is a constant, while the evaluation of A reflects the chosen cord path. For constant angle:

$$\text{put } C = \cot^2 \alpha$$

so that:

$$A = (\rho_m^2 - \rho^2) \exp \left[c \int_{\rho}^{\rho_o} \frac{1}{\rho} d\rho \right]$$

$$= (\rho_m^2 - \rho^2) (\rho_o/\rho)^c$$

Substituting in equation (14):

$$r = \frac{\rho_o^2 - \rho_m^2}{c\rho_m^c \rho_o^c/\rho^{c+1} + (2 - c)\rho_o^c/\rho^{c-1}} \qquad (18)$$

In appendix V, computer program FTCAPR is listed. It uses equation (18) in conjunction with the geometrical construction represented by equations (17). Again a double iterative algorithm is employed to obtain a required section width but, because the bias angle is fixed:

ρ_m is adjusted to give the required width;
but ρ_o is adjusted to give the required terminating radius (ρ_b).

To investigate the profiles which are obtained by this design method, the following sets of data were input to FTCAPR:

section width (w) = 130 mm with $\alpha = 55^\circ$, 45° and 35°
section width (w) = 130, 150 and 170 mm with $\alpha = 45^\circ$
radius to terminating point (ρ_b) = 130 mm
terminating angle (β) = 40°
inflation pressure (p) = 200 kPa

The profiles resulting from varying the bias angle for a constant width are shown in figure 4.14 and are seen to exhibit a reducing section height as the bias angle is decreased. In figure 4.15, different section widths are shown, all with a bias angle of 45°. Typical output from the program are included in appendix V, while the principal dimensions and tensions per unit length are listed in table V.

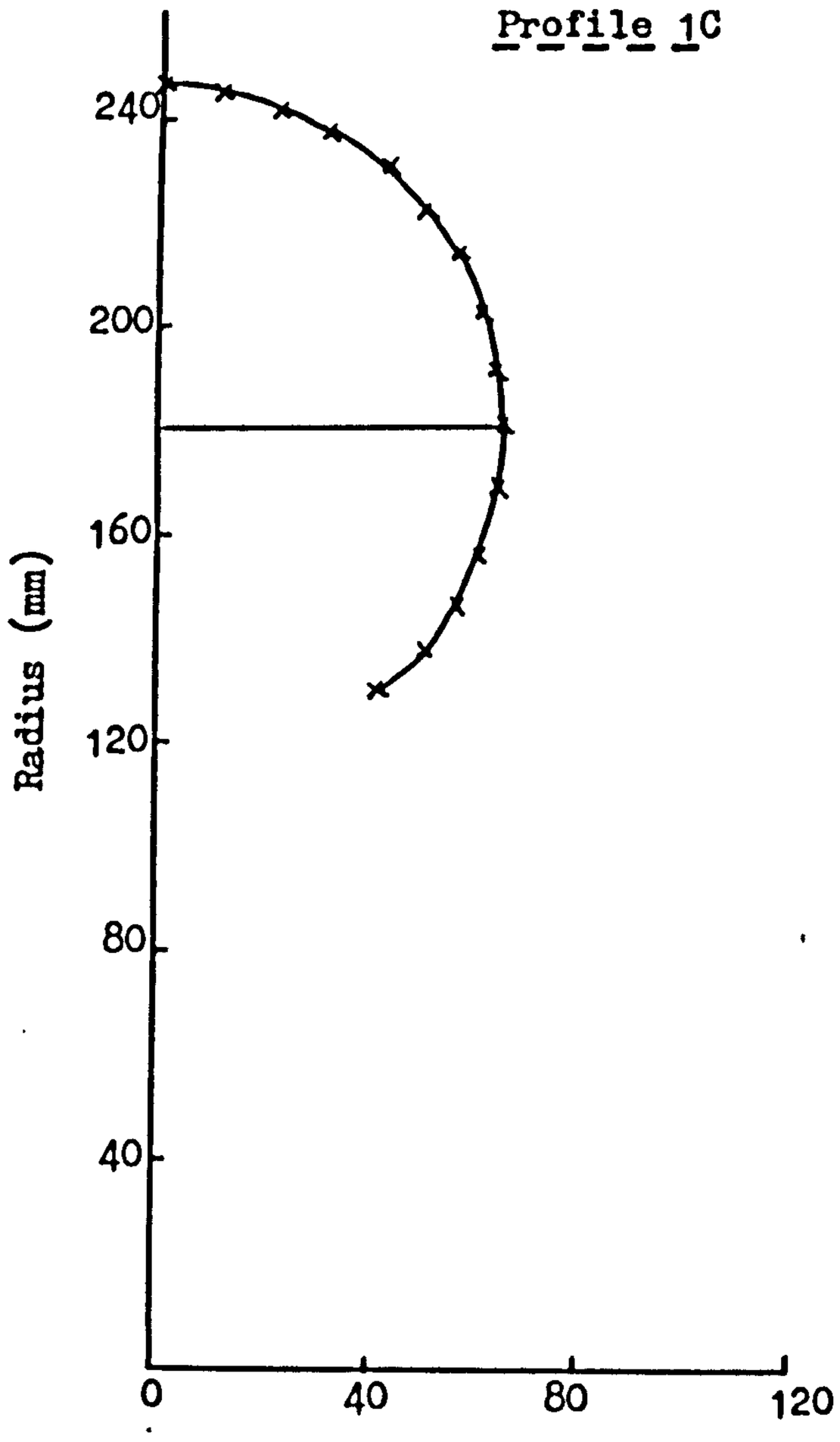
Profile 1C
240
200
160
120
80
40
Radius (mm)
0
40
80
120

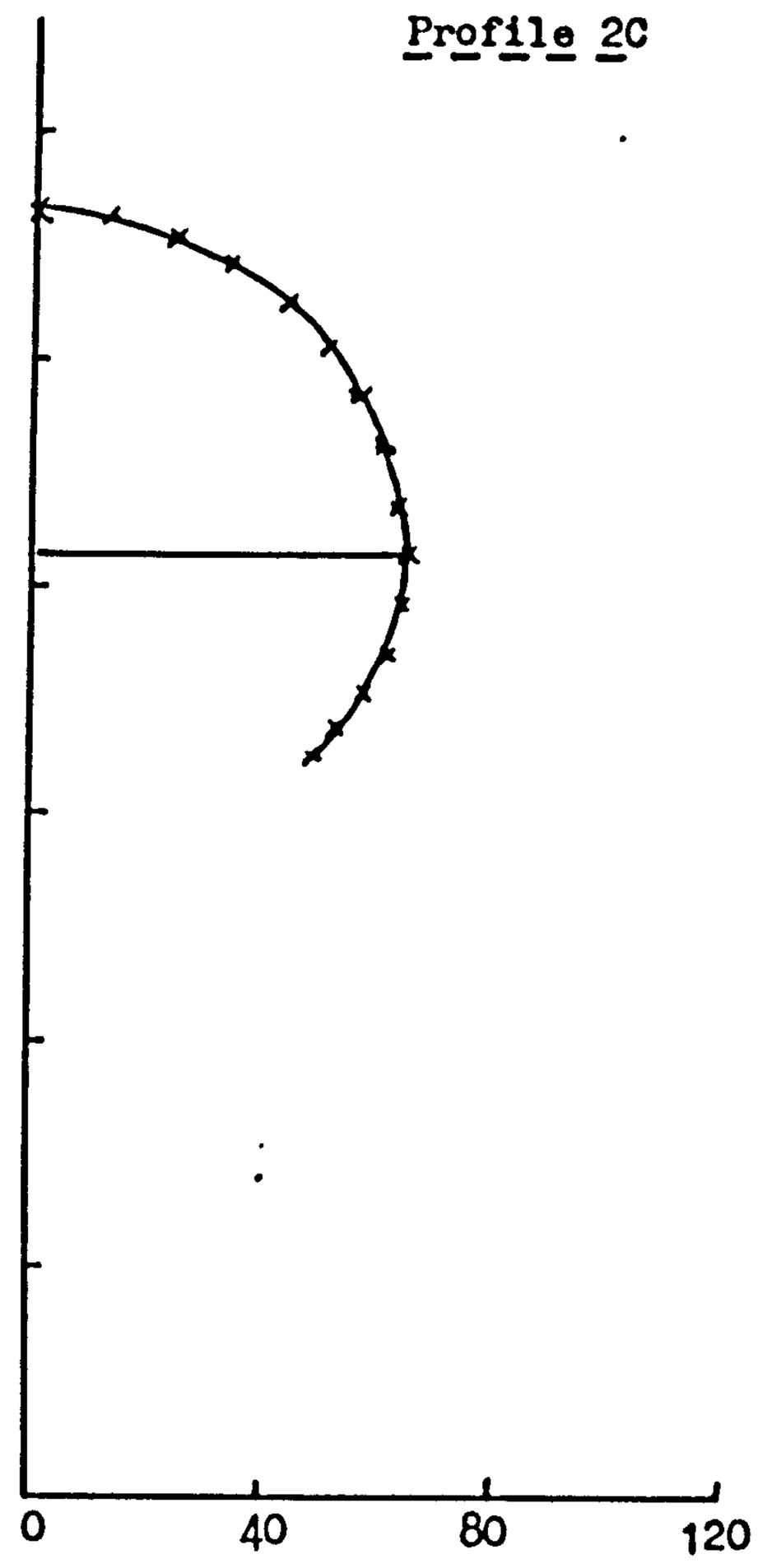
Profile 2C
0
40
80
120

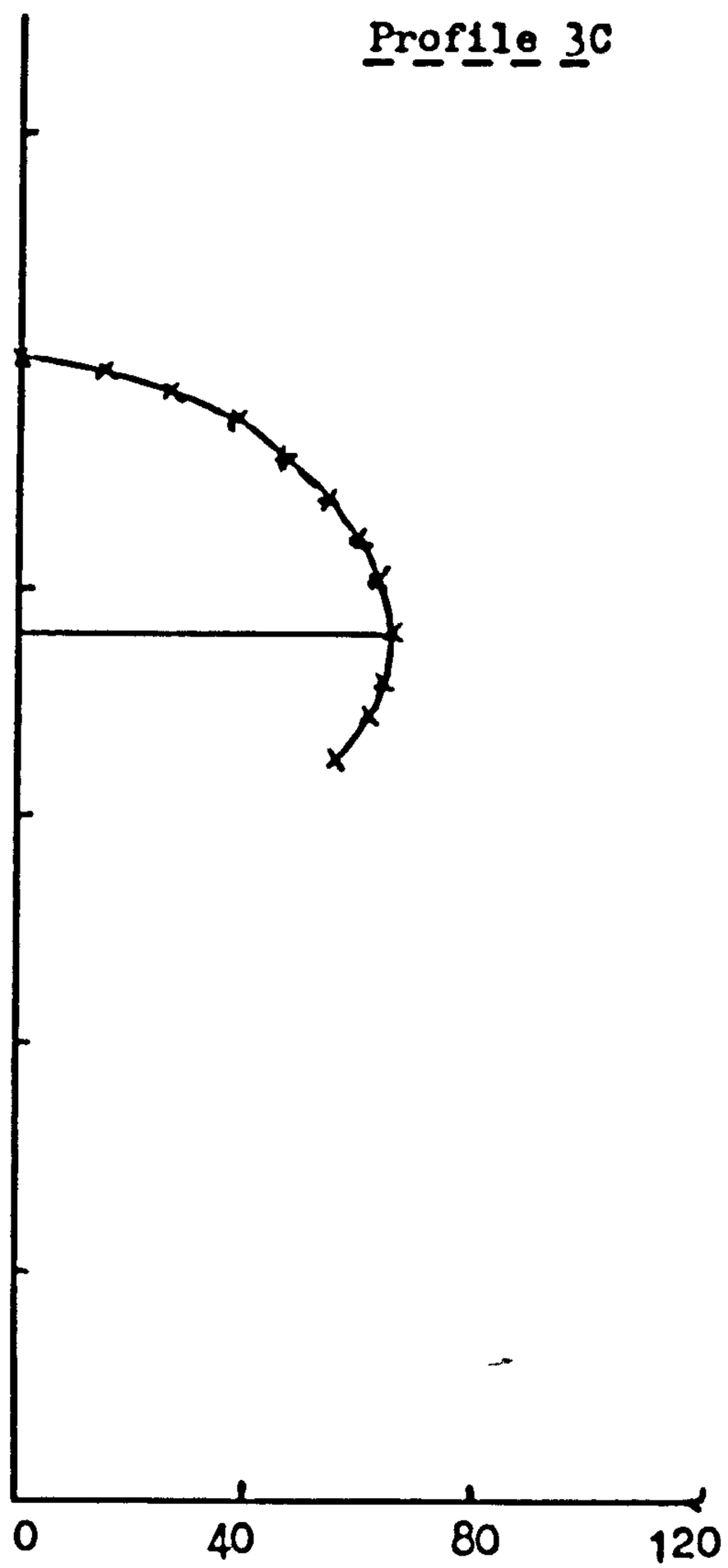
Profile 3C
0
40
80
120
Half Width (mm)

Figure 4.14

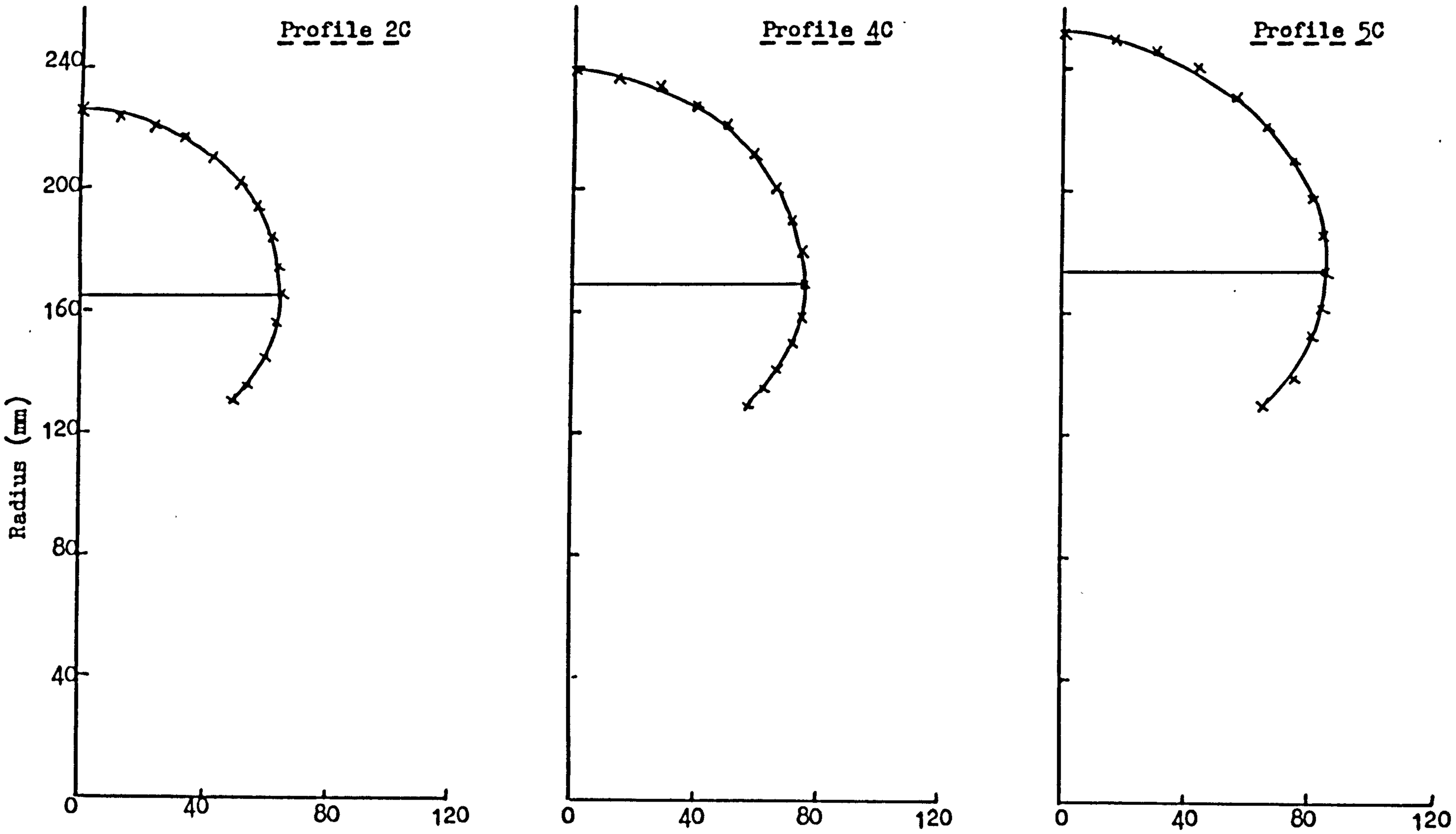
Profile 2C
Profile 4C
Profile 5C
240
200
160
120
80
40
0
40
80
120
Radius (mm)
Half Width (mm)

Figure 4.15

Table V

Principal Dimensions of Constant Angle Analogues

		Profile No.				
		1C	2C	3C	4C	5C
Bias angle	(°)	55	45	35	45	45
Radius to crown	(mm)	246.7	226.0	200.1	239.1	251.9
Radius to max. width	(mm)	180.8	165.7	150.3	169.9	173.9
Section width	(mm)	130.0	130.0	130.1	150.0	170.0
Radius to term. point	(mm)	130.0	130.1	130.1	130.1	130.0
Width at term. point	(mm)	83.0	98.5	112.8	115.0	131.7
Aspect ratio	(%)	90	74	54	73	72
Circumferential tension	(kN/m)	7.76	10.4	11.4	11.8	13.2
Meridional tension	(kN/m)	15.8	10.4	5.57	11.8	13.2

The changes in aspect ratio with bias angle are similar to those exhibited by the drum built, cross-biassed analogues. However, it is the tensions per unit length which are of greater interest. As explained, these are constant over the tyres' surfaces and their ratio is a function of the bias angle. Thus for $\alpha = 55^{\circ}$, the meridional tension is about twice that of the circumferential tension, whilst the opposite is true for $\alpha = 35^{\circ}$. At $\alpha = 45^{\circ}$, the interesting case of equibiaxial tensions occurs.

IV.3 Modulus of Carcass Material

In this chapter on design, four alternative methods for defining the meridional profiles of fabricless tyres have been developed. These result in different distributions of the principal tensions per unit length, both in terms of their magnitudes and their ratios. It is now necessary to calculate the Young's modulus required of any candidate carcass material, taking into account possible wall thicknesses.

When inflated, the growth of a fabricless tyre must be strictly limited for two reasons : variations in inflation pressure owing to poor maintenance or temperature rise when run must not result in significant changes in dimensions, particularly the overall diameter; also, the greater the growth, the greater is the stored energy available for flaw propagation. Associated with the latter is the sensitivity of elastomers to cutting when in tension. Thus, in calculating the required modulus,

an elasticity theory restricted to small strains is acceptable although, because elastomers are under consideration, Gaussian is preferable to classical elasticity.

The statistical or Gaussian theory of rubber elasticity, reference (14), results in an expression for the stored energy density:

$$W = \tfrac{1}{2}G\,(I_1 - 3) \qquad (19)$$

where G may be identified as the shear modulus of elasticity.

I_1 is the first strain invariant and is a function of the three principal extension ratios (λ):

$$I_1 = \lambda_1^{\,2} + \lambda_2^{\,2} + \lambda_3^{\,3} \qquad (20)$$

Now for any general strain condition, the volume of an element which, unstressed, was a unit cube, is:

$$v = \lambda_1\,\lambda_2\,\lambda_3$$

so that a small change in volume may be expressed as:

$$\delta v = \frac{\partial v}{\partial \lambda_1}\,\delta\lambda_1 + \frac{\partial v}{\partial \lambda_2}\,\delta\lambda_2 + \frac{\partial v}{\partial \lambda_3}\,\delta\lambda_3$$

But $$\frac{\partial v}{\partial \lambda_1} = \lambda_2\,\lambda_3 \quad \text{etc}$$

and thus:

$$\delta v = \frac{\delta\lambda_1}{(\lambda_2\,\lambda_3)^{-1}} + \frac{\delta\lambda_2}{(\lambda_3\,\lambda_1)^{-1}} + \frac{\delta\lambda_3}{(\lambda_1\,\lambda_2)^{-1}}$$

However, elastomers are virtually incompressible, so that:

$$\lambda_1\,\lambda_2\,\lambda_3 = 1$$

and $$\frac{\delta\lambda_1}{\lambda_1} + \frac{\delta\lambda_2}{\lambda_2} + \frac{\delta\lambda_3}{\lambda_3} = 0 \qquad (21)$$

Suppose that the triaxial strains represented by λ_1 λ_2 and λ_3 were brought about by corresponding forces f_1 f_2 and f_3, so that a small change in stored energy density is given by:

$$\delta W = f_1 \delta\lambda_1 + f_2 \delta\lambda_2 + f_3 \delta\lambda_3$$

Substituting for $\delta\lambda_3$ from (21) gives:

$$\delta W = (\lambda_1 f_1 - \lambda_3 f_3) \frac{\delta\lambda_1}{\lambda_1} + (\lambda_2 f_2 - \lambda_3 f_3) \frac{\delta\lambda_2}{\lambda_2} \qquad (22)$$

However, such a change in energy can also be derived from equations (19) and (20):

$$W = \tfrac{1}{2}G\,(\lambda_1^2 + \lambda_2^2 + \lambda_3^2 - 3)$$

or $$\delta W = G\,(\lambda_1 \delta\lambda_1 + \lambda_2 \delta\lambda_2 + \lambda_3 \delta\lambda_3)$$

Again substituting for $\delta\lambda_3$ from (21):

$$\delta W = G\,[(\lambda_1^2 - \lambda_3^2) \frac{\delta\lambda_1}{\lambda_1} + (\lambda_2^2 - \lambda_3^2) \frac{\delta\lambda_2}{\lambda_2}] \qquad (23)$$

Comparing equations (22) and (23):

$$\lambda_1 f_1 - \lambda_3 f_3 = G(\lambda_1^2 - \lambda_3^2)$$

$$\lambda_2 f_2 - \lambda_3 f_3 = G(\lambda_2^2 - \lambda_3^2) \qquad (24)$$

But for biaxial stresses, $f_3 = 0$ and the true stresses (σ) are:

$$\sigma_1 = \frac{f_1}{\lambda_2\,\lambda_3} = \lambda_1 f_1 \quad , \sigma_2 = \lambda_2 f_2$$

so that:

$$\sigma_1 = G(\lambda_1^2 - \lambda_1^{-2}\lambda_2^{-2})$$

$$\sigma_2 = G(\lambda_2^2 - \lambda_1^{-2}\lambda_2^{-2}) \qquad (25)$$

To adapt equations (25) for tensions per unit length, let the original wall thickness of an element of a toroid be t_o, then when strained it is:

$$t = \lambda_3 t_o = t_o/\lambda_1\lambda_2$$

so that $N_1 = \sigma_1 t = \sigma_1 t_o/\lambda_1\lambda_2$ etc.

Replacing the subscripts 1 and 2 by m and c, for the meridional and circumferential directions, and substituting in (25):

$$N_m = Gt_o\,(\lambda_m/\lambda_c - \lambda_m^{-3}\lambda_c^{-3})$$

$$N_c = Gt_o\,(\lambda_c/\lambda_m - \lambda_m^{-3}\lambda_c^{-3}) \qquad (26)$$

These equations may be used to calculate the product of shear modulus and wall thickness required to limit λ_m and λ_c to specified maximum values.

Now, apart from the high aspect ratio toroids, the most highly stressed region is in the crown where $N_c > N_m$. It is, therefore, convenient to specify the maximum value for λ_c. Equations (26) can then be used to calculate λ_m and thus the product, Gt_o.

Taking the ratios of equations (26):

$$R = \frac{N_c}{N_m} = \frac{\lambda_m^2\lambda_c^4 - 1}{\lambda_m^4\lambda_c^2 - 1}$$

or $$R\lambda_c^2\lambda_m^4 - \lambda_c^4\lambda_m^2 - (R - 1) = 0$$

a quartic in λ_m

Putting $x = \lambda_m$, this equation becomes

$$ax^4 + bx^2 + c = 0$$

and may be solved by the Newton-Raphson iterative method, whereby an improved root following an initial guess is given by:

$$x_{r+1} = x_r - \frac{F(x_r)}{F'(x_r)}$$

where $F(x_r) = ax_r^4 + bx_r^2 + c$

$F'(x_r) = 4ax_r^3 + 2bx_r$, the first derivative.

The values of λ_m and λ_c can then be entered into one of equations (26) and the product Gt_o calculated.

To determine an effective Young's modulus, E, defined as the initial slope of the uniaxial stress-strain curve of an elastomer, equation (25) may be written as:

$$\sigma_1 = G(\lambda_1^2 - \lambda_1^{-1})$$

thus $$\frac{d\sigma_1}{d\lambda_1} = G(2\lambda_1 + \lambda_1^{-2})$$

and as $\lambda_1 \to 1$, $E \to 3G$

For comparison, the equations equivalent to (26) but derived from classical elasticity theory are:

$$Et_o = (N_m - \mu N_c)/e_m$$

$$Et_o = (N_c - \mu N_m)/e_c \qquad (27)$$

where E is Young's modulus

μ is Poisson's ratio

and e_m, e_c are the meridional and circumferential strains respectively.

To investigate the differences between the two theories, the circumferential tension per unit length (N_c) was held constant at 10 kN/m, while the meridional tension was varied from zero to 10 kN/m, the final condition being equibiaxial. For the Gaussian theory, the extension ratio λ_c was set at 1.05, 1.10, 1.15 and 1.20 in turn; and thus for equivalence, the strain, e_c, for classical theory was 5%, 10%, 15% and 20%.

Using the Gaussian theory, equations (26), table VI.A lists the second principal extension ratio, λ_m, and the required product of Young's modulus and initial wall thickness, t_o. Table VI.B presents the same information but using equations (27) from classical elasticity with Poisson's ratio equal to 0.5.

Table VI.A

Gaussian Theory (N_c = 10 kN/m)

λ_c =	1.05		1.10		1.15		1.20	
N_m (kN/m)	λ_m	Et_o (kN/m)	λ_m	Et_o (kN/m)	λ_m	Et_o (kN/m)	λ_m	Et_o (kN/m)
0	0.976	205	0.954	105	0.933	71	0.913	60
2	0.985	186	0.971	96	0.960	66	0.950	51
4	0.995	168	0.993	88	0.994	62	0.997	48
6	1.009	150	1.021	81	1.037	58	1.055	47
8	1.027	134	1.057	74	1.089	55	1.123	46
10	1.050	118	1.100	69	1.150	53	1.200	45

Table VI.B

Classical Theory (N_c = 10 kN/m)

e_c =	0.05		0.10		0.15		0.20	
N_m (kN/m)	e_m	Et_o (kN/m)	e_m	Et_o (kN/m)	e_m	Et_o (kN/m)	e_m	Et_o (kN/m)
0	−0.025	200	−0.050	100	−0.075	67	−0.100	50
2	−0.017	180	−0.033	90	−0.050	60	−0.067	45
4	−0.006	160	−0.013	80	−0.019	53	−0.025	40
6	0.007	140	0.014	70	0.021	47	0.028	35
8	0.025	120	0.050	60	0.075	40	0.100	30
10	0.050	100	0.100	50	0.150	33	0.200	25

It may be seen that at low strains, λ = 1.05 or e = 5%, the moduli x thicknesses calculated from the two theories are very similar, as would

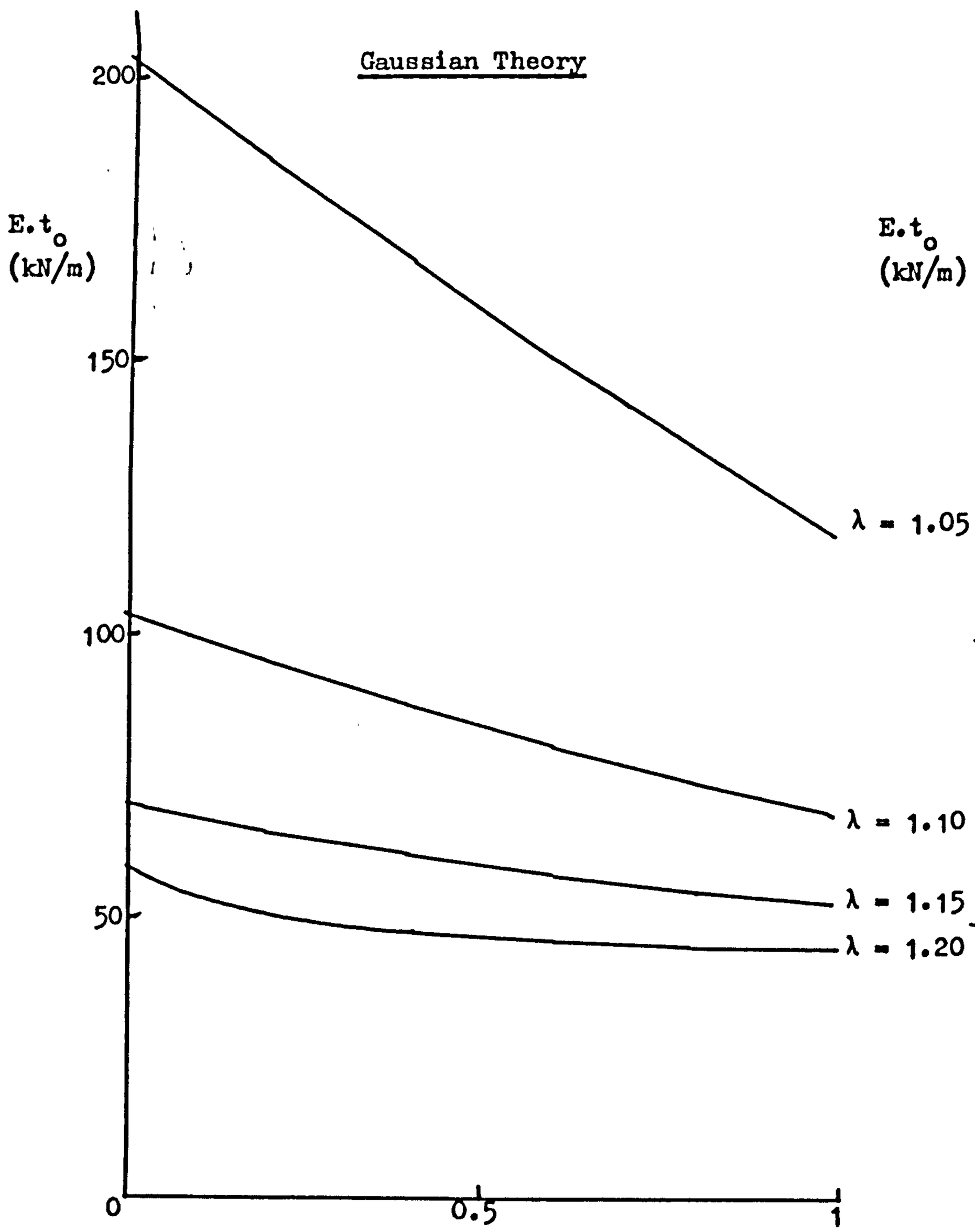
Gaussian Theory
200
150
100
50
0
E.t$_o$ (kN/m)
λ = 1.05
λ = 1.10
λ = 1.15
λ = 1.20
0.5
1
Ratio N$_m$/N$_c$

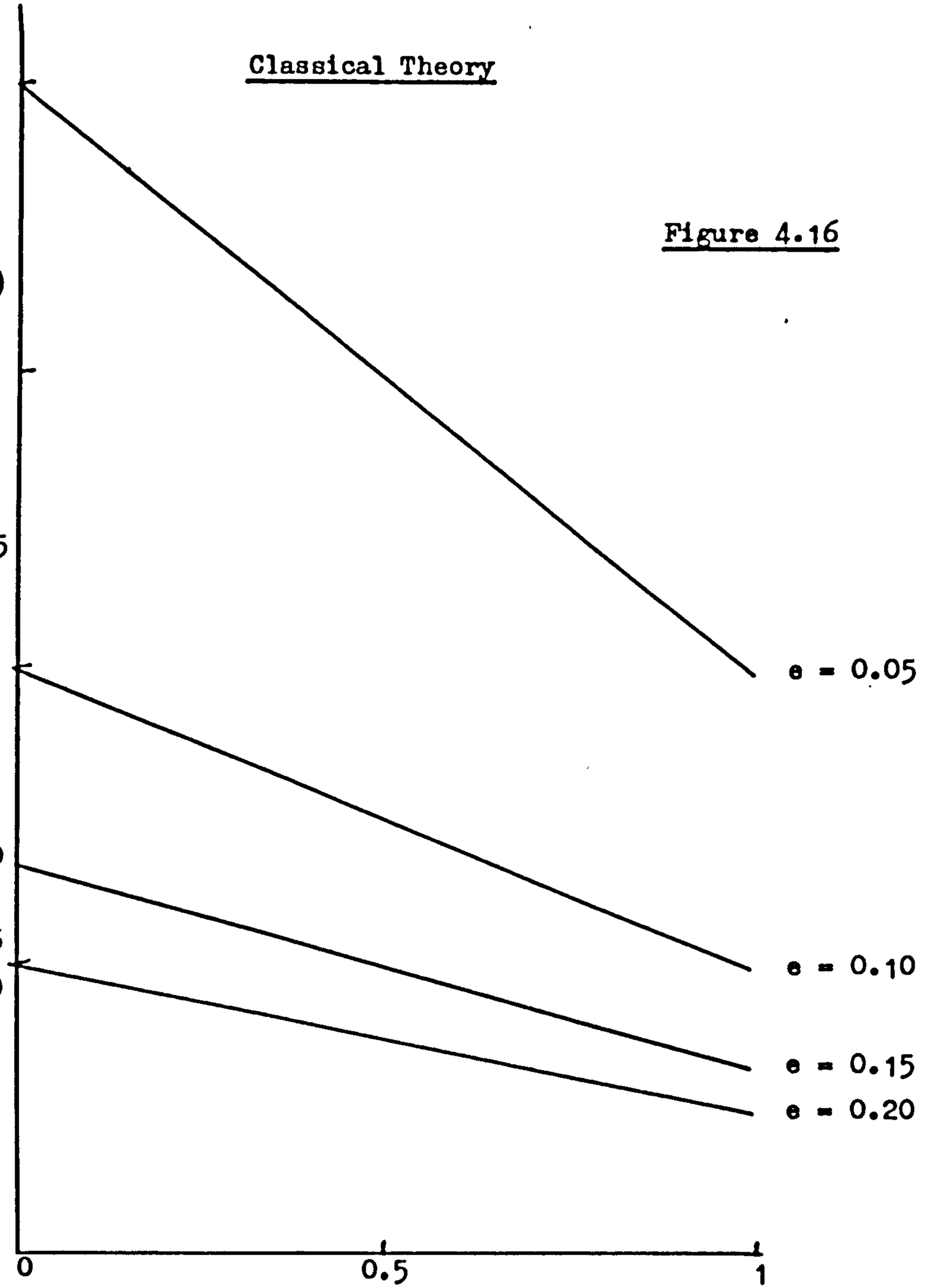
Classical Theory
E.t$_o$ (kN/m)
e = 0.05
e = 0.10
e = 0.15
e = 0.20
0
0.5
1
Ratio N$_m$/N$_c$

Figure 4.16

be expected. However, at the largest strain considered, $\lambda = 1.2$ or $e = 20\%$, significant differences are apparent, particularly under equi-biaxial conditions, 53 kN/m cf. 33 kN/m. It will be prudent, therefore, when designing fabricless tyres, to utilise Gaussian theory which reflects to some extent the non-linear behaviour of elastomers.

To illustrate the results given in tables VI.A and VI.B further, graphs are shown in figure 4.16 of the product of Young's modulus and initial wall thickness plotted against the ratio of the principal tensions per unit length, N_m/N_c with N_c held constant. It is immediately apparent that the modulus for a given wall thickness or the wall thickness for a given modulus are lowest when the two tensions are equal. This is a very important result and explains the interest in the fabricless tyre meridional profile based on the analogue of a cross-biassed tyre whose bias angle, α, is constant and equal to 45° throughout its construction. Clearly, minimising the modulus of the carcass material of a fabricless tyre allows the tyre to be more flexible when deflected under load. Similarly, minimising the wall thickness is efficient in terms of material usage and also allows the tyre to be more flexible.

IV.4 Bead Tension

In this chapter, methods for defining the cross-sections, or meridional profiles, of fabricless tyres have been established and, in the last section, a procedure for calculating the carcass wall thickness and material modulus to restrict growth, or strain, due to inflation has been developed. However, there is one tyre component which has not yet received attention, the bead wire. In fact, it has not been decided whether a bead wire is necessary in a fabricless tyre.

In reference (13), an expression is derived for the tension (T) in the bead wire of a cord-reinforced tyre and this can be used for the fabricless tyres based on the drum built and constant bias angle analogues. It is:

$$T = \frac{P}{2}\left[(\rho_m^2 - \rho_o^2)^2 \exp\left(-2\int_{\rho_b}^{\rho_o} \frac{\cot^2\alpha}{\rho}\, d\rho\right) - (\rho_m^2 - \rho_b^2)^2\right]^{\frac{1}{2}} \quad (28)$$

where the integration depends upon the cord path.

For the drum built tyre, to which the cosine rule applies, equation (28) becomes:

$$T = \frac{P}{2}\left[(\rho_m^2 - \rho_o^2)^2 \frac{\rho_o^2 \sin^2\alpha}{(\rho_o^2 - \rho_b^2 \cos^2\alpha_o)} - (\rho_m^2 - \rho_b^2)^2\right]^{\frac{1}{2}} \qquad (29)$$

A similar expression for the constant bias angle tyre is obtained by using the same substitution employed when calculating the meridional radius of curvature, ie:

$$c = \cot^2\alpha$$

with leads to:

$$T = \frac{P}{2}\left[(\rho_m^2 - \rho_o^2)^2 (\rho_b/\rho_o)^{2c} - (\rho_m^2 - \rho_b^2)^2\right]^{\frac{1}{2}} \qquad (30)$$

Equations (29) and (30) may now be used to calculate the bead tensions in the fabricless tyre profiles which illustrated the design methods in sections IV.2.3.3 and IV.2.3.4. They are listed, together with the principal design parameters of these tyres, in table VII.

Table VII
Bead Tensions

		Profile Reference							
		1B	2B	3B	1C	2C	3C	4C	5C
Rad. to crown	(ρ_o, mm)	240.0	240.0	240.0	246.7	226.0	200.1	239.1	251.9
Rad. to max. wd.	(ρ_m, mm)	178.5	175.6	173.7	180.8	165.7	150.3	169.9	173.9
Rad. to bead	(ρ_b, mm)	130.0	130.0	130.0	130.0	130.0	130.0	130.0	130.0
Bias angle	(α_o, ^{o})	45.01	38.35	34.67	55.0	45.0	35.0	45.0	45.0
Inflation pres.	(p, kPa)	200	200	200	200	200	200	200	200
Bead tension	(kN)	1.970	1.834	1.743	1.320	0.855	0.448	0.968	1.076

In general, the bead tension decreases as the bias angle is reduced. This is because the former is due to cord tension normal to the bead wire so that, in theory, if the bias angle were zero at the bead, no tension would be induced.

For the profiles considered, the tension ranges from 0.5 kN to 2.0 kN. For any tyre, the strain caused by this tension must be very low, say less than 0.1%, otherwise the tyre would become loose on the rim when inflated and the subsequent "shuffle" when run would cause abrasion of the rubber surrounding the bead and eventual failure.

Now if the cross-sectional area of the bead is A, whether it is a conventional multistrand steel wire or an integral part of the carcass of a fabricless tyre, and the material Young's-modulus is E, then to restrict bead extension to 0.1%:

$$\frac{T}{EA} < 0.001 \qquad \text{or} \qquad A > \frac{T}{0.001.E}$$

For steel, E is about 200 GPa so that:

with T = 0.5 kN $\qquad A = 2.5\ (mm)^2$

and with T = 2.0 kN $\qquad A = 10\ (mm)^2$

Clearly steel bead wires with these sections can be incorporated in the fabricless tyres listed in table VII.

If, however, the carcass material were used to form the bead, the situation is very different. Now a value for E of 100 MPa is not atypical of high modulus elastomers, with the consequence that,

for T = 0.5 kN $\qquad A = 5{,}000\ (mm)^2$

and for T = 2.0 kN $\qquad A = 20{,}000\ (mm)^2$

Thus it may be stated immediately that, if the fabricless tyres to be designed are fitted to rims in the same way as conventional tyres, then steel bead wires will be required. However, there is an alternative, which is to revert to Bartlett's bead-edge construction, figure 1.5 in Chapter I, whereby the bead regions are clamped in place by the rim.

CHAPTER V : DESIGN AND MANUFACTURE OF EXPERIMENTAL FABRICLESS TYRES

V.1 Introduction

There were a number of factors which influenced the choice of fabricless tyres to be made and tested in this research. Some were related to the range of available materials most likely to meet the demands made on their physical properties, while others were concerned with providing information on the effects of specific design variables on tyre performance. In addition, manufacturing methods had to be taken into account; and these were governed by the processing characteristics of the materials.

Candidate materials and manufacturing methods will be reviewed in the next two sections of this chapter; following which, the detailed design of the tyres will be described. Here it is worth emphasising the one most important design variable which could not be specified when discussing design methods in chapter IV : the carcass wall thickness. To limit growth of a tyre when freely inflated, the product of wall thickness and material modulus can be calculated and, for this loading case alone, it does not matter which combination is chosen; although economics, of course, would govern the final choice. When a tyre, however, is deformed radially, owing to the weight of the vehicle, the same argument cannot be applied. The sidewalls in the zone of the contact patch will be deflected and their bending stiffness will be proportional to the material modulus and some function of the wall thickness. If one were considering a bending beam, for example, its deflection is directly proportional to modulus but to the cube of its thickness. With the toroidal geometry of a tyre and non-axisymmetrical loading, such a simple relationship cannot be derived and thus one important goal of the experimental work was to ascertain the effect of wall thickness on radial stiffness. For this, the tyres to be designed, made and tested needed to include variants which differed only in this respect.

At this stage in the research, it was decided to introduce another design feature. In chapter IV it was shown that as the aspect ratio of a tyre is reduced, that is its section height is decreased relative to its section width, the tension per unit length in the circumferential direction at the crown rises steeply, although elsewhere in the meridian the changes are not so pronounced. Clearly this restricts the design of tyres with no fabric

reinforcement whatsoever to high aspect ratios. Consequently, the decision was taken to introduce a textile belt into some designs so that lower aspect ratio tyres could be investigated without the penalty of using materials of much higher Young's modulus or of increasing the wall thickness. It was argued that, if the addition of a belt resulted in very significant technical advantages, the complexity introduced into production would be acceptable, particularly if the belt could be of a simple construction designed only to restrict growth owing to inflation. In conventional tyres, it is the manufacturing stages required to prepare the composite materials, build and shape the carcass which dominate production, chapter I.

V.2 Materials

The research being described was not concerned with developing or modifying materials to meet the demands made by fabricless, pneumatic tyres. However choices had to be made from available materials and clearly those with the greatest potential were selected.

It must be stated that, early in the research, it was realised that no one polymer would be suitable for a complete tyre because the required physical properties of the tread material, such as high friction and abrasion resistance, are quite different to those of the carcass. The latter are primarily good fatigue life coupled to a greater Young's modulus to restrict growth due to inflation. It is well known (reference 15) that high modulus, or hardness, has a detrimental effect on road grip.

V.2.1 Tread material

Considering the tread material first, there is abundant information on many polymers, although much of it is not documented outside individual rubber companies. The commonly used hydrocarbon elastomers; such as natural rubber, cis-polybutadiene, styrene-butadiene copolymers, EPDM and butyls; all present different balances of properties ranging from the high abrasion resistance and poor grip of BR to the relative poor abrasion resistance but excellent grip of butyls. All these elastomers are reinforced with carbon black, and the choice of black and its quantity have strong influences.

Plastics in general, such as polyethylene and polyvinylchloride, have very poor properties when considered for tyre treads but one group of materials which has been subject to careful examination is polyurethanes. These can take many chemical forms but, because they are self-reinforcing, the additional freedom afforded by various carbon blacks is not available. For the more promising polyurethanes, it has been found that at low severities, defined in terms of tangential friction forces and slip (Ch.III.3), their abrasion resistance can be very high, for example Vulkollan (NDI-polyester), and this has been exploited in the shoe industry. However at high severities, their resistance to wear falls sharply and has precluded their use in pneumatic tyres, although they are acceptable for industrial solid tyres when the load carrying capacity of rubber is exceeded. Also, as will be demonstrated when the experimental work of this research is described, the road grip of polyurethanes is in conflict with their abrasion resistance. Either can be improved to the

required level but at the expense of the other, the compromise of carbon black filled conventional rubbers not being attainable.

Thus it appeared, when the research was commenced, that conventional rubbers would probably be required for the treads of fabricless tyres. However the possibility of using materials more compatible in terms of processing with that chosen for the carcass was to be explored.

V.2.2 Carcass material

It was shown in chapter IV that, to restrict growth due to inflation without needing an excessive carcass wall thickness, a material with a Young's modulus in the range 20 to 100 MPa is required. This immediately eliminates conventional rubbers because a modulus of about 8 MPa cannot be exceeded, even with very high loadings of carbon black, without destroying their elasticity. Thus the search for a suitable material must be directed towards polyurethanes, polymers containing both plastics and elastomeric segments and, perhaps, fibre filled polymers.

To guide the search, it is possible to specify properties other than Young's modulus, although this can only be done approximately and with reference to standard, routine laboratory tests. For example, to guard against catastrophic failure of tyres by splitting of the carcass, a tensile strength of about 30 MPa would be desirable. This corresponds to induced strains approaching 100%, depending upon the modulus, and such a value of elongation at break would mean that a potential failure would be easily detected by the appearance of localised swelling of the carcass. The swelling would also affect the dynamic balance of a tyre and would be transmitted as severe vibrations to the driver of the vehicle. Creep is another important property and should not be assessed from uniaxial data alone. Under the biaxial conditions present in the carcass of a tyre, creep is significantly lower, particularly if the stresses are equibiaxial. Nevertheless, if a material exhibits a tensile creep rate of more than 1%/day at 100°C and a stress of 3 MPa, its use should be questioned. Perhaps rates as low as 0.1%/day would be desirous.

Fatigue resistance is clearly a most important property but one which can only be assessed correctly under the conditions of strain, temperature and frequency present in a tyre. However as a guide, natural rubber in a routine test, which flexes samples containing a known cut, has a life of 2 to 3.10^7 cycles. Consequently, potential candidate carcass materials must have a life of at least 10^7 cycles under these conditions.

Finally, the temperature dependence of properties must be considered because, in the UK, tyres are operated in ambient temperatures from 0 to 25°C and their internal hysteresis can cause their body temperatures to rise to 80°C. Truck tyres run hotter and in other territories the ambient temperature range is greater. If the carcass material is a high modulus elastomer, its glass transition temperature should not exceed -40°C, otherwise its properties will be very temperature dependent over the range 0 to 80°C. On the other hand, if the material is a thermoplastics, its melting or softening point should be above 150°C to give adequate properties over the working range. For these latter materials there is an upper limit to the melting point because, during processing, a sufficiently low viscosity is required for injection moulding.

With these general comments on the required physical properties of candidate carcass materials, a list of groups of materials which may be suitable can be presented (reference 16).

1. Elastomers containing a multiplicity of polar interactions:
   a. hydrogen bonded polymers,
      (polyurethanes, polyamides);
   b. ionic polymers,
      (metal carboxylates, polyamopholytes).

2. Polymers containing plastics and elastomeric segments:
   a. hard block (plastics):
      (i) amorphous,
         (polycarbonate, aromatic polyether, PU);
      (ii) crystalline,
         (polyester, polyamide, PU);
   b. elastomeric block:
      (polyether, aliphatic polyester, polydienes, PU).

3. Blends of fibres and elastomers:
   a. fibre,
      (polyamide);
   b. elastomer,
      (polyacrylate, polydienes, PU).

Of these, those with ion cross-links can be eliminated because they suffer high creep, while those based on acrylate elastomers have poor dynamic properties. Moreover, when the remaining options were related

to commercially available polymers, the choice was reduced to two types. The option of fibre/elastomer blends was disregarded because of the material development which would be involved.

The first option is a polyurethane: polytetrahydrofuran end-tipped with tolylenediisocyanate, such as Du Pont's Adiprene L-100. There are several variants of the cross-linking agent aromatic amine which could be used, the best of which is probably methylene-bis-chloroaniline (MOCA) although diethyl tolylene diamine or chlorocarboxybutyl-m-phenylene diamine are also contenders. The last is costly and the second was finally chosen, although MOCA was used before being rejected on health grounds. The polyurethane elastomer so formed can be processed by liquid technology and can thus be cast or injected. A range of moduli are available by varying the ratios of ingredients.

The second material has the trade name Hytrel and is also manufactured by Du Pont. A range of grades is available with Young's moduli from 50 to 200 MPa. It contains crystalline polyester blocks of iso and terephthalic-acids with 1,4-butanediol, coestrified with hydroxyl terminated PTHF. It is prepared by co-reacting PTHF with the mixed acid-butanediol and numerous variations are possible by changing the amounts and types of aromatic acids. It is processed by conventional injection moulding.

It was decided that the experimental work should proceed on the basis of both materials : polyurethanes and Hytrel. Not only do they differ as types of polymer, but their processing characteristics are quite unlike and would call for contrasting manufacturing techniques. As noted in section V.2.1, conventional rubber compounds would be used for the treads initially.

V.3 Manufacturing Methods

V.3.1 Tyres with polyurethane carcasses

Because the type of polyurethane to be used for the carcass of the experimental tyres is liquid processing, the choice of manufacturing route lay between low pressure injection moulding, including simple pouring, and centrifugal casting. For two reasons the latter was preferred : firstly, a dispenser for mixing the ingredients and delivering the PU formulations

was in existence; and, secondly, there was some concern about trapping air bubbles in the PU as it reacted. It was argued that if the tyre mould were rotated about its axis and the liquid PU were fed into the cavity adjacent to the bead wires, air bubbles would not develop. Undoubtedly, liquid injection moulding would have advantages if properly engineered, as Polyair have shown (references 6 & 7), but the method chosen was considered adequate for experimental, as opposed to production purposes.

Casting a polyurethane tyre carcass is shown diagramatically in figure 5.1, where the following features are shown. The mould is the centrifuge and defines the outer profile of the carcass. It is fitted with a solid core to define the inner profile. The whole unit is fitted within a hot air oven and the mixed ingredients from a three stream dispenser are introduced close to the axis of the centrifuge and flow towards the crown of the tyre, gradually filling the cavity between the mould and the core.

The solid core, machined accurately to fit correctly, introduces a complication into centrifugal casting which could jeopardise this manufacturing method if taken into production. To remove it, after the tyre has been cast and the mould opened, it must be segmented along planes parallel to the tyre's axis but inclined either way from meridians. To automate such a system and protect it from long term damage would be a problem.

Now it was established in chapter IV that a fabricless, pneumatic tyre must be fitted with bead wires. With conventional tyres they are introduced as part of the building process but with liquid technology they need to be positioned prior to casting. This was achieved by wrapping them in low density, reticulated PU foam, having first treated them with a suitable bonding agent. Sufficient foam was used to provide an interference fit in the mould. When the PU was introduced, it passed through the foam and eventually filled the mould, so incorporating the bead wires correctly in the carcass.

For a typical PU formulation, the centrifuge or mould was rotated at 700 rpm with the hot air oven operating at 100°C. The liquid polymer mix was fed at 70°C from the dispenser and, with the available equipment, this operation took about 3 minutes. The time for the PU to react sufficiently, so that the centrifuge could be stopped and the mould opened, obviously depended upon the reaction rate of the particular

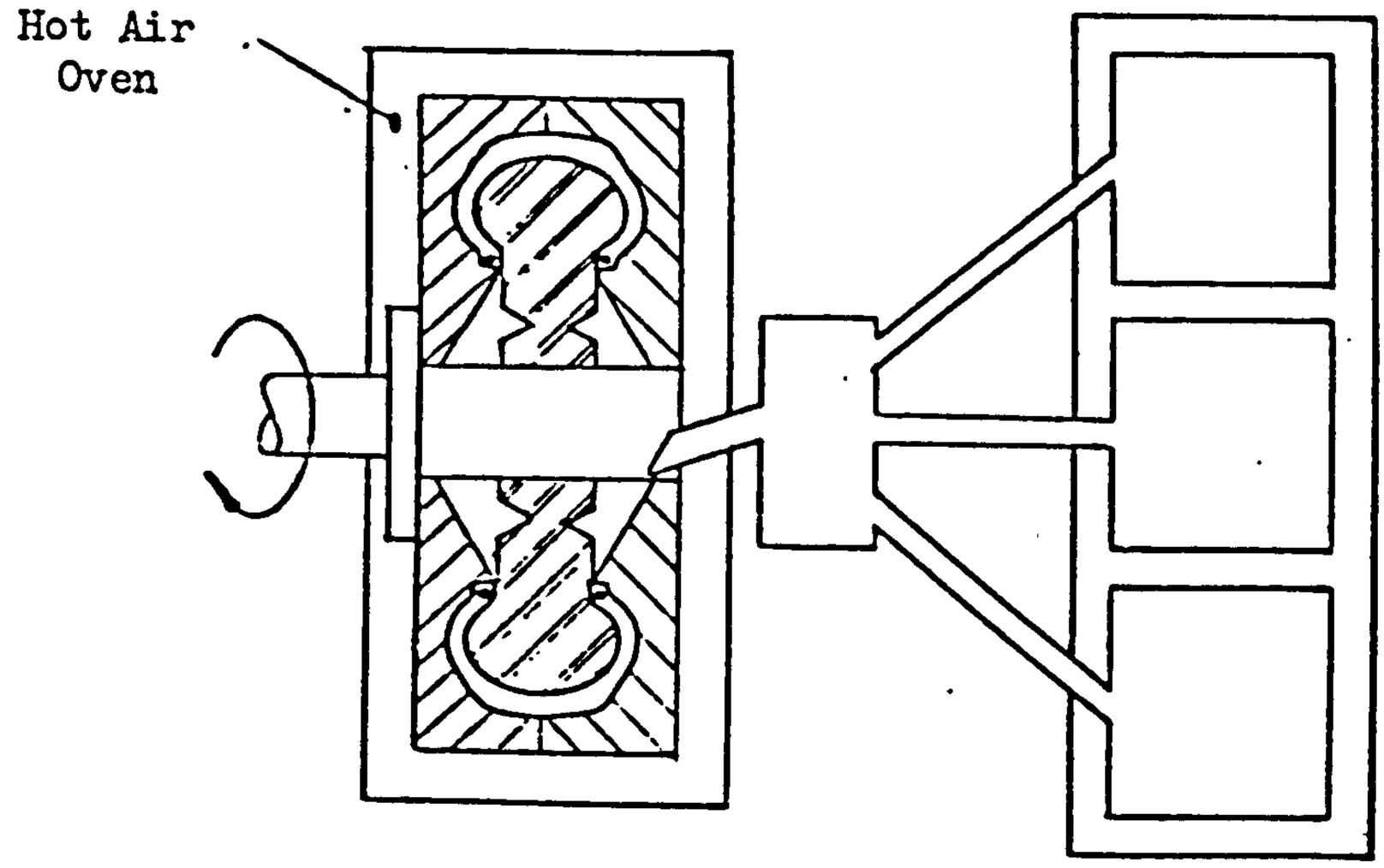

Figure 5.1

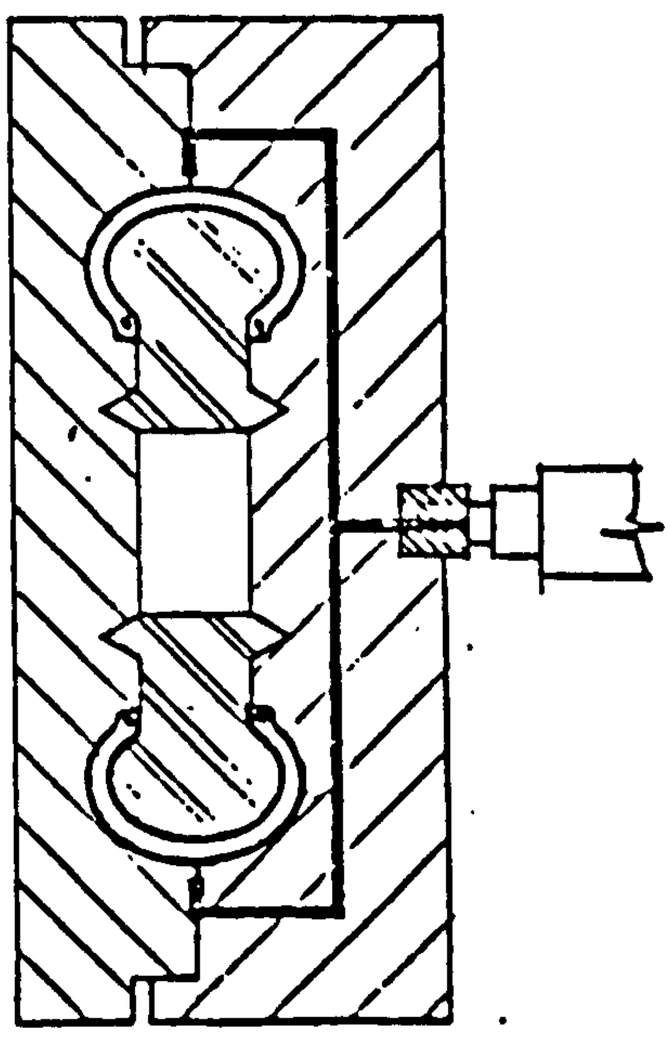

Figure 5.2

Figure 5.3

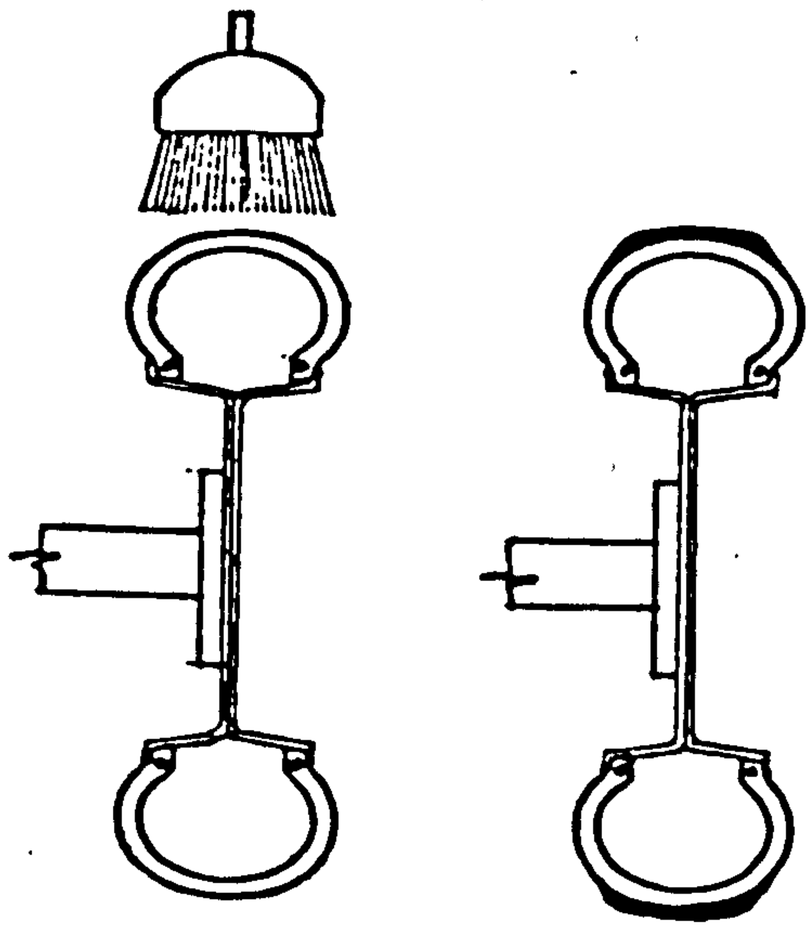

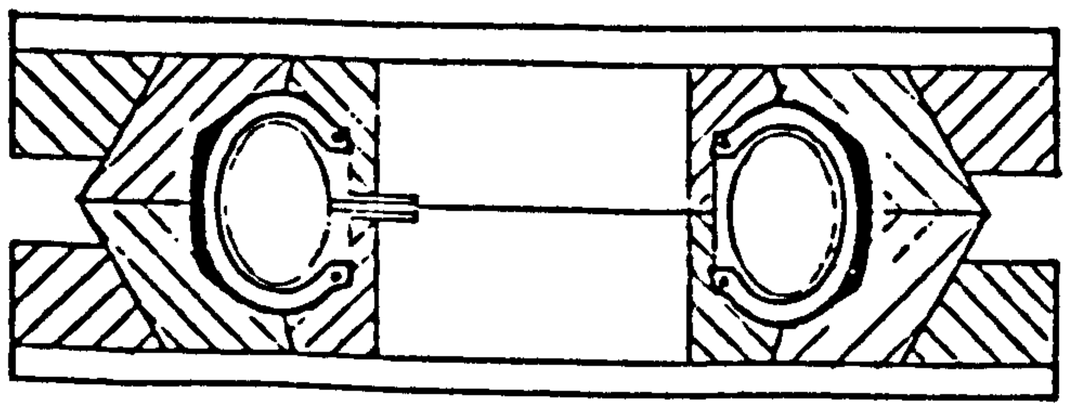

Figure 5.4

formulation being used. However when the tyre had been removed, it was placed in a storage oven for at least one hour to give the required post cure.

To manufacture the tyres complete with conventional rubber treads, at least three methods could be employed. The first is to mould and cure the treads separately and then fit them to the finished carcasses with a suitable adhesive. The tread would be stretch fitted to aid bonding. The second is to fit an uncured tread and, in effect, remould the tyre; while the third is to position a cured tread in the centrifuge mould and cast the carcass against it. The last has much to commend it as a production process and should result in a superior tyre because of the intimate chemical bonding. In the event, both methods one and three were tried with varying success.

V.3.2 Tyres with Hytrel carcasses

Products can be injection moulded from Hytrel in the conventional way and, in general, no difficulty was experienced in making tyre carcasses. The multicoil beads were wrapped with ductile steel wire in the form of a coarse helix, which supported them between the outer mould and the solid core. The latter, like those for centrifugal casting were segmented to allow removal.

During the moulding operation, the cavity was filled from a screw-ram injector through a hot runner system feeding two diametrically opposed ports on the carcass crown, figure 5.2. The Hytrel was at 240°C while the mould was heated to 100°C. The injector's hopper was purged continuously with nitrogen to inhibit oxidation of the Hytrel.

To complete the tyres, conventional rubber treads were added by remoulding. A carcass was cleaned with naphtha and its crown region treated with Desmodur R. After further cleaning, a 1 mm layer of dry bonding compound was applied, followed by an uncured extruded tread length, figure 5.3. Shaping and curing was accomplished by the standard remoulding technique, using an inflated inner tube for consolidating the tread, figure 5.4.

Now the pressures used in injection moulding are very high, in excess of 100 MPa in the case of the Hytrel carcasses. This required the solid core to be held very rigidly in the mould, otherwise variations in wall

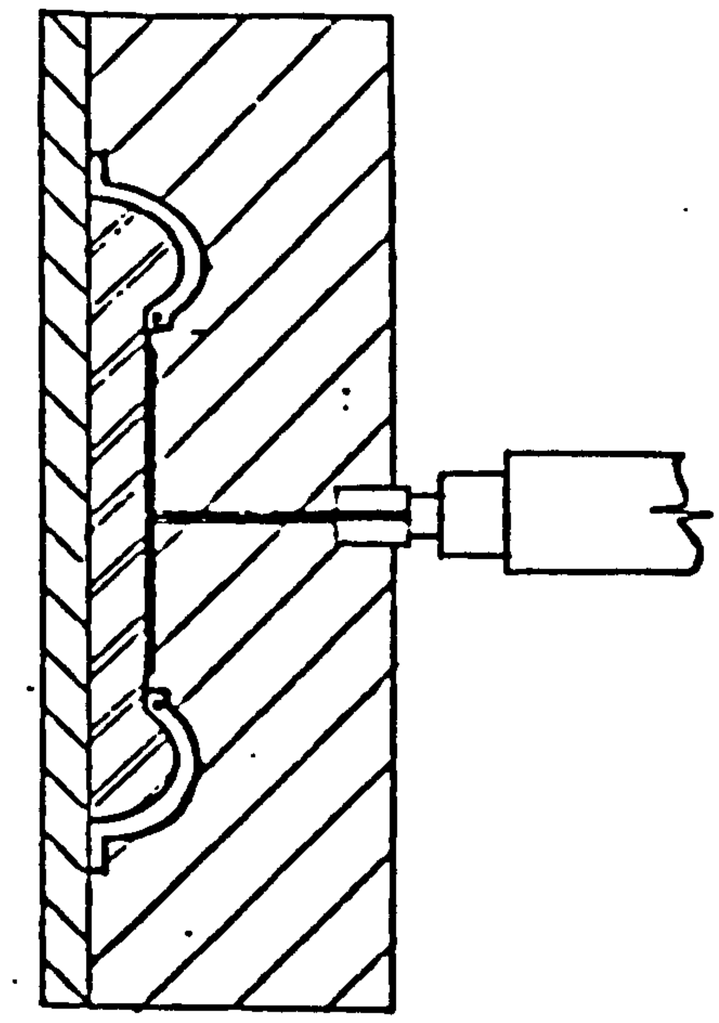

Figure 5.5

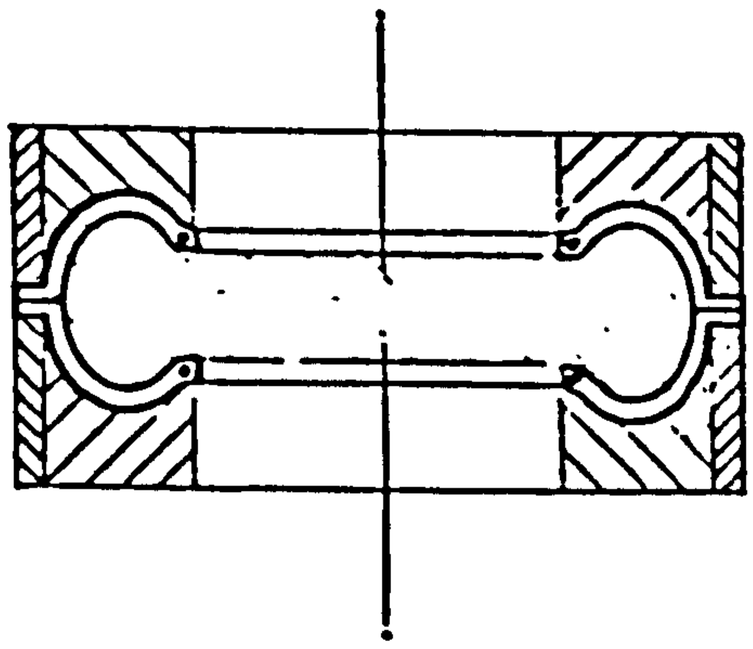

Figure 5.6

(Figure 5.4)

thickness would result. In fact it proved too difficult to produce carcasses with the thinnest wall planned and this prompted the development of a modified method of manufacture.

Being a thermoplastics, Hytrel can be welded to itself by local heating with, say, RF. Thus the concept of injection moulding half toroids, and subsequently welding them together around the crown line to form carcasses, was considered to be worth investigating. Figure 5.5 illustrates the moulding of half toroids, where it may be seen that Hytrel was injected through ports adjacent to the bead wires and that a circumferential "lip" was formed around the crown for welding. However, compared to moulding the complete toroid, the greatest difference when moulding a half toroid is that its inner surface is defined by the mould and not a solid core.

Welding was accomplished by constructing electrodes which clamped two half toroids together by their lips, figure 5.6. By adjusting the RF, successful welding was obtained, when a small bead of Hytrel formed around the inner circumferential line. This indicated the half-toroids were joined through their thickness. The lips were removed by cutting and buffing to give complete carcasses, to which treads were added as before, figure 5.4.

V.4 Detailed Design of Tyres

Although two types of material and two manufacturing methods were chosen and used for making fabricless tyres for the research, the injection moulding route was limited by the capacity of the available equipment. This only allowed a maximum of about 400 g of thermoplastics to be delivered in a single shot, which was not sufficient for producing carcasses of tyres similar in size to the smallest conventional tyres in regular production : 5.20–10 or 145–10 car tyres. Attempts were made to overcome this limitation by maintaining the mould at a higher temperature, just above the melting point of Hytrel, while repeated injections were made before cooling. However the joins between shots were detectable so that the resulting tyres were unsuitable for fatigue tests. Nevertheless, some pseudo–static tests were possible and these augmented the data obtained on PU tyres.

No such restrictions applied to centrifugal casting and the sizes chosen for the polyurethane tyres were equivalent to 5.20–10 biassed and 145–10 radial tyres, which are standard fitments to the British Leyland Min–Minor

car. Thus vehicle tests could be conducted on tyres considered suitable on the basis of laboratory results.

To investigate injection moulding and the use of thermoplastics, the main effort on Hytrel was directed towards model tyres. These had been used in Dunlop Technology Division for many years to assess materials for conventional tyres. They are about 300 mm in diameter and are fitted to wheels 200 mm in diameter, therefore their section dimensions are about half those of 5.20/145–10 tyres. Equipment was available for measuring the performance of these model tyres, including : radial and lateral stiffness; road grip and cornering power; rolling resistance or drag; fatigue life; and wear. The last facility was particularly important as no laboratory abrasion test has been developed which correlates to road wear. The other, very significant, advantage of using model tyres was that all the established test methods are rapid compared to those available for full-sized tyres. Thus the experimental programme could be conducted efficiently. In fact, it is the efficiency of the model tyre tests which led to their original development.

V.4.1 Series 'A' tyre carcasses

The first tyres chosen for manufacturing and testing were designated the 'A' series. They were based upon the equibiaxial tension design described in IV.2.3.4, which was shown to be the most efficient in terms of material usage. They would require no reinforcement whatsoever apart from bead wires and their wall thicknesses would be constant around their meridians. It was decided that, owing to the potential of this design, it should be investigated in both polyurethane and Hytrel versions.

Apart from the profile and wall thickness, the important dimensions of the tyres are shown in figure 5.7. Considering the full-sized tyre first to illustrate the design method, the rim chosen was the one used for 5.20–10 cross-biassed tyres, to which the high aspect ratio 'A' series may be compared. It is the 3.50B–10, has a well width (s_1) of 89 mm and a radius (r_1) of 127 mm. The bead wires (B) of the tyre, taken from production, have a mean radius (r_2) of 133 mm but their axial separation (s_2) would depend upon the thickness (t) of PU around them. Experience with some previous, crude fabricless tyres suggested that t = 15 mm was adequate and therefore s_2 was set at 74 mm. Now when calculating the profile of

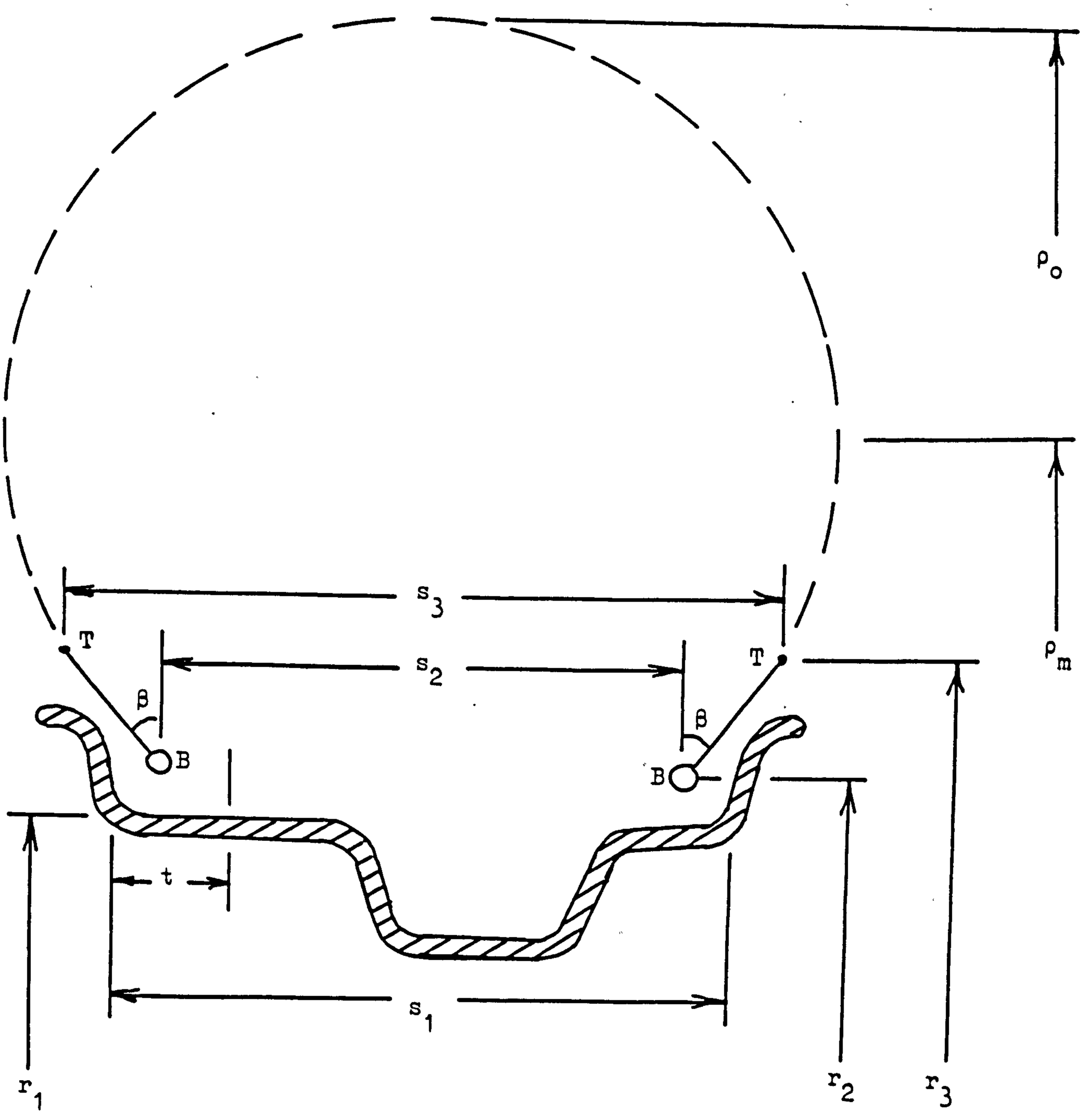

Principal Design Parameters

(all radii from axis)

Figure 5.7

the 'A' series or any other tyre, the meridian is not specified as far as the bead wires because reversed curvature must be introduced into this region, known as the clinch, in order to give the correct fit to the rim. Consequently a terminating point (T) was defined such that the mid-wall line to the bead (TB) was tangential to the calculated meridian at T. Thus it was required to specify the radius (r_3) to T, the width (s_3) at T and the final meridional angle (β). By trial and error on drawings, r_3 was put equal to 150 mm, β to 40° so that s_3 could be calculated as 102.6 mm.

Using computer program FTCAPR (appendix V), it was now possible to determine the carcass profile which terminated as required at T and had the approximate diameter and section width of the 5.20-10 conventional cross-biassed tyre. Its principal mid-wall dimensions were as follows:

radius to crown (ρ_o)		236.9 mm
radius to point of max. width (ρ_m)		179.8 mm
section width	122.6 mm)	
section height	110.1 mm)	aspect ratio = 89.8 %

For the polyurethane versions, three carcass wall thicknesses were selected : 3.0, 5.5 and 8.0 mm, requiring material moduli in the range 20 to 50 MPa if growth due to inflation were to be restricted to 3 to 5%. Now, ideally, all the resulting carcass sections should have the same mid-wall meridian but to achieve this would have been costly because three different segmented cores would have been required for the centrifugal casting process. Consequently it was decided to complete the design for the thinnest (3 mm) carcass first, designated the 'A1', and then to modify the outer mould to give the other thicknesses.

Using the data given above and the meridional profile, engineering drawings were prepared and converted into templates for machining the core and the 'A1' mould. The template for the mould was then modified to give the 'A2' (5.5 mm) and 'A3' (8 mm) moulds. In figure 5.8 it is shown how the profiles of the core and the moulds form the three carcasses. However, because the two thicker carcasses were based upon the meridian of the 'A1' carcass, it was necessary to check that the errors introduced by this procedure were not excessive. This was achieved by entering the principal dimensions of the 'A2' and 'A3' carcasses into program FTCAPR and comparing

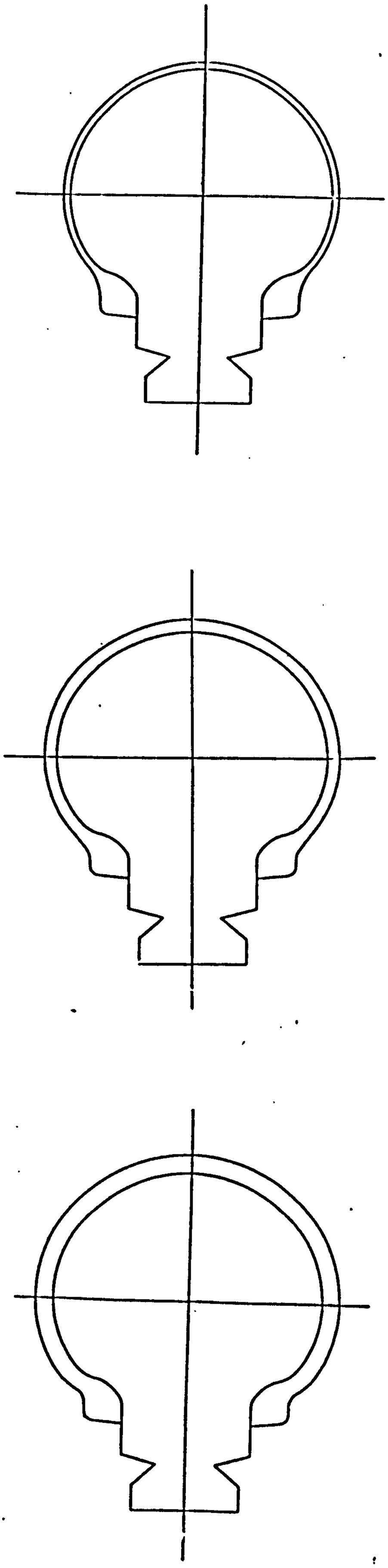

'A1'

'A2'

'A3'

Figure 5.8

the calculated and drawn profiles. Table VIII shows that the maximum error was less than 1 mm, considered to be quite satisfactory.

Table VIII

Mid-Wall Dimensions of A1, A2 and A3 Carcasses

	Radius to Crown (mm)	Radius to Max. Width (mm)	Section Width (mm)
'A1' Carcass (3 mm) :	236.9	179.8	122.6
'A2' Carcass (5.5 mm) drawn :	238.2	179.8	125.1
calculated :	238.6	180.2	125.2
'A3' Carcass (8 mm) drawn :	239.4	179.8	127.6
calculated :	240.2	180.7	127.7

To produce a Hytrel version of this tyre, a single wall thickness was chosen : 3.5 mm; somewhat less than the mid-range used for the PU tyres because of the generally higher Young's modulus of Hytrel. It was designated the 'A4' and the size nomenclature given to all four versions of these full-sized 'A' series tyres was 126-10.

The model 'A' series tyres were designed only for Hytrel and were the 73-8 'A1' and 73-8 'A2', with wall thicknesses of 1.2 and 2.2 mm respectively. Their other features, apart from size, were similar in every detail to the 126-10 tyres. The rim size was 2.0-8.

V.4.2 Series 'B' tyre carcasses

Although the 'A' series design is the most efficient in terms of material usage for withstanding the inflation pressure, it does have a high aspect ratio (~90%). For some years now, the trend in the tyre industry has been towards squatter, lower aspect ratio, designs; 70% being common, with many high performance tyres as low as 60% or even 50%. For a given tyre diameter, this means larger rims may be used, with the resulting greater space for brakes. Consequently, although it was realised some form of reinforcement would be needed in the crown region, it was decided to design, manufacture and test cast and injection moulded tyres with an aspect ratio of about 70%. These were designated the 'B' series.

To enable direct comparisons to be made between the two series of tyres, the same rim diameters were used. However as the 'B' tyres would be wider, the 4.50J-10 rim, standard for 145-10 radial tyres, was chosen

for the full-sized tyres, while for the model tyres the rim width was increased from 2.0 inches to 2.5 inches.

The detailed design procedure used for the 'B' series was the same as that used for the 'A' series. In fact, the bead and clinch regions for the two types were identical. Also the wall thicknesses chosen were the same, that is : 3.0, 5.5 and 8.0 mm for the PU full-sized carcasses and 3.5 mm for the Hytrel version, and 1.2 and 2.2 mm for the Hytrel model tyres. To define the meridional profiles, however, the method based on the analogue of a biassed construction was employed which, in chapter IV, was shown to give a suitable, smooth distribution of inflation tensions per unit length. In particular, the circumferential tension, although high at the crown of a low aspect ratio profile, falls rapidly in the sidewall. Thus material usage would be efficient if some form of reinforcement were incorporated in the crown region.

Using the specified terminating conditions and the approximate overall dimensions of the 145-10 radial tyre as a guide, meridional profiles for the full-sized and model carcasses were calculated using program BTPR (appendix IV). Using the meridional and circumferential tensions per unit length output by the program for an inflation pressure of 200 kPa, the products of wall thickness and shear modulus required around the profile to restrict growth to 5% were determined and are plotted against meridional angle in figure 5.9 for the full-sized 'B' series tyres. These data were used when specifying the required crown reinforcment.

To avoid the cost of different segmented cores for the various wall thicknesses, a common core based on the thinnest carcass was again used. Table IX, like table VIII for the 'A' series, shows that the errors introduced by this procedure were acceptable.

Table IX

Mid-Wall Dimensions of B1, B2 and B3 Carcasses

		Radius to Crown (mm)	Radius to Max. Width (mm)	Section Width (mm)
'B1' Carcass (3 mm)	:	224.0	174.2	139.4
'B2' Carcass (5.5 mm) drawn	:	225.3	174.2	142.1
calculated	:	225.3	174.7	142.2
'B3' Carcass (8 mm) drawn	:	226.5	174.2	144.6
calculated	:	226.5	174.1	144.7

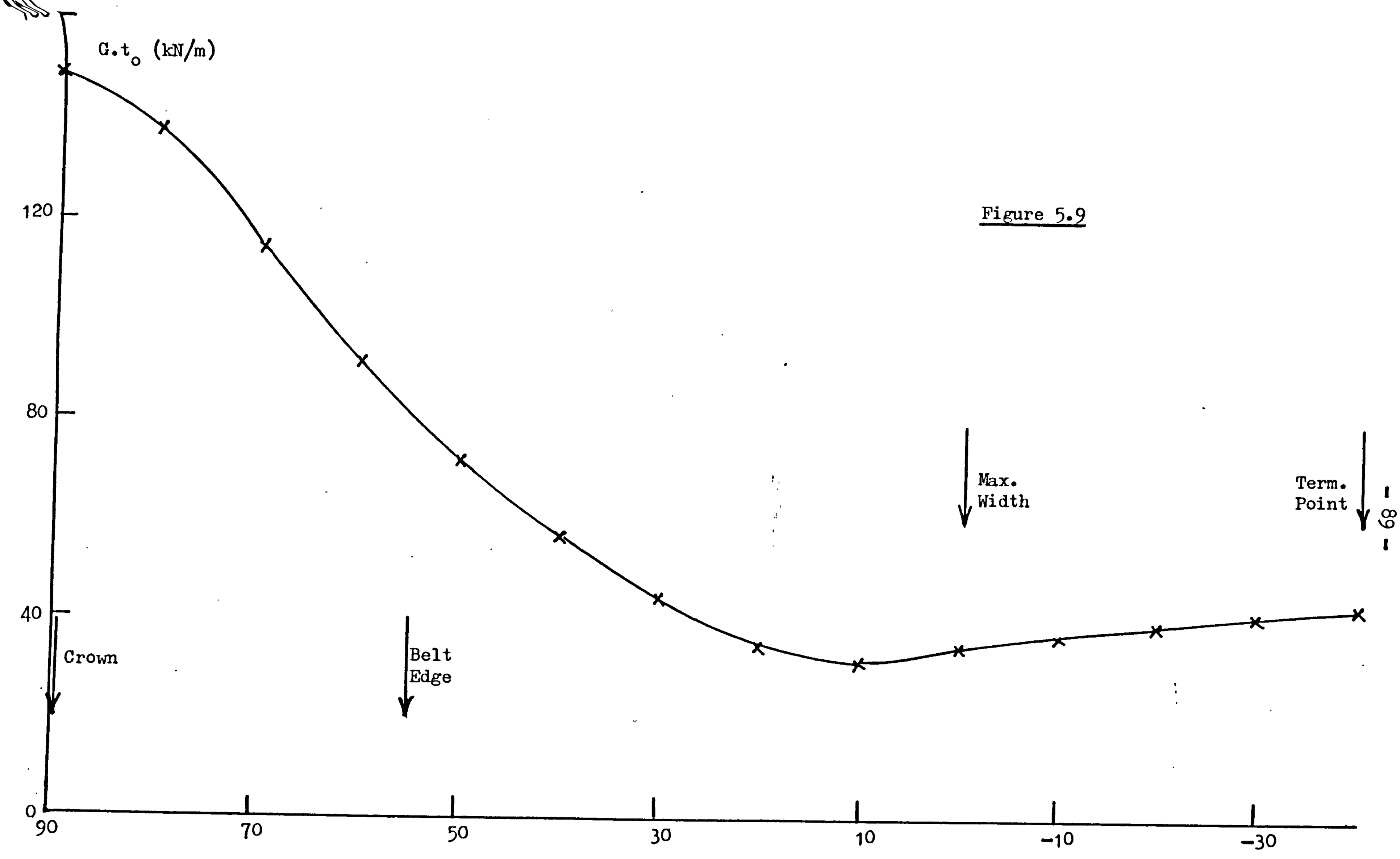
G.t$_o$ (kN/m)
120
80
40
0
Crown
Belt Edge
Max. Width
Term. Point
68
90
70
50
30
10
-10
-30
Meridional Angle (°)

Figure 5.9

The size nomenclatures chosen for the 'B' series were 143-10 for the full-sized tyres and 83-8 for the model tyres. Drawings of the complete 'A' and 'B' series tyres will be shown for comparison when the design of their treads has been described.

V.4.3 Tread profiles

As far as could be ascertained, no theoretical basis exists for deciding upon the cross-section of the tread of a pneumatic tyre. However, given the meridional profile of the carcass, two extremes can be identified, figures 5.10a and b. In the first the profile of the tread follows that of the carcass so that the tread depth is constant from the crown to the shoulder; whereas in the second, the tread profile is parallel to the tyre's axis and appears flat when the tyre is only inflated and not under load. Both extremes have their advantages and disadvantages.

The tread of uniform thickness, figure 5.10a, will suffer only compressive stresses when the tyre is under load and, because rubber compounds are virtually incompressible, the resulting strains are low. This behaviour is often represented by shape factors, a method of defining an increased modulus resulting from the geometry of the rubber component under consideration. Nevertheless, low strains mean low energy loss due to hysteresis so that tyres with this tread profile will have relatively low drag or rolling resistance. However the width of tread in contact with the road will depend upon the instantaneous radial deflection and this leads to difficulties when designing the tread pattern for water drainage.

The flat tread, figure 5.10b, gives a constant contact patch width whatever the radial force so that efficient tread patterns may be designed. Unfortunately, as the tyre deflects under load, the thick shoulder regions, where the misalignment of the tread and carcass profiles is the greatest, suffer significant shear as well as compressive strains. This leads to greater energy loss or drag. Moreover, because the shoulder regions restrict the freedom of the underlying carcass to flex, high radial reaction pressures are generated towards the edges of the contact patch. This leads to rapid and uneven wear.

Clearly, a compromise must be sought between the flat and profiled treads and, in addition, the width of the tread must be related to the section

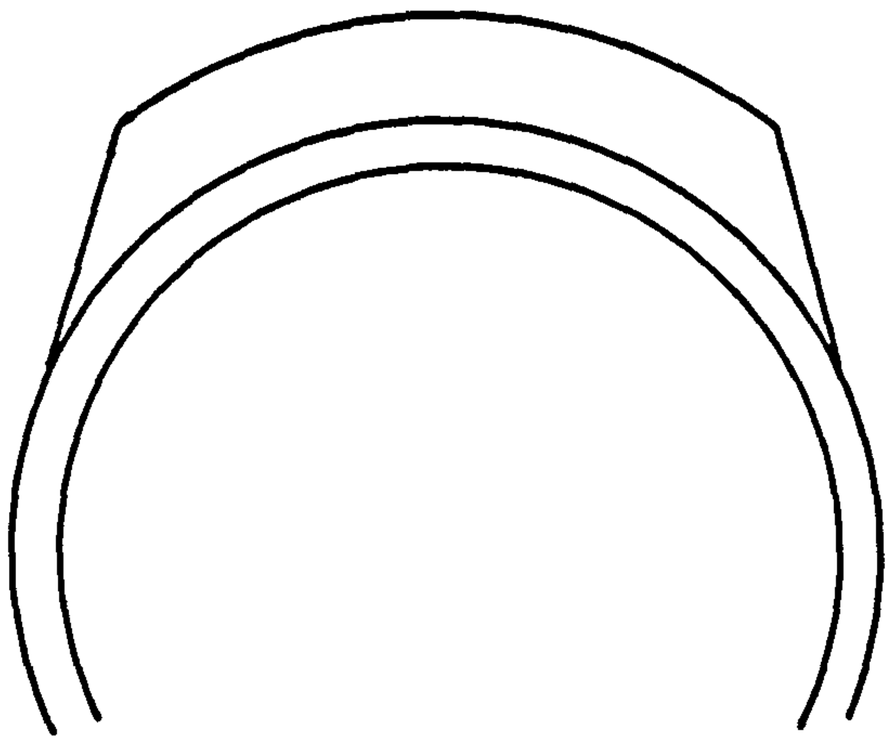

Figure 5.10a

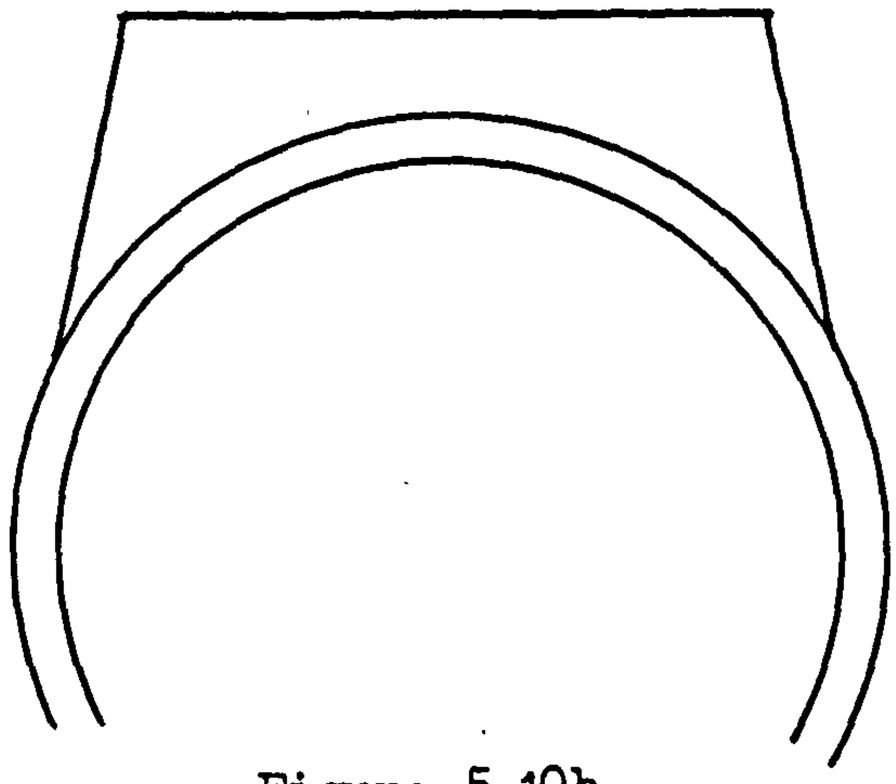

Figure 5.10b

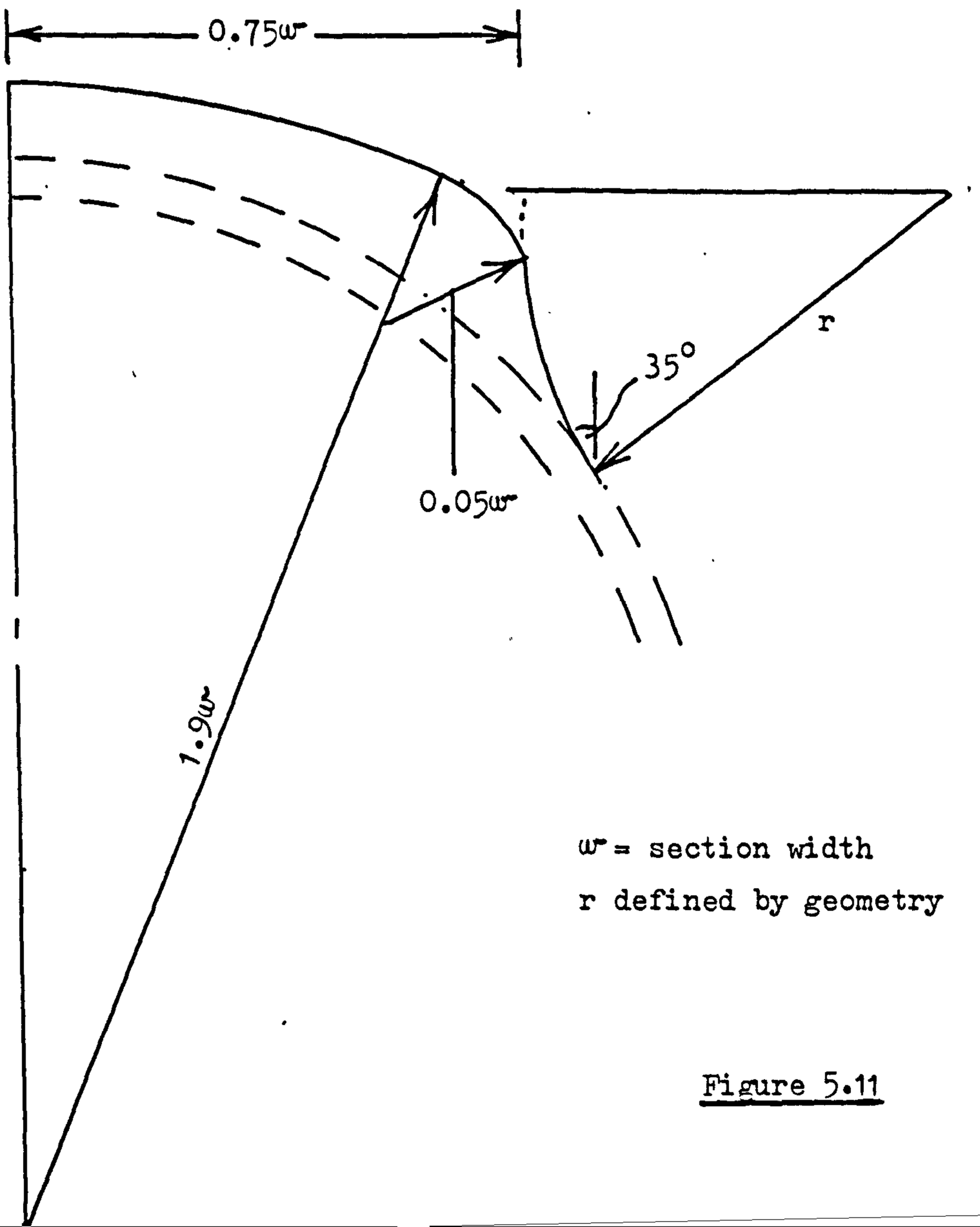

w = section width

r defined by geometry

Figure 5.11

width of the carcass. After discussing the problem with experienced tyre designers, the following empirical rules were established for this research.

(i) The radius of curvature of the tread profile should be 1.9 times the carcass section width (w).

(ii) The tread width should be 0.75 times the section width.

(iii) The tread profile should be chamfered at the shoulders using a radius of curvature about 0.05 times the section width.

(iv) The buttress of the tread, the portion from the tread edge to the sidewall, should be normal to the unchamfered edge and meet the sidewall where the meridian angle has fallen to 35^{o}.

The rules are illustrated in figure 5.11.

To accord with practice, the tread thicknesses at the crowns of the tyres were:

8.0 mm for the 126–10 'A' and 143–10 'B' tyres;

and 5.0 mm for the 73–8 'A' and 83–8 'B' model tyres.

No patterns were incorporated in the treads as these would add very significantly to the cost of the moulds. However they could be cut by hand using a hot knife should there be the need to conduct braking and handling tests on wet roads.

Although not part of the tread design per se, those for the 'B' series tyres, full-sized and model, were required to incorporate some reinforcement, primarily in the circumferential direction. This was achieved by using two plies of a rayon fabric, suitably topped with a rubber compound. It was cut at a bias angle of 20^{o} relative to the circumferential direction and laid as a balanced pair on the carcass prior to adding the tread. Its width was such that, on the 'B' series tyres, its edge was located at the meridional angle of 55^{o}, approximately below the shoulder of the tread. The tread thickness was reduced to accommodate this reinforcement which in radial tyres is known as the belt. It was biassed, rather than running circumferentially, to allow trellising when the tyres were distorted under load.

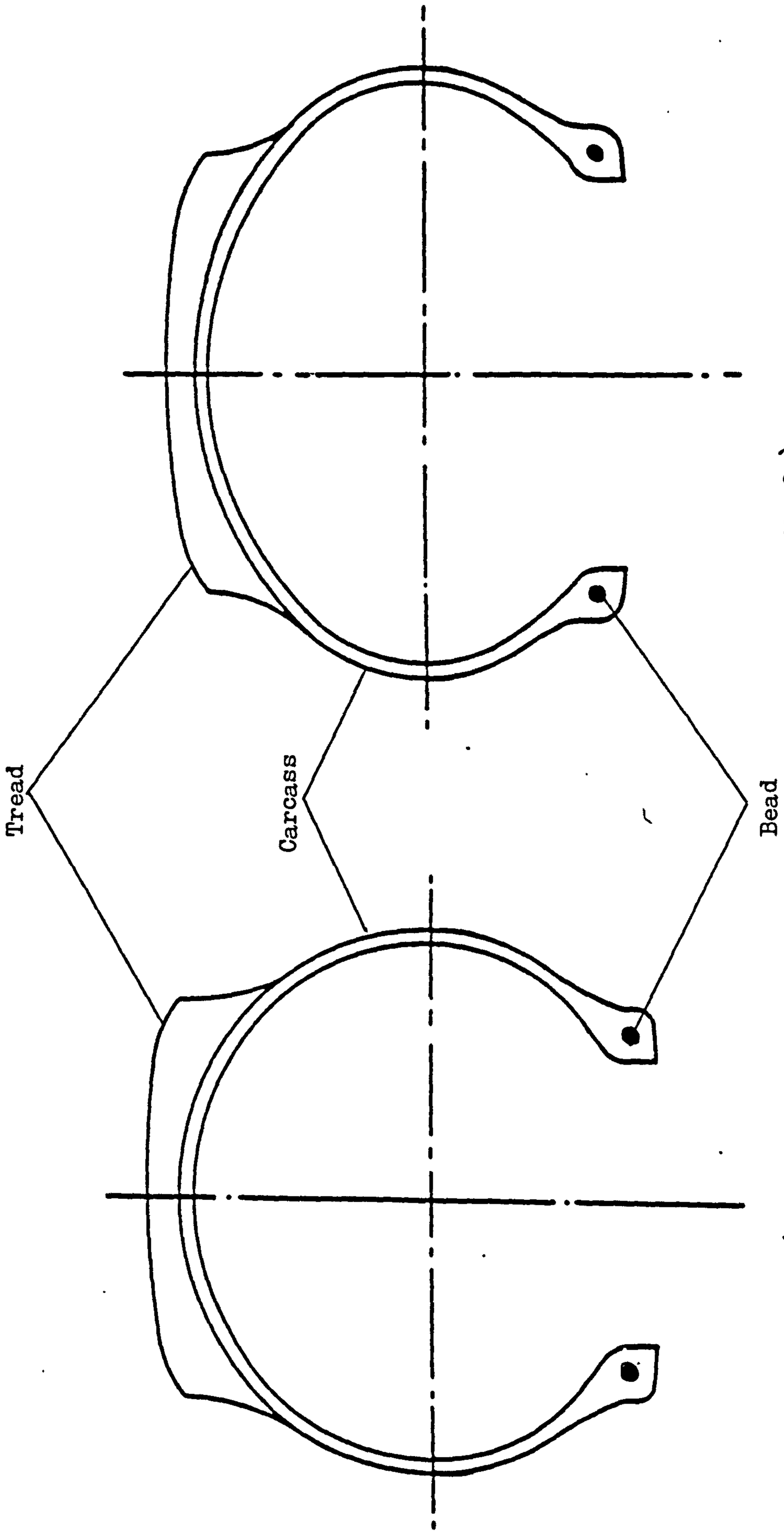

Figure 5.12

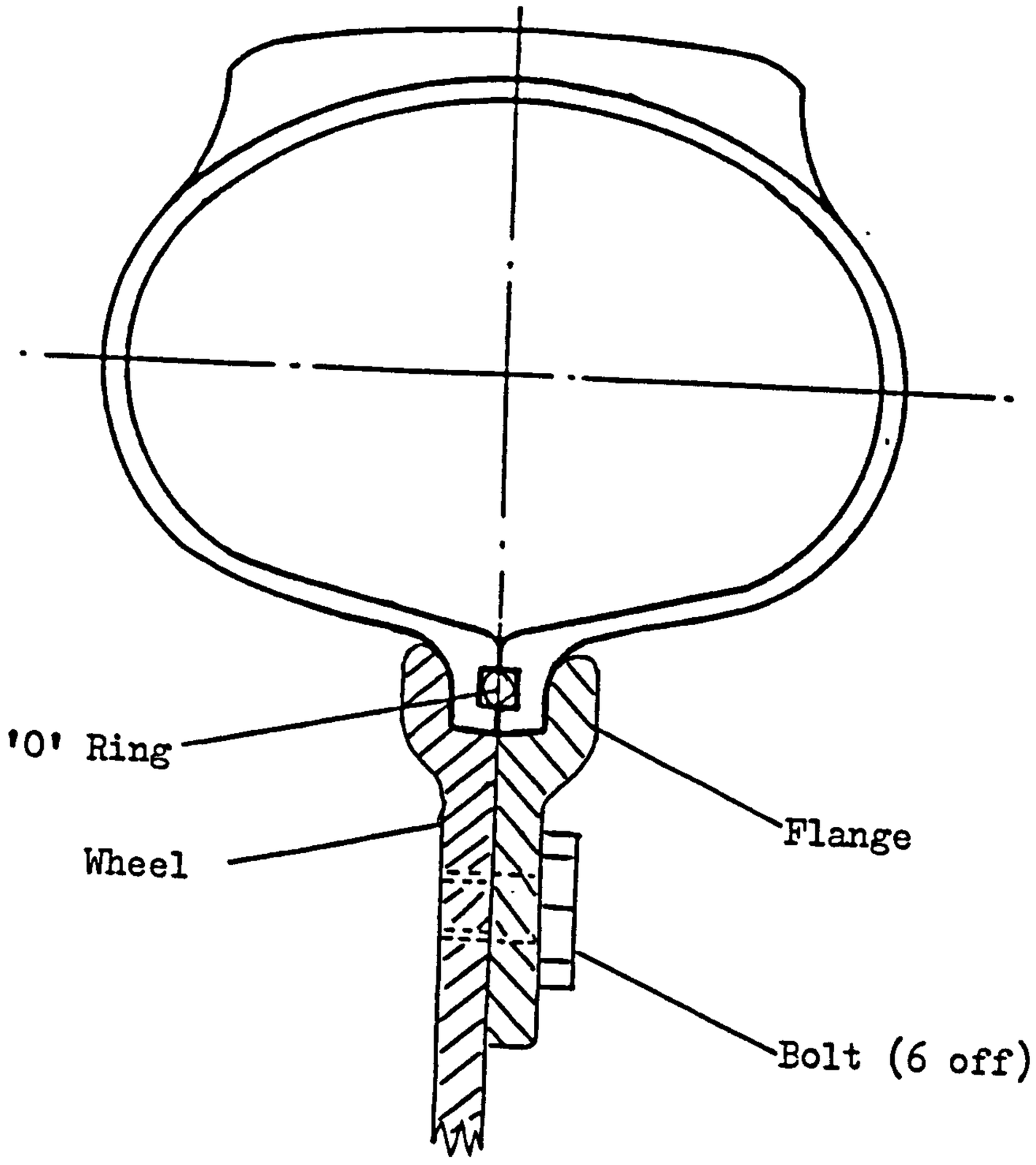

Figure 5.13

The profiles of the 'A' and 'B' series tyres, complete with their treads, are shown in figure 5.12 for comparison.

V.4.4 Series 'C' tyre carcass

The third and final tyre design chosen for investigation combined a number of features which, if successful, would have profound effects upon the future of fabricless tyres. First, it had no bead wires and would thus simplify manufacture considerably. To retain the tyre on the wheel the principle of the beaded edge was adapted which, as discussed in chapter I, was invented by Bartlett but finally gave way to the wired-on tyre still used today. However to avoid the use of a complicated rim, it was decided to bring the two bead regions together, the second feature, and to clamp them between flanges integral with the wheels, figure 5.13. To do this, the profile of the 83-8 B2 model tyre was extended using program BTPR until the sidewalls met on the centre line. Thus the meridian shape of the tyre, designated the 83-7 C, was still in equilibrium with the inflation pressure. Being, effectively, a low profile tyre, some reinforcement was necessary in the crown region like the 'B' series tyres. The same tread as the latter was fitted.

To seal the tyre for inflation, grooves were moulded in the "bead" regions where the two halves met so that a rubber 'O' ring could be inserted. Through this a short tube was positioned, connected to a conventional valve, to allow inflation.

The third distinguishing feature of the 83-7 C tyre was its method of manufacture. The two halves of the carcass were injected moulded separately from Hytrel and then joined by RF welding, see V.3.2.

V.5 Summary of Experimental Tyres to be Manufactured

The complete list of experimental tyres designed for the research is given in table X, together with their overall dimensions, carcass wall thickness, material type and rim size.

Table X

Experimental Tyres

	Tyre Designation	Overall Diameter (mm)	Section Width (mm)	Section Height (mm)	Wall Thickness (mm)	Carcass Material	Rim Size
	73–8 A1	331	71	64	1.2	Hytrel	2.0–8
*	73–8 A2	333	73	65	2.2	Hytrel	2.0–8
	83–8 B1	316	81	56	1.2	Hytrel	2.5–8
*	83–8 B2	318	83	57	2.2	Hytrel	2.5–8
*	83–7 C	318	83	65	2.2	Hytrel	0.5–7
*	126–10 A1	477	126	112	3.0	PU	3.5–10
*	126–10 A2	482	131	114	5.5	PU	3.5–10
*	126–10 A3	487	136	117	8.0	PU	3.5–10
	126–10 A4	478	127	112	3.5	Hytrel	3.5–10
*	143–10 B1	451	142	99	3.0	PU	4.5–10
*	143–10 B2	456	147	101	5.5	PU	4.5–10
*	143–10 B3	461	152	104	8.0	PU	4.5–10
	143–10 B4	452	143	99	3.5	Hytrel	4.5–10

As was stated before, owing to the limited size of shot from the injection moulding equipment, the 126–10 'A4' and 143–10 'B4' tyres were not suitable for testing dynamically. Also it proved too difficult to mould the thinner model tyres : the 73–8 'A1' and 83–8 'B1'. When the viscosity of the Hytrel was reduced sufficiently to cause adequate flow in the moulds, the material itself was degraded. Thus only the tyres marked with an asterisk in table X were available for the complete experimental programme.

CHAPTER VI. : ANALYSIS OF RADIAL STIFFNESS

VI.1 Introduction

It became apparent as the experimental work proceeded, described in the next chapters, that a method was required for analysing the radial stiffness of a pneumatic tyre. As discussed in chapter III, a tyre may be likened to a triaxial spring and, although all three modes are important, it is the radial mode which dominates the type of research being undertaken, when the technical feasibility of a radically different tyre design and construction is being assessed. The reason is that while the lateral and longitudinal stiffnesses require attention to give adequate wear resistance and handling, and to minimise vibration transmission, it is the radial stiffness which determines the distortions to which a tyre is subjected continuously as it rotates. If the resulting strain pattern cannot be accommodated by the design and the constituent materials, then fatigue will occur and the tyre may fail catastrophically.

Now the radial stiffness of a pneumatic tyre is a function of its design, the moduli of the materials used in its construction and, predominantly, the inflation pressure. Moreover it has been recognised for many years that the total stiffness is the sum of structural and pneumatic components, the former arising from inherent stiffness of the carcass. However, methods of analysis have been empirical in nature and have not taken into account the mechanics of how a tyre develops a radial force to oppose the axle load.

An example of a purely empirical approach is given in reference 17, where it is reported that the load, W, carried by aircraft tyres is related to the radial deflection, d, by equation (1).

$$\frac{W}{(p + 0.08p_r)\ w\sqrt{wD}} = f\left(\frac{d}{w}\right) \qquad (1)$$

where p is the inflation pressure;

$0.08p_r$ results from the effective carcass stiffness;

w is the tyre's section width;

and D is its overall diameter.

Moreover, if loads and pressures are limited to those close to the rated

operating conditions, the form of the function on the right hand side of equation (1) leads the simple relationship:

$$W = kpd^2 \qquad (2)$$

where k is a constant for a particular tyre.

Clearly, equations (1) and (2) are of little use in a fundamental study because they lead to neither a simple method of analysis nor an understanding of tyre behaviour.

A more suitable form of analysis is contained in reference 18 and is based upon the well known graphical method known as the carpet or Gough plot, after a pioneer of tyre mechanics Dr V.E. Gough. Figure 6.1 shows the form of a Gough plot and it may be drawn after the load-deflection curves of a tyre have been measured for a series of inflation pressures. The inflation pressure p_1 is the highest used and its load-deflection curve is constructed through the origin of the plot. The curve for next, lower, pressure p_2 is then constructed but with its origin displaced along the abscissa by an amount proportional to $(p_1 - p_2)$. Subsequently, the curves at pressures p_3 and p_4 are constructed displaced by $(p_1 - p_3)$ and $(p_1 - p_4)$ respectively. One is now able to join points of equal deflection to give the lines labelled d_1, d_2, d_3 and d_4. Thus on a single plot is is possible to judge load versus deflection at constant pressure and load versus pressure at constant deflection.

The work described in reference 18 recognised that the lines of load versus pressure are usually linear. It also assumed that the lines of load versus deflection at constant pressure would be linear apart from pronounced curvature at low deflections, as shown in figure 6.2. Thus an empirical equation was developed which recognised the two components of radial stiffness, structural and pneumatic, but did not depend upon an understanding of the mechanics involved. The equation is:

$$W = p\left[d - d_o\left(1 - \exp\left(-\frac{d}{d_o}\right)\right)\right] K_p + d\,K_s \qquad (3)$$

where K_s is the structural stiffness;
K_p was termed the pneumatic stiffness;
and d_o is a constant to account for the curvature at low deflection.

Figure 6.1

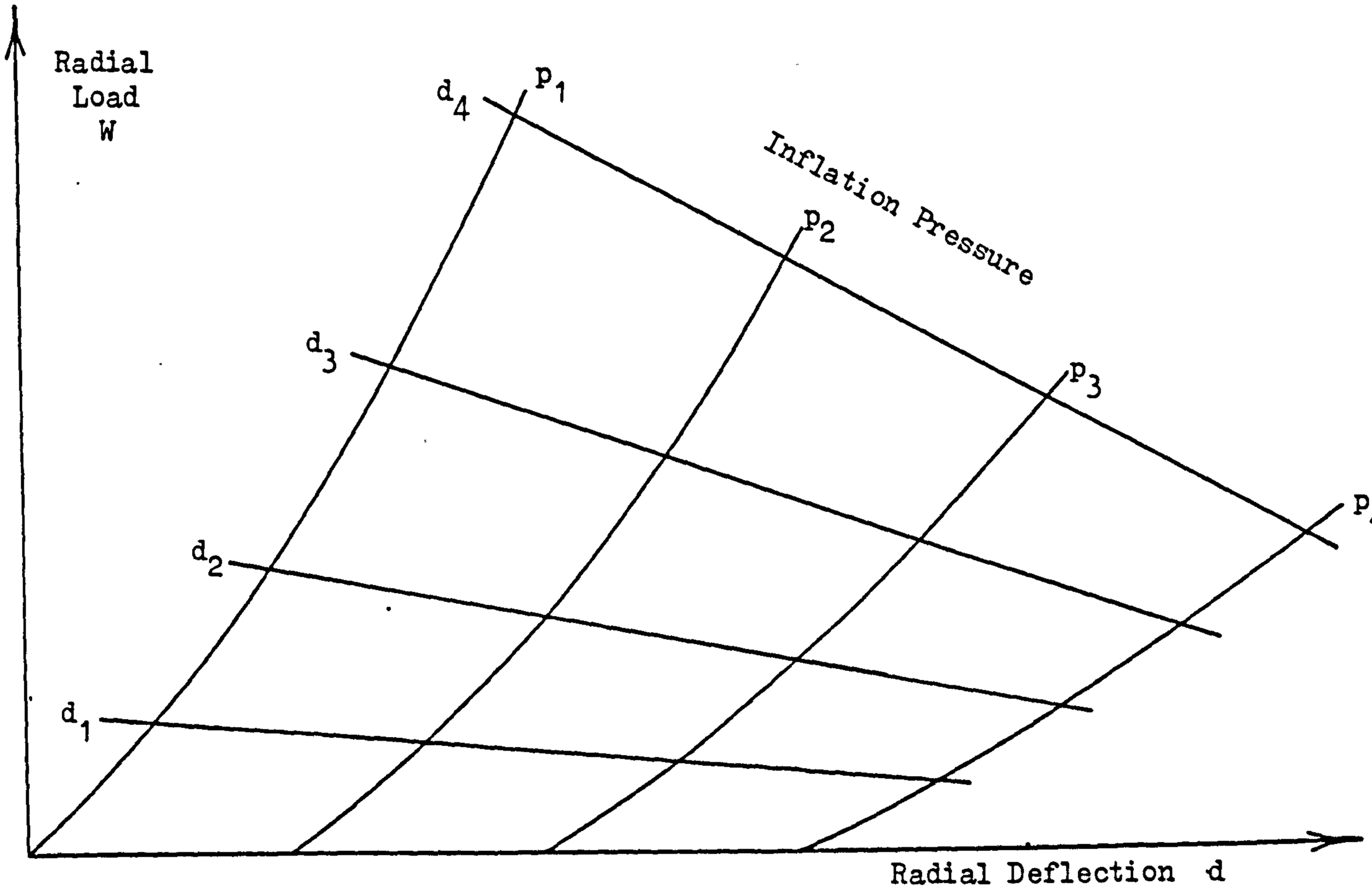

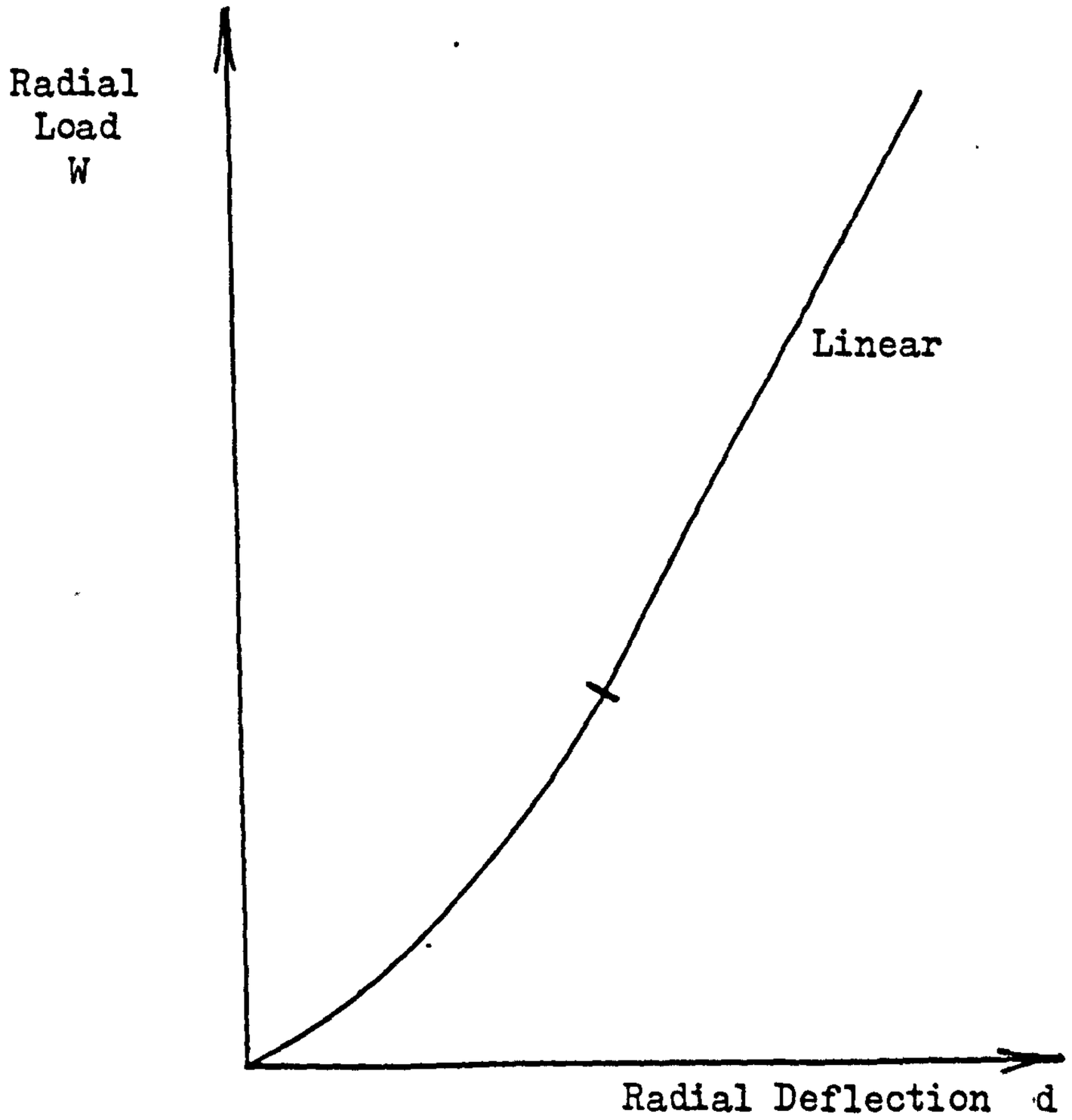

Figure 6.2

When cross-biassed tyres of different sizes, from cycle to truck tyres, were examined, it was found that the pneumatic "stiffness", K_p, was approximately proportional to the square root of the product of the tyre's diameter and section width:

$$K_p \propto \sqrt{wD}$$

However, overall, this approach makes assumptions about radial stiffness characteristics which are not necessarily correct and the form of equation (3) is not ideal for developing a method of analysis which characterises the behaviour of a tyre and separates the pneumatic and structural components.

VI.2 The Pneumatic Component of Stiffness

The mechanics of how a pneumatic tyre carries a radial load are not widely appreciated and have received only scant attention in the literature (reference 19). It is usually tacitly assumed that when a tyre is inflated it behaves like a balloon; in fact cycle tyres with a wide section are often referred to as "balloon tyres". However, this is misleading and, in order to develop a method for analysing radial stiffness, it is necessary to consider basic principles.

Ignoring the structural component of stiffness which, although complex, can be readily appreciated as resulting from the bending of a shell-like body with varying curvatures, consider a tyre's pneumatic behaviour. If its carcass is represented as a flexible but inextensible membrane then, when inflated, tensions are induced and these act on the bead wires. On a cross-section of the complete tyre, the result of the tension on the bead wires may be shown as vector forces, F_T, per unit circumference, figure 6.3. In addition the inflation pressure, p, acts directly on the rim of the wheel. Suppose the tyre is now deflected radially by a load applied to the axle. The pressure increase in the tyre will be small, because there will be little change in contained volume, and it will continue to act upon the rim uniformly around its circumference. Thus the pressure per se is not contributing directly to the load carrying mechanism. What does happen is that the tensions induced in the carcass in the zone of the contact patch are modified and, more importantly, the vector forces on the bead wires change their direction, F'_T, figure 6.4.

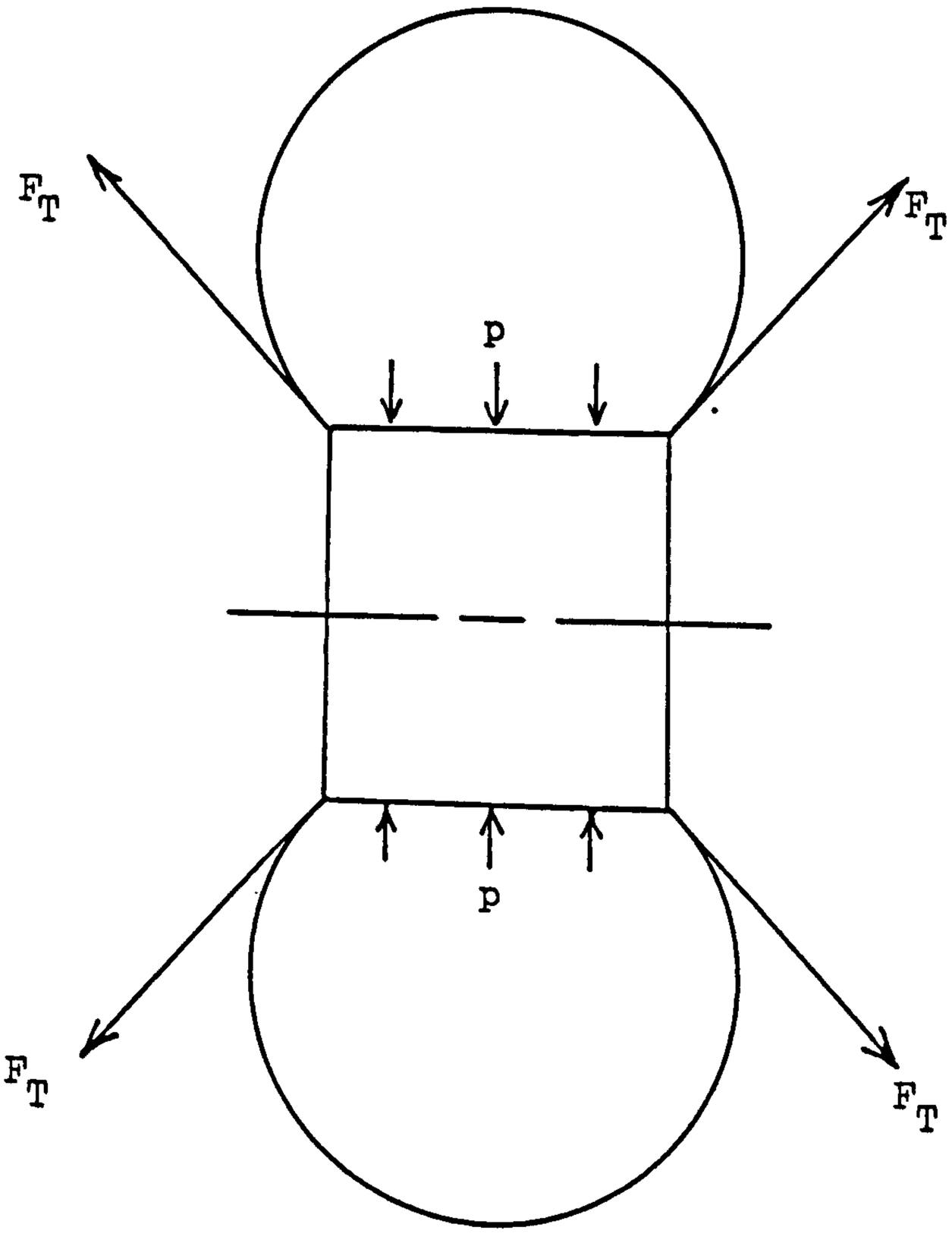

Figure 6.3

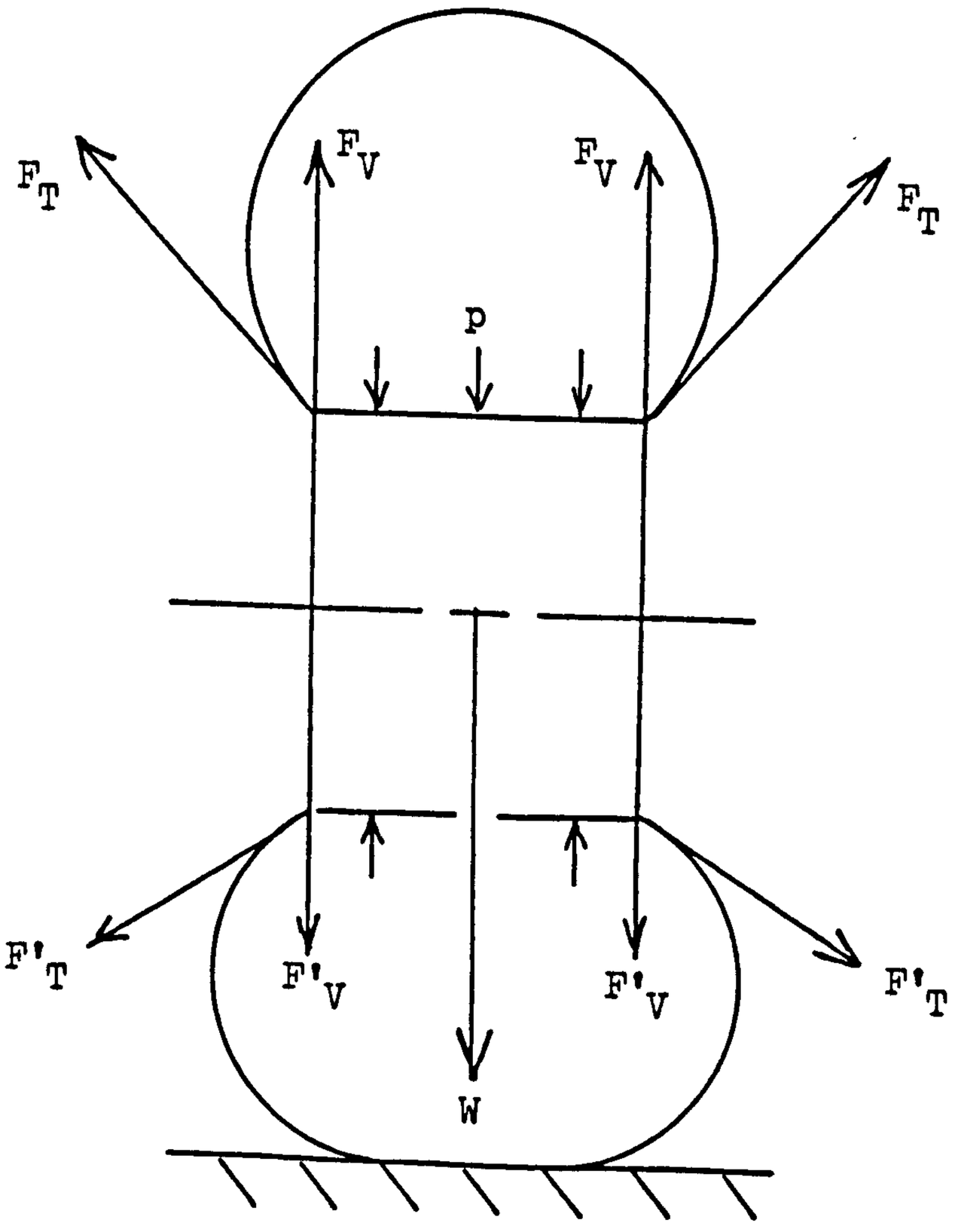

Figure 6.4

When the vector forces are resolved into vertical and horizontal components, these are completely balanced in the case of free inflation, figure 6.3. With the imposition of a radial deflection, the horizontal components remain balanced but the vertical components, F_V and F'_V, result in a net upward force, figure 6.4. In the sense that the vertical components at the top of the tyre are unchanged but those at the bottom adjacent to the contact patch are diminished, it may be said that the axle load, W, hangs from the top of the tyre.

Thus it may be seen that the interaction between a tyre and the rim on which it is fitted does not resemble the behaviour of a balloon. With the latter, the pressure over the area of a contacting surface directly opposes the applied load. If a tyre were a flexible membrane, the latter mechanism would occur where it makes contact with the road but the presence of the tread means that such a simple situation never occurs and the mean contact pressure is always significantly greater than the inflation pressure.

VI.3 Investigation of Pneumatic Stiffness

Before developing an expression which represents the radial behaviour of a pneumatic tyre adequately and which is based upon the mechanism by which a radial force is developed, it was decided that the explanation given in the last section should be tested by experiment. Thus the objective was to relate the measured pneumatic radial stiffness of a tyre to calculated changes in its meridional profile and associated tensions.

The basis of the calculations was the membrane theory described in chapter IV, although this is only applicable, strictly, to the freely inflated, axisymmetrical body. A radially loaded and deflected tyre is no longer axisymmetrical and with all conventional tyres and, indeed, the fabricless tyres of this research, there exist significant interactions between adjacent meridional sections because :

the carcass has a corded, biassed construction;

it is fitted with a circumferential belt;

or the material is isotropic.

Consequently it was necessary to use a very simple tyre construction in which the interactions were minimal; while, at the same time, it would be advantageous to keep the structural radial stiffness as low as possible so that measurements of pneumatic radial stiffness would be less prone to error. A construction which meets these criteria is a radial, single ply carcass with no belt and no tread.

Remembering that the mechanism put forward to account for pneumatic stiffness is related to modifications of the carcass tension and to changes in meridional angle at the beads in the zone of the contact patch, the next consideration was how to vary these two parameters without the need to build a range of tyres, each of which would require its own mould. The solution was to build a single tyre and fit it to wheels of different widths. By altering the bead separation in this way, the effect would be to change the meridional profile and the tensions induced by free inflation.

VI.3.1 Experimental work

To manufacture the tyre, a mould for a model tyre, designated 87-8 60S, was available. This is a low profile tyre with an aspect ratio of 60%, a width of about 87 mm and is fitted to an 8" OD wheel. The carcass was built in the usual way except that the turn-up of the single radial ply was made as short as possible. The fabric used was rayon. Also the outer rubber components, the tread and sidewall strips, were made from butyl so that, after moulding, they could be stripped from the carcass. This is possible because of the very poor adhesion between butyl and the natural rubber forming the topping of the ply.

The specially prepared tyre was fitted in turn to wheels with four different well widths to give the following assemblies.

Assembly	Well Width (mm)
'RA'	29
'RB'	49
'RC'	65
'RD'	81

In each case it was inflated and maintained at pressures (p) of 50, 100, 150 and 200 kPa, by permanently attaching an air supply with valves and a pressure gauge to the inner tube fitted to the tyre, while careful measurements of radial load (W) versus radial deflection (d) were made. A standard, laboratory Instron machine was used for this purpose.

The resulting carpet plot for assembly 'RC', typical of all four, is shown in figure 6.5. As may be seen, the load-pressure lines at deflections of 2 mm to 12 mm in 2 mm steps, when the loads were read from the Instron

Figure 6.5

Assembly 'RC'

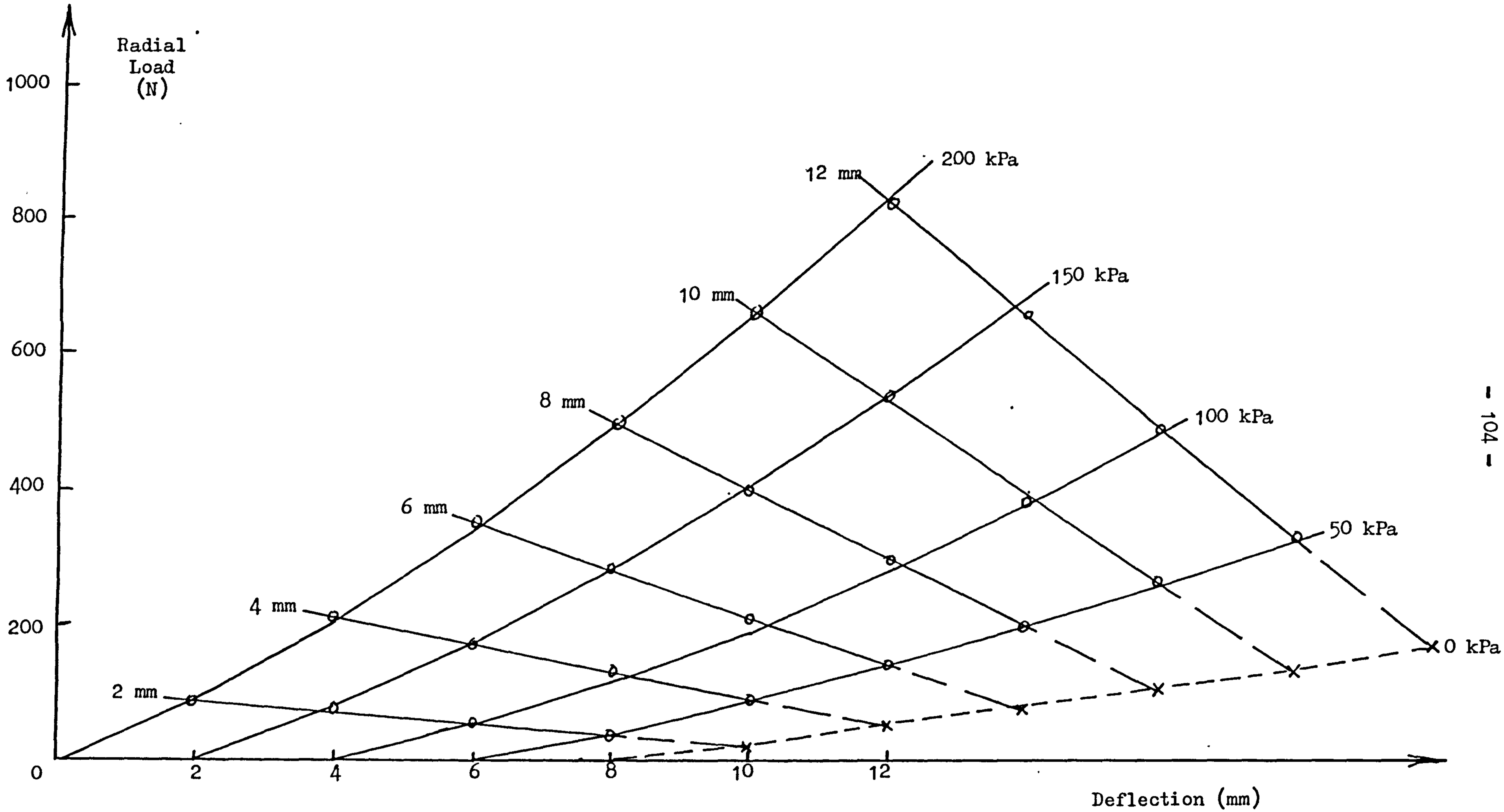

Figure 6.6

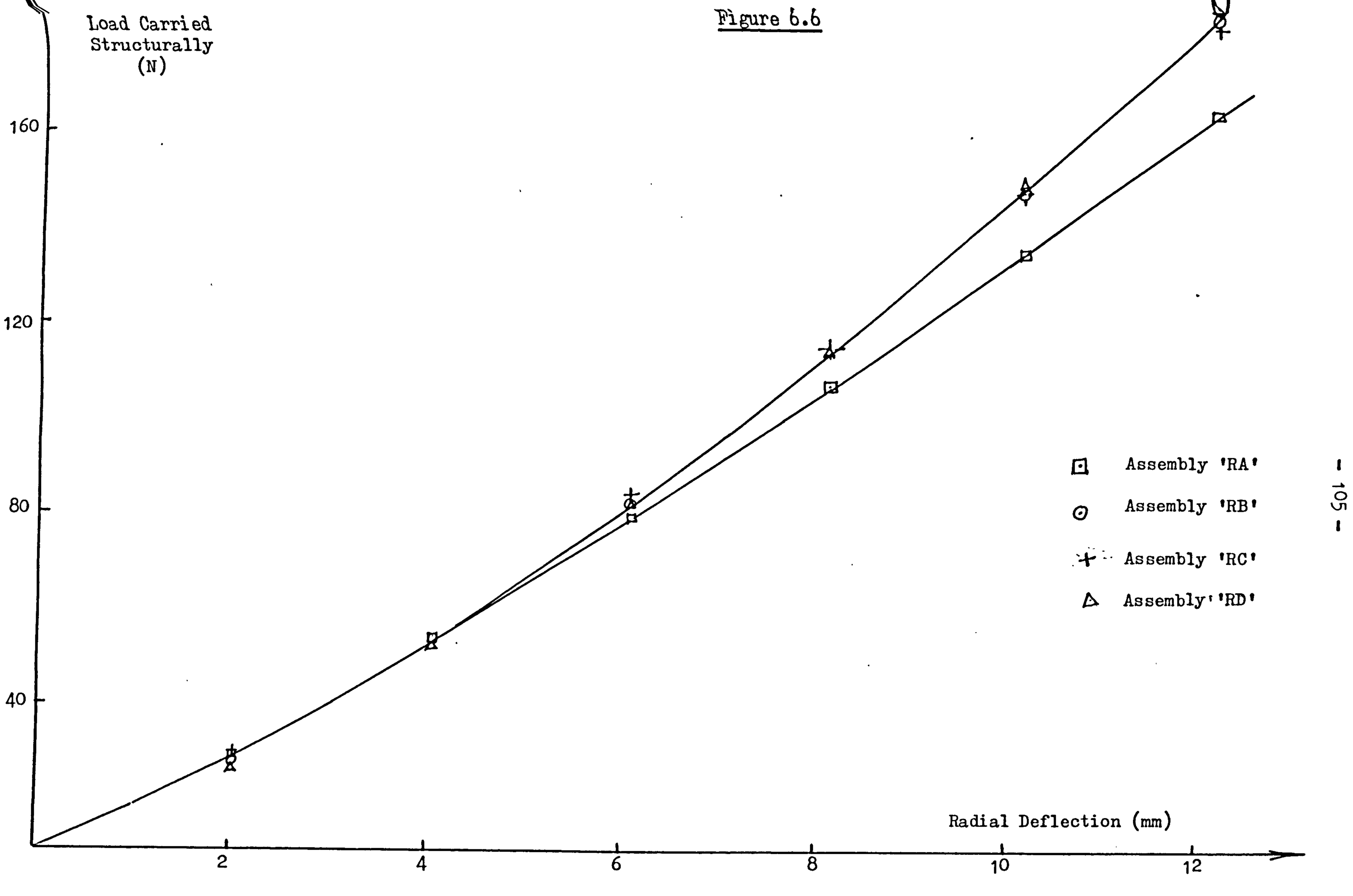
Load Carried Structurally (N)
160
120
80
40
2
4
6
8
10
12
Radial Deflection (mm)
Assembly 'RA'
Assembly 'RB'
Assembly 'RC'
Assembly 'RD'

Figure 6.7

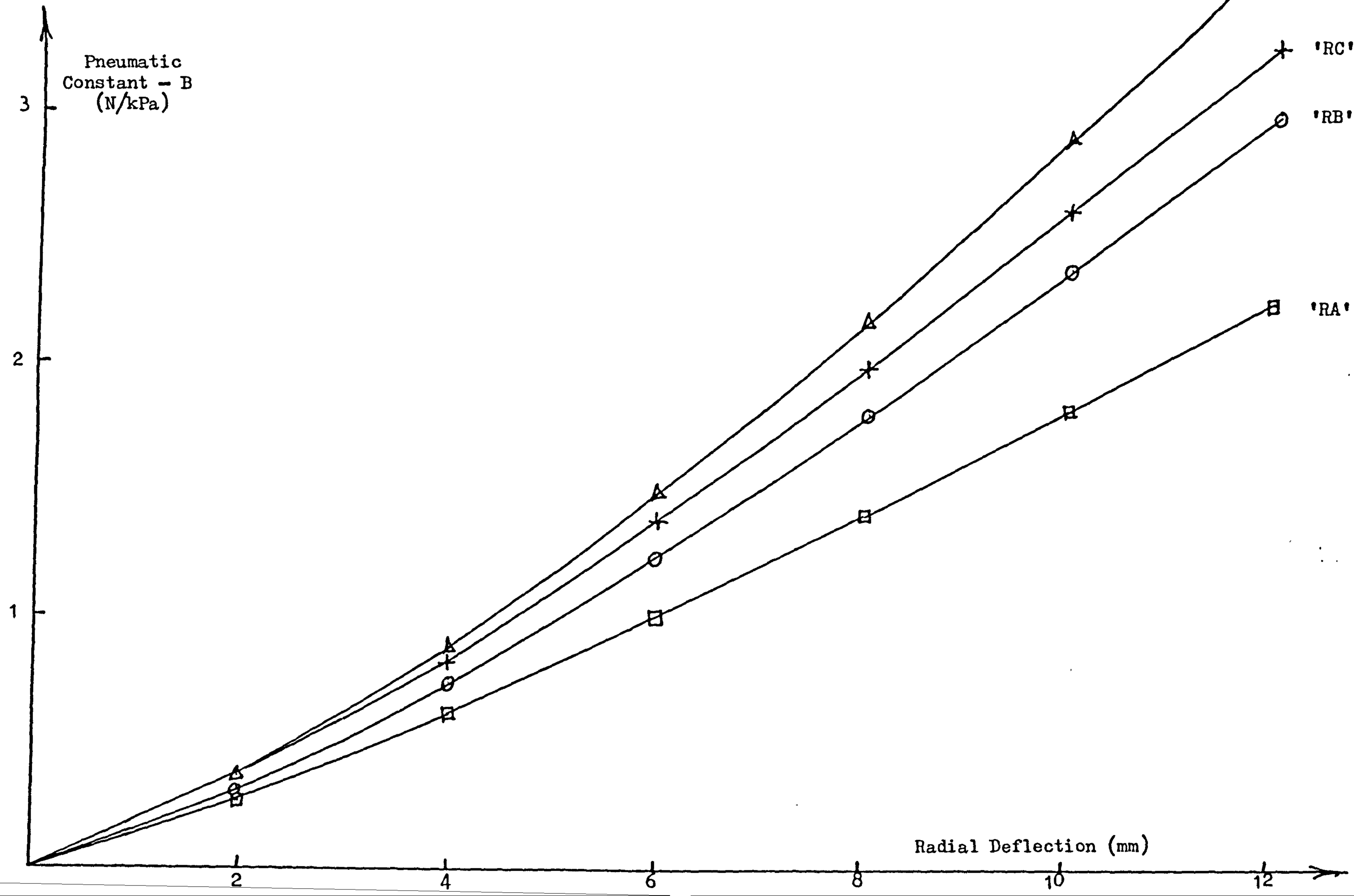
Pneumatic
Constant - B
(N/kPa)
3
2
1
'RC'
'RB'
'RA'
2
4
6
8
10
12
Radial Deflection (mm)

chart, are linear. Thus at each deflection, the total load carried may be expressed as:

$$W = A + B.p \qquad (4)$$

Moreover, the structural stiffness, obtained by extrapolating the load-pressure lines to p = 0, is small compared to the pneumatic component.

In figure 6.6, the values of A from equation (4), that is the loads carried structurally, are plotted against radial deflection for the four assemblies. It may be seen that the values for 'RB', 'RC' and 'RD' are very similar, while those for assembly 'RA' diverge somewhat. However, at the greatest deflection of 12 mm, the difference is only 20 N compared to total loads exceeding 800 N. Thus the assemblies have low structural stiffness, as required, and the effect of well width on this component is negligible.

The values of the pneumatic constant B, in units of N/kPa, are plotted against deflection in figure 6.7. A clear pattern of behaviour is exhibited with B rising progressively as the well width is increased, assemblies 'RA' to 'RD'. The ratio of the change from the lowest to the highest is about 1 to 1.6, which was sufficient to encourage the comparison with theory.

VI.3.2 Theoretical modelling

The calculations carried out were, basically, those described in IV.2.3.3 but with the bias angle (α_o in equation (15) of chapter IV) put equal to 90^o in order to represent the radial carcass. Moreover, because the circumferential tension per unit length would be zero for this case, there would be no interaction between adjacent meridional sections so that the theory developed for axisymmetrical bodies could be applied.

The computer program used for the calculations was based on the one listed in appendix IV but included an iterative procedure involving the user. At the commencement of a run, the following four fundamental parameters are displayed on the computer terminal and can be changed by use of the keyboard:

ρ_o, the radius to the crown;
ρ_m, the radius to the point of maximum width;
α_o, the bias angle at the crown, maintained constant at 90^o;
and β, the terminating meridional angle, as defined in IV.2.3.3.

When the user is satisfied with the values he has chosen for these parameters, the computer program calculates the equilibrium profile and outputs the following data on the terminal:

w_s, the section width;
ρ_b, the radius to the terminating point;
w_b, the "bead" separation at the terminating point;
and l_m, the cord length from terminating point to terminating point which, for $\alpha_o = 90^o$, is the same as the meridional length.

All the above parameters are shown on a diagram of a radial ply profile in figure 6.8. Thus if the user knows the values of:

1) the bias angle, 90^o;
2) the cord length, l_m;
3) the radius to the terminating point, ρ_b;
and 4) the "bead" separation at the terminating point, w_b;

the complete profile can be defined by adjusting the input variables: ρ_o, ρ_m and β; until the required values of l_m, ρ_b and w_b are obtained.

As explained in chapter V, the terminating point does not coincide with the actual bead wires because of both the interference of the rim of the wheel and the stiffness resulting from the ply turn-up. By examination of the carcass used for the experiments, the terminating radius (ρ_b) was put equal to 110 mm for all four assemblies, while the effective bead separations (w_b or s_3 in figure 5.7) was 3 mm greater than the well widths listed previously. The cord length, or meridional length (l_m), was measured as 150 mm.

With these data, the computer program was used to calculate the freely inflated profile of the radial carcass when mounted on the four wheels of different widths. The intention was to match the required parameters to within ∓ 0.1 mm but in the case of the cord length ∓ 2 mm had to be accepted because of inherent errors in the calculations. The values of the input and output parameters are listed in table XI, w_s being the section width at $\rho = \rho_m$.

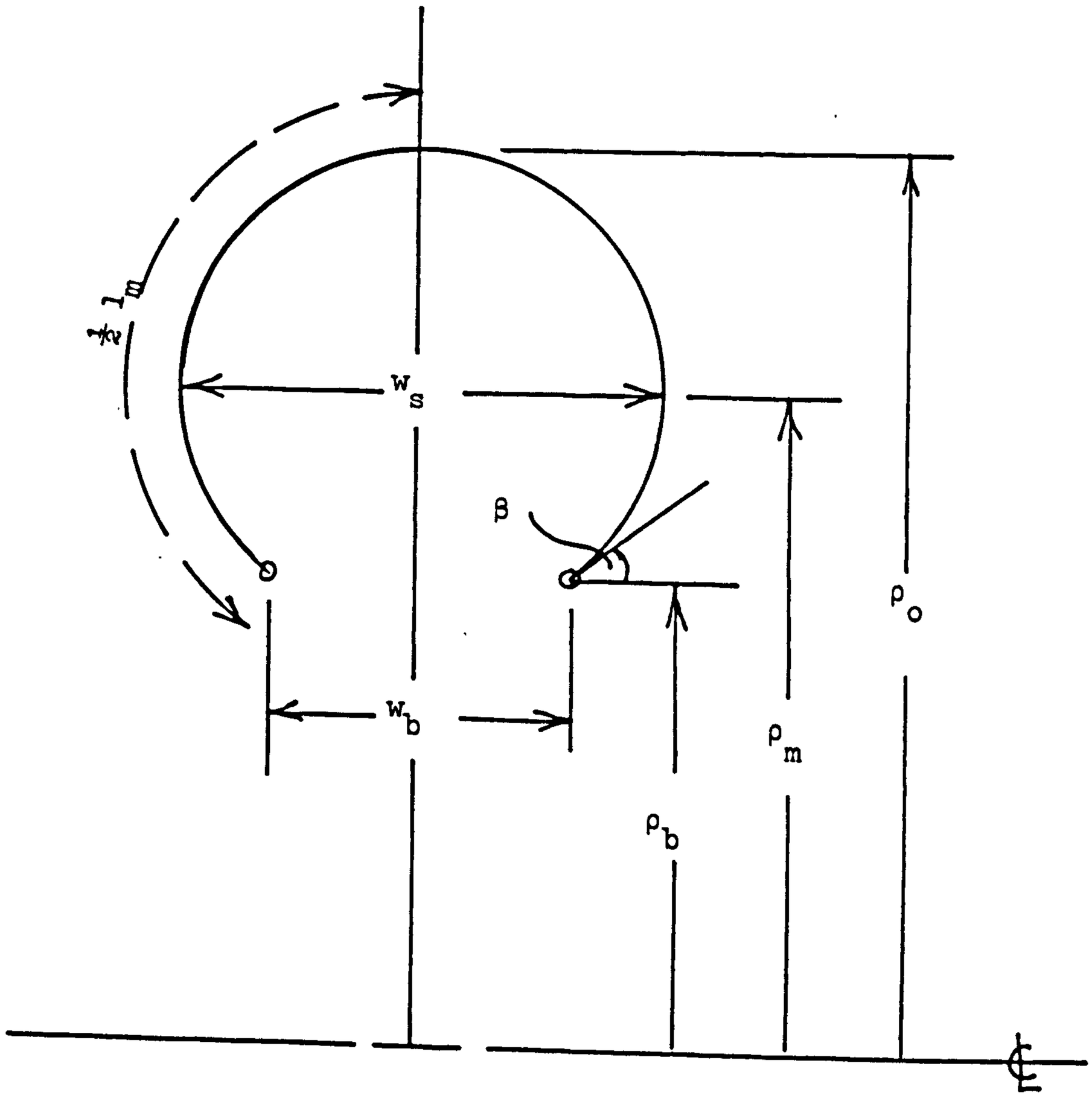

Figure 6.8

Table XI

Radial Carcass/Wheel Assemblies (Freely Inflated)

Assembly	Well Width (mm)	Input ρ_o (mm)	Input ρ_m (mm)	Input β (°)	Output w_s (mm)	Output ρ_b (mm)	Output w_b (mm)	Output l_m (mm)
'RA'	29	165.9	136.4	43	55.8	110.0	31.9	149.8
'RB'	49	166.5	132.0	59	64.6	110.1	52.1	150.9
'RC'	65	164.5	125.0	72	73.1	110.0	68.2	150.0
'RD'	81	162.5	116.0	84	84.6	110.0	83.9	151.4
Required values:						110.0	*	150.0

* Well width + 3 mm ie. 32, 52, 68, and 84 mm.

There is little upon which to comment in table XI except that the profiles were all successfully generated. However it is interesting to note that the radius to the crown (ρ_o) is a maximum for an intermediate well width, assembly 'RB'; while the radius to the point of maximum width (ρ_m) shows the greatest change. The four profiles are illustrated in figure 6.9.

To calculate the profiles when radially deflected, it was decided to limit the exercise to one deflection, 10 mm, at the centre of the contact patch. However, it was necessary to make use of the computer program just described in a different way and this is illustrated by figure 6.10.

When the profile is deflected by d, a new effective radius to the crown, ρ_o', is immediately defined:

$$\rho_o' = \rho_o - d$$

but the width of the contact patch, w_c is not known. Thus, values of ρ_m, ρ_m', and β, β', must be sought so that:

$$l_m - l_m' = w_c = w_b - w_b' \qquad (5)$$

where l_m' is the new cord length output by the program, equal to 2.C'T, and w_b' is the new effective "bead" separation at the terminating point, which is still defined by ρ_b. This relationship is, of course, unique to a radial ply tyre where the cords follow a meridian.

The parameters for both the freely inflated, F, and deflected, D, assemblies are listed in table XII, together with the differences given by equation (5).

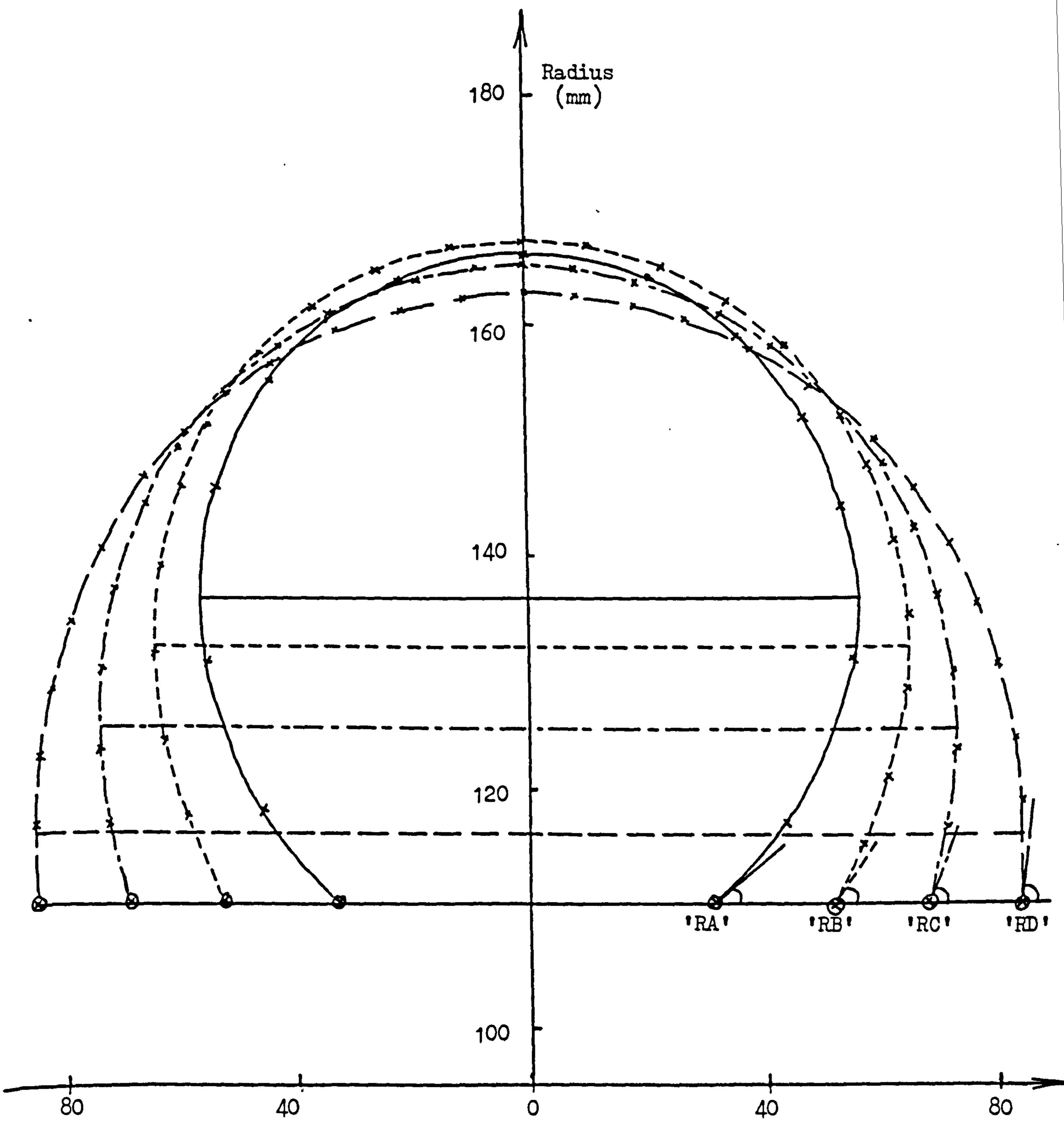

Figure 6.9 Freely Inflated Assemblies

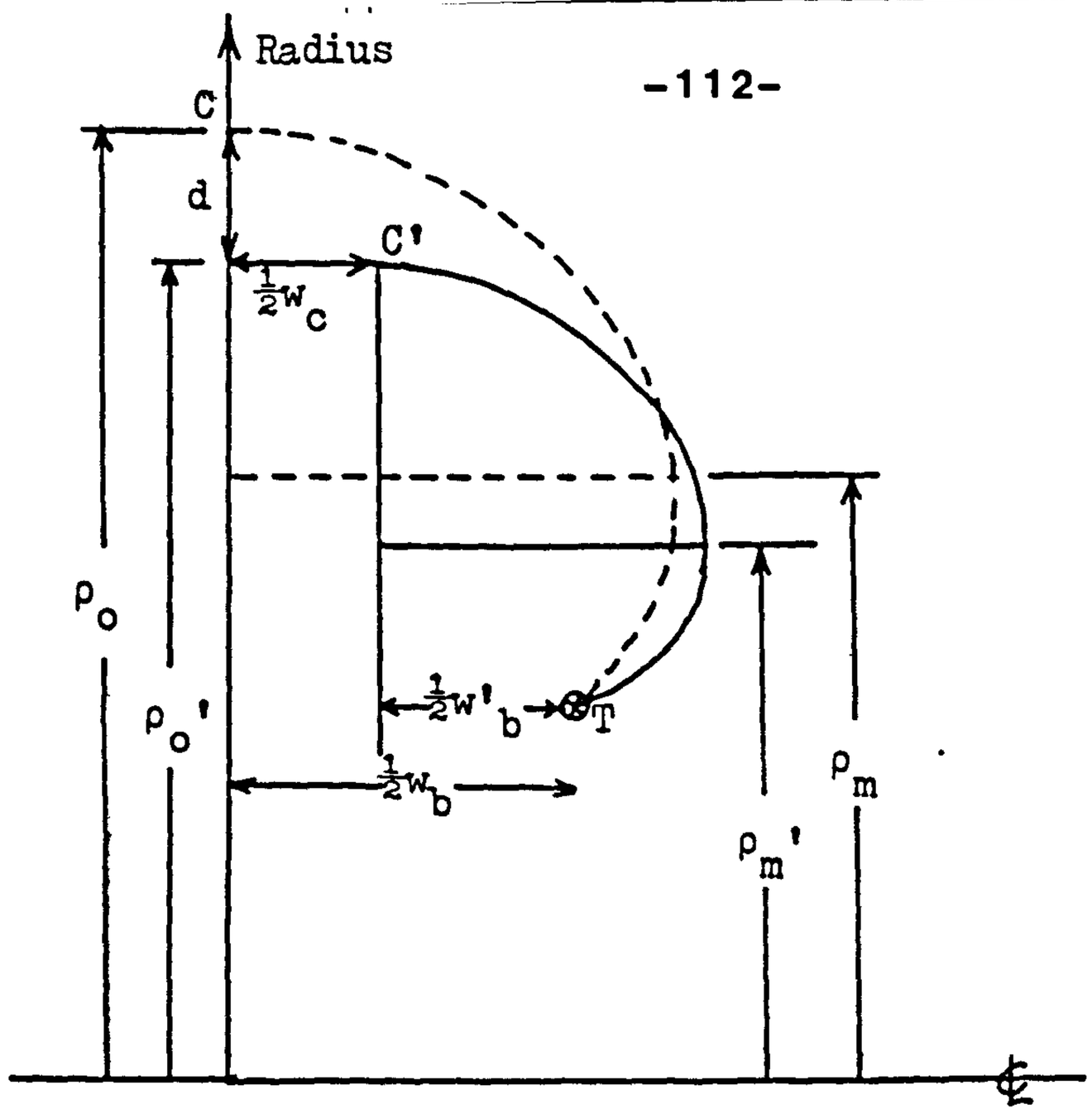

Figure 6.10

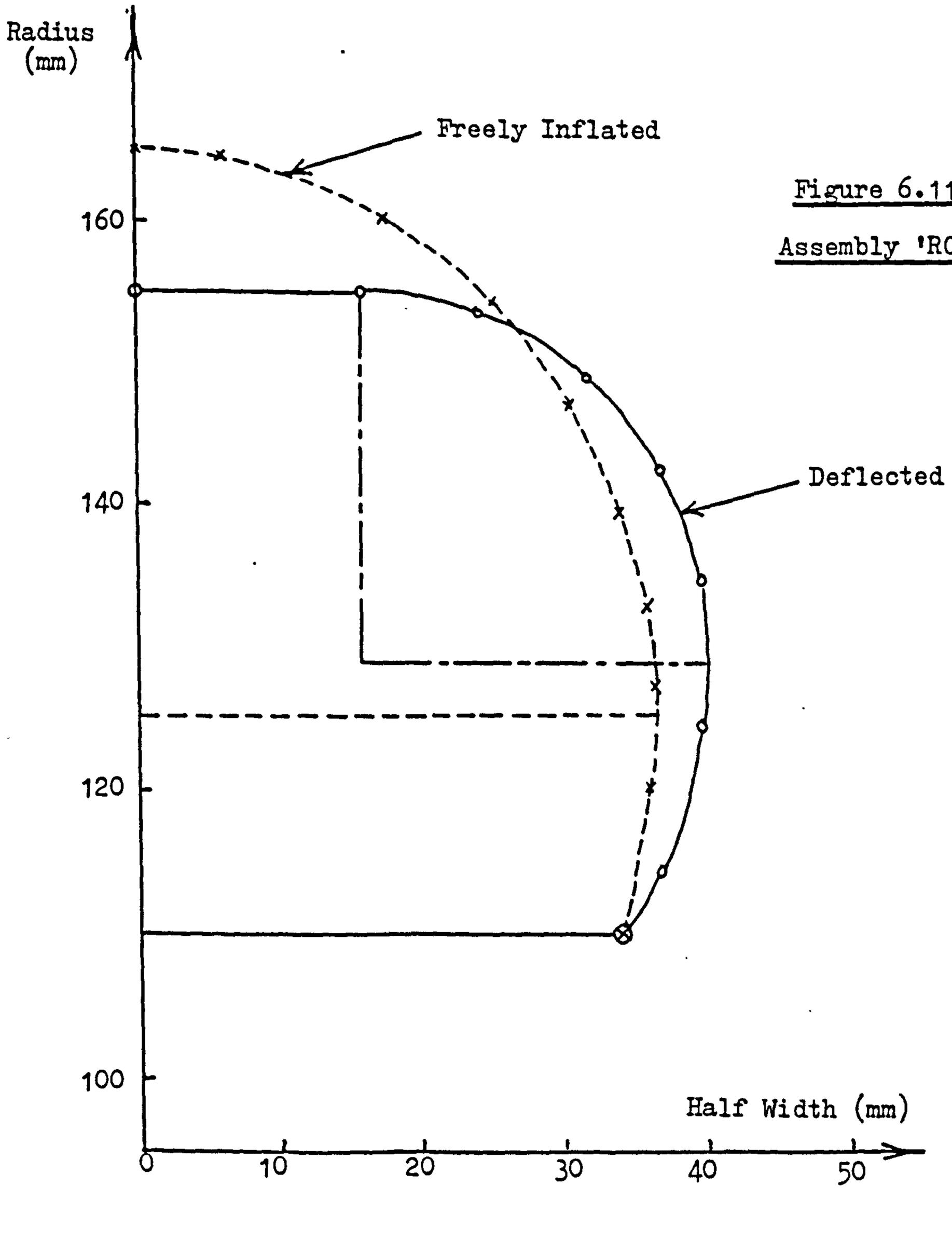

Figure 6.11

Assembly 'RC'

Table XII

Radial Carcass/Wheel Assemblies (Inflated and Deflected)

Assembly	Input			Output			
	ρ_o, ρ_o' (mm)	ρ_m, ρ_m' (mm)	β, β' (°)	w_s, w_s' (mm)	ρ_b (mm)	w_b, w_b' (mm)	l_m, l_m' (mm)
'RA' F	165.9	136.4	43	55.8	110.0	31.9	149.8
D	155.9	133.8	25	63.5	110.1	10.7	128.1
	10.0					21.2	21.7
'RB' F	166.5	132.0	59	64.6	110.1	52.1	150.9
D	156.5	132.1	41	72.8	110.2	25.8	124.7
	10.0					26.3	26.2
'RC' F	164.5	125.0	72	73.1	110.0	68.2	150.0
D	154.5	128.6	53	80.9	110.1	36.4	119.0
	10.0					31.8	31.0
'RD' F	162.5	116.0	84	84.6	110.0	83.9	151.4
D	152.5	123.5	67	89.5	110.1	49.0	115.9
	10.0					34.9	35.5

An example of a deflected profile, where it is compared to the freely inflated condition, is shown in figure 6.11 for the assembly "RC".

Some interesting trends emerge from table XII. For the assembly with the narrowest well width, 'RA', the radius to the point of maximum width (ρ_m) decreases as the tyre is deflected; while for the three wider wells ρ_m increases, the more the wider the wheel well. However, of greater importance to this study is the effect the changes have on the meridional tension per unit length. Now in a radial carcass, the cord tension, T, is constant around the meridian, that is it is a geodesic construction, and is given by:

$$T = \frac{\pi p \, (\rho_o^2 - \rho_m^2)}{n}$$

where p is the inflation pressure;
and n is the total number of cords in the carcass.

Consequently, the meridional tension per unit length at the terminating radius is:

$$N_m = \frac{Tn}{2\pi\rho_b} = \frac{p(\rho_o^2 - \rho_m^2)}{2\rho_b}$$

It follows that the radial component of this tension is $N_m \sin\beta$, which was calculated and is listed in table XIII with p = 200 kPa for the freely inflated and deflected conditions.

Table XIII

Radial Component of Meridional Tension

Assembly	Freely Inflated			Deflected (10 mm)		
	N_m (kN/m)	β (°)	$N_m \sin\beta$ (kN/m)	N_m (kN/m)	β (°)	$N_m \sin\beta$ (kN/m)
'RA'	8.11	43	5.53	5.82	25	2.46
'RB'	9.36	59	8.02	6.40	41	4.20
'RC'	10.40	72	9.89	6.67	53	5.33
'RD'	11.77	84	11.71	7.28	67	7.60

It may be seen that the reductions in the radial component of the meridional tension per unit width from the freely inflated to the deflected condition at the centre of the contact patch are due to changes in both the tension and the terminating angle.

With reference to figure 6.4 and noting that, with the particular carcass construction being modelled, the deflected zone will be virtually confined to the segment defined by the contact patch length, it may be inferred that the radial load carried pneumatically by the assemblies should be proportional to:

$$(N_m \sin\beta)_i - (N_m \sin\beta)_d = \Delta(N_m \sin\beta)$$

where the subscripts i and d refer to the inflated and deflected conditions respectively.

These differences, from table XIII, are:

assembly 'RA'	3.07 kN/m
assembly 'RB'	3.82 kN/m
assembly 'RC'	4.56 kN/m
assembly 'RD'	5.01 kN/m

and are plotted in figure 6.12 against the experimentally measured values of the pneumatic constant B, for the deflection of 10 mm. A straight line

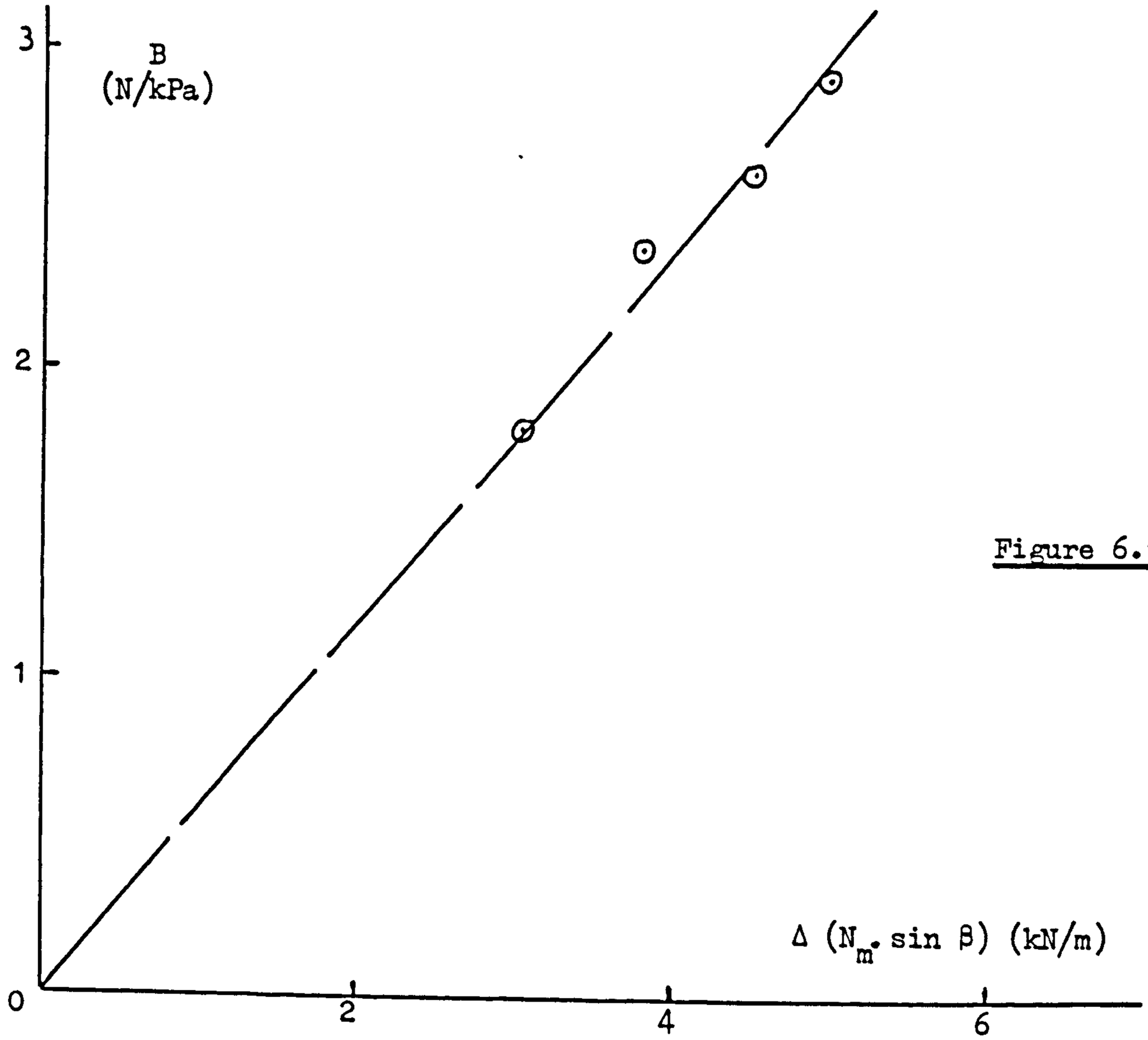

Figure 6.12

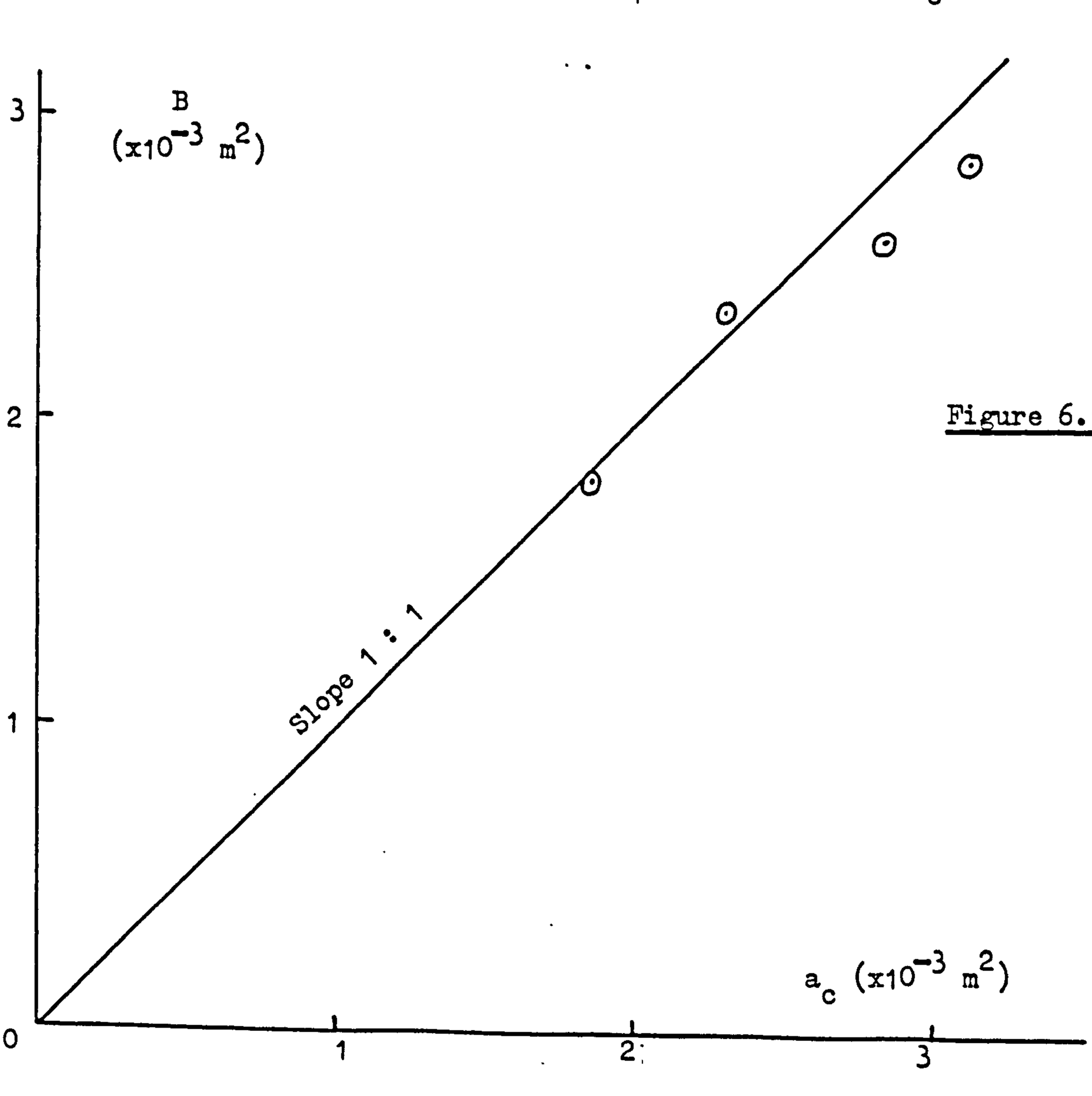

Figure 6.13

may be drawn through the points and the origin showing that the theoretical predictions are directly proportional to the load carried pneumatically by the four assemblies.

To be able to conclude that the results of this experimental and theoretical exercise support the explanation of how a pneumatic tyre develops a radial force to oppose the load, section VI.2, it is necessary to predict the load carried. However, to do this by calculating the radial components of tension on the beads throughout the lengths of the contact patches would be difficult because, although tensions per unit length are determined, the inflation pressure is actually contained by a finite number of textile cords and their spacing is not known within the contact zone. Consequently, an alternative approach was taken.

From the measured characteristics of the four assemblies, the constant B for each radial deflection gave the load carried pneumatically per unit inflation pressure, thus the units N/kPa. The latter, of course, may be simplified to square metres when divided by 10^3 so that B is also a measure of the area of the contact patch of this flexible carcass. Now the computer modelling gave the width of the contact patch, w_c, figure 6.10 and 6.11, and an estimate of its length (l_c) can be made from the known height (d) and radius (ρ_o) of a segment representing the deflected zone of the assemblies, ie:

$$l_c = 2.[\rho_o^2 - (\rho_o - d)^2]^{\frac{1}{2}}$$

If the reasonable assumption is then made that the contact patch is elliptical, its area, a_c, is given by:

$$a_c = \pi\, w_c\, l_c/4$$

The results of these calculated are given in table XIV.

Table XIV

Measured and Calculated Contact Patch Areas

Assembly	Width (w_c) (mm)	Length (l_c) (mm)	Area (a_c) (m^2)	B (m^2)
'RA'	21	113	$1.86.10^{-3}$	$1.82.10^{-3}$
'RB'	26	114	$2.31.10^{-3}$	$2.38.10^{-3}$
'RC'	32	113	$2.84.10^{-3}$	$2.62.10^{-3}$
'RD'	35	112	$3.11.10^{-3}$	$2.91.10^{-3}$

From the two final columns of table XIV, the agreement between theory and experiment is good and this is reinforced by figure 6.13.

To summarise, this investigation validated the qualitative description of how a pneumatic tyre carries load as the result of its being inflated. It was then possible to proceed with the examination of a range of tyre sizes as the next step in developing a general analytical expression suitable for characterising radial stiffness.

VI.4 Examination of a Range of Cross-biassed Tyres

As explained in the last section, the method of analysis developed for radial stiffness is only applicable to a tyre construction with little or no mechanical coupling between adjacent meridional sections. Thus it cannot be used for conventional cross-biassed and radial tyres. However the general approach may be followed and in appendix VI a simplified analysis is used to derive the following equation relating load, W, to radial deflection, d, and the inflation pressure, p:

$$W = \left[3.77\ k + \frac{5.66\ p}{\gamma}\right] R^{\frac{1}{2}}\ d^{3/2} \qquad (6)$$

where R is the overall radius;

k is a structural spring rate;

and $\gamma = \tan^{-1} \sqrt{[(w/w')^2 - 1]}$

with w = the tyre's section width,

and w' = the rim width.

This equation implies that:

at constant radial deflection, the load carried increases linearly with the inflation pressure;

at constant inflation pressure, load increases with deflection raised to the power of 1.5;

for tyres of different sizes, the load is proportional to the square root of the overall radius and is a function of the tyre and rim widths.

To establish whether the equation may be used to represent a range of tyre sizes, data for cross-biassed tyres were extracted from tables published by Dunlop Ltd. in 1965 (reference 20). These were chosen because, at that time, the variety of sizes was much greater than is currently available. Also the data themselves came from a single source, whereas similar data are now collated through the European Tyre and Rim Technical Organisation (ETRTO)

and take into account tyres from different manufacturers.

In tables of dimensional data, the following are listed:

overall diameter, giving the radius R;
axle height under load which, when subtracted from R, gives the radial deflection d;
tyre width, w;
and rim width, w'.

Other tables specify the schedule loads for a range of inflation pressures and are constructed from results taken at the deflection, d, in the dimensional data for each tyre size. Thus the load-pressure data are in the form:

$$W = A + B.p$$

so that, knowing W v. p, A and B were calculated and compared to equation (6), with:

$$A \equiv 3.77\ R^{\frac{1}{2}}d^{3/2} = f_1$$

$$\text{and } B \equiv 5.66\ \frac{R^{\frac{1}{2}}d^{3/2}}{\gamma} = f_2$$

Table XV lists the extracted dimensional data, together with the values of the angle γ, calculated from the tyre and rim widths, and the two functions f_1 and f_2 given above. Also included are the parameters A and B derived from the load-pressure data. A total of 17 tyres are represented from size 4.40 - 10 to 8.90 - 15, all being designated as "4 ply-rating" and having a similar construction. The Imperial units of the original data have been converted to S.I.

Table XV

Data for Cross-biassed Tyres

Size	Radius R (mm)	Section Width w (mm)	Rim Width w' (mm)	Angle γ (rad)	Radial Defl. d (mm)	f_1 $\times 10^{-3}$ (m^2)	f_2 $\times 10^{-3}$ (m^2)	A (kN)	B $\times 10^{-3}$ (m^2)
4.40–10	234	110	76	0.81	15	3.35	6.2	0.65	6.2
5.20–10	253	131	76	0.95	17	4.20	6.6	0.83	8.6
5.60–12	283	146	102	0.80	19	5.25	9.9	0.98	9.7
5.20–13	290	140	102	0.76	20	5.74	11.3	1.02	10.1
5.90–13	309	150	102	0.82	20	5.93	10.9	1.22	14.0
6.40–13	319	163	114	0.80	22	6.95	13.0	1.42	15.6
6.70–13	330	169	114	0.83	22	7.07	12.8	1.58	16.1
7.50–13	331	185	127	0.81	25	8.57	15.9	1.78	15.0
5.20–14	305	133	89	0.84	21	6.34	11.3	1.15	10.5
6.40–14	330	160	114	0.78	21	6.59	12.7	1.49	16.1
7.00–14	337	178	127	0.77	25	8.65	16.9	1.67	21.0
8.50–14	362	208	152	0.75	27	10.06	20.1	2.16	15.7
5.60–15	327	145	102	0.79	21	6.56	12.5	1.36	12.9
6.40–15	346	163	114	0.80	24	8.24	15.4	1.63	15.7
7.10–15	364	182	127	0.80	26	9.54	17.9	1.92	19.0
8.20–15	383	212	152	0.77	30	12.12	23.6	2.29	24.2
8.90–15	398	232	165	0.78	29	11.75	22.6	2.62	24.1

Figure 6.14 is a plot of the parameter A, which is the structural stiffness constant of a tyre, against the function f_1. As may be seen, the results cluster around a straight line passing through the origin, the slope of which gives the constant k, defined in appendix VI as the spring rate of a tyre's sidewall per unit circumferential length. Its value is 208 kN/m/m.

Figure 6.15 is a similar plot with the pneumatic stiffness parameter B compared to the function f_2. Now f_2 contains no unknown terms so that a direct comparison may be made between measurements and calculations. The straight line in figure 6.15 is for a 1 : 1 relationship and, allowing for some scatter, the agreement is good.

It may thus be concluded that equation (5) represents the behaviour of the range of cross-biassed tyres examined, both in terms of their structural and pneumatic stiffnesses.

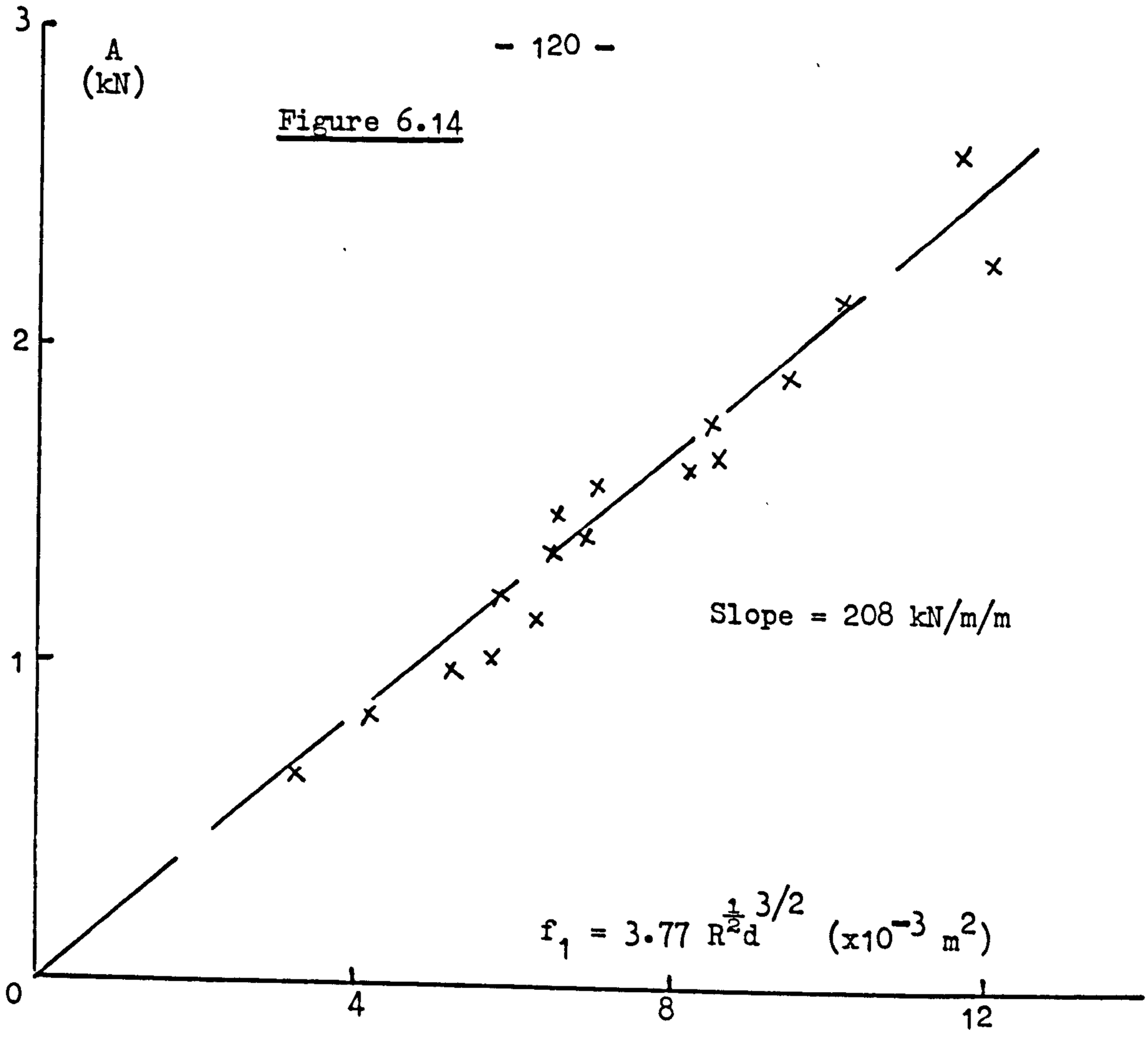

Figure 6.14

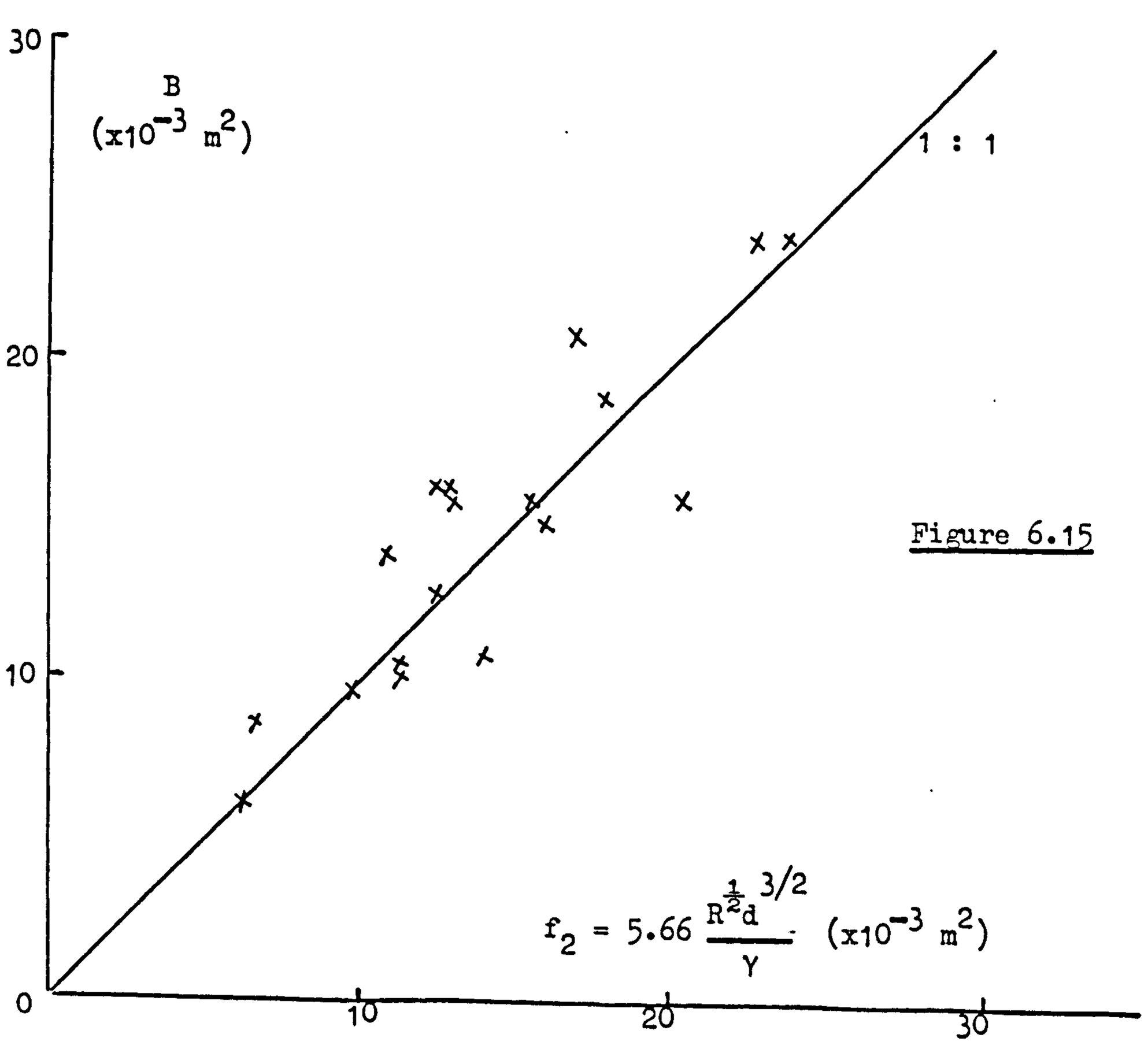

Figure 6.15

VI.5 Development of Simplified Equation and Analysis

It may be observed from table XV that the angle γ, which is a function of the section and rim width, does not vary much from the smallest to the largest tyre. This might be expected because tyres with a large section width are fitted to wide rims, and vice versa. Also the spring rate, k, does not vary from tyre to tyre. Consequently, equation (5) may be simplified to:

$$W = (A + B.p)\, R^{\frac{1}{2}} d^{3/2} \qquad (7)$$

where the parameters A and B now incorporate γ and k.

The dependence of load carrying on tyre size, as represented by the overall radius R, is clearly important to the general study of tyres but, for the purposes of this research, may be ignored because the comparisons to be made between fabricless tyres concern carcass wall thickness and, as will be seen, material modulus. Thus, by again modifying A and B, the above equation (7) may now be written as:

$$W = (A + B.p)\, d^{3/2} \qquad (8)$$

There then remains the question of whether $d^{3/2}$ accurately represents the dependence of load on radial deflection. Now the derivation of equation (5) in appendix VI assumed the distortion of a tyre was confined to a zone adjacent to the contact patch. If the crown region were radially stiff compared to the sidewalls, this would not be the case and the distorted zone would be spread further circumferentially around the tyre. Thus it was decided to generalise equation (8) into the form:

$$W = (A + B.p)\, d^{n} \qquad (9)$$

This equation, although simple, has features to commend it. Load is seen to rise linearly with pressure for a given deflection, known to be the case for many, if not all, conventional tyres. Also the structural and pneumatic components of stiffness may be identified conveniently by the parameters A and B. Finally, no assumptions are made about the exact dependence of load on radial deflection, although the raising rate characteristic which is often observed can be represented. However, the significance of the power index n will be investigated further in VI.6.

To analyse the radial stiffness characteristics of a tyre over a range of inflation pressures, in order to separate the structural and pneumatic components, the following procedure was adopted. Equation (9) was first rearranged to give:

$$\frac{W}{d^n} = A + B.p \qquad (10)$$

which is in the form:

$y = a + bx$ and can be treated statistically by linear regression analysis if the value of n is known. However, as it is not known, an iterative procedure was utilised and included in a computer program TWPD, listed in appendix VII. The power index (n) is first put equal to 0.9, 1.0 and 1.1 in turn and the three residual deviations of the values of W/d^n about the fitted lines calculated. If n = 1.1 gives the lowest deviation, that is the best fit, n is put equal to 1.0, 1.1 and 1.2 and the same procedure followed. However, when the central value of n gives the lowest deviation, the difference between the three values of n is halved, so that the program converges on the parameters A, B and n which give the best fit to the experimental data. To limit the accuracy to which n is adjusted, the program is terminated when the difference between successive values of n has reduced to 0.0125.

This method of analysis has the advantage that all the experimental data for a tyre are taken into account at the same time. In other words, neither the load–deflection curves at constant pressures nor the load–pressure lines at constant deflections are examined separately before being combined to give the final result. Also, compared to the graphical method, no extrapolations to zero pressure are involved.

The output of program TWPD includes the fitted values of A, B and n, together with the residual standard deviation of W/d^n and the standard deviation of the load (W) about the fitted equation. Also output is a list of calculated loads for selected combinations of pressure and deflection.

To illustrate the use of program TWPD, a 5.20–10 cross-biassed tyre and a 145–10 radial tyre were tested, the former at inflation pressures of 275, 220, 165 and 110 kPa and the latter at 190, 150, 110 and 70 kPa. Four or five values of load were measured at approximately equal increments

Figure 6.16 : 5.20-10 Tyre

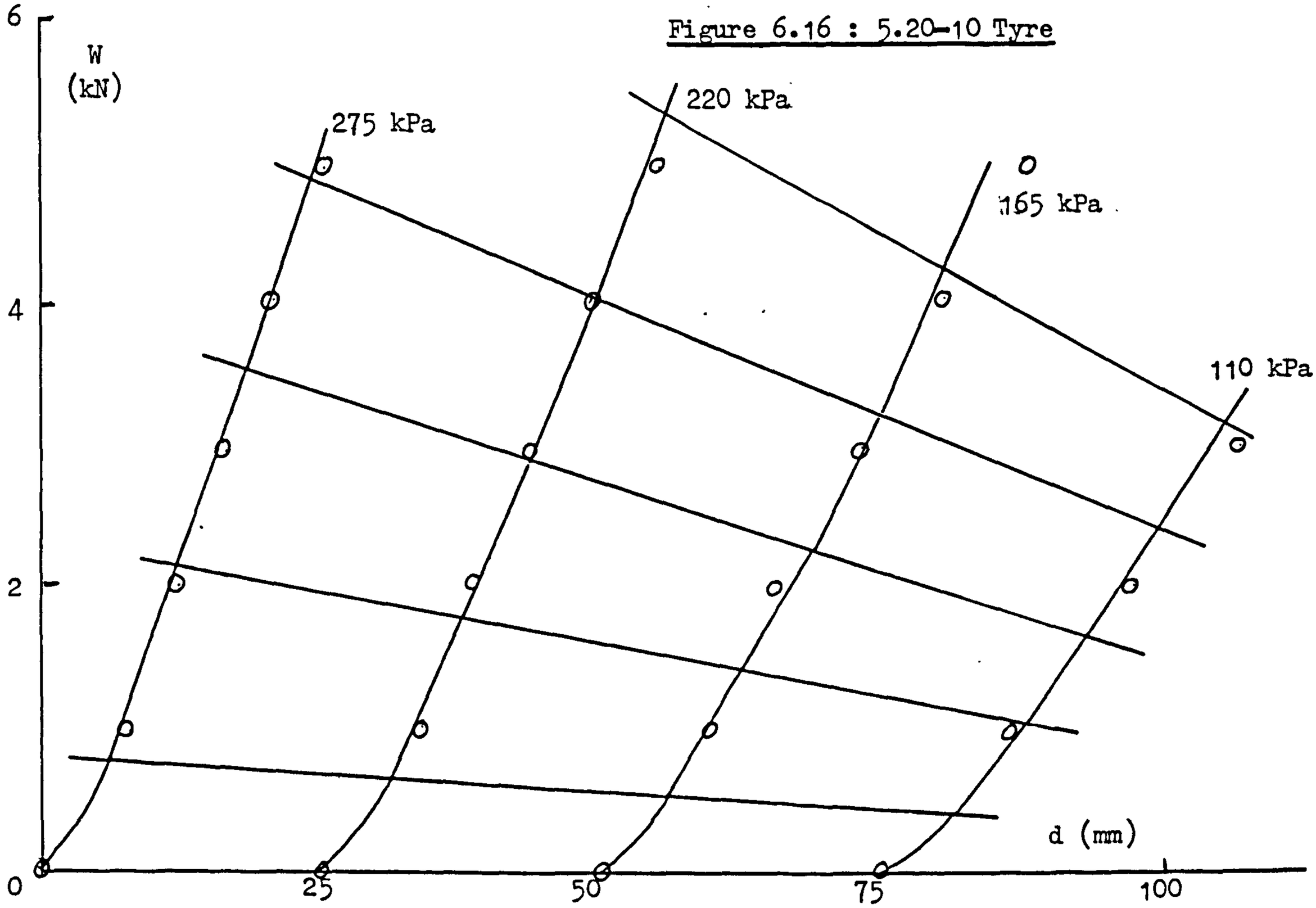

Figure 6.17 : 145-10 Tyre

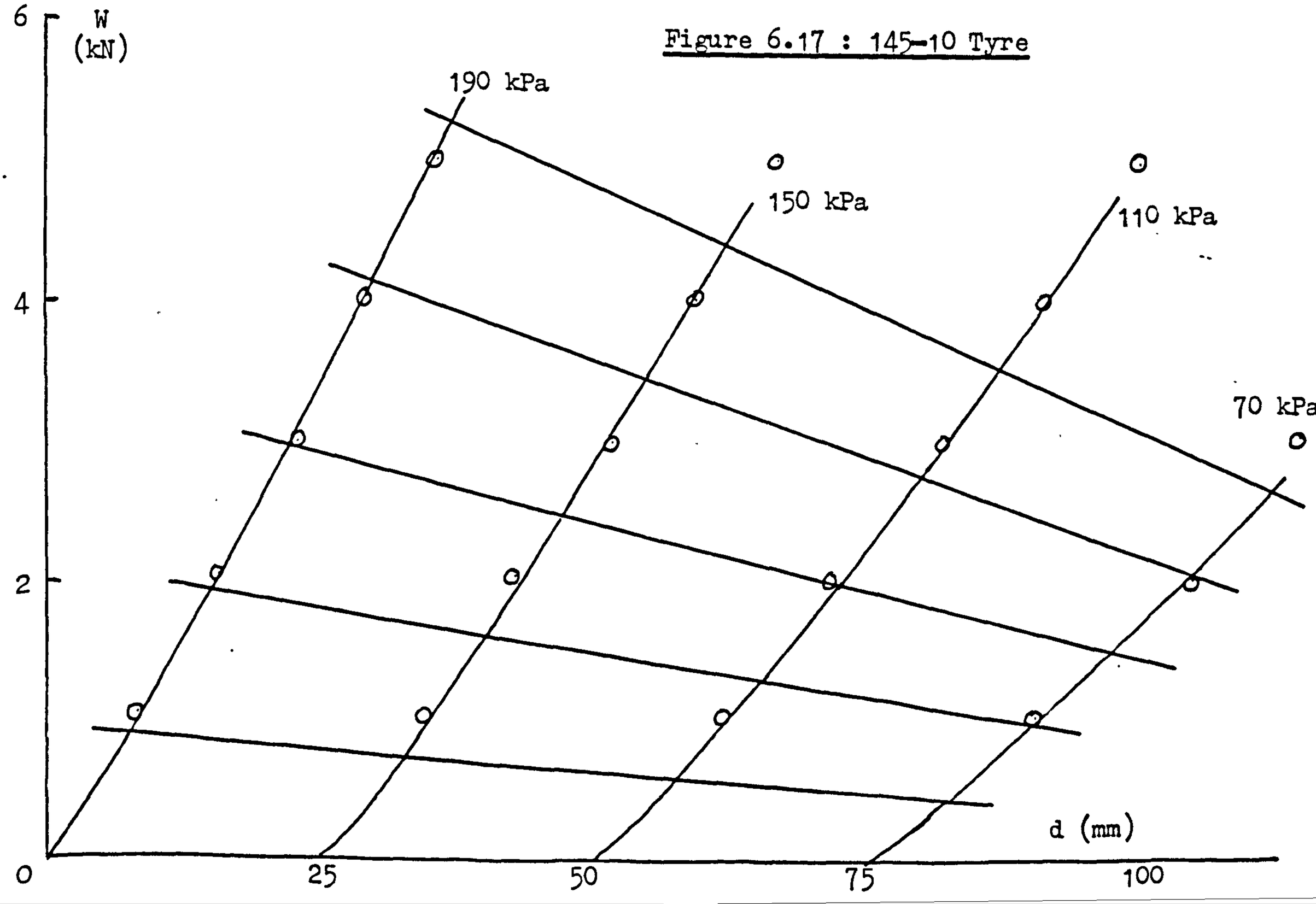

of deflection at each pressure. Results of the analyses are given in table XVI.

Table XVI

Radial Stiffness Analysis of Two Car Tyres

$$W = (A + B.p)\, d^n$$

Tyre	A	B	n	Res. S.D. (N)
5.20–10 cross-biassed	12.95	0.277	1.2375	171.9 (3.2%)
145–10 radial ply	23.56	0.374	1.1000	61.0 (1.1%)

(Units are consistent with loads in N, pressures in kPa and deflection in mm)

The lattice plots, with the experimental data represented by circled points, are shown in figures 6.16 and 6.17. The fits are excellent and this is supported by the residual standard deviations in table XVI, which amount to 3.2% and 1.1% of the maximum loads imposed on the two tyres respectively.

VI.6 Significance of the Power Index n

Although the parameters A and B in equation (9) relate, respectively, to the structural and pneumatic components of a tyre's radial stiffness, the significance of the power index n, controlling the dependence of the load carried on the radial deflection, is not immediately apparent. However the results of the stiffness analyses of the 5.20–10 and 145–10 tyres, listed in table XVI, and the comments about the extent of the distorted zone adjacent to the contact patch suggest an interpretation. The radial 145–10 tyre has a lower aspect ratio (~80%) than the 5.20–10 (>90%), therefore the circumferential tension per unit width at the crown of the former is considerably higher, see figure 4.13. It may also be noted from table XVI that the 145–10 tyre has the lower value of n, 1.10 cf. 1.24. Thus it may be argued that the effect of the circumferential tension is to extend the distorted zone further around the tyre from the contact patch. In the ultimate, if the crown zone were infinitely rigid by virtue of its construction and tension, it would remain circular when the tyre was deflected but would move in the direction opposite to the applied load relative to the beads. In this extreme case, the power index would approach unity.

To test this hypothesis, a number of tyres were required which differed primarily in their aspect ratio, and thus crown circumferential tension. Data for suitable car tyres were not available but three truck tyres were identified which met this criterion. They are:

11-R-22.5, having an aspect ratio of about 85%;
11/70-R-22.5, with an aspect ratio of 70%;
and 360/50-R-22.5, with an aspect ratio of 50%.

The load-deflection characteristics of the three tyres were measured at four inflation pressures in the range 200 kPa to 850 kPa, with a maximum load at the highest pressure of about 40 kN. When analysed using program TWPD, the results shown in table XVII were obtained.

Table XVII

Radial Stiffness Analysis of Three Truck Tyres

Tyre	A	B	n	Res. S.D. (N)	Aspect Ratio
11-R-22.5	48.2	0.385	1.238	167	85%
11/70-R-22.5	56.0	0.518	1.163	264	70%
360/50-R-22.5	96.7	0.649	1.100	706	50%

(Units consistent with load in N, inflation pressure in kPa and radial deflection in mm)

The fit of the equation to the data is excellent, as shown by the residual standard deviations which amount to 0.4%, 0.6% and 1.7% of the maximum loads carried. Moreover, the value of n decreases progressively through the range of tyres as the aspect ratio is reduced, supporting the hypothesis.

To provide further evidence confirming this interpretation of the significance of n, the tyres were loaded until their radial deflections were 30 mm at each of the four inflation pressures in turn. Careful measurements were then made of tyre radius from the centre of the contact patch round to the diametrically opposite point, defined by circumferential angles Φ from 0^{o} to 180^{o}. By subtracting the tyre's freely inflated radius from these measurements, values of radial distortion were obtained. The results are plotted against circumferential angle in figure 6.18 for the three tyres at the highest and lowest inflation pressures. The curves for the intermediate pressures were consistent but have been omitted for clarity. It

Figure 6.18

11-R-22.5

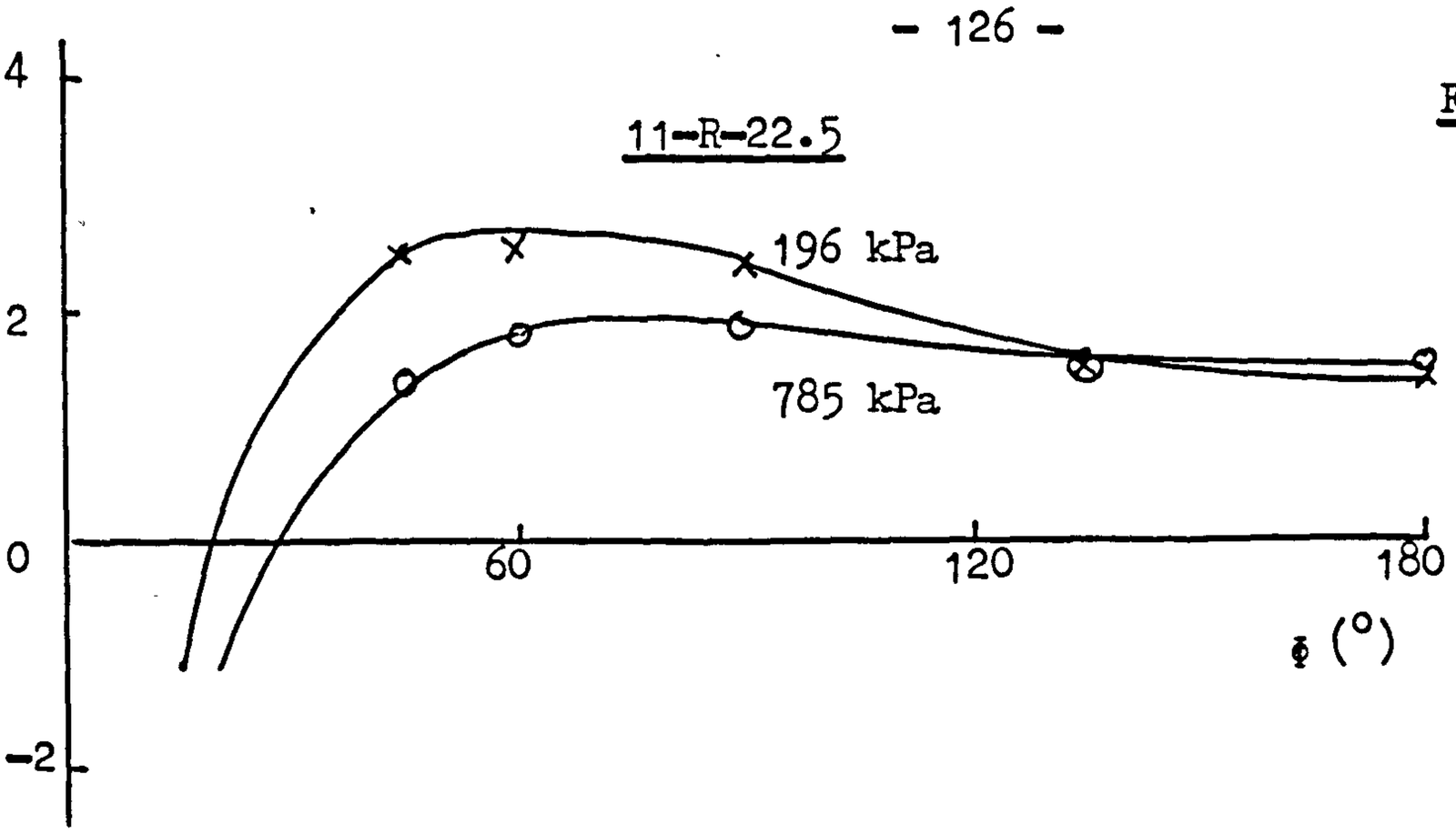

11/70-R-22.5

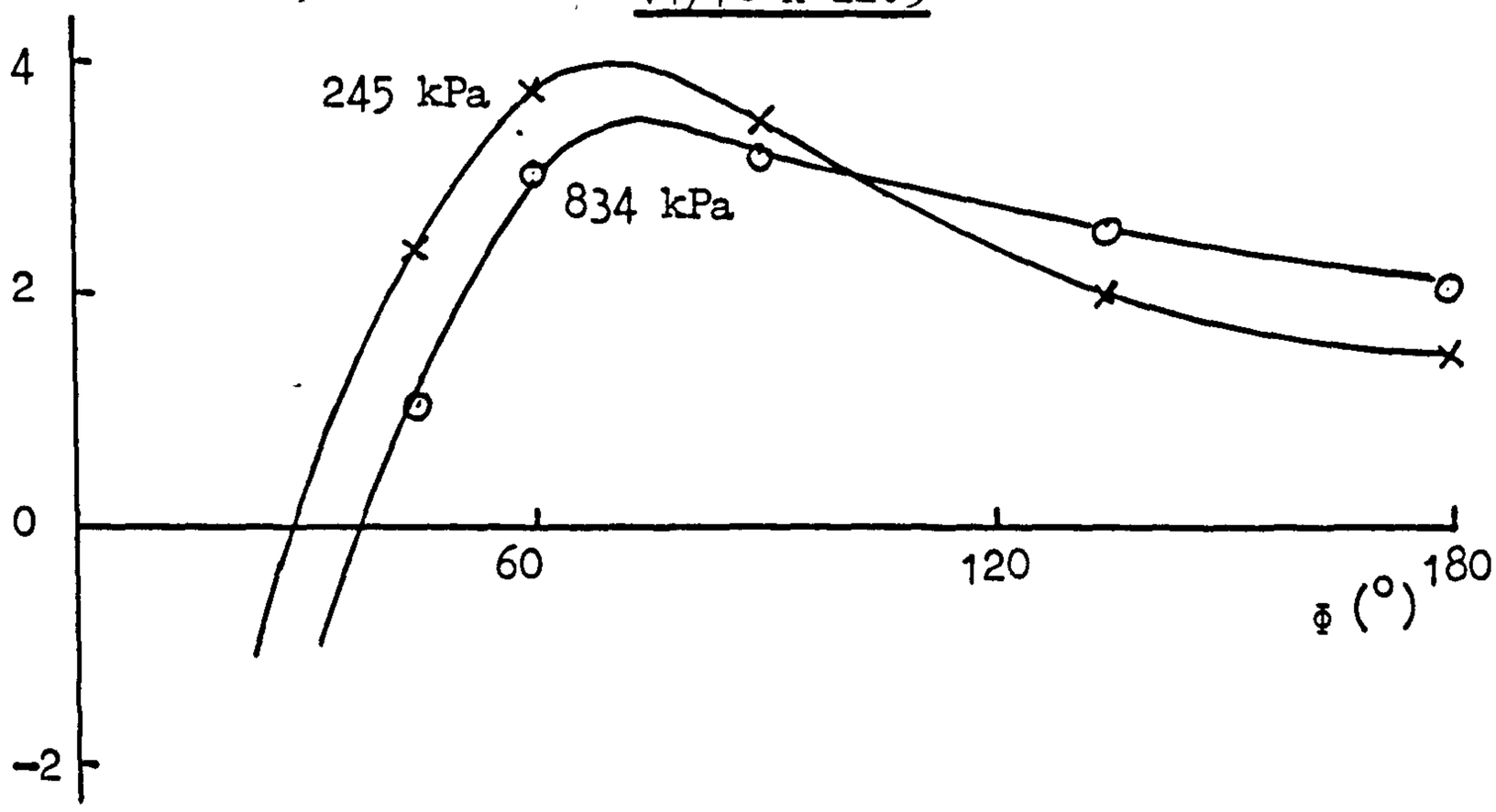

360/50-R-22.5

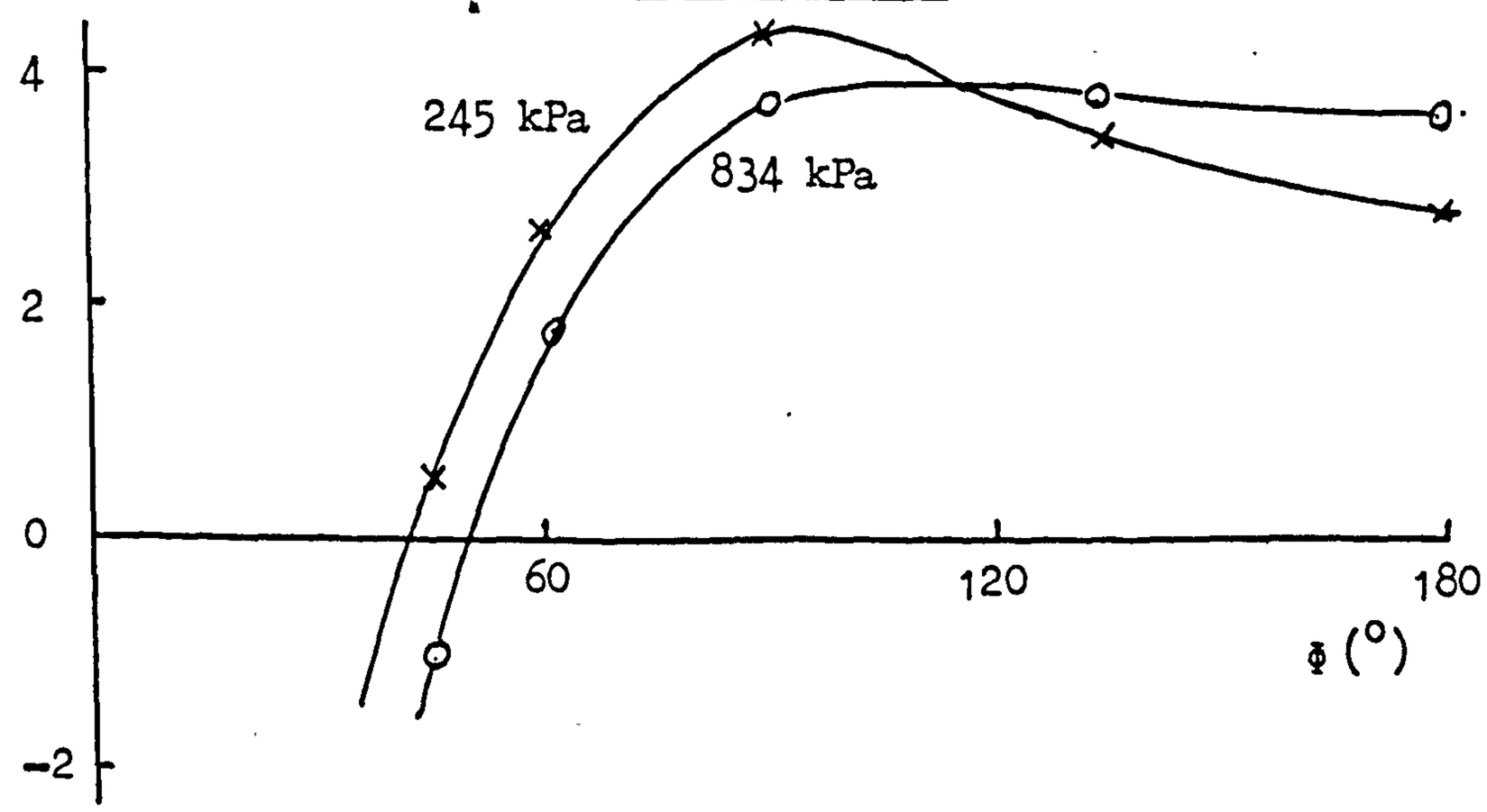

may be observed that the distortion of the 11-R-22.5 tyre recovers more quickly from the maximum value at the centre of the contact patch compared to the lower aspect ratio 11/70-R-22.5. This in turn recovers more quickly than the 360/50-R-22.5. Moreover, it may be discerned that all three tyres recover more slowly at the higher inflation pressure, when the circumferential tension is greater.

If recovery is described by the angle Φ at which the distortion returns to zero, and by the reversed distortion at $\Phi = 180^{\circ}$ where all three tyres exhibit an increase in radius when loaded, then the following table may be constructed for the highest pressures used.

Table XVIII

Distortion of Truck Tyres

Tyre		Max. Distortion (mm)	Φ at Zero Distortion ($^{\circ}$)	Distortion at $\Phi = 180^{\circ}$ (mm)
11-R-22.5	(85%)	- 30	35	1.5
11/70-R-22.5	(70%)	- 30	40	2.0
360/50-R-22.5	(50%)	- 30	48	4.0

These data are subject to some uncertainty as the measurements were difficult to make with the available equipment, but they do indicate that the hypothesis put forward for interpreting the power index n is correct.

Because the power index does vary between tyres, care must be taken when assigning total stiffness to structural and pneumatic components. Clearly the proportions will depend upon the inflation pressure chosen but, for illustration, consider the three truck tyres when operating under their schedule loads and pressures. These are:

	Schedule Load	Pressure
11-R-22.5	29.42 kN (3000 kgf)	785 kPa
11/70-R-22.5	29.42 kN (3000 kgf)	834 kPa
360/50-R-22.5	36.78 kN (3750 kgf)	834 kPa

Knowing the values of A, B and n (table XVII), equation (9) may be used to calculate the radial deflection d, and also the structural and pneumatic

proportions of the total load for each tyre. These are given in table XIX as percentages.

Table XIX

Structural and Pneumatic Components of Load

	Radial Defl^{n} (mm)	Structural Component	Pneumatic Component
11-R-22.5	36	14%	86%
11/70-R-22.5	34	12%	88%
360/50-R-22.5	40	15%	85%

Thus, although the values of the structural and pneumatic stifness parameters (A and B) in table XVII show clear trends with aspect ratio, the changing power index (n) negates these differences to give similar divisions of the total loads between the two mechanisms.

With the understanding derived from the subsidiary study described in this chapter, the analysis of radial stiffness characteristics of the fabricless tyres of the research could be undertaken with confidence.

CHAPTER VII : EXPERIMENTS ON THE MODEL TYRES

VII.1 Introduction

This chapter describes the experiments carried out on the model tyres and records, analyses and discusses the results obtained. The reasons for using model tyres at this stage of the research were : equipment and experimental methods were already in existence for this size of tyre; the results would be obtained more rapidly, compared to using car tyres; and the experience gained would guide the work on car tyres, when this was undertaken.

First, the test data obtained on the 73-8 A2 and 83-8 B2 tyres will be given, together with an outline of the experimental methods used. These tyres comprise the core of the model tyre work and, as explained in chapter V, all were manufactured with Hytrel carcasses and conventional rubber treads. This was also the case for the 83-7 C closed toroid tyre, whose assessment will be described next and related to the equivalent, open toroid, 83-8 B2 tyre. Next, to allow a direct comparison of the two candidate carcass materials, the results obtained on the 73-8 A2 Hytrel tyre will be examined in relationship to a model tyre with a polyurethane carcass. The design of this last tyre was not described in chapter V because it has exactly the same profile as the 73-8 A series but with a wall thickness of 3.2 mm. However, owing to manufacturing difficulties, its tread was cast from the same grade of polyurethane as its carcass and, to compensate for the greater bending stiffness of this component compared to a conventional rubber tread, its tread thickness was reduced from 5 mm to 3 mm. Finally, the results of a parallel study carried out to assess the suitability of polyurethane formulations as tread materials are summarised. Although not part of the research reported in this thesis, the conclusions reached are important to the overall view of the technical feasibility of fabricless tyres.

VII.2 Tests on 73-8 A2 and 83-8 B2 Tyres

VII.2.1 Grades of Hytrel

Owing to the difficulty of injection moulding the carcasses with the lesser wall thickness chosen, 1.2 mm, the research concentrated upon determining

the effects of carcass material modulus and inflation pressure on the behaviour of the tyres with a wall thickness of 2.2 mm. Thus, although the design calculations gave the modulus required to limit growth with inflation, these predictions had not been checked experimentally. Also the calculations gave no information on other tyre properties such as radial stiffness.

To obtain a range of Young's modulus, two grades of Hytrel were selected : 4050 and 5550; and blended. Table XX lists the four variants chosen and used to manufacture the carcasses.

Table XX
Blends of Hytrel

Hytrel		Blend	Young's Modulus at 25°C
parts 4050	parts 5550	Ref.	(MPa)
0	100	(i)	118
25	75	(ii)	82
50	50	(iii)	65
100	0	(iv)	30

Young's modulus was measured as the secant slope of a uniaxial stress-strain curve at 5% strain, within the elastic limit (about 10%). Moreover, because the blends gave almost linear characteristics over this range, modulus defined as the initial slope was very similar.

Both 73-8 A2 and 83-8 B2 carcasses, having aspect ratios of 90% and 70% respectively, were injection moulded from the four blends of Hytrel. Neither treads nor, in the case of the 83-8 B2 tyres, belts were fitted at this time.

VII.2.2 Burst strength

The first property of the carcasses to be measured was burst strength, in order to establish safe working pressures. A method standard in the tyre industry was used which involves fitting a tyre, or carcass in this case, to a wheel, filling it with water and pressurising it hydraulically. In this way, little energy is dissipated on burst which, otherwise, could

destroy any evidence of the mode of failure. The results obtained are listed in table XXI, where the safety factor is calculated assuming a working pressure of 150 kPa. The burst pressure per unit modulus is also given.

Table XXI

Burst Strength, 73-8 A2 and 83-8 B2 Carcasses

Tyre Type	Blend Ref.	Young's Modulus (E) (MPa)	Burst Pressure (P) (kPa)	Safety Factor	P/E $\times 10^3$
73-8 A2	(i)	118	970	6.5	8.2
	(ii)	82	760	5.1	9.3
	(iii)	65	720	4.8	11.1
	(iv)	30	510	3.4	17.0
83-8 B2	(i)	118	1090	7.3	9.2
	(ii)	82	830	5.5	10.1
	(iii)	65	640	4.3	9.8
	(iv)	30	570	3.8	19.0

The safety factors are lower than those for conventional tyres, which are almost 7 when failure usually occurs in the rim of the wheel rather than in the tyre itself. Nevertheless, all apart from those for the lowest material modulus were considered satisfactory for general use, especially as failure in every case followed the formation of a thin walled bubble at the crown due to cold flow of the material. This would be very obvious and would thus lessen the chance of a catastrophic burst. For experimental purposes, with care, all four material variants could be used.

The burst pressure per unit material Young's modulus generally increases as the latter is reduced but the absolute pressure decreases. Thus, for these tyres with a wall thickness of 2.2 mm and mamufactured from a single type of material, the highest modulus variant is most able to contain the inflation pressure.

VII.2.3 Growth with inflation pressure

The next property to be measured was growth in section height and section width as the carcasses were inflated. For this test, a carcass was mounted on a rim and then placed horizontally on a flat surface. One point on its circumference rested against a vertical stop while, diametrically opposite to this, a dial gauge registered the change in diameter. A second gauge recorded the change in section width by reference to the flat surface.

The results are given in table XXII as percentages when the inflation pressure was increased from 0 to 200 kPa, well below the burst pressures.

Table XXII

Growth of Carcasses owing to Inflation

Blend Ref.	Young's Modulus (MPa)	% Growth at 200 kPa			
		73-8 A2		83-8 B2	
		Height	Width	Height	Width
(i)	118	+2.7	-1.4	+6.3	-3.7
(ii)	82	+2.7	-0.7	+8.0	-3.3
(iii)	65	+3.2	-0.4	+8.0	-3.3
(iv)	30	+5.2	+1.4	+13.3	-2.8

Consider, first, the data for the 73-8 A2 carcass, designed to have an equibiaxially stressed equilibrium profile. They may be compared to the predictions of the theory developed in chapter IV.

The principal dimensions which determine the stress level in this carcass are:

radius to crown (ρ_o) = 165.6 mm

and radius to point of max. width (ρ_m) = 132.3 mm

giving meridional and circumferential tensions per unit length due to a pressure of 200 kPa equal to 5.99 kN/m, equation (7) in chapter IV. Now classical elasticity theory, acceptable for low strains, gives for the equibiaxial case:

$$Et_o = \frac{N}{2e} \qquad \text{(equation (27), ch. IV)}$$

where E is Young's modulus;

t_o is wall thickness;

N is the meridional or circumferential tension;

and e is the induced biaxial strain.

Substituting the values of E for the four Hytrel blends, with t_o = 2.2 mm and N = 5.99 kN/m, will give the expected strains:

blend (i) e = 1.2 %

(ii) e = 1.7 %

(iii) e = 2.1 %

(iv) e = 4.5 %

Now the measured percentage growths are not strains but may be interpreted as such if the carcass profile is considered elliptical and its changes in meridional length calculated. For the four carcasses, the experimental data give:

blend (i) e = 1.3 %

(ii) e = 2.0 %

(iii) e = 2.8 %

(iv) e = 6.7 %

It may be seen that the theoretical and experimental strains are in reasonable agreement for the high modulus Hytrel blends but diverge as the modulus decreases. In all cases the experimental values are greater.

To explain this discrepancy, at least qualitatively, the data in table XXII for the lower profile 83–8 B2 carcass may be examined. This carcass was designed using the analogue of a cross-biassed, cord-reinforced, conventional tyre. When made from an isotropic material and with a uniform wall thickness, it will not contain the inflation pressure only through stresses developed parallel to its surfaces. Bending stresses will be induced and the carcass will change in meridional shape, behaviour which is compounded by the unbalanced biaxial tensions at its crown : 5.33 kN/m and 16.77 kN/m in the meridional and circumferential directions respectively (ρ_o = 157.8 mm; ρ_m = 128.4 mm). This change in shape is very apparent from the experimental data, with increases in height of 6% to 13%, depending upon the material modulus, but decreases in width. However growth is also taking place, with the overall result that the lowest modulus carcass changes the least in width.

It may be surmised that the 73–8 A2 carcass behaves in the same way, although the changes in meridional shape are much less because it was designed

specifically for an isotropic material. However, the design theory does not allow for the fact that the bead wires are fixed in radius and separation; consequently, on inflation, growth will be non-uniform : greater at the crown and less in the sidewalls due to the restraint of the beads. This, in turn, will lead to an imbalance of stresses, particularly at the crown of the carcass. As explained in chapter IV, table V, a higher modulus is required to limit strains, or growth, in these circumstances; thus the greater growth of the 73-8 A2 carcass than predicted.

Overall, the measurements of growth with inflation show that a carcass material modulus of at least 50 MPa is required to ensure that the 73-8 A2 carcass does not increase in dimensions by more than 3%. As expected, the 83-8 B2 carcass would not be acceptable unless a much higher modulus were available, approaching 250 MPa. Thus this carcass requires a belt to reinforce its crown region.

As detailed in chapter V, the belts for the 83-8 B2 tyres were constructed from two rubberised plies of 2/244 rayon having a twist of 335/m and an end count of 75 ends/10 cm. Bias angles relative to the circumferential direction of $\mp 21^{\circ}$ were used. With belts fitted, the carcasses were retested to 200 kPa and the results obtained are given in table XXIII.

Table XXIII

Growth of 83-8 B2 Carcasses with Belts

Blend Ref.	Young's Modulus (MPa)	% Growth Height	% Growth Width
(i)	118	+3.3	-0.5
(ii)	82	+2.8	-1.9
(iii)	65	+2.7	-1.4
(iv)	30	+2.1	+2.1

Growth is now satisfactory. Indeed the lowest modulus blend gives the least change in section height, presumably because its relatively large increase in width lowers the stresses at the crown of this carcass. It then remained to recheck the burst strength with a belt fitted. An 83-8 B2 (i) carcass was chosen and a 50% increase in strength found, with failure at the edge of the belt.

VII.2.4 Creep at elevated temperature

Having established a material modulus to limit growth of these carcasses due to inflation, it was important to check long term creep. Now the creep of elastomers is accelerated by elevated temperatures and, in operation, car tyres reach an internal temperature of about 75°C, depending upon their size and running speed. However, they rarely maintain this temperature for more than a few hours and so it was decided to measure creep over a period of 150 hours at the temperature of 75°C. If this were not excessive, the 73-8 A2 and 83-8 B2 carcasses would be deemed acceptable.

The eight toroids were inflated to 150 kPa and placed in an oven at 75°C. Periodically their section heights and widths were measured, both of which increased. After 150 hours, the average percentage creeps exhibited are those listed in table XXIV. The 83-8 B2 carcasses were fitted with belts for this test.

Table XXIV

Creep of 73-8 A2 and 83-8 B2 Carcasses

Blend Ref.	% Creep at 75°C after 150 hours	
	73-8 A2	83-8 B2
(i)	+1.0	+0.5
(ii)	+1.5	+0.9
(iii)	+1.9	+1.6
(iv)	+3.7	+3.8

Only the lowest modulus blend, (iv), resulted in significant creep so that this property of the model fabricless tyres may be considered satisfactory if the burst strength and growth with inflation are acceptable.

VII.2.5 Radial stiffness

Before measurements of load and radial deflection were made, to give radial stiffness, the 73-8 A2 and 83-8 B2 carcasses were fitted with rubber treads by the remoulding technique. In the case of the 83-8 B2 tyres, the two ply fabric belt was included at the base of the tread. Now, although the inherent stiffness of a rubber tread itself is low, its geometrical presence affects the mode of deformation of the carcass in the zone of the contact patch.

Thus at this stage of the experimental work it was no longer acceptable to measure the properties of the carcasses alone, with or without belts.

The complete tyres were inflated to pressures of 100, 125, 150, 175 and 200 kPa and, at each pressure, were deflected incrementally against a flat surface. At each of four deflections, the radial load generated was measured. A standard laboratory Instron machine was used.

The data for each tyre were analysed according to equation (9), developed in chapter VI:

$$W = (A + B.p)d^n$$

using computer program TWPD listed in appendix VII.

To allow the results to be compared directly to conventional tyre constructions, the following model tyres were included in the experiments:

1) a high aspect ratio cross-biassed tyre, the 3.00-8, which has a 2-ply rayon reinforced carcass with a crown bias angle of about 40^o;
2) a squatter radial tyre, the 83-R-8, having a single ply rayon carcass and a 2-ply belt identical to that of the 83-8 B2 fabricless tyre (bias angle = $\mp 21^o$).

These two would be the basis for comparison of the 73-8 A2 and 83-8 B2 tyres respectively.

The results of the analyses are listed in table XXV in terms of the parameters A, B and n. Also included is a total stiffness, which is defined as the ratio of load to radial deflection with a load of 560 N and an inflation pressure of 150 kPa. These values were chosen because the latter is the schedule inflation pressure of the two conventional model tyres and the former is approximately the mid-range load of these experiments and is used in a number of established tests to be employed later in the research. It is less than the schedule load of the conventional tyres, 1150 N.

Table XXV

Radial Stiffness Analysis, 73-8 A2 and 83-8 B2 Tyres

Tyre	Blend Ref.	Young's Modulus (MPa)	Stiffness Parameters* A	B	n	Total Stiffness (kN/m)
73-8 A2	(i)	118	65.7	0.14	1.24	125.0
	(ii)	82	49.4	0.15	1.21	103.7
	(iii)	65	47.5	0.14	1.20	98.3
	(iv)	30	13.7	0.10	1.28	55.5
3.00-8 Cross-biassed		-	22.0	0.19	1.30	86.0
83-8 B2	(i)	118	44.2	0.14	1.28	103.7
	(ii)	82	27.8	0.12	1.40	92.6
	(iii)	65	24.3	0.26	1.19	88.9
	(iv)	30	26.9	0.16	1.20	76.2
83-R-8 Radial	-	-	17.5	0.24	1.13	70.0

* Units consistent with W in N, p in kPa and d in mm.

The fit of the equation to the load, pressure, deflection data for the tyres was good, as illustrated by figure 7.1 which is the lattice plot for the 73-8 A2 tyre made from Hytrel blend (iii). However, the three parameters in table XXV, although exhibiting some clear trends, show some inconsistencies which may be attributed to the statistical analysis used in calculating their values. This is particularly noticeable with the 83-8 B2 tyres whose structural stiffness parameter values, A, do not fall progressively with material modulus as would be expected. This is caused by the other two parameters, B and n, taking exceptional fitted values such as B = 0.26 for blend (iii), compared to 0.12 to 0.16, and n = 1.40 for blend (ii), compared to 1.19 to 1.28. Nevertheless, some conclusions may be drawn from the analyses.

a) The structural stiffnesses of the 73-8 A2 tyres, parameter A, are generally higher than that of the conventional cross-biassed tyre and increase with carcass material modulus; while their pneumatic stiffnesses, parameter B, are lower.

b) The same trends are apparent for the 83-8 B2 tyres when compared to the conventional radial, although the dependence on carcass material modulus is less marked.

Figure 7.1

73-8 A2 (iii) Tyre

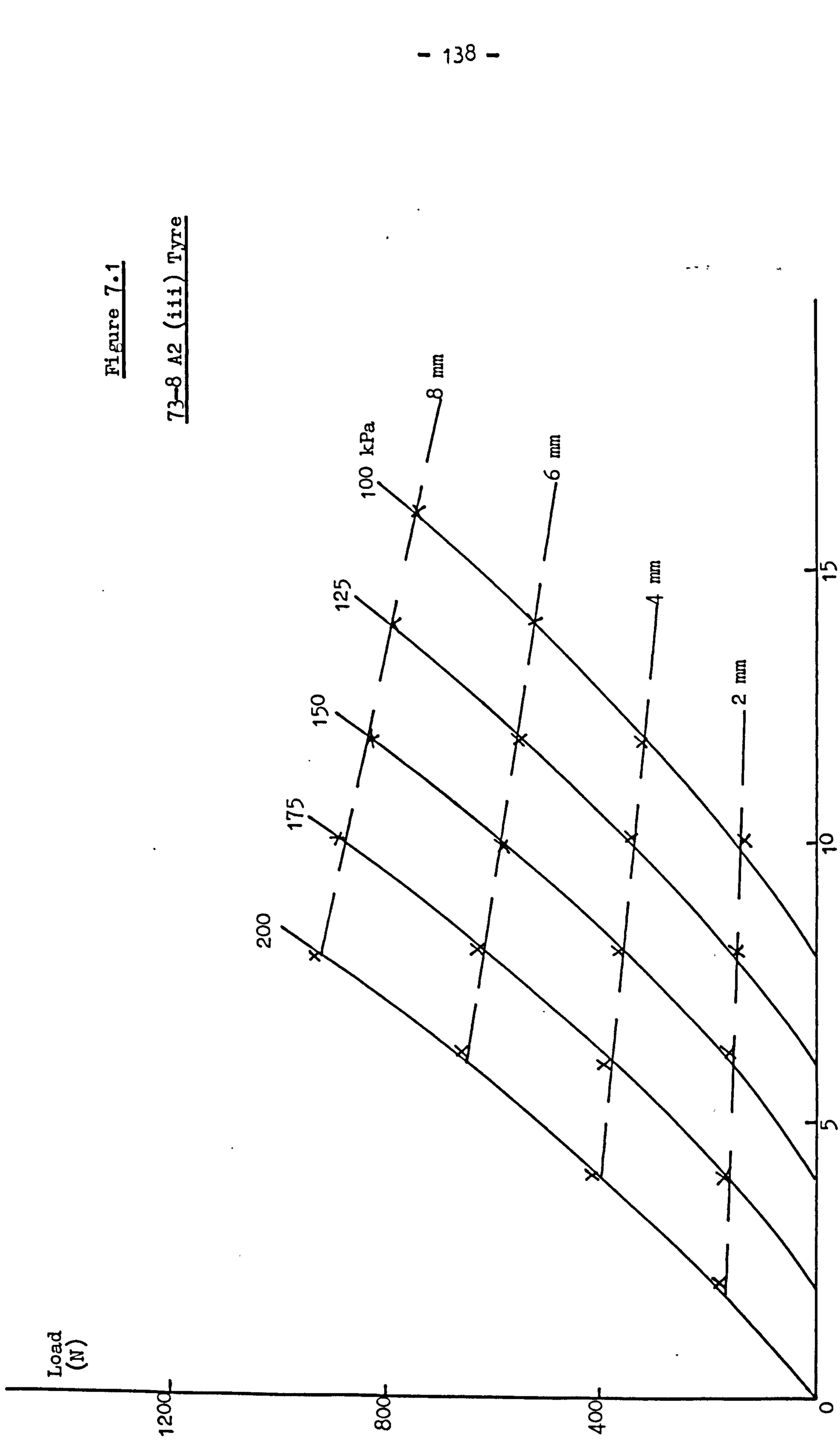

To obtain a clearer view of the behaviour of the tyres, their total stiffness may be examined. These were calculated from the fitted values of A, B and n by substituting W = 560 N and p = 150 kPa into the equation to give the values of deflection. By this means the total data for each tyre were used to assess its behaviour under these conditions, rather than relying upon single measurements. From the final column of table XXV, it may be seen that, for both tyres, total stiffness decreases progressively as the carcass material modulus is reduced. Figure 7.2 shows this graphically, where the stiffnesses of the two conventional tyres are marked for reference. As observed before, the radial stiffness of the completely unreinforced 73–8 A2 tyre is more dependent upon the modulus of its carcass material than is the 83–8 B2 tyre fitted with a restraining belt. This behaviour may be related to the growth characteristics of the former tyre, particularly when made from the lowest modulus Hytrel blend. For this variant, which emphasises the curvature of the 73–8 A2 line in figure 7.2, it may be suggested that its wall thickness is reduced sufficiently by inflation to lower the bending stiffness of its sidewalls and thus the tyre's total structural stiffness; while its change in shape, particularly in section width, modifies its pneumatic behaviour, as discussed in chapter VI with respect to the meridional angle at the beads. These hypotheses are supported by the data in table XXV for the 73–8 A2 (iv) tyre whose A and B parameters are low and are not compensated by a high power index, n.

Taking the total stiffness curves of figure 7.2 as drawn, it may be concluded that for a 73–8 A2 tyre to match the equivalent 3.00–8 cross-biassed tyre requires a carcass material modulus of about 60 MPa. The 83–8 B2 is stiffer than the 83–R–8 radial tyre for all carcass material moduli. Using the schedule pressure and load (W = 1150 N), the radial deflections of all the tyres examined are given in table XXVI.

Table XXVI

Radial Deflections, 73–8 A2 and 83–8 B2 Tyres

Blend Ref.	Young's Modulus (MPa)	Radial Deflection (mm) 73–8 A2	83–8 B2
(i)	118	8.0	9.4
(ii)	82	10.1	10.0
(iii)	65	10.5	11.4
(iv)	30	17.7	13.4
3.00–8 Cross-biassed	–	11.0	
83–R–8 Radial	–		15.1

Figure 7.2

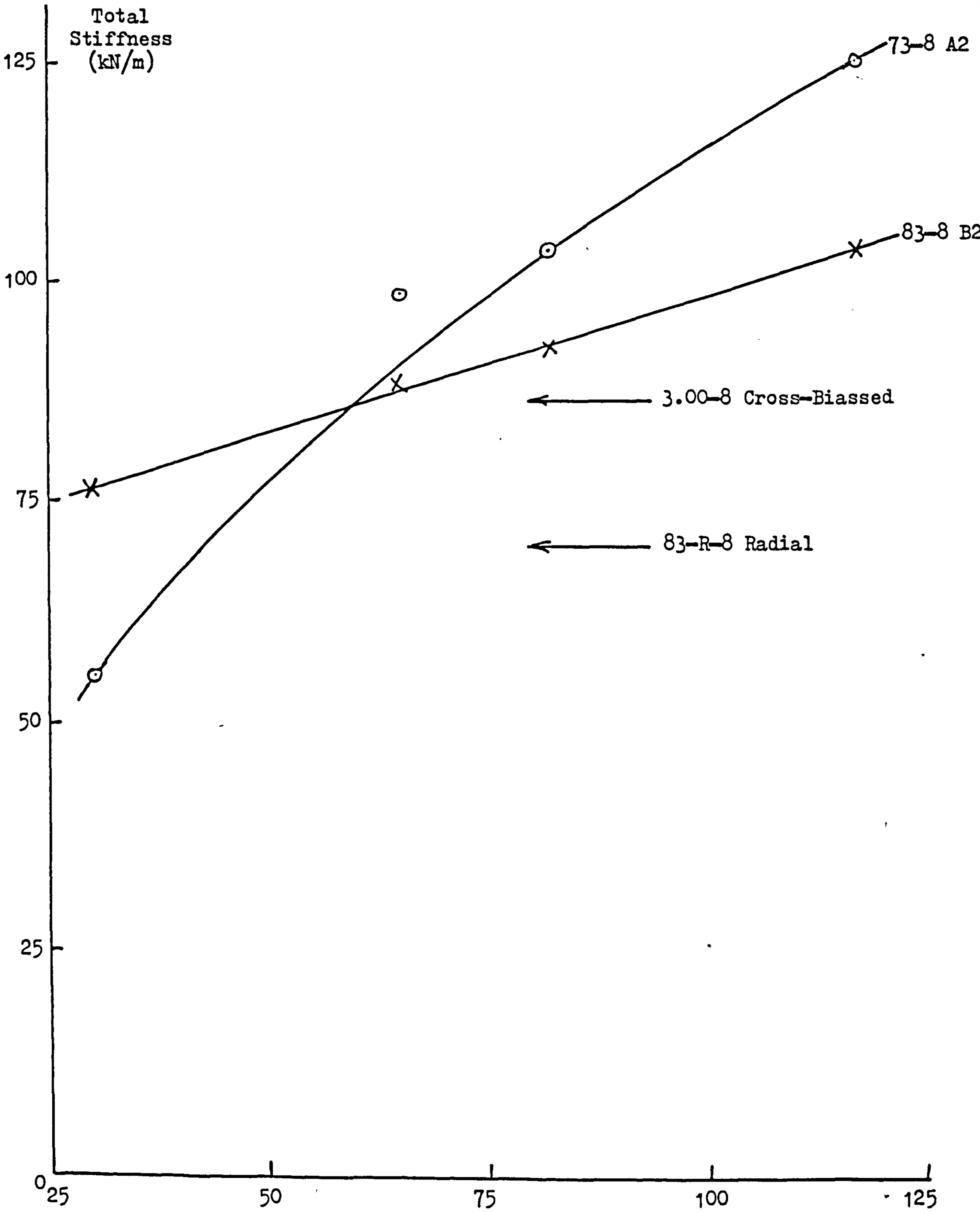
Total Stiffness (kN/m)
125
100
75
50
25
0
25
50
75
100
125
73-8 A2
83-8 B2
3.00-8 Cross-Biassed
83-R-8 Radial
Carcass Material Modulus (MPa)

VII.2.6 Cornering power

Cornering power is defined as the initial slope of the curve obtained by plotting the cornering or lateral force generated by a tyre when it is steered, against the angle of steer, or slip angle. The form of this curve was illustrated in chapter III, figure 3.5. To measure this characteristic, a method was available for model tyres based upon a specially constructed trailer which may be towed over any chosen road surface.

The trailer consists of two trailing arms pivoted at their forward ends to a cross-frame, which is itself rigidly attached to the back of the towing vehicle (a Land Rover). At their rear ends they carry horizontal, freely rotating axles on which test wheels and tyres may be mounted. Load on the tyres is provided by weights attached to the arms. The lateral separation of the forward ends of the arms may be adjusted by a screw mechanism driven by an electric motor; while their rear ends are restrained by a lateral link incorporating a load cell. When the two trailing arms are parallel, the tyres are running straight ahead with zero slip angle and therefore developing no cornering force. However, as the forward ends of the arms are driven apart, the tyres are steered in opposite directions and the resulting slip angle causes a cornering force to be generated. By this means, force as a function of slip angle may be measured.

The curvature of the force-slip angle curve only became noticeable with angles greater than 4^{o} and thus initial cornering power in $N/^{o}$ was quite satisfactory for describing the behaviour of the tyres over the range encountered in normal motoring (reference 21). It was decided to limit the inflation pressures examined to two : 100 kPa and 150 kPa; while maintaining the load at 560 N. The results obtained are given in table XXVII.

Table XXVII

Cornering Power, 73-8 A2 and 83-8 B2 Tyres

Blend Ref.	Young's Modulus (MPa)	Cornering Power ($N/^{o}$) 73-8 A2 100 kPa	73-8 A2 150 kPa	83-8 B2 100 kPa	83-8 B2 150 kPa
(i)	118	76	78	119	120
(ii)	82	72	75	108	109
(iii)	65	64	64	101	105
(iv)	30	26	32	83	102
3.00-8 Cross-biassed		53	73		
83-R-8 Radial				67	95

A contrast in behaviour between the Hytrel tyres and the conventional tyres is very obvious. With the former, cornering power changes very little with inflation pressure; whereas the cornering powers of the cross-biassed and radial tyres increase, approximately, in proportion to the pressure. In magnitude, all the 83-8 B2 tyres more than match the radial tyre, while the 73-8 A2 tyres made from the two higher modulus Hytrel blends have cornering powers similar to that of the cross-biassed tyre at its schedule pressure, 150 kPa.

Using the analogy of a beam on an elastic foundation , described in chapter III, the performance of the two types of Hytrel tyre may be compared. Now they have the same wall thickness and so the stiffnesses of their sidewalls, the elastic foundation of the analogy, are similar. However their widths, which control the second moments of area of the analogous beam, are 73 mm and 83 mm respectively; thus the ratio of the beam stiffnesses (EI) is:

$$\frac{83^3}{73^3} = 1.47 \qquad (83\text{-}8\ B2/73\text{-}8\ A2)$$

For the three higher modulus tyres, the ratios of the cornering powers are:

(i) 1.54; (ii) 1.45; and (iii) 1.57;

all in reasonable agreement with the prediction. The lowest modulus variants have a ratio of over 3.0 and therefore do not support the theory. However, as with the radial stiffness analysis, it may be suggested that the excessive growth of the 73-8 A2 tyre, in particular, modifies its cornering behaviour adversely.

A further conclusion which may be drawn from the comparison of the two types of Hytrel tyre is that the belt fitted to the 83-8 B2 has little effect upon its cornering properties. This is contrary to experience with conventional radial tyres, when the design and materials of the belt are crucial to its performance.

VII.2.7 Wear resistance

Related to cornering power is wear resistance and for these measurements another trailer technique was employed. Similar but shorter trailing arms each carry two identical tyres, allowing four tyres to be assessed under the same conditions. The forward ends of the arms are held at a fixed separation by the supporting framework attached to the towing vehicle, while a double acting pneumatic cylinder in place of the link incorporating the load cell

is located between the trailing arms at their rear ends. When pressure is applied to the cylinder via a precision regulator, the arms are either forced apart or together thus causing the tyres to run at the slip angle required to generate the cornering force to oppose the applied force. By this means, irrespective of the relative cornering powers of the two pairs of tyres, all the tyres run at the same cornering force but possibly different slip angles, thus reproducing the behaviour of tyres fitted to a cornering vehicle. A driver, on entering a bend, does not turn the steering wheel through a given angle but adjusts the angle to negotiate the bend. The latter demands a given radial acceleration, or cornering force, for a particular approach speed.

For the experiments to determine wear, the tyres were run for about 8 km, reversing the direction of the cornering force every 1 km. They were weighed before and after each run using a sensitive balance able to measure a weight loss of about 5 g, in a combined tyre/wheel weight of 1.5 kg, to within 10 mg. The levels of cornering force used were 112 N and 168 N which, for a load of 560 N, correspond to cornering coefficients, lateral force divided by radial force, of 0.2 and 0.3. These two cornering coefficients correspond to those encountered in normal driving (reference 21). The results in g/km are listed in table XXVIII for inflation pressures of 100 and 150 kPa.

Table XXVIII

Wear of 73-8 A2 and 83-8 B2 Tyres

Tyre Type	Blend Ref.	Young's Modulus (MPa)	Wear Rate (g/km) c.cf. = 0.2		c.cf. = 0.3	
			100 kPa	150 kPa	100 kPa	150 kPa
73-8 A2	(i)	118	0.042	0.052	0.161	0.156
	(ii)	82	0.052	0.060	0.169	0.179
	(iii)	65	0.060	0.068	0.195	0.185
	(iv)	30	0.218	0.205	0.775	0.629
3.00-8 Cross-biassed		-	0.088	0.055	0.252	0.172
83-8 B2	(i)	118	0.036	0.039	0.099	0.107
	(ii)	82	0.044	0.042	0.130	0.109
	(iii)	65	0.049	0.042	0.172	0.101
	(iv)	30	0.056	0.044	0.159	0.104
83-R-8 Radial		-	0.053	0.047	0.174	0.114

Figure 7.3

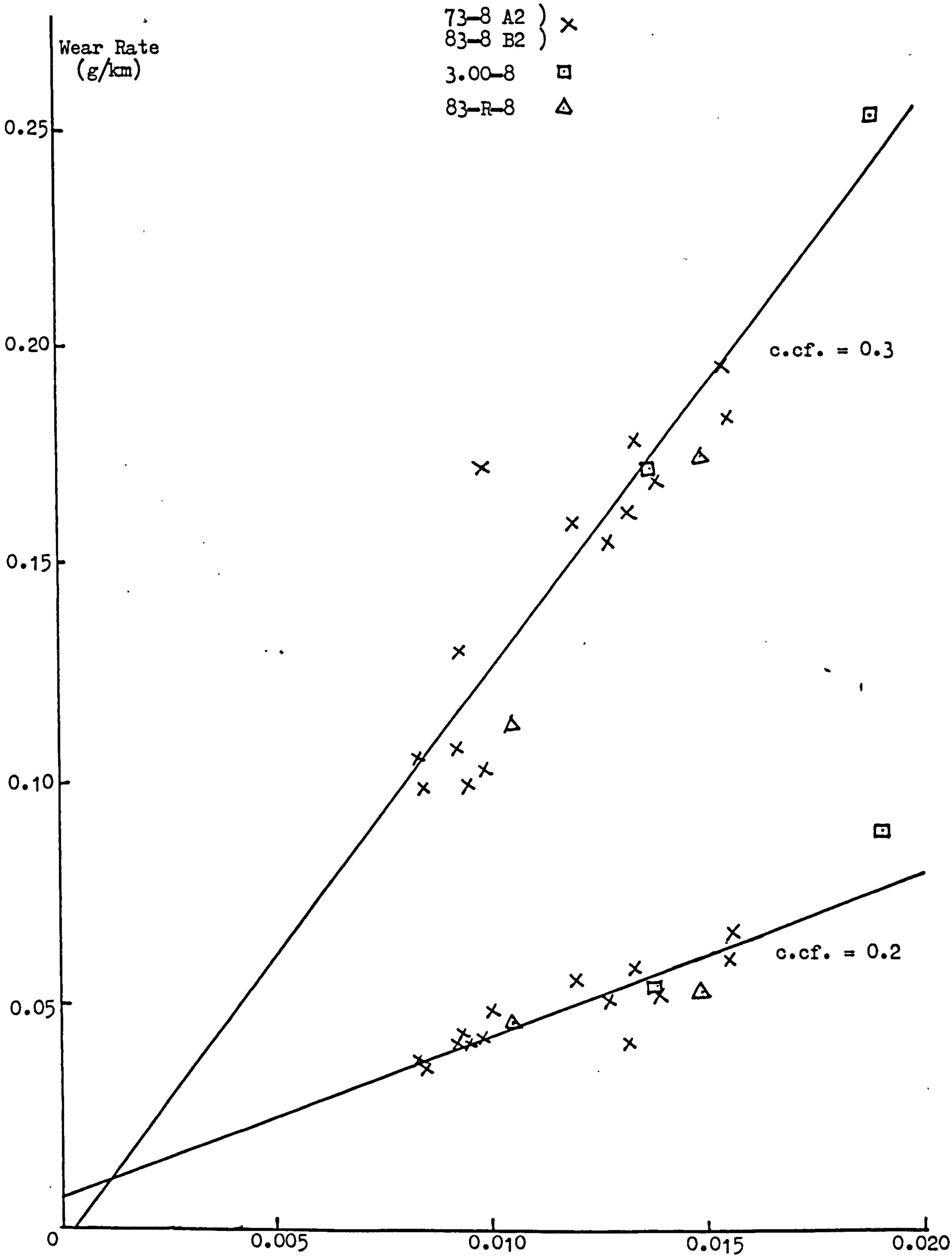
73–8 A2
83–8 B2
3.00–8
83–R–8
Wear Rate (g/km)
0.25
0.20
0.15
0.10
0.05
0
0.005
0.010
0.015
0.020
c.cf. = 0.3
c.cf. = 0.2
1/Cornering Power (°/N)

These data show that the wear resistances of the conventional tyres can be matched by the two types of fabricless tyre if the carcass material modulus is sufficiently high. It is also worth noting that inflation pressure has little effect upon the wear of the higher modulus tyres, reflecting their cornering behaviour. To be specific, the wear of the 73-8 A2 tyre is similar to that of the cross-biassed tyre inflated to 150 kPa if the carcass material modulus is greater than about 80 MPa at the lower severity (c.cf. = 0.2) or greater than 60 MPa at the higher severity (c.cf. = 0.3). All four versions of the 83-8 B2 tyre have wear rates lower than the conventional radial tyre (at 150 kPa) at both severities.

The data in tables XXVII and XXVIII also present a unique opportunity for testing the theoretical relationship between wear and cornering power outlined in chapter III. There it was explained that if the amount of lateral slip occurring during cornering is decreased, by stiffening the tyre, the work done against the frictionally induced cornering force, and thus the wear, is also lessened. In the tests just described, a wide range of tyre constructions were compared at two cornering coefficients or, because the radial load was constant, two levels of cornering force. Consequently, according to theory, wear should be inversely proportional to cornering power.

Figure 7.3 shows the wear rates of all the tyres, apart from the lowest modulus 73-8 A2 which exhibited excessive wear, plotted against the inverse of cornering power. The results for both inflation pressures are included. Regression lines were fitted to the data:

$$y = a + b.x$$

where y is the wear rate and x is the inverse cornering power, with the results:

for c.cf. = 0.2 : a = 0.007 b = 3.66

and for c.cf. = 0.3 : a = -0.002 b = 12.74

The correlation coefficients are 0.885 and 0.922 respectively which, for 16 degrees of freedom, both indicate significances greater than 99.9%. Thus the experiments support the theory, particularly as the fitted lines in figure 7.3 pass close to the origin.

VII.2.8 Rolling resistance or drag

Rolling resistance is the more commonly used term to describe the drag of a rolling tyre caused by its internal hysteresis (reference 22). More

correctly, "rolling resistance" is the non-dimensional ratio of the drag force to the radial load, analogous to a coefficient of friction.

To measure the drag of the model tyres, they were run on a 300 mm diameter steel drum driven by a synchronous motor at a speed equivalent to about 35 km/h. Both the drum and the motor are contained in a pivoted cradle, which reacts against a leaf spring under the action of the moment caused by a tyre's drag. In this way, no corrections are necessary to allow for the driving motor's internal losses. The deflection of the leaf spring is detected by a linear potentiometric transducer whose output was calibrated in terms of drag by hanging a series of weights on a cord wrapped around the periphery of the drum, when stationary.

The drags of the tyres were measured with a radial load of 560 N and an inflation pressure of 150 kPa. These conditions resulted in a greater radial deflection than in the trailer tests but is still less than the deflection under the schedule conditions for these tyres. Measurements were taken immediately a tyre was loaded on the drum and after about 10 minutes, when drag had reduced because of the temperature rise in the tyre and had reached equilibrium. The results are given in table XXIX; although, because of a developing fault, measurements could not be made on the 73-8 A2 (iii) tyre.

Table XXIX

Drag of 73-8 A2 and 83-8 B2 Tyres

Blend Ref.	Young's Modulus (MPa)	Drag (N) 73-8 A2 0 min.	73-8 A2 10 min.	83-8 B2 0 min.	83-8 B2 10 min.
(i)	118	19.5	17.0	22.0	19.0
(ii)	82	21.5	19.0	21.0	18.0
(iii)	65	-	-	21.5	19.0
(iv)	30	28.5	24.0	22.0	19.0
3.00-8 Cross-biassed		39.0	29.5		
83-R-8 Radial				28.5	22.5

These data show the expected difference between the two conventional tyres, the radial having the lower drag. The two types of fabricless tyre show only a small decrease in drag with time, or temperature, and, initially, all except the lowest modulus 73-8 A2 have drags lower than the radial. At

equilibrium, they are similar to the radial and thus exhibit drags less than the cross-biassed tyre.

The reason for the relative lack of temperature dependence of the Hytrel tyres is probably as follows. As the temperature rises, the loss modulus of the carcass material, which governs the hysteretic bending losses, will fall. However the elastic or Young's modulus will also decrease so that the radial deflection of these structurally stiff tyres will increase. Thus, although energy loss per unit strain is reduced as the temperature rises, the induced strains increase with the radial deflection. With these opposing mechanisms, the overall consequence is that the measured drags do not change as much as those of conventional tyres. The latter have much lower structural stiffnesses and so maintain their initial radial deflections, so exhibiting reducing drag as the loss moduli of their component materials fall with temperature.

VII.2.9 Temperature build-up

From the discussion of drag, it may be appreciated that temperature independence cannot be interpreted necessarily as a low running temperature. In fact, it was essential to determine from separate tests the magnitude of temperature rise to be expected in fabricless tyres. However, experimentally, it is not easy to measure the temperatures in a running tyre. If thermocouples are used, they are prone to breakage if positioned in high strain zones where heat generation will be large; also wires must be routed along isothermals as far as possible, otherwise the measured temperature will be in error because of the large difference between the thermal conductivities of metals and polymers. In practice, using thermocouples was the best option but it was decided to limit the experiments to two tyres:

the 73-8 A2 (i)

and the 3.00-8 cross-biassed.

Thermocouples were positioned in the rubber treads of both tyres in four locations:

a) carcass-tread interface in the shoulder;

b) mid-tread in the shoulder;

c) carcass-tread interface at the crown;

d) mid-tread at the crown.

The wires were run parallel to the carcass, as the greatest temperature

gradient would be through the thickness of the tread, and were brought out to slip rings fitted to the wheel axle of the machine used for the drag measurements. A potentiometric recorder was used to measure the outputs from the thermocouples as this takes minimal current and would thus be less affected by any electrical resistance in the slip rings.

The two tyres were tested with an inflation pressure of 150 kPa but with three radial loads : 560 N, 700 N and 840 N. As before, the speed was 35 km/h. The temperatures recorded at equilibrium, when the ambient temperature was about 20°C, are listed in table XXX.

Table XXX

Running Temperatures, 73-8 A2 (i) and 3.00-8 Tyres

Tyre and Load (N)	Temperature (°C)			
	Shoulder		Crown	
	Interface	Mid-tread	Interface	Mid-tread
73-8 A2 (i)				
560	73	60	59	47
700	87	70	64	53
840	101	78	67	56
3.00-8 Cross-biassed				
560	73	74	65	56
700	87	87	70	60
840	93	94	73	62

Apart from the temperature at the tread-carcass interface in the shoulder, the fabricless tyre ran significantly cooler than the conventional tyre. In all cases, the shoulder temperature is higher than the equivalent crown temperature, which is readily explained. In the tread, the crown region is subjected to simple compression, while the shoulder suffers both compression and shear because the tread surface and carcass interface are not parallel in this region. Also it can be envisaged that more bending occurs beneath the shoulder in the carcass as a section of the tyre passes into and out of the contact zone. Higher strains lead to greater energy loss and increased local temperatures.

VII.2.10 Structural performance or fatigue

The structural performance of conventional tyres is usually assessed by running them on drums, inflated to the schedule pressure but with the radial load increased by 50% or 65%. This is thus an overload test. With the fabricless tyres, however, there was no history of their pattern of failure and therefore it was decided that the effects of both load and pressure should be investigated. Moreover, because the strains induced in their carcasses would be functions of the radial deflection, careful note of the latter would be made.

The equipment available for structure testing consists of a 600 mm diameter drum mounted with its axis vertical. Four tyres can be loaded against it, equally spaced around its periphery, and are carried on short swinging arms. The loads are generated by pneumatic cylinders controlled by adjustable reducing valves and solenoid valves. The last are wired through microswitches held adjacent to the tyres so that, if failure of a tyre occurs, its increased deflection will operate the valves and the tyre will be withdrawn from the drum. Electromagnetic counters record the distances travelled.

The testing procedure developed is illustrated by table XXXI and was adopted for each of four inflation pressures : 50, 100, 150 and 200 kPa.

Table XXXI

Structure Testing Procedure

Tyre Station	Load as Percentage of Standard (560 N)					
	100%	125%	150%	175%	200%	
1	2	-	2	-	2	)
2	1	2	-	2	-	) Running
3	2	-	2	-	2	) Periods
4	1	2	-	2	-	)

With reference to this table, four nominally identical tyres inflated to the same pressure were fitted to the machine and run for periods defined as 1250 km at 65 km/h. Initially, all four tyres carried the standard load of 560 N but, after 1 period, two of the tyres had their loads increased to 125% of the standard. The other two tyres completed 2 periods at the

first load before being loaded to 150% of the standard. The loads on the two pairs of tyres then increased alternately up to a maximum of 200%. When a tyre failed, its total distance to failure and its radial deflection at that time were recorded.

The results obtained with the two types of fabricless, Hytrel tyres are given in table XXXII, where the figures in brackets are the radial deflections at failure.

Table XXXII

Fatigue, 73-8 A2 and 83-8 B2 Tyres

Tyre Type and Blend	Young's Modulus (MPa)	Fatigue Life (km) and Radial Deflection (mm) Inflation Pressure (kPa) 50	100	150	200
73-8 A2 (i)	118	650(7.0)	1150(7.0)	1500(8.5)	2650(9.0)
(ii)	82	550(10.0)	1050(7.0)	1350(8.5)	2700(10.0)
(iii)	65	350(12.0)	1250(10.5)	1400(9.5)	2600(9.0)
(iv)	30	150(19.5)	700(13.0)	1450(14.0)	2000(9.0)
83-8 B2 (i)	118	200(7.5)	300(6.0)	2750(10.5)	4500(10.5)
(ii)	82	150(8.0)	250(7.5)	2750(12.0)	2950(10.5)
(iii)	65	200(9.5)	100(8.0)	2050(9.0)	2750(10.5)
(iv)	30	50(11.0)	300(11.0)	2700(14.0)	3700(13.0)

Without exception, all the tyres failed by circumferential crack growth in the carcass below the shoulder. In this region, bending of the tread to contact the running surface and increased curvature of the sidewall to give the radial deflection combine to maximise the dynamic strain. This is where the tyres exhibited the highest running temperatures, as noted in the last section.

Although conventional cross-biassed 3.00-8 tyres were subjected to the same fatigue test, failure of their carcasses was never observed. Tread looseness, however, did occur and limited their life to around 3500 km when inflated to 150 kPa. Thus it is difficult to make a direct comparison of fabricless and conventional tyres on the basis of these model tyres alone. This must await the experimental investigation of the car tyres.

Table XXXII, however, does provide a valuable insight into the structural behaviour of fabricless tyres. Clearly, both the 73–8 A2 and 83–8 B2 tyres exhibit greater lives when inflated to higher pressures but, when the radial deflections at failure are examined, it may be inferred that it is not the inflation pressure per se that leads to this improvement. Given the inaccuracy of a stepped load test, where failure is the cumulative effect of a number of loads, and the exception of the very low modulus 73–8 A2 (iv) tyre, it may be observed that the failure deflections vary very little between the inflation pressures. Thus the failure mechanism would appear to depend only upon the radial deflection, there being a critical value above which rapid failure occurs. Of course, the higher the inflation pressure, the greater the distance travelled before this deflection is reached in a stepped load test. Now the internal strains induced in the carcasses will be functions, primarily, of the deflection; thus, from the data, it is apparent that it is the strains which cause failure, not the stored energy. However, the latter increases with material modulus and there is a slight trend for the critical deflection to decrease with increasing modulus.

To check whether fatigue life is dependent upon the carcass material modulus and to allow an overall comparison of the two types of fabricless tyre, analysis of variance was used to examine the variations within each type. For the 73–8 A2 tyres, the resulting table is as follows with the fatigue lives scaled by 10^{-3}.

Source of Variance	Sum of Squares	Degrees of Freedom	Mean Square	'F' Ratio
Carcass Modulus	0.40	3	0.13	4.6
Inflation Pressure	9.01	3	3.00	103.9
Residual	0.26	9	0.029	
Total	9.67	15		

With 3 and 9 degrees of freedom, the 'F' ratio for the effect of carcass modulus is just significant (95%); while the effect of pressure is highly significant (99.9%) as observed. The unscaled standard deviations calculated from the components of variance are:

carcass modulus variation	161 km
inflation pressure variation	862 km
error	170 km

For the 83–8 B2 tyres, the analysis of variance table is the following, again with the fatigue lives scaled.

Source of Variance	Sum of Squares	Degrees of Freedom	Mean Square	'F' Ratio
Carcass Modulus	0.93	3	0.31	2.04
Inflation Pressure	33.60	3	11.20	73.68
Residual	1.37	9	0.152	
Total	35.90	15		

For these tyres, the effect of carcass modulus is not significant; while again the inflation pressure is a highly significant factor. The standard deviations with the modulus factor sum of squares and degrees of freedom summed with the residual are:

inflation pressure variation	1659 km
error	438 km

Thus, from the statistics, the modulus of the carcass material has only a minor effect, if any, on the behaviour of the two types of tyre. Pressure is important;although, as discussed, it is its effect on radial deflection which controls fatigue life. In this respect the 83–8 B2 is more sensitive than the 73–8 A2 tyre, as the following lives averaged over the carcass moduli show.

Table XXXIII

Average Fatigue Lives of 73–8 A2 and 83–8 B2 Tyres

Inflation Pressure (kPa)	Fatigue Life (km) 73–8 A2	83–8 B2
50	425	150
100	1038	238
150	1425	2563
200	2488	3475

If an inflation pressure of 150 kPa or, presumably, greater is used, then the 83–8 B2 tyre is the superior.

VII.3 Tests on the 83-7 C Tyre

In chapter V, the closed toroid tyre was introduced as a possible means of overcoming the difficulty of injection moulding carcasses with a conventional meridional profile. The latter require the use of a solid, segmented core and in production it was anticipated that such a core would be vulnerable to damage and wear, leading to inaccuracies in wall thickness. The 83-7 C tyre was designed to be moulded in two halves and joined around its crown by RF welding. Its profile is identical to that of the 83-8 B series and it has the additional feature of sidewalls which extend until they meet to form a single bead region.

83-7 C carcasses with a wall thickness of 2.2 mm were made from the three higher modulus blends of Hytrel listed in table XX. The lowest modulus blend was omitted because of its generally poor performance in the 73-8 A2 and 83-8 B2 tyres. Burst strength of the carcasses was not assessed successfully because they expanded out of the rim at about half the expected burst pressure. This problem could be solved by redesigning the bead region and rim to provide a more positive lock.

Growth of the 83-7 C carcasses was measured with and without a belt although, because the design is essentially one with a low profile, a belt would almost certainly be needed. The results obtained are given in table XXXIV.

Table XXXIV

Growth of 83-7 C Carcasses.

Blend Ref.	Young's Modulus (MPa)	% Growth at 200 kPa			
		Without Belt		With Belt	
		Height	Width	Height	Width
(i)	118	+8.2	-2.9	+3.3	-1.6
(ii)	82	+8.8	-2.9	+3.1	-1.3
(iii)	65	+9.8	-3.0	+1.7	+0.2

The percentage changes in height and width are very similar to those for the 83-8 B2 carcasses, tables XXII and XXIII, confirming that a belt must be fitted to prevent excessive growth. Thus, for all the remaining tests, belts were fitted and the tyres were completed by adding a rubber tread as before by remoulding.

The radial stiffness characteristics of the 83-7 C tyres were measured and analysed in the same way as those of the other model tyres and using the same range of inflation pressures : 100 kPa to 200 kPa in 25 kPa increments. The results are listed in table XXXV, together with the total stiffness data for the 83-8 B2 tyres from table XXV.

Table XXXV

Radial Stiffness Analysis, 83-7 C Tyres

Blend Ref.	Young's Modulus (MPa)	Stiffness Parameters A	B	n	Total Stiffness (kN/m) 83-7 C	83-8 B2
(i)	118	52.0	0.16	1.18	100.2	103.7
(ii)	82	34.7	0.13	1.28	92.5	92.6
(iii)	65	24.5	0.19	1.23	82.1	88.9

As may be seen, the total stiffnesses of the two tyres, which share a common meridional profile and are identical in every respect apart from the extended sidewalls of the 83-7 C, are very similar. The same is true of the stiffness parameters A, B and n when the data in the above table are compared to those in table XXV, allowing for some uncertainty in the fitting procedure.

Cornering power was measured next and table XXXVI compares the results obtained with those given previously in table XXVII for the 83-8 B2 and 83-R-8 tyres. The two inflation pressures : 100 kPa and 150 kPa; were again employed.

Table XXXVI

Cornering Power, 83-7 C and 83-8 B2 Tyres

Blend Ref.	Young's Modulus (MPa)	Cornering Power (N/°) 83-7 C 100 kPa	83-7 C 150 kPa	83-8 B2 100 kPa	83-8 B2 150 kPa
(i)	118	113	113	119	120
(ii)	82	102	107	108	109
(iii)	65	87	98	101	105
83-R-8 Radial		67	95		

The 83-7 C tyre exhibits the same independence of inflation pressure as the

other fabricless tyres when compared to the conventional radial. For all carcass material moduli, it generates a somewhat lower cornering force per angle of steer than the 83-8 B2 but is superior to the radial ply tyre at both inflation pressures. This result was most encouraging because, of all properties, it was thought this closed toroid design would have poor cornering ability owing to the meridional angle in its clinch, adjacent to the bead. There existed the possibility of its being unstable. Clearly the high structural lateral stiffness of the sidewalls of a fabricless tyre give it both stability and the means of transmitting the cornering force to the rim.

Because the cornering data for the 83-7 C tyres showed promise, it was decided to proceed to the determination of wear. Using the trailer, measurements were made for inflation pressures of 100 kPa and 150 kPa, and at the two cornering coefficients : 0.2 and 0.3. These were the conditions used for the other model tyres, table XXVIII. A 83-R-8 conventional radial tyre was included in these later runs to act as a control because experience has shown that wear can vary from day to day. It certainly varies according to the time of the year, largely because of the ambient temperature but also, it is suspected, owing to the state of the road surface. The results obtained are listed in table XXXVII.

Table XXXVII

Wear of the 83-7 C Tyres

Blend Ref.	Young's Modulus (MPa)	Wear Rate (g/km) c.cf. = 0.2 100 kPa	150 kPa	c.cf. = 0.3 100 kPa	150 kPa
(i)	118	0.051	0.053	0.126	0.128
(ii)	82	0.066	0.058	0.167	0.158
(iii)	65	0.091	0.066	0.223	0.182
83-R-8 Radial		0.071	0.044	0.174	0.132

As observed with the other fabricless tyres, the wear of the 83-7 C is not sensitive to inflation pressure, particularly when its carcass material modulus is high. However, the variability of the conventional tyre is sufficient to invalidate any direct comparisons with the 73-8 A2 and 83-8 B2 tyres but, unlike them, the 83-7 C tyre can only match the conventional tyre at the higher cornering severity.

Drag and running temperature measurements were not made on the 83-7 C tyre as there was no reason to suppose it would be significantly different to the other model Hytrel tyres. Consequently, the next and final assessment was fatigue. The stepped load procedure given by table XXXI was followed, although only three inflation pressures were used; at 200 kPa; the weakness of the bead/rim design lead to a slow leak and testing was discontimued. The results for the three lower pressures are listed in table XXXVIII, including the radial deflections at failure.

Table XXXVIII

Fatigue of 83-7 C Tyres

Blend Ref.	Young's Modulus (MPa)	Fatigue Life (km) and Radial Deflection (mm) Inflation Pressure (kPa)		
		50	100	150
(i)	118	1110(7.5)	600(7.5)	2300(10.0)
(ii)	82	420(10.0)	1240(11.5)	1900(10.0)
(iii)	65	348(14.0)	1283(12.0)	3000(14.0)

As before, failure occurred by the development of a circumferential crack in the carcass below the shoulder of the tyres but the data are more variable than before, table XXXII, and because of their number are less amenable to statistical analysis. However, assuming their dependence on carcass material modulus is small, as demonstrated for the other model tyres, averages for the three inflation pressures may be calculated and compared to those for the 83-8 B2 tyre.

Table XXXIX

Average Fatigue Lives of 83-7 C and 83-8 B2 Tyres

Inflation Pressure (kPa)	Fatigue Lives (km)	
	83-7 C	83-8 B2
50	626	150
100	1041	238
150	2400	2563

At 150 kPa inflation, the more likely condition, the two tyre designs are similar but it does seem that the 73-7 C closed toroid tyre has greater life at the lower pressures.

VII.4 Tests on the 73-8 PU Tyre

It was explained in the introduction to this chapter that a 73-8 model tyre centrifugally cast from polyurethane was included in the experimental investigation. The original intention was to make the comparison between the two candidate carcass materials using car tyres but the difficulties experienced in injection moulding such tyres in Hytrel, owing to the limited shot size of the available equipment, prompted a change in the programme of the research.

The additional model tyre, which will be designated the 73-8 PU, has a meridional profile identical to that of the 73-8 A series of Hytrel tyres but with a wall thickness of 3.2 mm. Its tread was cast integrally with the carcass from the same material because a satisfactory means of bonding a rubber tread was not available. Also, as already stated, the tread thickness was reduced from 5 mm to 3 mm to counter the effect on structural stiffness of a higher modulus tread material.

The polyurethane chosen for limited testing was a polyether : Adiprene L-100, supplied by DuPont. It is representative of good quality, engineering polyurethanes and has a Young's modulus of 46 MPa. In the results which follow, the tyre made from this material is compared directly to the highest modulus Hytrel tyre, the 73-8 A2 (i).

The experimental data for burst strength and growth with inflation are presented in table XL, and include the stiffnesses per unit circumference of the tyres' sidewalls, calculated as the product of modulus and wall thickness.

Table XL

Burst Strength and Growth, 73-8 PU and 73-8 A2 (i) Tyres

Tyre	Young's Modulus (E) (MPa)	Wall Thickness (t) (mm)	Sidewall Stiffness (E.t) (kN/m)	Burst Pressure (kPa)	% Growth at 200 kPa	
					Height	Width
73-8 PU	46	3.2	147	620	+0.75	+0.13
73-8 A2 (i)	118	2.2	260	970	+2.7	-1.4

Given its greater wall thickness but lower Young's modulus, the polyurethane tyre has a burst pressure commensurate with the Hytrel tyre. However its growth with inflation pressure is significantly lower, even allowing for its higher modulus tread, and perhaps reflects the difference in properties of the two types of material. Hytrel is a thermoplastic whereas the polyurethane is an elastomer, so that growth of a tyre made from the former may induce limited yield. No measurements of permanent set, unfortunately, were made to test this hypothesis.

The radial stiffness characteristics of the tyres were measured and analysed as before. The results are given in table XLI.

Table XLI

Radial Stiffness Analysis, 73-8 PU and 73-8 A2 (i) Tyres

Tyre	Young's Modulus (MPa)	Stiffness Parameters A	B	n	Total Stiffness (kN/m)
73-8 PU	46	65.7	0.09	1.24	115.5
73-8 A2 (i)	118	65.7	0.14	1.24	125.0

Although the modulus of the polyurethane is less than half that of the Hytrel, the stiffnesses of the tyres are very similar. Moreover, their structural stiffness parameters, A, are equal showing the importance of carcass wall thicknesses; an aspect of tyre mechanics which will be investigated in more detail in the next chapter.

The cornering and wear characteristics of the 73-8 PU tyre were not assessed because separate experiments had shown that an acceptable balance between friction and wear could not be achieved with available materials of this type. For completeness, the results of these experiments will be summarised in the next section. Thus the next property measured was drag and, for this, a single load of 560 N was used with the tyres inflated to 150 kPa, table XLII.

Table XLII

Drag of 73-8 PU and 73-8 A2 (i) Tyres

Tyre	Young's Modulus (MPa)	Drag (N) after 0 min.	Drag (N) after 10 min.
73-8 PU	46	10.1	7.0
73-8 A2 (i)	118	19.5	17.0

As may be seen, the polyurethane tyre exhibits the very much lower drag, both initially and when the tyres have reached their equilibrium temperatures after 10 minutes. Remembering that the Hytrel tyre itself has similar or lower drag than the conventional radial tyre, this result is outstanding.

Finally, the structural fatigue life of the 73-8 PU tyre was assessed, comparing it directly to the Hytrel tyre which was run again. However, because no further insight into the mechanics of failure was sought, only one load was used but the inflation pressure of the two PU tyres tested was adjusted to 186 kPa so that they ran at the same radial deflection as the conventional 3.00-8 cross-biassed tyre. Two Hytrel tyres were run at pressures of 150 kPa and 200 kPa, thus bracketing the PU tyre. The results are listed in table XLIII.

Table XLIII

Fatigue, 73-8 PU and 73-8 A2 (i) Tyres

Tyre	Young's Modulus (MPa)	Inflation Pressure (kPa)	Fatigue Life (km)
73-8 PU	46	186	3335
73-8 PU	46	186	3479
73-8 A2 (i)	118	150	1500
73-8 A2 (i)	118	200	2650

Failure of the polyurethane tyres occurred in the same manner as all the other tyres tested : a circumferential crack in the carcass beneath the shoulder of the tread. However, from this limited test, it does appear to have a superior life compared to the Hytrel tyre.

VII.5 Wear and Wet Grip of Polyurethane Treads

The experiments, the results of which are summarised in this section, were performed to determine the suitability of polyurethane as the tread material for pneumatic tyres (reference 23). This work does not constitute a part of the research being described but the conclusions reached must be taken into account when assessing the technical feasibility of fabricless tyres.

In chapter III, when discussing the mechanics of pneumatic tyres, it was emphasised that the ability of a tyre to develop a longitudinal force, to allow a vehicle to accelerate or brake, depends not only upon the coefficient of friction between the tread material and the road but also, in wet conditions, on the removal of water through the tread pattern and the establishment of dry contact. Moreover, the removal of the final film of water is a function of the asperity height of the road texture and the hardness of the tread material. Now the friction of a rubber-like material is a visco-elastic phenomenon and therefore its magnitude depends upon the glass transition temperature (T_g) of the material. For example, cis-polybutadiene with a T_g of $-105^{\circ}C$ exhibits lower friction at normal ambient temperatures than natural rubber with a T_g of $-72^{\circ}C$. This in turn develops less friction than SB-R with a T_g of $-55^{\circ}C$. Consequently, when studying wet grip, which is the development of frictional forces by tyres on wet roads, the two material parameters which must be considered are the glass transition temperature and hardness, the second measured by a standard indenter (reference 15).

For abrasion, with respect to tread material as opposed to the structure of the tyre, the situation is far more complex and no laboratory measured parameters have been identified which correlate with any confidence to road wear. Thus the need for such techniques as trailer testing, outlined in VII.2.7. In addition, because wet grip on different road surfaces cannot be predicted with the accuracy required, a trailer technique has also been developed for this purpose. Essentially, the trailer consists of a hinged framework, the upper half of which is attached to the towing vehicle, while the lower half carries a solid axle on which are mounted two identical tyre/wheel assemblies. The wheels are about 1 m apart to give the trailer stability and the connecting axle also carries a disc brake operated by an observer in the towing vehicle. When the brake is applied, the lower half of the framework of the trailer would pivot backwards owing to the action

of the longitudinal force developed by the tyres. However it is restrained by a load cell which, therefore, measures the magnitude of the force. The signal generated is recorded on a UV recorder, together with a signal from a tachometer attached to the trailer's axle. From the two signals, the force-slip velocity curve may be constructed and the maximum and final values of braking force identified. The former usually occurs at slip velocities around 20% of the forward velocity, while the latter corresponds to the locked condition when the slip is 100%.

For the experiments, a total of eight polyurethane formulations were employed, three of which are supplied by DuPont : Adiprenes L-42, L-83 and L-100, the last being the one used in the carcass and tread of the 73-8 PU tyre. To maintain as constant as possible the construction of the tyres to be fitted with treads of these materials, the 3.00-8 cross-biassed tyre was modified so that, when moulded, a circumferential recess extending almost the whole width of its tread region was formed. The polyurethane materials were manufactured separately as tread bands reinforced with a two ply belt but with the cords disposed at 0^{o}, that is circumferentially. When a band was fitted in the recess moulded in a 3.00-8 tyre and the tyre was inflated, a sufficiently good "bond" between the carcass and tread band was obtained.

To act as a standard for comparison, a normal 3.00-8 tyre with a tread composed of Intol 1500 polymer (SB-R) reinforced with 50 p.p.h.p. of HAF black was used. All the results obtained, table XLIV, are expressed as indices with Intol 1500/50 HAF rated as 100. An index greater than 100 indicates a superior performance. In the table, the compositions D to H inclusive were obtained using experimental PU polymers and oil extension; the wear results were obtained at a cornering coefficient of 0.25; while the maximum and final values of wet grip were measured on two contrasting road surfaces, smooth asphalt and Dorset pebbles whose micro-textures are rough and smooth respectively. "Smooth" asphalt refers to its macro-texture, not its micro-texture.

Table XLIV

Wear and Wet Grip of Polyurethane Formulations

Tread Material	T_g (°C)	Hardness (Shore A)	Wear Index	Wet Grip Index			
				Smooth Asphalt		Dorset Pebbles	
				Max.	Final	Max.	Final
A (L - 42)	-36	80	92	93	104	84	73
B (L - 83)	-45	84	169	116	114	81	68
C (L - 100)	-28	88	316	118	115	85	71
D	-44	72	30	90	96	87	73
E	-36	64	8	62	65	95	83
F	-47	56	4	-	-	-	-
G	-19	73	54	116	108	119	99
H	-19	68	15	113	102	140	111
Intol 1500/50 HAF	-55	63	100	100	100	100	100

It may be seen that with these polyurethane compositions, which are not exclusive but indicate the problem to be solved, those with high wear resistance, such as B (L - 83) and C (L - 100), have poor wet grip particularly on Dorset pebbles. This surface represents a highly polished road, a situation which can occur at just those locations where good grip is required, on a bend for instance or the approach to a junction. In contrast, the polyurethanes compounded to reduce hardness and thus improve friction, especially when combined with a high glass transition temperature, have very poor wear resistance, G and H for example.

To conclude this section, it may be stated that a major materials development programme would be needed to produce a liquid-processing polyurethane with the required balance of properties. Moreover, properties other than wear and friction could not be overlooked because even passenger car tyres are sometimes run over extremely rough surfaces when cutting could be a problem.

VII.6 Summary of Model Tyre Results

Owing to the failure to manufacture model tyres with the thinner carcass, 1.2 mm, only limited conclusions may be drawn from the experiments reported in this chapter. Nevertheless, additional information has been obtained which contributes to the understanding of the behaviour of fabricless, pneumatic tyres.

Almost all the tyres tested had carcasses made from the thermoplastic Hytrel but with conventional rubber treads. By blending two grades of the former material, carcasses with a range of moduli were produced in two basic designs : the high profile 73–8 A tyre and the low profile 83–8 B and 83–7 C tyres. It is instructive to consider, first, the measurements made of burst strength, growth and creep, all associated with inflation only.

Perhaps the most fundamental observation is that freedom of design is more limited than for conventional tyres if no reinforcement whatsoever is incorporated. The comparison of the 73–8 A and 83–8 B tyres showed that growth with inflation is excessive, without using an unacceptably high material modulus or presumably wall thickness, if the tyre's profile does not conform to that dictated by the requirement of equibiaxial tensions. These take advantage of the isotropic nature of a homogeneous material. Thus to restrict growth, the lower profile 83–8 B and 83–7 C tyres must be fitted with a belt. With this proviso and confining the discussion to a single carcass wall thickness, 2.2 mm, it was seen that to give a burst strength of about 600 kPa, four times the presumed operating pressure, and to limit growth and creep to less than 3% and 2% respectively, all require a material Young's modulus of at least 50 MPa.

When external forces are applied or generated by the tyres, such as radial load and cornering force, the performances of the high and low profile tyres differ. The latter, 83–8 B and 83–7 C when fitted with a belt, are less sensitive to carcass modulus and are able to match a conventional radial tyre with a modulus as low as 30 MPa. However, the 73–8 A tyre requires a carcass material modulus of 50 MPa to give it the same radial stiffness as a cross-biassed tyre and a value of 80 MPa to match its cornering power. For all the tyres tested, having rubber treads, wear resistance was proportional to cornering power. It should also be noted that the 83–7 C tyres, designed for ease of manufacture, performed almost as well as the equivalent, more conventionally shaped, 83–8 B.

All the experimental fabricless tyres excelled in one respect, their drags were lower than those of the conventional tyres. As this property depends upon the hysteresis of the component materials, it was reflected in the measurements of equilibrium running temperatures. With the exception of the carcass–tread interface beneath the shoulder, temperatures in the one fabricless tyre examined were lower than those at the equivalent locations of a conventional tyre. However the one exception became significant when the structural fatigue of the tyres was assessed.

Every model fabricless tyre run to test its structural integrity failed in the same way : a circumferential crack in the carcass below the shoulder of the tread. From the high temperature recorded in this location, it may be inferred that it is a region of high stress concentration. That this is so may be implied qualitatively because, as a meridian of a tyre is bent into and then flattened in the contact zone, the sidewalls are simultaneously deflected to give a combined distortion in the shoulder.

Unfortunately it was not possible to rate the structural or fatigue lives of the fabricless tyres relative to the conventional tyres. The latter failed by tread looseness with their carcass structures intact. Even so, the lives of the fabricless tyres were less, although the 83-8 B and 83-7 C tyres were superior to the 73-8 A tyres, all with Hytrel carcasses. It is also noteworthy that the 73-8 PU (polyurethane) tyre had a life twice that of its Hytrel equivalent, a fact which encouraged the work on car tyres, described in the next chapter, as most of these were to be manufactured using polyurethanes.

A more fundamental finding on the fatigue of fabricless tyres is that life is critically dependent on radial deflection. The tests were carried out for a wide range of inflation pressures using a stepped load procedure and, allowing for some uncertainty and the exceptional behaviour of the lowest modulus variants, failure occurred when a certain radial deflection was reached. If confirmed by the car tyre experiments, this is a most important observation because it means there is a conflict with fabricless tyres between a low radial deflection to prolong life and a higher deflection, comparable to conventional tyres, to give acceptable ride and handling.

Finally, it should be remarked that the work on the wear and wet grip of polyurethane formulations for treads indicates that their optimisation to meet the demands of modern pneumatic tyres will not be easy. For this purpose, hydrocarbon, high molecular weight elastomers which can be reinforced with carbon black appear to be unique.

CHAPTER VIII : EXPERIMENTS ON THE CAR TYRES

VIII.1. Introduction

As listed in table X, chapter V, two types of car tyre were designed, equivalent in size to 5.20/145-10 cross-biassed or radial tyres fitted to the Leyland "Mini" car. They have aspect ratios of 90% and 70%, their meridional profiles being identical in shape to the 73-8 A and 83-8 B model tyres. Moulds were manufactured to allow the tyres to be made with one of four carcass wall thicknesses : nominally 3.0, 3.5, 5.5 and 8.0 mm, the second suitable for multi-shot injection moulding from Hytrel and the others for centrifugal casting using polyurethanes. The higher aspect ratio tyres were designated the 126-10A and the lower aspect ratio the 143-10 B series.

The previous chapter showed how the model tyres were employed to examine the effects of carcass material modulus and inflation pressure on the performance of fabricless tyres. The former, with the section geometry, controls the radial and lateral structural stiffnesses but also determines the allowable inflation pressure and therefore, indirectly, the corresponding pneumatic stiffnesses. The purposes of the work on car tyres were : to confirm and extend the findings, particularly with respect to carcass wall thickness; to relate the structural performance or fatigue of fabricless tyres to that of conventional tyres; and, if appropriate, conduct vehicle tests to assess handling and comfort, the latter being a combination of the generation and transmission of vibrations by a tyre.

To provide a range of material modulus for the tyres to be cast from polyurethane, three grades of Adiprene : L-42, L-100 and L-315, ex. DuPont; were blended. For the tyres to be injection moulded, only the highest modulus Hytrel was chosen, grade 5550. As mentioned earlier, difficulties were experienced in using this last type of material owing to the limited shot size of the available injection moulding machine. Also the limited data on model tyres suggested that polyurethane was a superior material for the carcass. The complete list of materials used for the 126-10 A and 143-10 B tyre carcasses is given in table XLV, together with their nominal Young's moduli.

Table XLV

Carcass Materials - Car Tyres

Reference No.	Adiprene parts L-42	Adiprene parts L-100	Adiprene parts L-315	Young's Modulus at 25°C (MPa)
(i)	0	45	55	160
(ii)	0	55	45	110
(iii)	0	70	30	80
(iv)	0	85	15	55
(v)	0	100	0	45
(vi)	50	50	0	35
(vii)	100	0	0	20
(viii)	——— Hytrel 5550 ———			118

Because the manufacture of each polyurethane tyre involved an individual chemical reaction between the polyol, cross-linker and catalyst, variability between nominally identical blends could not be avoided. Consequently, test samples were produced at the same times as the tyres and used for determining the actual Young's moduli. These will be quoted in the tables of results for the tyre tests. It should also be noted that, due to shrinkage and perhaps other sources of variability in manufacture, the measured carcass wall thicknesses were generally less than the design values.

VIII.2 Burst Strength

A limited number of 126-10 A and 143-10 B carcasses, the latter with no belt fitted, were subjected to the burst test in order to establish safe working pressures and the relationship between burst pressure, material modulus and carcass wall thickness. The results are given in table XLVI, together with : the safety factor assuming an operating pressure of 150 kPa, typical of 5.20/145-10 conventional tyres; the sidewall membrane stiffness, given by the product of Young's modulus (E) and wall thickness (t); and the ratio of burst pressure (P) to the sidewall stiffness.

Table XLVI

Burst Strength, 126-10 A and 143-10 B Carcasses

Tyre Ref.	Material Ref.	Young's Modulus (MPa)	Wall Thickness (mm)	Burst Pressure (P) (kPa)	Safety Factor	Stiffness E.t (kN/m)	Ratio P/E.t (m^{-1})
126-10 A1	(v)	46.1	2.7	324	2.2	124.5	2.60
126-10 A2	(vii)	21.6	5.2	311	2.1	112.3	2.77
126-10 A2	(vi)	35.4	5.2	414	2.8	184.1	2.25
126-10 A2	(v)	46.8	5.2	518	3.5	243.4	2.19
126-10 A2	(v)	45.5	5.2	518	3.5	236.6	2.19
126-10 A3	(vii)	21.9	7.6	442	2.9	166.4	2.66
126-10 A3	(vi)	34.1	7.6	511	3.4	259.2	1.97
126-10 A3	(v)	42.8	7.6	725	4.8	325.3	2.23
143-10 B1	(v)	46.5	3.0	317	2.1	139.5	2.27
143-10 B2	(v)	49.6	5.3	523	3.5	262.9	1.99
143-10 B3	(vi)	37.2	7.7	496	3.3	286.4	1.73
143-10 B4	(viii)	118.0	3.5	930	6.2	413.0	2.25

The one Hytrel tyre failed like the model tyres by the formation of a local bubble by cold flow prior to a split at the crown. The polyurethane tyres grew in a regular manner before splitting either at the crown or in a sidewall, there being no clear pattern of behaviour due, presumably, to failure occurring at a point of weakness.

The first comment to make on these results is that the burst pressure of the 143-10 B4 carcass injection moulded from Hytrel 5550 is similar to that of the equivalent model tyre, table XXI, showing that the scaling of the section dimensions was correct. This observation would be important if tyres of other sizes were to be designed.

Overall, the results in table XLVI show that the carcasses exhibit a range of burst pressures, and thus safety factors, as would be expected. However, there is a correlation between pressure and sidewall membrane stiffness, as the consistency of the final column of data (P/E.t) illustrates. Undoubtedly there is some variation due to the non-linearity of the stress strain properties of the materials but, for design purposes, it may be stated that burst pressure (P) is directly proportional to the product of material Young's modulus (E) and carcass wall thickness (t). Moreover, the one Hytrel carcass obeys this empirical relationship, although the physical

behaviour of this thermoplastic differs from that of the polyurethanes, particularly in terms of its yield strain. Also aspect ratio has little effect upon this ultimate pressure, as exemplified by the 143-10 B carcasses.

Taking the mean value of the ratio P/E.t in table XLVI, the burst pressure (P) may be related to Young's modulus (E) and wall thickness (t) by equation (1):

$$P = k.E.t \qquad (1)$$

where $k = 2.26 \mp 0.30\ m^{-1}$

and with P in kPa

E in MPa

and t in mm

Now a safety factor of 4 is probably the minimum which can be specified for a production, as opposed to an experimental, tyre. Thus for an operating pressure of 150 kPa, equation (1) may be used to calculate the required Young's moduli for a range of wall thicknesses. These are given in table XLVII.

Table XLVII

Carcass Modulus/Thickness Requirements for Burst Strength

Wall Thickness (mm)	Young's Modulus (MPa)
2.0	133
4.0	66
6.0	44
8.0	33

VIII.3 Growth with Inflation Pressure

The next property to be measured was growth with inflation and, because this is not a destructive test, a greater number of carcasses were examined. Difficulties, however, were met because these larger tyres would not seat correctly in the rims until a pressure of about 100 kPa was reached. This meant that changes in section width could not be measured with any accuracy, although the growths in section height were consistent. Thus only the latter are given in tables XLVIII.A and XLVIII.B for the 126-10 A and 143-10 B carcasses respectively, as percentage changes from 100 kPa to 200 kPa

pressure. Now as growth will be a function of the membrane compliance of a carcass, the latter calculated as the inverse of the membrane stiffness (E.t) is also listed in the tables.

Table XLVIII.A

Growth of 126-10 A Carcasses owing to Inflation

Tyre Ref.	Material Ref.	Young's Modulus (MPa)	Wall Thickness (mm)	% Growth in Height	Compliance 1/E.t (μm/N)
126-10 A1	(v)	46.1	2.7	5.68	8.03
	(iv)	54.8	2.7	4.01	6.76
	(iii)	71.8	2.7	2.25	5.18
	(ii)	105.9	2.7	1.33	3.50
126-10 A2	(vii)	21.6	5.2	6.64	8.90
	(vi)	35.4	5.2	2.81	5.43
	(v)	46.8	5.2	1.87	4.11
	(v)	45.5	5.2	1.53	4.23
	(iv)	53.7	5.2	1.24	3.58
126-10 A3	(vii)	21.9	7.6	2.53	6.01
	(vi)	34.1	7.6	1.80	3.86
	(v)	42.8	7.6	1.19	3.07
126-10 A4	(viii)	118.0	3.5	1.04	2.42

It may be noted that the lowest modulus materials were not used with the thinnest wall thickness and vice versa.

Table XLVIII.B

Growth of 143-10 B Carcasses owing to Inflation

Tyre Ref.	Material Ref.	Young's Modulus (MPa)	Wall Thickness (mm)	% Growth in Height	Compliance 1/E.t (μm/N)
143-10 B1	(v)	49.5	3.0	5.75	6.76
	(iii)	84.5	3.0	4.17	3.94
	(ii)	117.1	3.0	2.90	2.84
	(i)	162.8	3.0	2.38	2.04
143-10 B2	(v)	49.4	5.3	3.25	3.82
	(iv)	62.5	5.3	2.79	3.02
	(iii)	85.4	5.3	1.93	2.21
143-10 B3	(vi)	36.0	7.8	3.25	3.56
	(v)	45.5	7.8	2.14	2.82
	(iv)	52.3	7.8	1.86	2.45
143-10 B4	(viii)	118.0	3.5	2.23	2.42

A greater range of modulus was employed for these lower aspect ratio carcasses because they were not fitted with belts and would therefore be expected to exhibit more growth than the 126-10 A carcasses.

Figure 8.1 shows percentage growth from 100 kPa pressure to 200 kPa plotted against carcass membrane compliance for the two series of tyres and the greater growth of the lower aspect ratio 143-10 B is very apparent. In fact, in the region of low compliance, up to 5 μm/N, growth of these carcasses is over twice that of the high aspect ratio 126-10 A carcasses, in excellent agreement with the findings of the model tyre experiments, table XXII. In the region of high compliance, greater than 5 μm/N, the growth of the 126-10 A carcasses increases rapidly. This is probably caused by thinning of the wall and by unbalancing the otherwise equibiaxial stresses. On the other hand, the growth of the 143-10 B carcasses is dominated by the changes in meridional profile owing to their not being cast or moulded to an equilibrium shape, as discussed in the last chapter.

Now growth of no more than 3% at an inflation pressure of 200 kPa, somewhat greater than the nominal operating pressure of 150 kPa, can be tolerated which, in figure 8.1, corresponds to 1.5% because the pressure was increased from 100 kPa to 200 kPa in the experiments. Up to this level of growth,

Figure 8.1

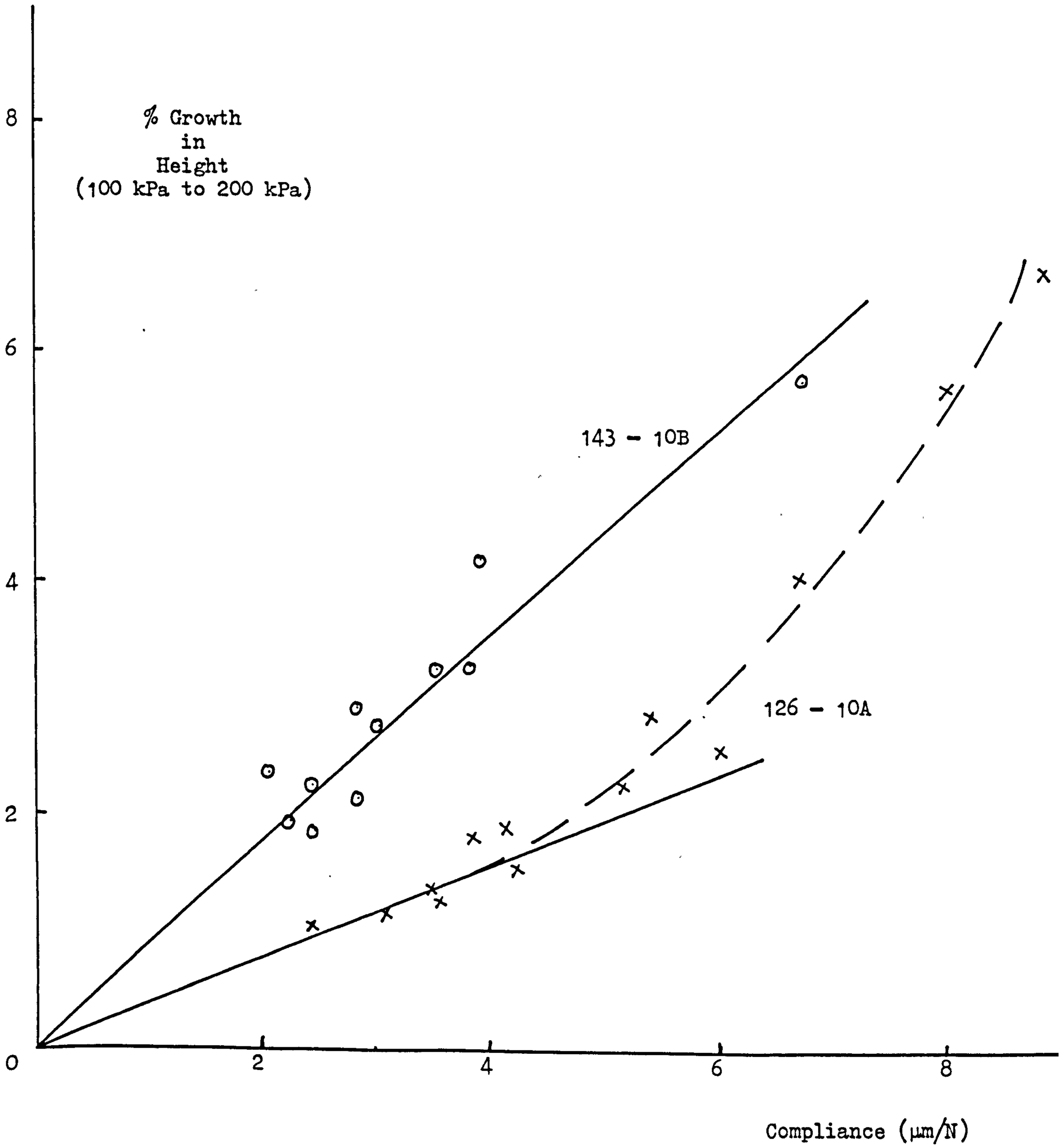
% Growth
in
Height
(100 kPa to 200 kPa)
8
6
4
2
0
2
4
6
8
143 - 10B
126 - 10A
Compliance (μm/N)

linearity can be assumed as shown by the straight lines in figure 8.1, so that the behaviour of the two carcass types may be expressed by equations (2) and (3):

for the 126–10 A

$$\% \text{ growth} = \frac{780}{E.t} \qquad (2)$$

and for the 143–10 B

$$\% \text{ growth} = \frac{1740}{E.t} \qquad (3)$$

with Young's modulus, E, in MPa
and wall thickness, t, in mm.

Using these equations, the moduli required to limit growth in section height to 3% may be calculated for a range of carcass wall thickness. However, it may be anticipated from examination of figure 8.1 that values for the lower profile 143–10 B will be large unless the wall thickness is considerably greater than that necessary for the 126–10 A. Consequently a restraining belt will be required, as was the case with the model 83–8 B tyres when this option reduced growth by about 50% or more, depending upon the material modulus, tables XXII and XXIII. If it is assumed the same effect will be achieved with the larger tyre, noting that scaling between the two sizes, model and car, was successful for burst strength and growth without a belt, then estimates of the material moduli required to limit growth to 3% with a belt fitted may also be made. The results of these calculations are given in table XLIX.

Table XLIX

Carcass Modulus/Thickness Requirements for 3% Growth

Wall Thickness (mm)	Material Young's Modulus (MPa)		
	126–10 A	143–10 B Without Belt	143–10 B With Belt
2.0	130	290	145
4.0	65	145	73
6.0	43	97	49
8.0	33	73	37

As may be seen, the moduli for the 126–10 A and 143–10 B tyres, the latter fitted with a belt, are not very different and when they are compared to

those given in table XLVI, calculated to give adequate burst strength, similar values occur for the range of wall thickness. This is an important observation for design purposes because it implies that a carcass which meets the requirements of burst strength, by virtue of its wall thickness and material Young's modulus, will not exhibit excessive growth when inflated to the normal operating pressure.

Related to growth with inflation is creep but, because of the results obtained on the model tyres, it was not examined in detail. However, a 126-10 A4 Hytrel tyre and a 126-10 A2 polyurethane tyre, blend (v), were inflated to 150 kPa and their section heights monitored over a period of 9000 h. The increase due to creep only amounted to 0.3%.

VIII.4 Radial Stiffness

One of the most important investigations afforded by the 126-10 A and 143-10 B series of fabricless tyres was the examination of the effects of both carcass material modulus and wall thickness on radial stiffness. As has been shown, membrane theory can be used to assess the ability of carcasses to contain the inflation pressure but a tyre when it is loaded radially is no longer axisymmetrical and, at present, not susceptible to theoretical analysis.

The measurements of load and radial deflection were made using the same technique employed for the model tyres, except that more robust equipment was necessary : an Avery tensile/compressive rig with a capacity of 50 kN. Detachable tread bands were made from a conventional tread rubber compound for the two series of tyre, incorporating a two ply rayon belt in those for the 143-10 B tyres. These were fitted to the uninflated carcasses and were found to be satisfactory for these pseudo-static tests. As explained in VII.2.5, it is important to measure radial stiffness of complete tyres because the absence of a tread affects the geometry of the distortion of the carcass, even if tread stiffness per se is negligible.

The tyres were tested at four inflation pressures : 50, 100, 150 and 200 kPa; and the results were analysed statistically as before according to equation (9) in chapter VI :

$$W = (A + B.p)d^n$$

Two conventional tyres were included in the experiments, a 5.20–10 cross-biassed tyre and a 145–R–10 radial. The results for these tyres are included in both table L, the analyses of the 126–10 A series, and table LI for the 143–10 B series. Total stiffness is calculated for a load of 2.25 kN and from the radial deflection at a pressure of 150 kPa.

Table L

Radial Stiffness Analysis, 126–10 A Tyres

Tyre Ref.	Material Ref.	Young's Modulus (MPa)	Wall Thickness (mm)	Stiffness Parameters A	B	n	Total Stiffness (kN/m)
126–10 A1	(v)	46.1	2.7	25.3	0.176	1.15	84.5
	(iv)	54.8	2.7	24.6	0.200	1.14	85.8
	(iii)	71.5	2.7	30.8	0.287	1.11	104.2
	(ii)	105.9	2.7	43.2	0.320	1.08	114.0
126–10 A2	(vii)	21.6	5.2	28.4	0.217	1.14	94.2
	(vi)	35.4	5.2	35.4	0.218	1.09	101.7
	(v)	46.8	5.2	52.9	0.265	1.10	118.0
	(v)	45.4	5.2	38.5	0.213	1.18	123.8
	(iv)	53.7	5.2	62.3	0.318	1.05	127.1
126–10 A3	(vii)	21.9	7.6	48.3	0.294	1.08	115.4
	(vi)	34.1	7.6	67.4	0.267	1.09	137.0
	(v)	42.8	7.6	95.2	0.254	1.10	172.3
5.20–10 Cross-biassed			-	18.4	0.369	1.18	122.7
145–R–10 Radial			-	18.9	0.401	1.08	99.9

Table LI

Radial Stiffness Analysis, 143-10 B Tyres

Tyre Ref.	Material Ref.	Young's Modulus (MPa)	Wall Thickness (mm)	Stiffness Parameters A	B	n	Total Stiffness (kN/m)
143-10 B1	(v)	49.5	3.0	29.6	0.337	1.08	101.2
	(iii)	84.5	3.0	26.4	0.208	1.24	116.2
	(ii)	117.1	3.0	51.7	0.353	1.11	142.5
	(i)	162.8	3.0	61.5	0.314	1.13	152.1
143-10 B2	(v)	49.4	5.3	48.0	0.223	1.18	133.5
	(iv)	62.5	5.3	59.7	0.260	1.16	152.7
	(iii)	85.4	5.3	94.1	0.275	1.13	185.0
143-10 B3	(vi)	36.0	7.8	70.8	0.284	1.10	148.8
	(v)	45.5	7.8	71.2	0.214	1.19	168.2
	(iv)	52.3	7.8	101.6	0.238	1.16	203.2
5.20-10 Cross-biassed			-	18.4	0.369	1.18	122.7
145-R-10 Radial			-	18.9	0.401	1.08	99.9

The units of A, B and n are consistent with W in N, p in kPa and d in mm.

Examination of table L and LI reveals a number of obvious conclusions:

a) total stiffness increases with carcass material modulus;

b) total stiffness increases with carcass wall thickness, material blend (v) is common to all tyre types and shows this trend clearly;

c) the structural stiffness parameter, A, of the fabricless tyres is always higher than those of the two conventional tyres and can be as much as five times greater;

d) the pneumatic stiffness parameter, B, of the fabricless tyres is less than those of the conventional tyres;

e) although some variants are comparable with the conventional tyres, the overall stiffnesses of the fabricless tyres are generally greater, showing that their higher structural stiffnesses more than compensate for their lower pneumatic stiffnesses.

However, to establish the relationship between the radial stiffness of a fabricless tyre and its carcass material modulus and wall thickness, it is necessary to analyse the results further. Consider first the power index n, which describes the curvature of the load-deflection lines at equal pressure. It is apparent by inspection of table L and LI that this parameter does not vary systematically with either material modulus or wall thickness. In fact the range of values is small so that a mean value and its standard deviation may be calculated for each series of tyre:

126-10 A mean value of $n = 1.11 \mp 0.04$
143-10 B mean value of $n = 1.15 \mp 0.05$

Now it has already been observed that the structural stiffness parameter, A, varies with both modulus and thickness. This is confirmed by figures 8.2a and 8.2b for the 126-10 A and 143-10 B series respectively. On these graphs, separated lines for the three wall thicknesses may be constructed showing the dependence of A on material modulus. However there is some scatter in the data which might be attributable to the statistical method used for calculating the three stiffness parameters, including A.

Figures 8.3a and 8.3b are the corresponding graphs for the pneumatic stiffness parameter, B. Although there appears to be a trend for B to increase or decrease with modulus for some wall thicknesses, there is no overall pattern to the data. It may be concluded, therefore, that this parameter is independent of material modulus and wall thickness, thus allowing mean values and their standard deviations to be calculated:

126-10 A mean value of $B = 0.252 \mp 0.047$
143-10 B mean value of $B = 0.271 \mp 0.051$

Having shown that neither the pneumatic stiffness parameter, B, nor the power index, n, varies with wall thickness (t) and material modulus (E), their averaged values may be used to recalculate the structural stiffness

Figure 8.2a

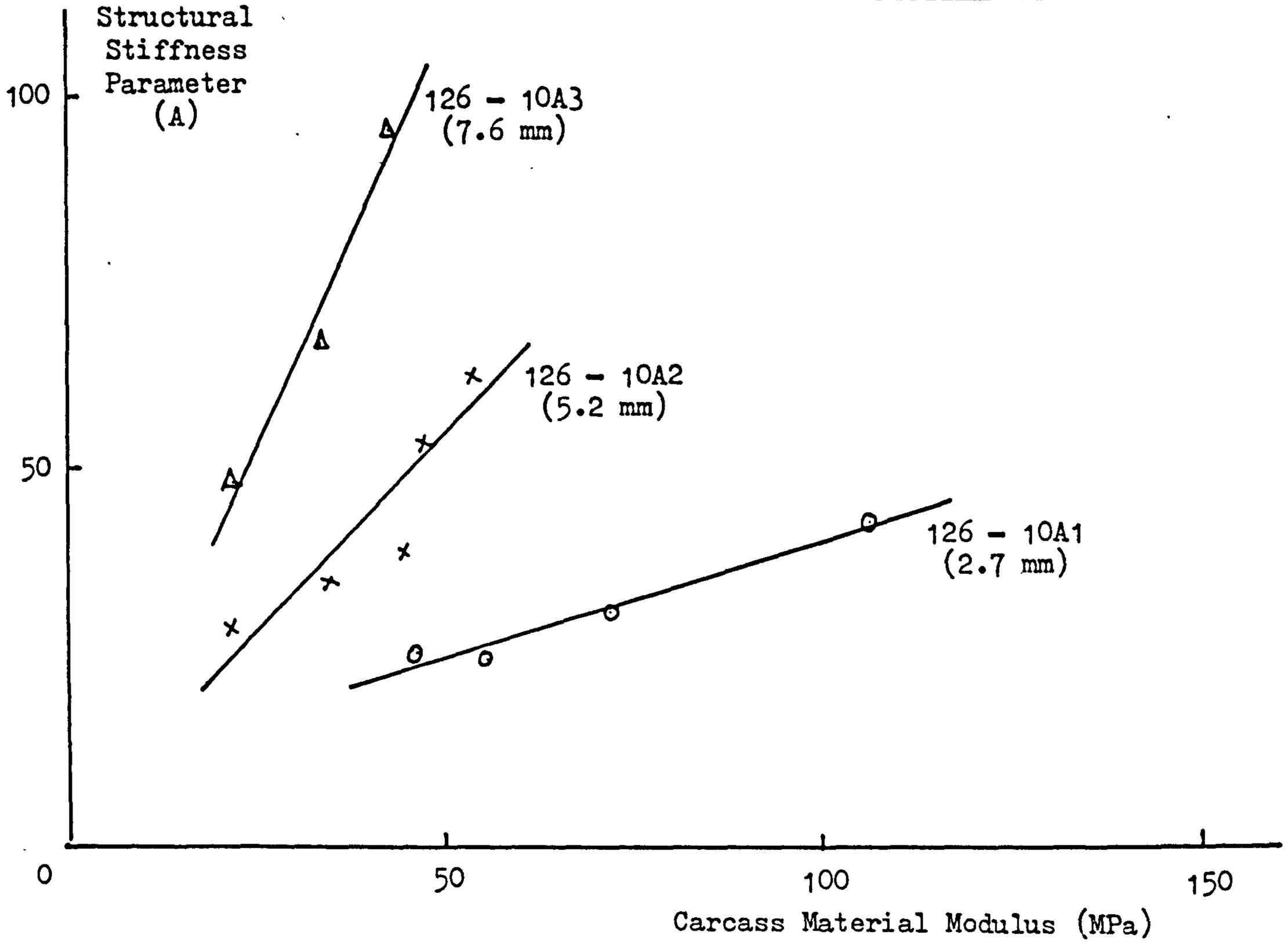

Figure 8.2b

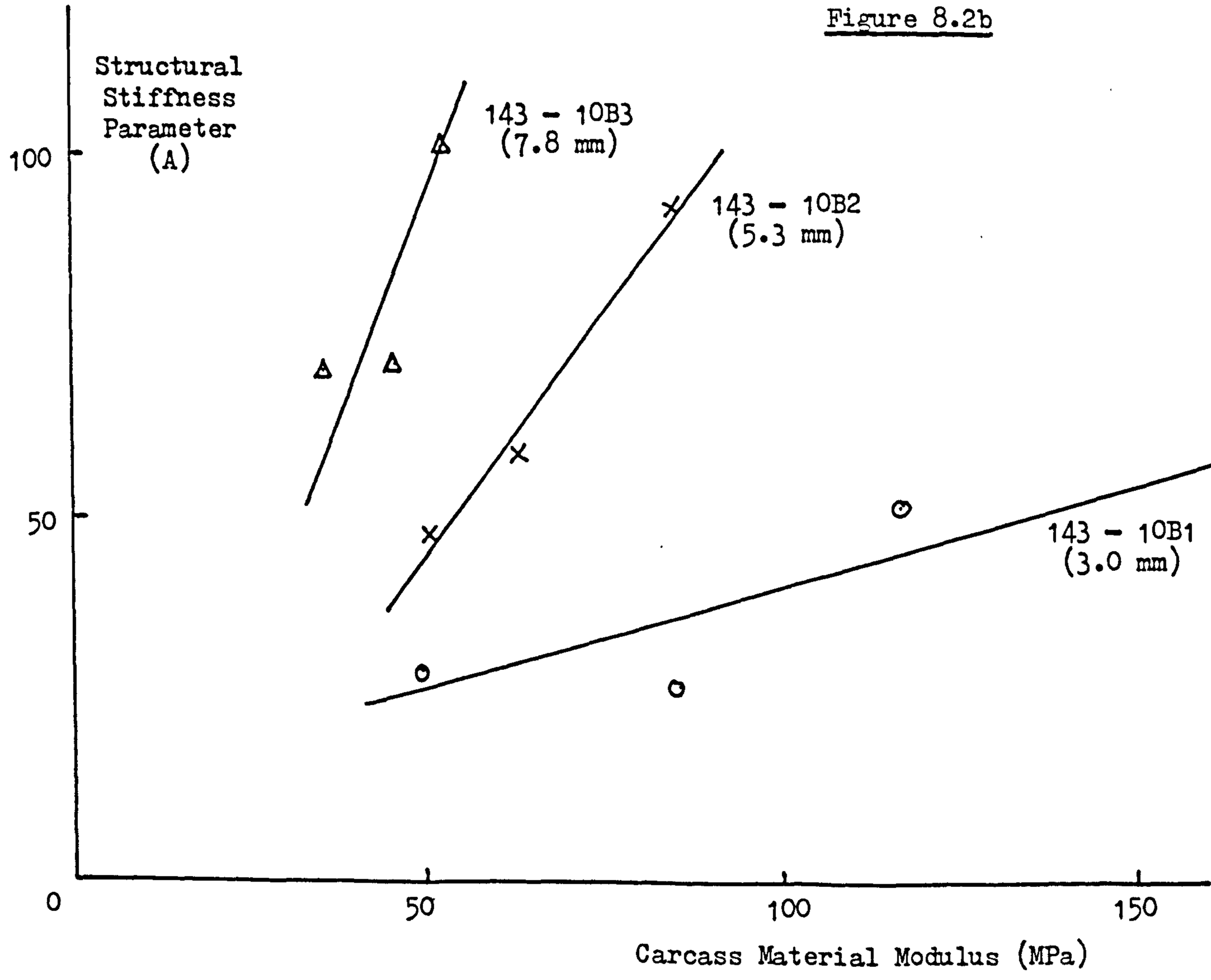

Figure 8.3a

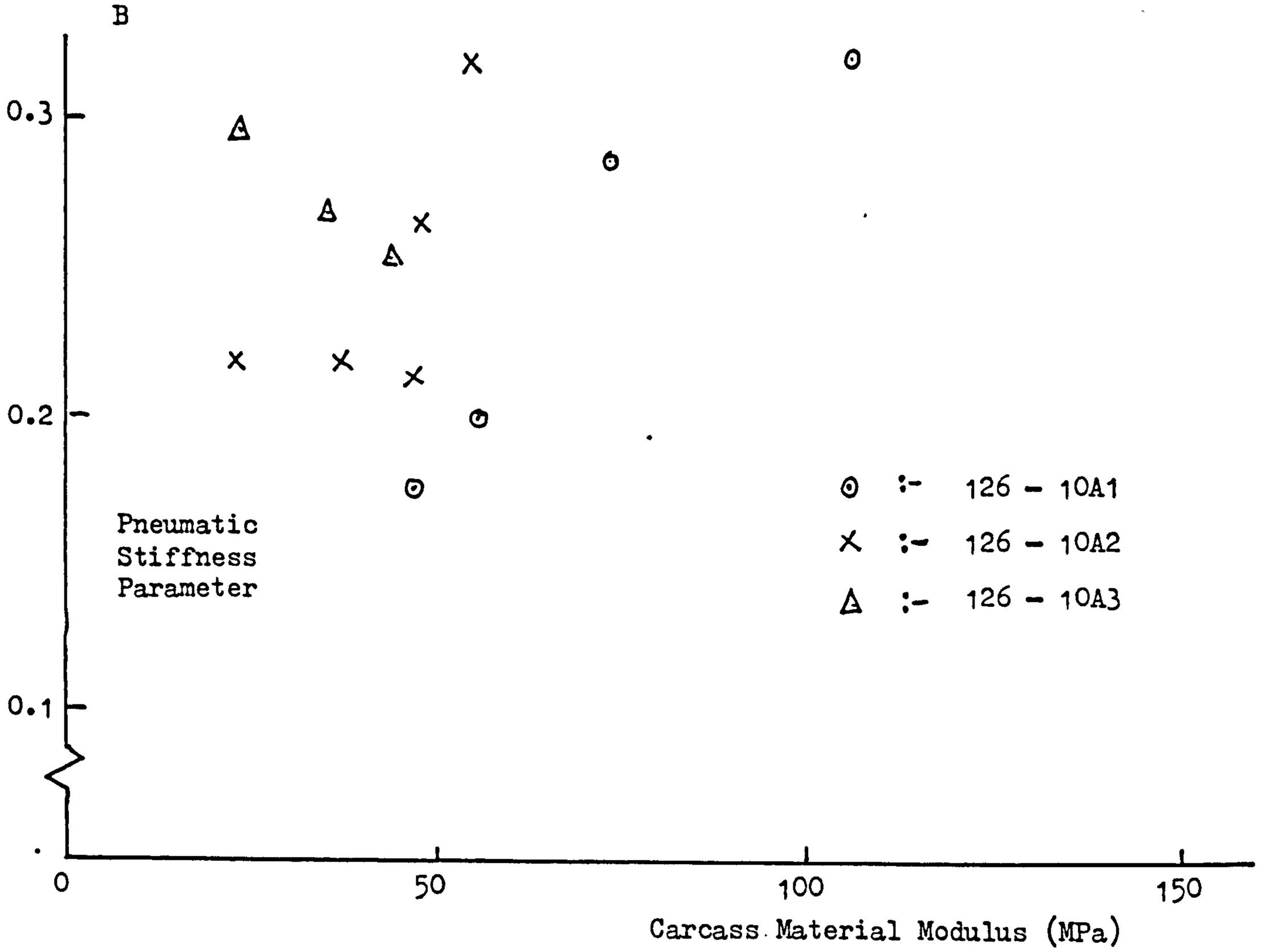

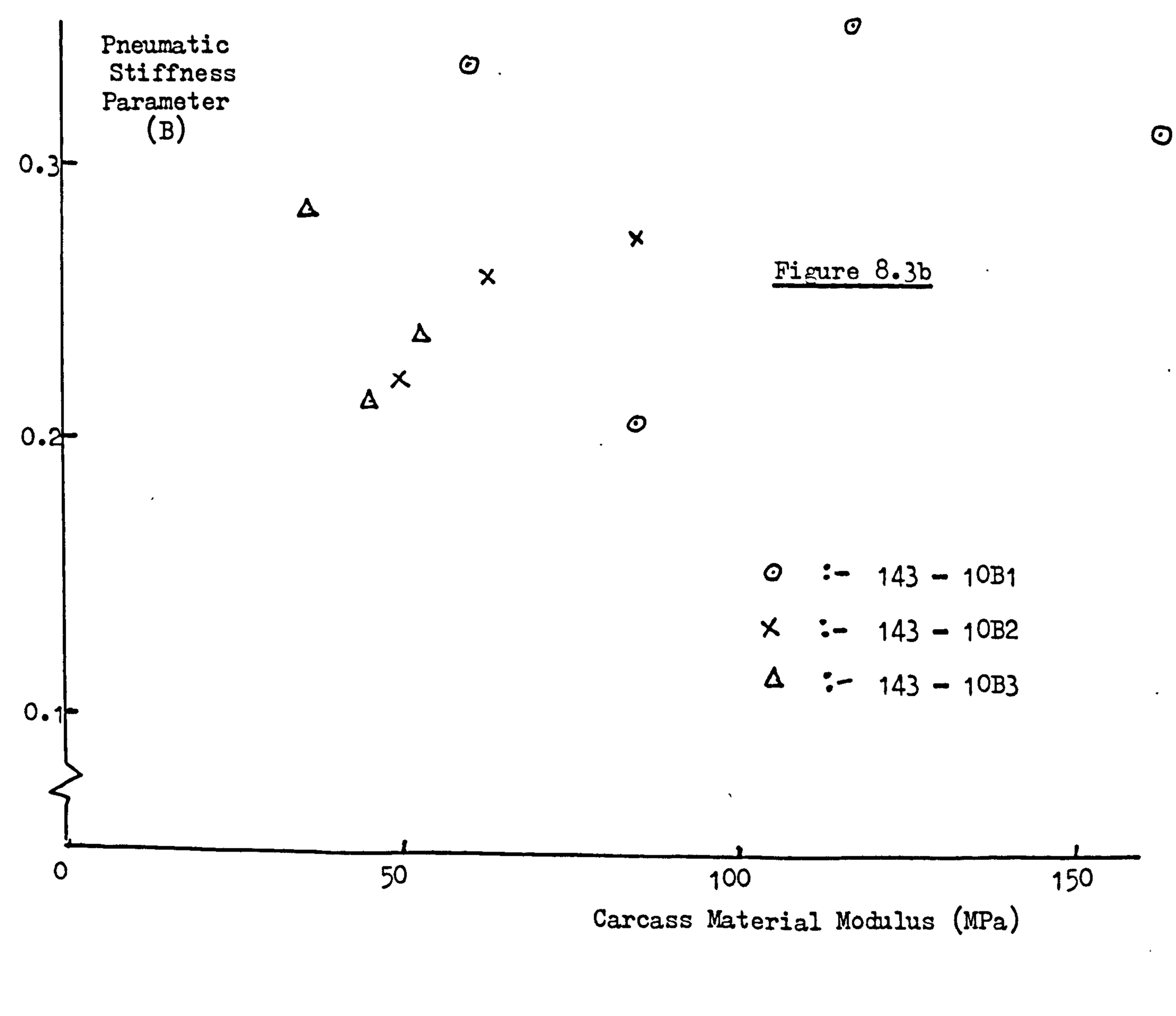

Figure 8.3b

parameter, A, of each tyre with the objective of reducing the scatter. This would allow A to be related to E and t with more confidence.

Equation (9) from chapter VI can be rearranged as:

$$A = \frac{W}{d^n} - B.p$$

so that by substituting the load (W), calculated from the original values of A, B and n, at a pressure (p) of 150 kPa and a radial deflection (d) of 20 mm, together with the averaged values of B and n for each series of tyre, normalised values of A are obtained. These are listed in tables LII and LIII for the 126-10 A and 143-10 B series respectively. Also given is the ratio of A to the carcass material modulus (E).

Table LII

Structural Stiffness Parameter, 126-10 A Tyres

Tyre Ref.	Material Ref.	Young's Modulus (MPa)	Wall Thickness (mm)	Normalised Parameter A	Ratio A/E
126-10 A1	(v)	46.1	2.7	21.3	0.46
	(iv)	54.8	2.7	22.5	0.41
	(iii)	71.5	2.7	37.4	0.52
	(ii)	105.9	2.7	45.4	0.43
126-10 A2	(vii)	21.6	5.2	29.2	1.35
	(vi)	35.4	5.2	35.7	1.01
	(v)	46.8	5.2	48.9	1.05
	(v)	45.4	5.2	53.2	1.17
	(iv)	53.7	5.2	55.3	1.03
126-10 A3	(vii)	21.9	7.6	46.4	2.12
	(vi)	34.1	7.6	63.7	1.87
	(v)	42.8	7.6	93.0	2.17

Table LIII

Structural Stiffness Parameter, 143-10 B Tyres

Tyre Ref.	Material Ref.	Young's Modulus (MPa)	Wall Thickness (mm)	Normalised Parameter A	Ratio A/E
143-10 B1	(v)	49.5	3.0	24.2	0.49
	(iii)	84.5	3.0	35.0	0.41
	(ii)	117.1	3.0	53.8	0.46
	(i)	162.8	3.0	61.4	0.38
143-10 B2	(v)	49.4	5.3	48.2	0.98
	(iv)	62.5	5.3	62.9	1.01
	(iii)	85.4	5.3	86.5	1.01
143-10 B3	(vi)	36.0	7.8	58.2	1.62
	(v)	45.5	7.8	76.5	1.68
	(iv)	52.3	7.8	103.8	1.99

When the normalised structural stiffness parameters are plotted against carcass material modulus for the three wall thicknesses, figures 8.4a and 8.4b, it may be seen that the scatter is reduced and straight lines passing through the origin may be fitted to the data points. Consequently, an empirical relationship has been established:

$$A = a.E$$

where a is a function of wall thickness.

In tables LII and LIII, 'a' corresponds to the mean value of the ratio A/E for any wall thickness. They are as follows:

126-10 A tyres, t = 2.7 mm : a = 0.46
t = 5.2 mm : a = 1.12
t = 7.6 mm : a = 2.05

143-10 B tyres, t = 3.0 mm : a = 0.43
t = 5.3 mm : a = 1.00
t = 7.8 mm : a = 1.76

Clearly 'a' increases more rapidly than the wall thickness and therefore the two were related by a logarithmic plot, figure 8.5. From this, the final form of the dependence of the structural stiffness parameter, A, on

Figure 8.4a

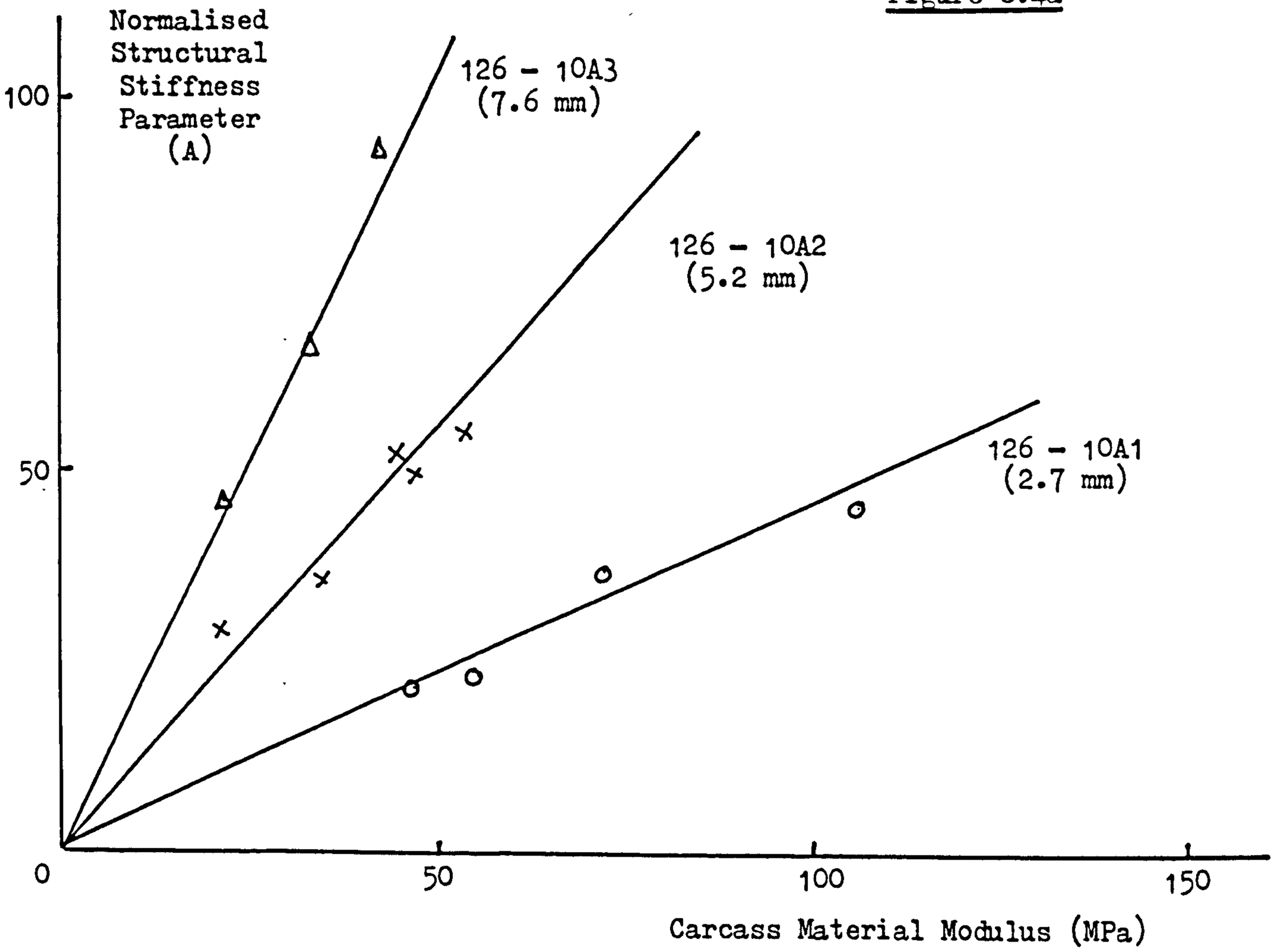

Figure 8.4b

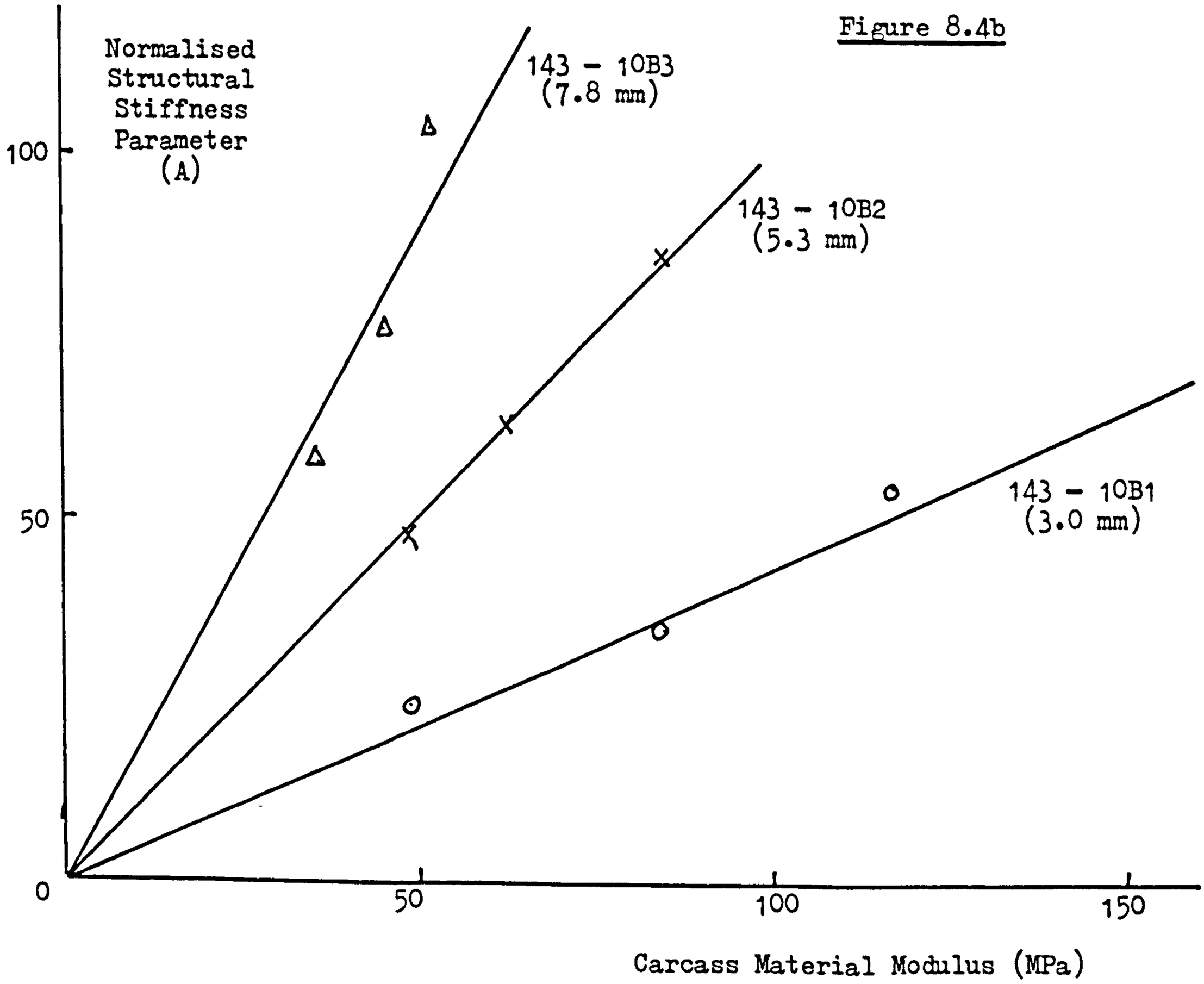

Figure 8.5

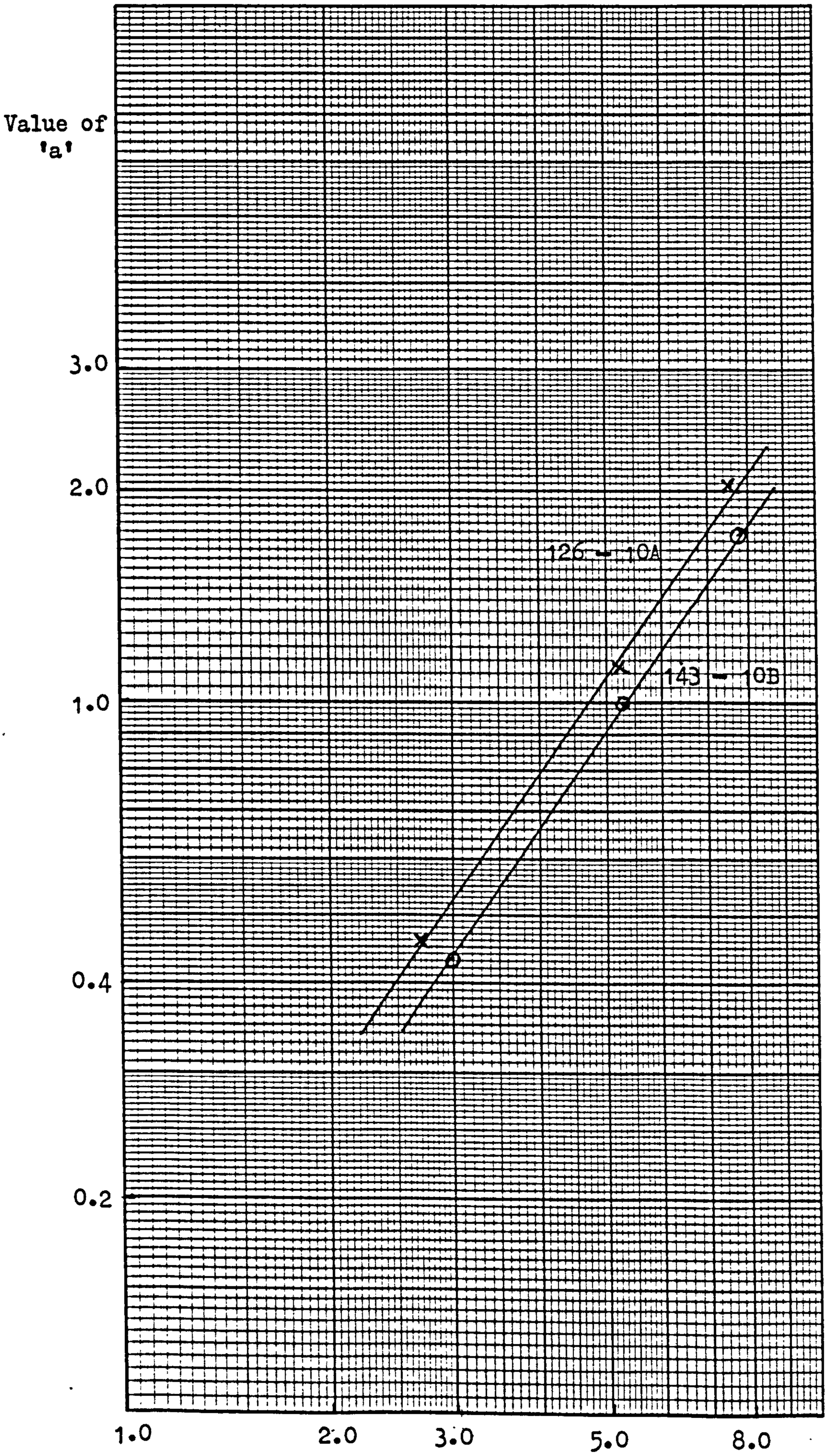
Value of 'a'
3.0
2.0
1.0
0.4
0.2
126 – 10A
143 – 10B
1.0
2.0
3.0
5.0
8.0
Wall Thickness (mm)

carcass material Young's modulus, E, and wall thickness, t, is obtained. For the 126–10 A series of tyre it is:

$$A = 0.109\ E.t^{1.45} \tag{4}$$

and for the 143–10 B series it is:

$$A = 0.089\ E.t^{1.45} \tag{5}$$

Equations (4) and (5) illustrate an interesting and unexpected result. From the analogy of a bending beam, it would be anticipated that the structural radial stiffness of a toroid would be proportional to the cube of its wall thickness and yet, experimentally, it has been shown to vary with the thickness raised to the power of about 1.5. The reason for this is not apparent; it may be due to the complex geometry of a toroid and its distortion under the action of a localised radial load when bending in the meridional and circumferential planes will be involved. Further study will be necessary to elucidate this behaviour, perhaps involving finite element stress analysis of hypo-elastic shell-like bodies. Computer programs for this are being developed but are not yet available. However, for the research being described, the result is very significant because wall thickness, although still important, is not so critical as would have been the case if stiffness were proportional to its cube.

To summarise the investigation of the radial stiffness characteristics of the fabricless tyres, the various empirical relationships which have been established may be brought together into equations describing the behaviour of the two types of tyre. The basic equation is:

$$W = (A + B.p)d^{n}$$

Now B and n were evaluated by averaging the results for the individual tyres in each series. The standard deviations of the mean values were also calculated, so that Student's 't' test may be used to determine whether the two series give significantly different results. For B, 't' = 0.91 and for n, 't' = 2.07, both with 20 degrees of freedom. These indicate that neither the values of B nor n for the two series of tyre are significantly different at the 95% confidence level. Thus averaged values may be taken. Thus, for the 126–10 A series the load, pressure, deflection relationship becomes:

$$W = (0.109.E.t^{1.45} + 0.26.p)d^{1.13} \tag{6}$$

and for the 143-10 B series is:

$$W = (0.089.E.t^{1.45} + 0.26.p)d^{1.13} \qquad (7)$$

where W is the radial load (N)
E is the carcass material Young's modulus (MPa)
t is the carcass wall thickness (mm)
p is the inflation pressure (kPa)
and d is the radial deflection (mm)

Using equations (6) and (7), alternative combinations of wall thickness, material modulus and inflation pressure may be considered when optimising the design of a fabricless tyre. This will be undertaken in the final chapter.

VIII.5 Comfort

There are many factors which affect the noise and vibrations perceived by passengers in a car. Tyres and the road surface on which they are running are responsible for generating a spectrum of vibrations and the former also transmit these vibrations to the axles of the vehicle. Thus there are two aspects of tyre behaviour which are important : generation and transmission. However, a detailed examination of these properties with respect to the fabricless tyres of the research was considered unnecessary for a general assessment but would receive attention should such constructions be considered for commercial manufacture.

To establish whether fabricless tyres, in general, present any unusual problems with respect to comfort, a simple test was established which combines both generation and transmission. A two metre diameter drum, on which the tyres could be run under load, was equipped with a series of transverse slats of various heights and lengths. By careful choice of these, it was ensued that, in one revolution of the drum at 58 km/h, a wide frequency range of vibrations would be generated by a tyre. An accelerometer on the tyre/wheel axle was used to record the waveform transmitted to it through the tyre, again in one revolution of the drum. The recorded waveform was analysed into its Fourier components and the harmonic response coefficients thus calculated were divided into three frequency bands and averaged.

A total of five tyres were examined by this procedure : the conventional 5.20–10 and 145–R–10 tyres; the 126–10 A2 and 143–10 B2 tyres with carcasses made from polyurethane blend (v) and rubber treads; and a 126–10 A2 with both carcass and tread cast in PU blend (v). The last tyre was included because great difficulties were experienced in bonding rubber treads to PU carcasses, particularly for dynamic testing, so that the option of an all–polyurethane tyre had to be considered if all the planned investigations were to be completed.

The results of the comfort tests are given in table LIV, the radial load was 2.6 kN and the inflation pressure was 150 kPa. Included in the table are the measured radial deflections.

Table LIV

Harmonic Response Coefficients

Tyre Ref.	Tread Material	Radial Deflection (mm)	Mean Coefficient (arb. units) Low Frequency (20 – 55 Hz)	Mid Frequency (55 – 80 Hz)	High Frequency (80 – 150 Hz)
5.20–10	Rubber	21.1	43	3	12
145–R–10	Rubber	25.6	43	8	18
126–10 A2	Rubber	17.4	48	32	13
143–10 B2	Rubber	~ 17.8	60	8	20
126–10 A2	PU	8.1	210	40	55

It is immediately apparent that the all–polyurethane tyre is very poor. Both its harder tread, which will generate more vibrations because of its inability to envelop the slats on the drum, and its high radial stiffness will contribute to its performance. The results for the fabricless tyres with rubber treads are more promising. Given their lower radial deflections, or greater radial stiffnesses, their transmitted vibrations are only marginally worse than those from the conventional tyres. Thus it would appear that if a fabricless tyre has a tread material comparable in hardness to current production tyres and it has similar radial stiffness, then its "comfort" properties should be acceptable.

It was decided not to proceed to full vehicle tests to confirm the results of the drum tests. However a Leyland Mini car was fitted with four of the 126–10 A3 all–polyurethane tyres and their poor performance was

immediately apparent. Also, because their radial deflection was less than half that of conventional cross-biassed tyres, handling in terms of very low self-aligning torque and general feel through the steering wheel was quite unacceptable.

VIII.6 Structural Performance or Fatigue

The investigation of fatigue of the fabricless car tyres when run continuously under load proved far from satisfactory. The intention was to assess both the 126-10 A and 143-10 B series with rubber treads because measurements of comfort, wear resistance and wet grip, the latter two with model tyres, had shown that polyurethane treads were unsuitable. However, when 126-10 A2 tyres with adhered rubber treads were manufactured and run, most failed prematurely after a few kilometres owing to tread looseness. Nevertheless, two tyres did run until failure of their carcasses was observed. They were made from polyurethane blend (v), with a nominal Young's modulus of 45 MPa, and were inflated to 150 kPa pressure. Under the schedule load (2.25 kN), one tyre had a life of 4000 km; while the other tyre with 50% overload only lasted for 20 km. In both cases the cause of failure was . . a circumferential split in the upper sidewall adjacent to the shoulder.

None of the lower profile 143-10 B tyres was run successfully to give an indication of its structural performance. It was decided, therefore, that there was no alternative to examining a number of the 126-10 A tyres with integral polyurethane treads of the same blends as their carcasses. To make these tyres, a mould similar to the one used for the 126-10 A2, 5.5 mm thick, carcasses was obtained but with an enlarged cavity to form the tread. A simple four-rib pattern was incorporated to reduce bending stiffness in the plane of the meridian. This approach could not be followed for the 143-10 B series because the required belt could not be located and held in place during centrifugal casting.

A total of seventeen 126-10 A2 tyres with integral treads were made and tested. The radial load was 150% of the schedule (2.25 kN) and the tyres were inflated to 150 kPa. The measured structural lives of the tyres are given in table LV, together with the references to one of the three blends of polyurethane from which the tyres were made and measured or estimated radial deflections.

Table LV

Fatigue Lives, 126-10 A2 Tyres with Integral Treads

Blend Ref.	Young's Modulus (MPa)	Radial Deflection (mm)	Life (km)
(v)		13.6	6166
(v)		13.6	8222
(v)	45	13.6	15311
(v)		13.6	28184
(v)		13.6	38019
(vi)		16.8	135
(vi)		15.4	616
(vi)	35	15.5	2163
(vi)		17.0	10012
(vi)		16.8	7674
(vii)		19.4	248
(vii)		18.7	9886
(vii)		19.0	1905
(vii)	20	19.2	871
(vii)		19.6	882
(vii)		19.3	692
(vii)		19.6	670

Failure of the tyres occured as the result of splits in the upper sidewall but, as may be seen, the range of fatigue lives is large, both between tyres made from the three blends of polyurethane and within groups of nominally similar tyres. However, there is a clear trend for tyres with low radial deflection to have greater lives. This hypothesis was tested statistically by regression analysis with radial deflection as the independent variable and log (fatigue life) as the dependent variable. The correlation coefficient is:

$$r = -0.6429 \quad \text{with 15 degrees of freedom;}$$

which, from the tables, is between 99.0% and 99.9% significant. The calculated regression equation is:

$$\log (\text{fatigue life}) = 6.607 - 0.190.d$$

and is illustrated by figure 8.6.

Figure 8.6

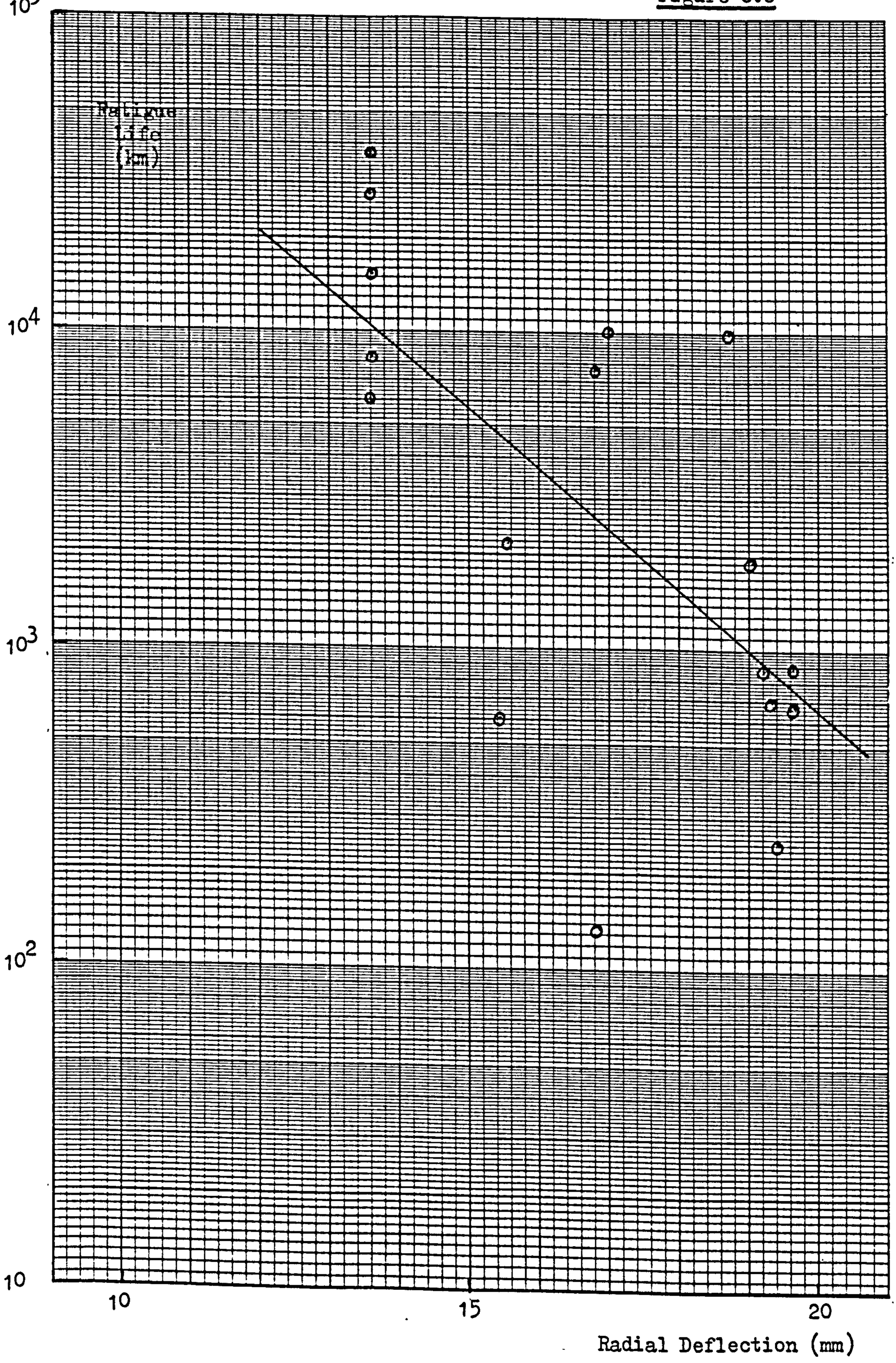
Refrigue life (km)
10^5
10^4
10^3
10^2
10
10
15
20
Radial Deflection (mm)

Thus it has been established that, like the model tyres, the life of the 126–10 A2 polyurethane tyre with an integral tread is critically dependent upon the radial deflection at which it runs. The latter is governed by the Young's modulus of its carcass material and the inflation pressure but, as will be discussed, these two controlling variables are not independent. The maximum allowable pressure is set by the material modulus for any given wall thickness.

Now the radial deflection of a conventional cross-biassed 5.20–10 tyre under 50% overload is about 27 mm and under this condition its fatigue life would exceed 20,000 km. Consequently, none of the 126–10 A2 tyres tested approaches this structural performance. In the final chapter, consideration will be given to whether the required improvement could be made.

To complete the examination of the structural performance of fabricless car tyres, it is worth citing the evidence provided by Firestone, already referred to in chapter I, reference 3. The tyre size employed was 7.35–14, much larger than the equivalent 5.20–10 manufactured and tested in this research, and therefore direct comparisons cannot be made. Nevertheless, it may be assumed that, relative to their respective schedule loads, the two sizes of tyre would run at similar radial deflections calculated as proportions of their section widths. This assumption is supported by data given by Firestone on the radial deflection of its fabricless tyre. Under the schedule load, this is 22.4 mm compared to 29.6 mm for the equivalent conventional cross-biassed tyre and 37.1 mm for the equivalent radial. Referring back to table L, the total stiffnesses of typical 126–10 A tyres would result in similar relative deflections.

A graph illustrating the structural testing of the Firestone tyre is reproduced as figure 8.7. Ten tyres were run, first under the schedule load of 5.15 kN for 400 km. The load was then increased in steps with four tyres proceeding to 6.35 kN, when two were removed without failure after running a total distance of 2900 km and the others failed after 5600 km and 5900 km. Of the remaining six tyres, four were removed without failure with a load of 6.05 kN and two were loaded to 6.85 kN (about 33% overload) when they failed after 4200 km and 5600 km. With this regime of testing, it is difficult to analyse the data further except to note that, with an overload of more than 20%, the tyres failed with lives between 4200 km and 5900 km. Referring to figure 8.6, it may be seen that this range corresponds to a deflection of 15 mm for the 126–10 A2 tyres, typical of the tyres tested.

Figure 8.7

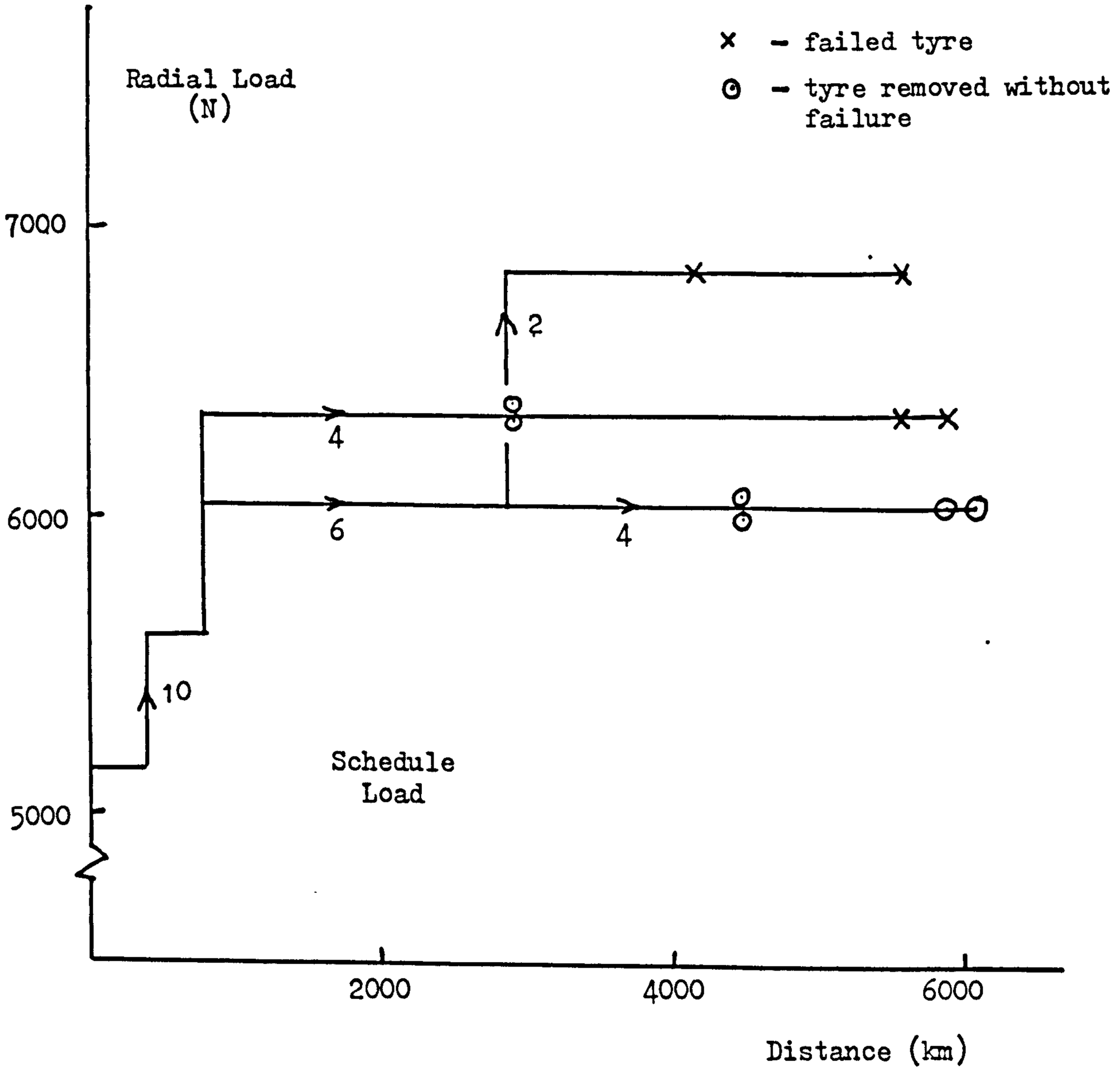

Reproduced from :

G.Alliger, CMRA Paper No. 725, New York, Mar '80

VIII.7 Summary of Car Tyre Results

Although practical difficulties were experienced in this study of fabricless car tyres, primarily due to the unsolved problem of bonding a rubber tread to a polyurethane carcass, progress was made in quantifying the behaviour of such tyres, particularly with respect to wall thickness.

Wall thickness and the Young's modulus of the carcass material determine the membrane stiffness of a carcass, thus controlling growth with inflation and, ultimately, contributing to its burst strength.

When burst strength was examined, it was found to be directly proportional to the product of Young's modulus and wall thickness, irrespective of the type of material : grade of polyurethane or Hytrel; and the aspect ratio of the carcass : A or B series. Similarly, when growth was measured, the change in section height on inflation was directly proportional to the carcass membrane compliance, which is the inverse of the product of modulus and wall thickness. However, in this case, the constants of proportionality for the A and B series were different, the growth of the 143-10 B tyres being much greater. This design, therefore, requires a reinforcing belt to limit growth to an acceptable level, a conclusion also reached for the corresponding model tyre.

Radial stiffness and its dependence upon carcass material modulus and wall thickness was the subject of an important investigation because, with the model tyres, only the effects of modulus had been determined. By analysing the data statistically, it was shown that the pneumatic stiffness parameter and the power index of the load-pressure-deflection equation did not vary significantly for all the tyres examined. Advantage was taken of this to normalise the structural stiffness parameter values in order to reduce their scatter. It was then possible to relate this parameter directly to the carcass material modulus and show that it is also proportional to the wall thickness raised to a power of about 1.5.

When comfort, or the generation and transmission of vibrations, was investigated briefly, two conclusions could be drawn. First, a fabricless tyre must deflect radially under load by about the same amount as a conventional tyre. Second, the hardness of its tread must not exceed that of a conventional rubber compound. A radially stiff tyre with a hard polyurethane tread resulted in accelerations at the axle four times the magnitude of those recorded with a conventional tyre.

Finally, the structural performance or fatigue of fabricless tyres was

measured. Unfortunately, the preferred tyres with rubber treads failed prematurely owing to tread looseness and so reliance had to be placed on results from tyres with integral polyurethane treads. The results were very scattered but, nevertheless, statistical analysis showed there was a very significant dependence of life on radial deflection. If run at the same deflection as the equivalent conventional tyre, these fabricless tyres would have very inferior structural lives, a conclusion which is supported by data published by Firestone.

In the next and final chapter, the relationships established in this and the preceeding chapter will be used to assess the technical viability of fabricless tyres. Apart from the meridional profile, other parameters which are available for optimisation are carcass material Young's modulus, wall thickness and inflation pressure. The question to be answered is whether a combination of these can be identified which will raise the performance of fabricless tyres to the level where they can compete with conventional tyres, particularly those with a radial construction and steel reinforced belt.

CHAPTER IX : DISCUSSION AND CONCLUSIONS

IX.1 Introduction

The aim of the research undertaken is to assess the technical viability of fabricless tyres as alternatives to the modern, conventional designs used on passenger cars. However before examining the experimental data obtained in this context, it is worth summarising the principal aspects of the research and some of the more general conclusions.

IX.2 Design of Fabricless Tyres

Stress analysis by the method of finite elements (FEA) is becoming the preferred technique for assessing the designs of products and engineering components whose geometries or loading conditions are sufficiently complex to preclude the well established analytical methods. Moreover FEA is now being extended to hyper-elastic materials, with their attendant problems of large distortions and non-linear elasticity, and therefore will soon become suitable for fabricless tyres. However, at present, it can only be used for the case of free inflation, when the tyre and its loading are, and remain, axisymmetrical. This is demonstrated in appendix I but, for the purposes of the research, FEA was rejected in favour of the simpler shell theory, shown to be sufficiently accurate for predicting changes in the profiles of fabricless tyres and for determining their growth when inflated.

Shell theory has been developed to cover the cases of tyre profiles with a circular meridian, a meridian composed of elliptical and circular arcs, and meridians based on the analogy of cross-biassed tyres for which a theory was in existence. It was apparent, when these alternatives were examined, that the profile based on the analogy of a cross-biassed tyre with a constant bias angle of 45^{o} is superior for withstanding inflation. It results in uniform equibiaxial stresses when the tyre is inflated, so allowing the tyre's carcass to be manufactured with a uniform wall thickness, while the equibiaxial stresses minimise the required modulus of the carcass material to contain the pressure. It was anticipated that minimising the modulus would be important because of its effect on radial stiffness, although the magnitude of this could not be calculated.

Using the theory of a constant bias angle tyre, a computer program was written whereby a tyre profile of any required radius and width could be determined. Two of these profiles were used as the basis for the A series model and car tyres. However, one disadvantage of these designs is that they have a high aspect ratio of about 90%. Modern passenger car tyres have aspect ratios of 80%, 70% or even 60% so that, by comparison, the A series fabricless tyres resemble the older cross-biassed tyres which were fully developed and widely used in the 1950s and 1960s, after which the radial tyre began to dominate the market.

To produce a lower aspect ratio tyre with a fabricless construction would require a higher modulus material to contain the large circumferential stress induced in its crown. This would lead to sidewalls which were unnecessarily stiff. Alternatively, the carcass could be designed to have a significant thickness gradation around its meridian to counter the non-uniform stresses induced by inflation. In practice, neither approach is acceptable and consequently it was decided to incorporate some fabric reinforcement as a belt beneath the tread to withstand the highest stresses. In this way it was possible to design otherwise fabricless tyres with an aspect ratio of 70%, the B series. The profiles of these model and car tyres were also based on the analogy of a cross-biassed design but one in which the bias angle varies from a minimum at the crown to a maximum at the bead. This gives stress distributions which change smoothly around the meridian, whereas profiles constructed geometrically from arcs of ellipses and circles give local high stresses in the shoulder where the restraint of the belt would be least effective.

One further design was assessed in the research and it was chosen solely because it offers a simpler manufacturing route. It is the C tyre and differs from the B series only because its lower sidewalls are extended to meet and form a single bead region. A second computer program was written to calculate the profiles of both the B and C tyres.

The original intention was to manufacture model and car tyres with carcasses of Hytrel, the most promising thermoplastics material available, and of polyurethane, perhaps the most obvious candidate material because, compared to conventional rubbers, it maintains its hyper-elastic nature to much higher values of Young's modulus. However, limitations dictated by the available processing equipment meant that Hytrel was used mainly for the

model tyres, by injection moulding, while the car tyres were cast from polyurethanes. Nevertheless, a single model tyre was cast from a polyurethane and a few car tyre carcasses were made from Hytrel, by multi-shot injection moulding, so that data obtained on the two sizes of tyres could be related.

IX.3 Experiments on Fabricless Tyres

When the experimental programme for the fabricless tyres was being planned, it was argued that radial stiffness and its dependence upon carcass material modulus and wall thickness would be one of the most important properties to be characterised. In operation, tyres are continually subjected to radial deflection and it is the stresses induced by this mode of deformation which lead to their eventual failure by fatigue.

Guidance on the properties of free inflation : growth, creep and burst strength; would be obtained from shell theory, although any predictions would have to be checked by experiment, but radial stiffness would require an entirely empirical approach. Consequently, it was thought appropriate to re-examine the mechanics of radial stiffness. This lead to a simple equation relating load, inflation pressure and radial deflection but based on fundamental principles, rather than being a curve fitting exercise. It allows the structural and pneumatic components of stiffness to be isolated, an advantage which will become more apparent later in this chapter.

The experiments performed to measure a wide range of tyre properties were largely successful, although curtailed by the inability to injection mould the thinner of the two carcasses chosen for the model tyres and by failure to bond conventional rubber treads to the polyurethane carcasses of the car tyres. However, the data which were obtained were self-consistent, showed the expected trends and, when appropriate, agreed with theoretical predictions. By considering the results obtained on both the model and car tyres, the following broad conclusions may be drawn.

a) The burst strength of both the A and B series of tyres, which have aspect ratios of 90% and 70% respectively, is directly proportional to the product of the Young's modulus of the material used for the carcass and its wall thickness. Moreover, this empirical relationship applies equally to polyurethanes and Hytrel, although there was some evidence that the lower modulus blends of the latter material exhibited greater burst strengths

than would be anticipated. For the car tyres : 126-10 A and 143-10 B, without a belt; the established relationship is:

$$P = 2.26\ E.t \qquad (1)$$

where P is the burst pressure, kPa;
E is the Young's modulus, MPa;
and t is the wall thickness, mm.

Assuming the effect of fitting a belt to a 143-10 B tyre would be the same as measured for the 83-8 B model tyre, that is a 50% increase in burst strength, the relationship for the B series car tyres is:

$$P = 3.39\ E.t \qquad (2)$$

b) When growth of the tyres was measured over the range of pressures at which they could be operated safely, agreement with the predictions of the shell theory was satisfactory for the A series model and car tyres. With the model tyres, the measured and calculated strains were in reasonable agreement; while with the car tyres, which presented greater experimental difficulties, it was shown that growth is directly proportional to the membrane compliance of the carcass, that is inversely proportional to the material Young's modulus and wall thickness.

As expected, the B series tyres exhibited much greater growth, primarily because their low profiles changed shape and induced large bending stresses. Thus it was confirmed that they required a reinforcing belt to withstand the high circumferential crown stresses, otherwise the wall thickness and/or material modulus in this region of the carcass would need to be unacceptably high.

For the 126-10 A series car tyres, the relationship established is:

$$\%\ \text{growth} = \frac{780}{E.t} \qquad (3)$$

which also applies with sufficient accuracy to the 143-10 B series tyres when fitted with a belt.

c) Creep of a fabricless tyre does not appear to present any problems. Although only a few tests were made, the data obtained indicate that, if a carcass meets the requirements of burst strength and growth with inflation, the long term changes in its dimensions only amount to a

maximum of about 2%. This value applies to the higher modulus blends of Hytrel, the one polyurethane carcass examined was significantly better in this respect.

d) The radial stiffness data for the many model and car fabricless tyres examined were all analysed according to the equation derived in chapter VI:

$$W = (A + B.p)d^n \qquad (4)$$

where W is the radial load, N;
p is the inflation pressure, kPa;
and d is the radial deflection, mm.

The constants A and B are the structural and pneumatic stiffness parameters; while n is the power index which describes the curvature of the lines of load versus deflection at constant pressure. When the behaviour of conventional tyres was examined, it was shown that the power index is a function of the radial deflection of a tyre around its periphery but was not found to vary significantly between the designs of fabricless tyres. Thus the main interest in equation (4) lies in the relative magnitudes of the structural, A, and pneumatic, B.p, components of stiffness and their dependence upon the geometry and carcass material modulus of the tyres.

For the 126-10 A tyres, it was shown that equation (4) has the form:

$$W = (0.109.E.t^{1.45} + 0.26.p)d^{1.13} \qquad (5)$$

and for the lower profile 143-10 B tyre fitted with a belt:

$$W = (0.089.E.t^{1.45} + 0.26.p)d^{1.13} \qquad (6)$$

Thus the difference in the radial stiffness behaviour of the two series of tyres appears in the structural component.

Through legitimate but confidential contacts in the tyre industry, data obtained by other workers on the radial stiffness behaviour of fabricless tyres made and tested by them were obtained. These workers will be referred to as 'X' and 'Y' and the tyres they manufactured are equivalent to sizes 165-R-13 ('X') and 155-R-13 ('Y'). No information on their constructions is available apart from the facts that they have polyurethane carcasses and are both fitted with belts.

The load-pressure-deflection data provided were analysed according to equation (4) and the results expressed in percentages to allow different sizes of tyre to be compared directly. Thus the structural stiffness component is given by:

$$\frac{A}{A + B.p} \cdot 100\%$$

and the pneumatic stiffness component by:

$$\frac{B.p}{A + B.p} \cdot 100\%$$

Now the results for the 126-10 A and 143-10 B tyres, using equations (5) and (6), depend upon the wall thickness and material modulus chosen; these values for the tyres made by 'X' and 'Y' are unknown. Therefore, for the tyres of this research, the average wall thickness of 5 mm and a typical polyurethane modulus of 50 MPa were selected. For all the tyres and their equivalent conventional designs, an inflation pressure of 200 kPa was used. The results obtained are summarised in table LVI.

Table LVI

Structural and Pneumatic Components of Radial Stiffness

Tyre Size and Type	Structural Stiffness Component (%)	Pneumatic Stiffness Component (%)
126-10 A, fabricless without belt	52	48
5.20-10, cross-biassed	20	80
143-10 B, fabricless with belt	47	53
145-R-10, radial	19	81
165-13 'X', fabricless with belt	43	57
165-R-13, radial	19	81
155-13 'Y', fabricless with belt	39	61
155-R-13, radial	15	85

The most obvious feature of table LVI is the high structural stiffness of

all the fabricless tyres relative to the conventional tyres. The average is 45% compared to less than 20%. It also appears that the workers 'X' and 'Y' have produced fabricless tyres with lower structural stiffness than those of this research, but their tyres are somewhat larger and, in any case, criteria for a true comparison could not be established with the available data. In general, the results from 'X' and 'Y' confirm those of this research.

When the two components of stiffness for the 126-10 A and 143-10 B tyres are summed and compared to the cross-biassed and radial tyres, ignoring the influence of the power index, n, the total stiffnesses for the inflation pressure, wall thickness and material modulus chosen are similar:

126-10 A	total stiffness	=	108.2 kN/m
5.20-10	" "	=	92.2 kN/m
143-10 B	" "	=	97.9 kN/m
145-R-10	" "	=	99.1 kN/m

However, it must be remembered that the power indices for the two conventional tyres, 1.18 and 1.08 (table L), result in their carrying different loads at the same radial deflection : 3162 N and 2519 N respectively at 20 mm. Thus in use with a given load, the radial 145-R-10 would deflect more than the cross-biassed 5.20-10, a conclusion well established in the tyre industry. As far as the two designs of fabricless tyre are concerned, the lower profile B series has the lower stiffness and more nearly matches the conventional tyres.

e) Experiments to measure <u>cornering power</u> could only be carried out on the model tyres. An interesting observation was the almost complete lack of inflation pressure dependence with the fabricless tyres, whereas the cornering power of the conventional designs increases approximately in proportion to the pressure. In general, the performance of the fabricless tyres was superior to the conventional tyres, particularly in the case of the lower profile 83-8 B tyres whose greater width increases their lateral bending stiffness, and thus cornering power, in accordance with theory.

f) The measurements of <u>wear resistance</u>, noting that the model tyres had conventional rubber treads, reflected the greater cornering power of

the fabricless tyres. The experiments also provided a unique opportunity to test the theory that wear is proportional to the slip induced in a tyre while it is generating the cornering force. The measurements on the wide range of model tyres were made at given cornering forces so that wear should have been inversely proportional to cornering power. The results confirmed this statistically to a high level of confidence.

g) Rolling resistance or drag was assessed only with the model tyres but, like cornering and wear, relative results could be scaled to car tyres with confidence. Again, the fabricless tyres were superior to the conventional designs, with the polyurethane version exhibiting especially low drag. The few measurements of running temperatures confirmed these results but did indicate that an exceptionally high temperature was occurring at the tread carcass interface in the shoulder of a fabricless tyre, an observation which proved to be very significant when fatigue was investigated.

h) To assess comfort, it was essential to use car tyres because no work on model tyres of this nature had been undertaken in the past and so there were no established criteria for judging performance. The tests on selected 126-10 A and 143-10 B tyres, the former including one with a polyurethane tread integral with its carcass, showed that : a tread of conventional hardness is essential to avoid the generation of excessive vibrations from road irregularities; a carcass of comparable radial stiffness to a conventional tyre is needed to minimise the transmission of the vibrations.

i) Structural performance or fatigue proved to be the least satisfactory investigation for two reasons. First, although the experiments on model tyres were comprehensive and examined the effects of carcass material modulus, inflation pressure and radial load on the fatigue lives of the A and B series, only one wall thickness was included because it was not possible to injection mould the thinner of the two carcasses planned for each design. Second, the programme on car tyres was undermined by the unsolved problem of bonding conventional rubber treads to polyurethane carcasses. Thus, while it was planned to examine three wall thicknesses, time dictated that only a single mould was adapted to produce tyres with an integral tread cast from the same grade of polyurethane as the carcass.

The model tyre results highlighted the dependence of fatigue life on

radial deflection, rather than inflation pressure and radial load per se. At a given deflection, the blend of Hytrel used for the carcass had little effect but limited tests proved polyurethane to be a superior material. Likewise, at normal operating pressures, the low aspect ratio B tyre had a greater life than the A tyre, although neither could be compared directly to conventional tyres because, in model form, the last suffered from premature tread looseness without exhibiting failure of their carcasses.

When the car tyres with integral polyurethane treads were run, the dependence of life on radial deflection was confirmed in spite of considerable scatter in the data. Overall, none of the fabricless tyres tested approached the life expected of a conventional tyre, even though some were running at only half the radial deflection. This result is confirmed by other workers (reference 3).

Failure of all the fabricless tyres occurred by circumferential splits in the shoulder region of the carcass, where the high temperature was recorded when investigating energy loss as manifested in drag. This is clearly where the highest stress concentration occurs when the meridian of a tyre distorts as it enters and leaves the contact zone.

j) Wear and wet grip of polyurethane formulations were measured in another study to assess their suitability for the treads of tyres (reference 23). The main conclusion is that a formulation can be chosen whose wear or wet grip matches or is superior to that of a conventional tread rubber compound but no formulation was identified with the required balance of properties.

k) Tests on the 83-7 C, closed toroid, tyre showed that it matched the performance of the conventionally shaped 83-8 B tyre in most respects. However its cornering power was lower but not to the extent that had been anticipated. Thus if Hytrel, or any other thermoplastics which can be RF welded, was deemed suitable for the carcass of a fabricless tyre, then the closed toroid design could be a contender. In any case, the manufacturing route of injection moulding the carcass in two halves and subsequently joining them together offers considerable advantages with any tyre design, but only with thermoplastics.

l) To summarise the experimental data on the fabricless tyres of this research, table LVII relates their performance to that of conventional

tyres by rating the properties measured as +, - or =. When a property is inferior (-), the third column of the table indicates whether it would be acceptable. In particular, the B series tyre with a belt is considered because it has exhibited a higher level of performance than the completely fabricless A series.

Table LVII

Summary of Fabricless versus Conventional Tyre Properties

Property	Relative Performance	Acceptable
Burst strength	-	Yes
Growth with inflation	-	Yes
Creep	-	Yes
Radial stiffness	=	
Cornering power	+	
Wear resistance*	+	
Wet grip*	=	
Drag or rolling resistance	+	
Temperature build-up	+	
Comfort	=	
Fatigue or structural life	-	No

* With a conventional rubber tread.

Two points should be noted when interpreting Table LVII. First, steel belted conventional radial tyres are still being improved so that the superior performance indicated for fabricless tyres with respect to cornering power and wear resistance may be eroded. Second, comfort can only be rated equal if fabricless tyres can be run at radial deflections approaching those of conventional tyres and have treads of similar hardness. The evidence on fatigue suggests this to be unlikely. It should also be remembered that second order effects such as handling response and uniformity of wear across the tread pattern have not been considered. These are now very important to the tyre industry, especially when selling to original equipment manufacturers, but it can be anticipated that, should fabricless tyres be adopted, the large technical effort required would solve these and similar problems of detail. In fact a recent paper (reference 24) reports that Polyair have produced tyres which are indistinguishable in

handling and comfort to modern radial tyres, although the other claims made must be treated with caution.

The over-riding shortcoming of the fabricless tyres of this research, indicated in table LVII, is their structural life. Moreover, this is critically dependent upon the radial deflection at which the tyres are run and this, in turn, affects comfort and handling. Thus there is a conflict between a low deflection to maximise life and a larger deflection to give acceptable comfort if fabricless tyres are to be considered as alternatives to conventional tyres on passenger cars. Their greatest advantage is undoubtedly low drag, leading to reduced fuel consumption.

IX.4 Optimisation of Radial Stiffness

The detailed constructions of conventional and fabricless tyres are very different : the one having reinforcing cords of textile or steel embedded in a rubber matrix; and the other, apart from the belt if fitted, being homogeneous and of a different material, say polyurethane. However, the relatively poor fatigue performance of fabricless tyres must be related to their high structural stiffness. As a section of such a tyre distorts into and out of the contact zone, more energy is stored elastically in its structure and is available for propagating flaws. Thus it can be argued that a fabricless tyre with a lower structural stiffness component should exhibit greater fatigue resistance.

The feasibility of designing such a tyre may be assessed from the empirical relationships established in this research. To recapitulate, it has been shown that:

$$\text{burst strength (pressure)} = k.E.t$$

where k is a constant of proportionality, therefore, if a safety factor of 4 is specified, the maximum operating pressure is:

$$p = k.E.t/4 \qquad (7)$$

It has also been shown that the load carried by either an A series or B series tyre can be expressed as:

$$W = (A'.E.t^m + B.p)d^n \qquad (8)$$

where A', B, m and n are constants for a particular design.

Substituting for p from equation (7) into equation (8):

$$W = (A'.E.t^m + B.k.E.t/4)d^n \qquad (9)$$

Now for any chosen ratio, R, of the structural to pneumatic components of stiffness, the two terms within the brackets, equation (9) will yield a value for the wall thickness, t:

$$R = \frac{A'.E.t^m}{B.k.E.t/4} = \frac{4A'.t^{m-1}}{B.k} \qquad (10)$$

to give: $$t = \left[\frac{R.B.k}{4A'}\right]^{\frac{1}{m-1}} \qquad (11)$$

If the load, W, and radial deflection, d, are then specified, equation (9) will also give the required carcass material Young's modulus, E. Finally, the values of E and t may be substituted into equation (7) to obtain the operating inflation pressure, p. It is also possible to predict the growth of the tyre by reference to equation (3).

The first stage in this feasibility exercise is to define the load to be carried and the pressure at which the conventional tyre to be matched operates. The ETRTO publishes such data and for a 145-R-10 and its equivalent cross-biassed tyre the Economic Load is given as 2.7 kN when inflated to a pressure of 190 kPa. Now the radial stiffness parameters for these tyres in the equation:

$$W = (A + B.p)d^n$$

are (tables L and LI):

	A	B	n
5.20 - 10	18.4	0.37	1.18
145-R-10	18.9	0.40	1.08

which, for the ETRTO load and pressure, give the following radial deflections:

5.20 - 10	18.1 mm
145-R-10	22.2 mm

In the following calculations, the 126–10 A design will be matched to the 5.20–10 cross-biassed tyre, while the 143–10 B will be matched to the 145–R–10 radial.

Consider, first, the 126–10 A fabricless tyre design for which the constants in equation (9) have the following values, the units of which are consistent with load (W) in N, inflation pressure (p) in kPa, radial deflection (d) and wall thickness (t) in mm and Young's modulus (E) in MPa.

$A' = 0.109$ $\quad B = 0.26$ $\quad n = 1.13$

$m = 1.45$ $\quad k = 2.26$

Using these values and $W = 2700$ N, $d = 18.1$ mm, table LVIII may be constructed from equations (11), (9), (7) and (3). It shows the wall thickness, carcass material Young's modulus, inflation pressure and growth with inflation for structural stiffness components which account for 10% to 60% of the total stiffness.

Table LVIII

Optimisation of the 126–10 A Fabricless Tyre

Structural Stiffness (%)	Structural/Pneumatic Ratio R	Wall Thickness (mm)	Young's Modulus (MPa)	Inflation Pressure (kPa)	Growth (%)
10	0.111	0.01	63257	361	1.2
20	0.250	0.09	6148	315	1.4
30	0.429	0.30	1613	276	1.6
40	0.667	0.80	519	236	1.9
50	1.000	1.98	174	197	2.3
60	1.500	4.87	57	157	2.8

It may be seen from table LVIII that, to match the 5.20–10 cross-biassed tyre which has about a 20% structural stiffness component, the 126–10 A tyre should have a carcass manufactured from a material with a modulus over 6 GPa but with a wall thickness of only 0.1 mm. This is clearly impracticable. In fact, the best which can be achieved is a structural stiffness component between 50% and 60%, using a material with a modulus

in the range of polyurethanes and with a wall thickness between 2 mm and 5 mm. Growth with inflation is less than 3%. This description is typical of the experimental 126–10 A tyres of this research.

For the 143–10 B fabricless tyre design, the values of the constants in equation (9) are:

$A' = 0.089$ $B = 0.26$ $n = 1.13$
$m = 1.45$ $k = 3.39$

With W = 2700 N, d = 22.2 mm, table LIX may be constructed.

Table LIX

Optimisation of the 143–10 B Fabricless Tyre

Structural Stiffness (%)	Structural/Pneumatic Ratio R	Wall Thickness (mm)	Young's Modulus (MPa)	Inflation Pressure (kPa)	Growth (%)
10	0.111	0.06	5506	281	2.4
20	0.250	0.35	840	250	2.7
30	0.429	1.15	224	219	3.0
40	0.667	3.06	72	188	3.5
50	1.000	7.54	24	156	4.3
60	1.500	18.55	8	125	5.3

Even though the 143–10 B is operating at a higher radial deflection than the 126–10 A, in order to match the 145–R–10 radial, viable constructions are possible to lower percentage structural stiffnesses. A value below 40% would seem to be possible, with a wall thickness of, say, 2.5 mm and a material Young's modulus of about 100 MPa. The inflation pressure would be around 190 kPa, the same as that specified for the conventional radial tyre. However, this structural stiffness is still twice that of the radial tyre but corresponds to the tyre produced by the workers 'Y', table LVI. Its growth with inflation pressure is marginally acceptable.

It may be concluded, therefore, that although the meridional profile of the 126–10 A design is superior for containing the inflation pressure, its high structural stiffness makes it less suitable than the squatter 143–10 B when attempting to match the radial stiffness characteristics of

a conventional tyre. Consequently the further discussion will be limited to the 143-10 B.

Suppose this tyre were allowed to run at a lower radial deflection than the 145-R-10 radial. This could arise if it were possible to adjust the suspension on a passenger car to accommodate this situation, or an application for the tyre might be identified for which comfort is less important, in agriculture for example. Whatever the reason, it is instructive to calculate the consequences to the design of the optimised tyre.

Now from equation (10), the ratio of structural to pneumatic stiffness for a particular tyre design depends only upon the wall thickness and is independent of the carcass material Young's modulus. Thus increasing the total stiffness of a tyre to reduce its radial deflection under a given load will not lessen this ratio. Nevertheless, the ratio can be maintained at any chosen level and increased stiffness obtained by using a higher modulus material for the carcass, coupled with a greater inflation pressure. To illustrate this, the values calculated for deflections of 22 mm, used in table LIX to match the radial tyre, 18 mm to match the cross-biassed tyre, 15 mm and 12 mm are listed in table LX. The structural stiffness component chosen is 40%, approximately the lowest practicable level and requiring a wall thickness of 3 mm. Also included in the table is the energy stored elastically in the carcass, calculated from:

$$\frac{1}{n+1} A'.t^{m}.E.d^{n+1}, \qquad \text{the integral of the structural term in equation (9).}$$

Table LX

Optimised 143-10 B Fabricless Tyre at Reduced Deflections

Radial Deflection (mm)	Young's Modulus (MPa)	Inflation Pressure (kPa)	Growth (%)	Stored Energy (J)
22	72	188	3.5	11.2
18	91	237	2.8	9.1
15	112	291	2.3	7.6
12	145	377	1.8	6.1

It may be seen that reducing the radial deflection decreases the growth with inflation which, at 22 mm deflection, is greater than the 3% arbitrarily chosen; the elastically stored energy falls significantly because it is a fixed proportion of a lessening total.

Overall, this optimisation exercise has shown that, using available hyper-elastic materials such as polyurethanes, a carcass for a fabricless tyre equivalent in size to a 145-R-10 cannot be designed to carry less than about 40% of its load structurally, compared to under 20% for the conventional tyre. However, the quantity of energy stored elastically in the fabricless tyre can be reduced but only by causing it to run at a lower radial deflection. This strategy, although compromising comfort and handling, would lead to improved fatigue resistance as the experiments on the 126-10 A tyres with integral polyurethane treads showed. Whether the improvement would lead to a viable tyre is doubtful but open to some speculation because fatigue tests were not carried out on either the 83-8 B model or 143-10 B car tyres with carcasses cast from polyurethane and fitted with restraining belts and rubber treads. With Hytrel carcasses, the model 83-8 B tyres were superior to the 73-8 A tyres, but not by a margin which would suggest viability could be achieved. It must also be appreciated that it is not the total stored energy which controls fatigue but the peak energy density. In a rolling tyre this travels around the tyre circumferentially like a wave and is thus available once per revolution to propogate a flaw which, eventually, leads to failure. If, as is suspected, it is the inner surface of the carcass in the shoulder zone of the tyre which is most highly stressed, there is no way at present for predicting how this would be affected by the tyre's radial deflection. When the finite element method can be used to model an inflated and radially deflected tyre, further evidence will become available on which to base any speculation and, indeed, progress towards improved designs of fabricless tyres. Indeed, the method would allow tyres of different sizes to be assessed without recourse to experiment. For withstanding the inflation pressure, carcass wall thickness for a given material modulus increases linearly with tyre size but the effects on radial stiffness and fatigue life are largely unknown. Nevertheless, the experimental evidence from the model and car tyres of this research and data from reference 3, which between them include tyres whose section widths differ by a factor of 2.5, suggest that tyre size is not an important parameter in deciding the viability of fabricless constructions.

IX.5 Final Conclusions

The original aim of the research was to establish the technical feasibility of a pneumatic tyre for modern passenger cars which is constructed with no directional reinforcement in its carcass. If bead wires are exempted, then only the A series of tyres, made and tested in the course of the work undertaken, meet this specification. In both model and car sizes, the carcasses of these tyres were designed to contain the inflation pressure using minimal wall thicknesses and material Young's moduli. Nevertheless, when their radial stiffnesses were measured and analysed, it was found that, for all practicable combinations of thickness and modulus, less than 50% of the radial load was carried pneumatically; compared to over 80% for tyres with a conventional construction. Thus it is arguable whether the A series of tyres can be described as pneumatic, although this is a question of semantics because the definition of a pneumatic tyre has never been expressed in these terms.

The mechanical behaviour of the completely fabricless A tyres was in most respects moderate but acceptable when compared with a cross-biassed tyre having a similar high aspect ratio. Moreover, when made with a polyurethane carcass, exceptionally low drag was exhibited which might make this design particularly suitable for light, electrically powered urban cars of the future, for which energy consumption and thus range are of paramount importance. However, before such an application can be realised, fatigue life or structural performance must be improved. The tyres of the research were poor in this respect, even when run at reduced radial deflections.

The hypothesis was put forward that one reason for the poor fatigue life of the fabricless tyre is its high structural stiffness. This implies that more energy is stored elastically in its carcass than in a conventional tyre, energy which is available for propogating any flaws. Thus it may be seen that there is a conflict between the various properties required of the material used for the carcass of a fabricless tyre.

To withstand the inflation pressure, a high modulus in tension is necessary for any acceptable wall thickness. This must be coupled with high ultimate strength, otherwise the tyre would grow excessively when inflated normally and burst if over-inflated. The stiffness of the carcass in bending, however, should be low so that the tyre is sufficiently compliant when loaded radially by the weight of the vehicle to allow the pneumatic

behaviour of the carcass to dominate this mode of deformation. Structural compliance also leads to a more uniform load distribution in the contact patch. Radial stiffness and, to a lesser extent, contact pressure distribution both affect comfort, handling, braking, cornering and wear.

With a conventional tyre, the textile cords in a multi-ply construction have the required modulus and strength in tension to withstand the inflation pressure. However, the twist imparted to the cords during manufacture, giving them a much lower modulus in compression than in tension, and the very low shear modulus of the rubber matrix combine to give such a construction a low bending stiffness. Thus the conflict experienced with fabricless tyres is not met. This is also true for modern mono-ply constructions in which a single layer of, say, steel cords can remain in tension when the tyre is deflected radially, while the orthotropic properties of the carcass, its reduced thickness and the shear modulus of the rubber give the low bending stiffness.

There is another advantage to using a composite for the carcass of a tyre, which is not shared by a fabricless tyre and is a further reason for the latter's poor fatigue resistance. If, during the life of a conventional tyre, a flaw is propogated in the rubber matrix, the cords can limit the size to which the flaw will grow. Also, if a cord fatigues and ruptures, the rubber matrix redistributes the stresses to adjoining cords and thus inhibits catastrophic failure. Neither of these mechanisms is available in the homogeneous, isotropic material of the carcass of a fabricless tyre, so that once a flaw is initiated in a zone of high energy density, catastrophic failure is inevitable.

The realisation that the meridional profile of a completely fabricless tyre is limited to one with a high aspect ratio, 90%, lead to the B series of tyres, for which a compromise was made by fitting a directionally reinforced belt below the tread. This belt was only introduced to limit growth with inflation pressure of, otherwise, fabricless tyres with a lower aspect ratio. For the B series, an aspect ratio of 70% was chosen, equivalent to many modern radial tyres.

In general, the mechanical behaviour of the B tyres was superior to that of the A tyres. Their cornering and wear were equal to or better than a conventional radial and, with respect to these properties, it was confirmed that the presence of the belt had little effect. Higher

lateral stiffness is derived from the greater meridional width and inherent stiffness of the design. Thus the construction of the belt does not need to conform to that of conventional radial tyres, bias angles of $\mp 20^{\circ}$, but could be a single 0° ply able to withstand the higher circumferential stresses induced by inflation in the crown region of a low profile tyre. Moreover, it would be possible to adopt the meridional profile of the A series for the sidewalls only of a low profile tyre to give the advantage of constant equibiaxial stresses due to inflation. This is possible because the mathematical description of a meridian does not contain section width as a parameter, only the radial distances from the tyre's axis to the point of maximum width and, in this case, the effective crown (equation 18 in chapter IV). Equibiaxial stresses have been shown to minimise the required product of material Young's modulus and carcass wall thickness to limit growth with inflation. This in turn would minimise the bending stiffness of the sidewalls and thus the total structural stiffness.

Although tests on the model B tyres showed them to have greater fatigue lives than the completely fabricless, higher profile A tyres, even when running at a greater radial deflection, definitive trials of the equivalent car tyres could not be undertaken because of manufacturing difficulties. However, in the light of the limited evidence available, it would seem that the structural performance of fabricless tyres can be maximised by adopting the following:

(i) a low profile with a simple 0° belt to limit growth;
(ii) a sidewall meridian between the belt edge and bead wire which results in constant equibiaxial stresses in this unreinforced region of the tyre when it is inflated;
(iii) a polyurethane, as opposed to Hytrel, material for the carcass;
(iv) an optimal combination of carcass wall thickness, material Young's modulus and inflation pressure;
(v) a reduced radial deflection, consistent with acceptable comfort and handling.

Of these, the choice of wall thickness and Young's modulus is the most difficult to make because, in the research, no fatigue tests have been carried out to determine the effect of the former. However, on the basis

of the bending strains and stored energy as a meridional section enters and leaves the contact zone, preference must be given to a lesser wall thickness and a greater Young's modulus. However the improvement given to structural performance by this choice must be in doubt.

The elastically stored energy in the optimised low profile tyre fitted with a belt still accounts for 40% of the total energy of deformation, while the reduction in the induced strains by minimising the wall thickness may not be so great as might be first thought. If the carcass in the region of the shoulder of a fabricless tyre is the position of the greatest strains and stored energy density, as the results obtained indicate, then the presence of the tread must not be ignored. In effect, the tread and carcass form the equivalent of a composite beam, the tread being the thicker component although having a lower modulus. Consequently, the strains induced at the inner surface of the carcass will be less dependent upon the carcass thickness than would be the case, say, in the sidewall where the carcass resembles a simple, one component beam.

The final comment which must be made about the viability of fabricless tyres concerns the choice of the tread material. The standards of road-holding and wear attained by and expected of modern radial tyres are such that no significant dimimution of properties would be tolerated. If the carcass of a fabricless tyre were cast or injection moulded from a polyurethane, it would be preferable to use a compatible version of the same type of material for the tread in order to obtain a bond of the required integrity. However, evidence from a related study suggests that a polyurethane with the correct balance of wear resistance and friction will be very difficult to formulate. Consequently, in this research, the decision was made to use a conventional, carbon black filled rubber compound but the inability to bond it to polyurethane curtailed the experimental programme and remains a problem to be solved if alternative materials compatible with polyurethanes, or any other high modulus elastomer chosen for the carcass, are not identified.

To conclude, there are fundamental reasons why a fabricless tyre cannot be designed to match the pneumatic behaviour of a conventional tyre. These are related to the isotropic properties of the material used for its carcass, compared to the orthotropic properties of a cord-rubber composite. In this sense, a fabricless tyre represents a step backwards

in the history of pneumatic tyres, because it is the exploitation of directional reinforcement which has lead to the major advances in the past. Undoubtedly material developments will make possible fabricless tyres which approach the performance of conventional tyres more closely and perhaps allow them to be used for some, less demanding, applications. A carcass material with greater fatigue resistance would be one required development but, possibly of greater importance, is a tread material which can be bonded to high modulus materials like polyurethanes while exhibiting the wear and friction properties of existing rubber compounds.

REFERENCES

(1) D L Richards, Chem.Mark.Reporter, Vol 218, No 4, 28 Jul 1980.

(2) Anon, Auto Eng, Vol 87, No 4, Apr 1981.

(3) C Aliger, CMRA Paper No 725, New York, Mar 1980.

(4) Air Force Flight Dynamics Lab.,
Tech Report AFFDL-TR-71-51, Jul 1977.

(5) Air Force Flight Dynamics Lab.,
Tech Report AFFDL-TR-78-42, Mar 1978.

(6) F G Faxa, Plas. & Rubb. Int., Vol 5, No 3, Jul 1980.

(7) J E Morgan, SAE Paper No 810133, Detroit, Feb 1981.

(8) A Schallamach, NBS Monograph 122, Mechanics of Pneumatic Tyres,
Ch.6.

(9) D H Cooper, V E Gough, J H Hardman, Rev. Gen. du Caoutchouc, Oct 1959.

(10) V E Gough, SAE Paper No. 667A, Detroit, Mar 1963.

(11) S Timoshenko, Strength of Materials Part II, 3rd Edition,
D van Nostrand, 1958.

(12) W Hofferberth, Kautschuk u Gummi, 9, WT255, 1959.

(13) R B Day, S D Gehman, Rub. Chem. and Tech., 36, 1963.

(14) L R G Treloar, The Physics of Rubber Elasticity, Oxford Univ. Press, 1949.

(15) G D Hubbard, D Bulgin, M H Walters, Proc. of Fourth Rub. Tech. Conf.,
London, 1962.

(16) W Cooper, Dunlop Technology Division, private communcation.

(17) R F Smiley, W B Horne, Nat. Ad. Comm. for Aeronautics, Tech. Note 4110.

(18) D H Cooper, Trans. IRI, Vol 40, No. 1, Feb 1964.

(19) S K Clark (Ed), NBS Monograph 122, Ch. 3.

(20) Technical Data - Car Tyres, Dunlop Ltd., 1965.

(21) J G Smith, J E Smith, Automobile Eng., Dec 1967.

(22) P S Oubridge, MSc Thesis, University of Birmingham, 1965.

(23) M H Walters, Dunlop Technology Division, private communication.

(24) S Marshall, paper C284/83, Conference Proceedings, Automobile Wheels
and Tyres, I.Mech.E, Sutton Coldfield, Oct 1983.

APPENDIX I

Inflation Stresses from Finite Element Analysis

To justify the decision taken not to employ finite element stress analysis when designing the fabricless tyres assessed in this research, chapter IV, but also to show how the method could be used to guide further work, a single design was chosen for examination.

The tyre chosen was the 126-10 'A2' described in chapter V. Its profile conforms to the constant bias angle analogue, IV.2.3.4, with $\alpha = 45^{o}$ so that the tensions per unit length induced by inflation are equibiaxial and constant around its meridian. For the analysis, the tread was ignored because, even allowing for its greater thickness, its Young's modulus is low compared to that of the carcass, 3 MPa cf. 20 MPa, and would have only a small effect on the overall stiffness of the tyre under conditions of free inflation.

Inflation of a tyre is a case of an axisymmetrical body subjected to axisymmetrical boundary conditions. A number of FE methods exist for such cases but most were developed, primarily, for metals and other materials at low strains. To be more specific these methods make the following assumptions:

> the strains are very small so that no change in geometry occurs under load;
> the materials are linear in behaviour, strain directly proportional to stress, and are usually isotropic;
> their elastic behaviour can be described by two constants, Young's modulus and Poisson's ratio.

When considering elastomers, these assumptions are incorrect (reference 1) and limit the usefulness of any analysis. In particular:

> the large strains which will be encountered lead to significant changes in geometry;

although isotropy may be assumed, elastomers have non-linear elastic characteristics;
the use of Poisson's ratio (μ) leads to difficulties because, as elastomers are nearly incompressible, μ tends to 0.5 and the calculated stresses become very sensitive to small errors in μ.

For these reasons, the choice of method lay between one developed in Dunlop Technology Division (reference 1) which uses simple triangular elements and assumes complete incompressibility, and one developed at the University College of Swansea, Applied Science Faculty, for Dunlop Ltd. The latter uses more advanced elements, allows for some compressibility and, in general, is superior. Consequently, the Swansea method was used for this exercise.

The computer program written at Swansea is called DEFEN 3 (reference 2). It uses 8-noded, isoparametric, quadrilateral elements of the type shown. By isoparametric, it is meant that in the two in-plane principal directions, the geometry and stress distributions are described by similar functions, in this case quadratic. Stresses are calculated by integration and are presented at four positions, known as Gauss points.

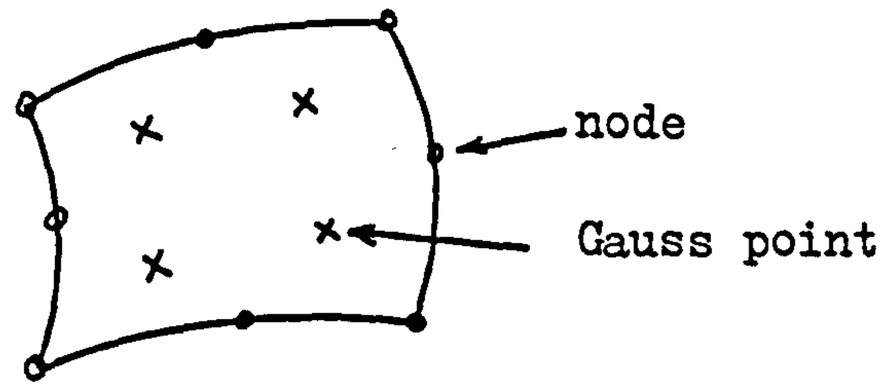

To characterise the elastic behaviour of elastomers, a modified truncation of the Rivlin stored energy function is used which, in its simplest form was used in chapter IV, equation (19). The complete modified function is:

$$W = \Sigma\, C_{ij}\,(I_1 - 3)^i\,(I_2 - 3)^j + \Sigma\, H_k\,(I_3 - 1)^k$$

where I_1, I_2 and I_3 are the strain invariants and the second series of terms allows for bulk compression. If each series is limited to two terms:

$$W = C_{10}\,(I_1 - 3) + C_{01}\,(I_2 - 3) + H_1\,(I_3 - 1) + H_2\,(I_3 - 1)^2$$

there is left the task of determining four elastic constants C_{10}, C_{01},

H_1 and H_2.

For elastomers, which have bulk moduli very much greater than their Young's moduli, by a factor of between 100 and 1000, it has been shown possible (reference 3) to measure the constants by two separate experiments. C_{10} and C_{01} are obtained from biaxial plane stress experiments (references 1, 4 and 5), while H_1 and H_2 may be calculated if the bulk modulus (k) is measured by compressing a small cylinder of elastomer contained in a close-fitting cylinder and piston. It may be shown (reference 3) that:

$$H_1 = -(C_{10} + C_{01})$$

$$\text{and } H_2 = k/8 + \tfrac{1}{3}(C_{10} + C_{01})$$

However, because C_{10} and C_{01} are small compared to k:

$$H_2 \simeq k/8$$

The elastomer chosen for the FE analysis was a polyurethane, Adiprene L-100, and its measured elastic constants are:

$$C_{10} = 4.125 \text{ MPa}$$

$$C_{01} = -0.831 \text{ MPa}$$

$$\text{and } k = 2657 \text{ MPa}$$

$$\text{to give } H_1 = -3.294 \text{ MPa}$$

$$H_2 = 332.1 \text{ MPa}$$

The 126-10 'A2' tyre has a carcass wall thickness of 5.5 mm and, to generate the FE mesh, a x2 drawing was produced and divided approximately into the required elements. A digitising tablet was then used to enter the co-ordinates of the nodes into the computer. A drawing of the resulting mesh is shown in figure I.A, where the crosses represent the nodes of the isoparametric elements. There is a total of 31 elements in the half section with the abscissa (r) representing a line of symmetry.

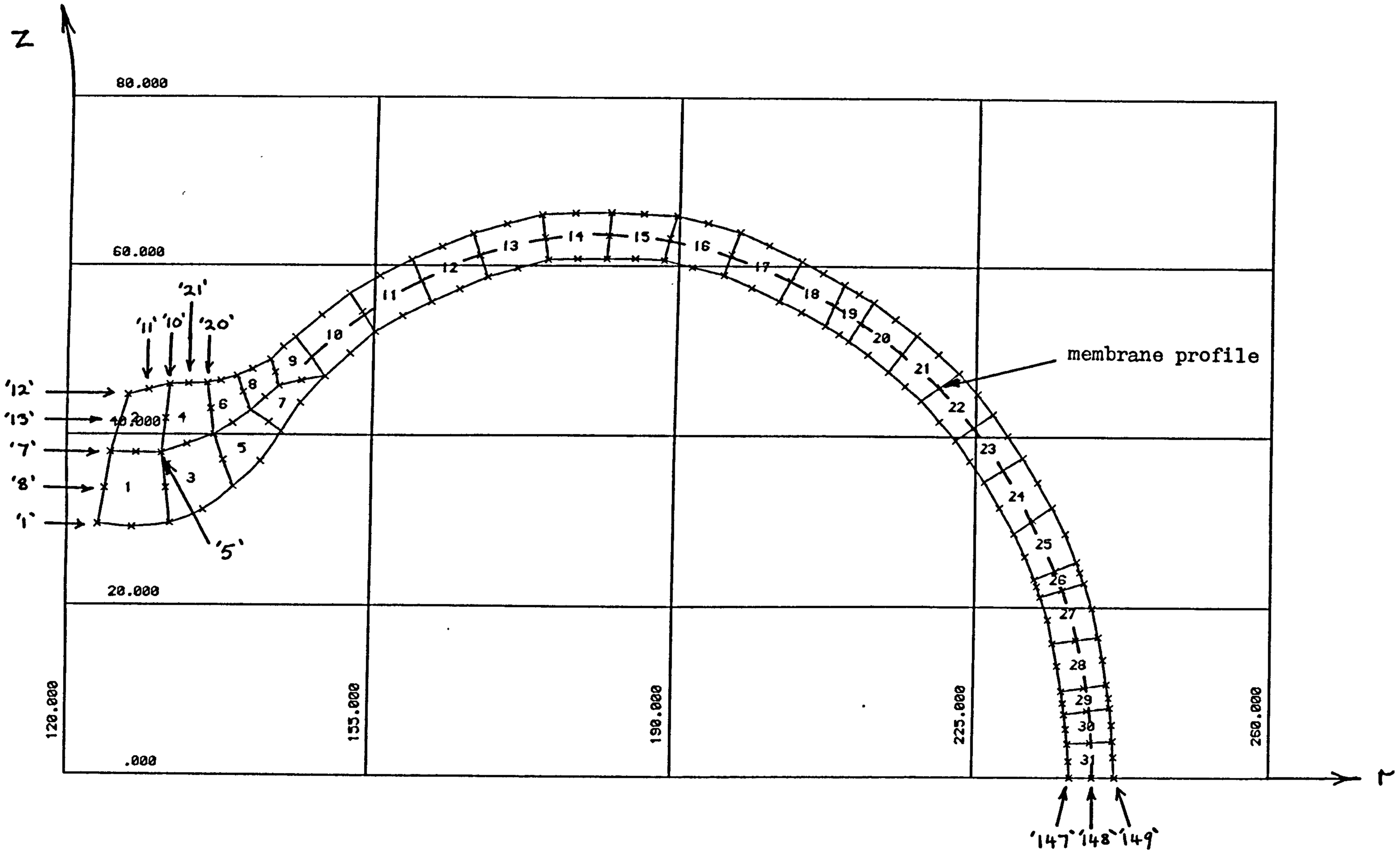

TITLE.

TYRE CARCASS MESH 31 ELEMENTS UNDEFORMED MESH.

Units - mm	Figure I.A
SCALE. 1.5/1.0	

The nodes which are restrained during the analysis are shown by their numbers in figure I.A. Those in contact with the rim of the wheel:

1, 8, 7, 13, 12, 11, 10, 21 and 20

together with the one in the position of the bead wire, number 5, were fixed in both the axial (z) and radial (r) directions; while 147, 148 and 149 on the line of symmetry were fixed in z but free in r. Finally the edges of the elements along the inner surface were all subjected to normal pressures in steps up to a maximum of 200 kPa.

The analysis, which uses the Newton-Raphson iterative technique to arrive at a solution, outputs the displacements of the nodes from their original positions together with the components of stress at the four Gauss points of every element: σ_{zz}, σ_{rr}, σ_{rz} and σ_{tt}, the last normal to the section. Also output are the in-plane principal stresses and their orientation relative to the axes.

Now the maximum principal stress will correspond to the meridional stress if it is correctly orientated and the minimum principal stress is small and only represents the pressure gradient from the inside to the outside of the tyre. These criteria were satisfied by the results and thus the maximum principal stress and the stress normal to the section (σ_{tt}), averaged over each element, may be compared to the tensions per unit length calculated from membrane theory. The latter (N) can be expressed as stresses (σ) by dividing by the wall thickness (t):

$$\sigma = \frac{N}{t}$$

To calculate the membrane tensions, the profile shown by the broken line in figure I.A was used. Its principal dimensions are:

ρ_o (radius to crown) = 240.0 mm

ρ_m (radius to max. width) = 180.8 mm

which, for an inflation pressure of 50 kPa, give:

$N_m = N_c = 2.6$ kN/m

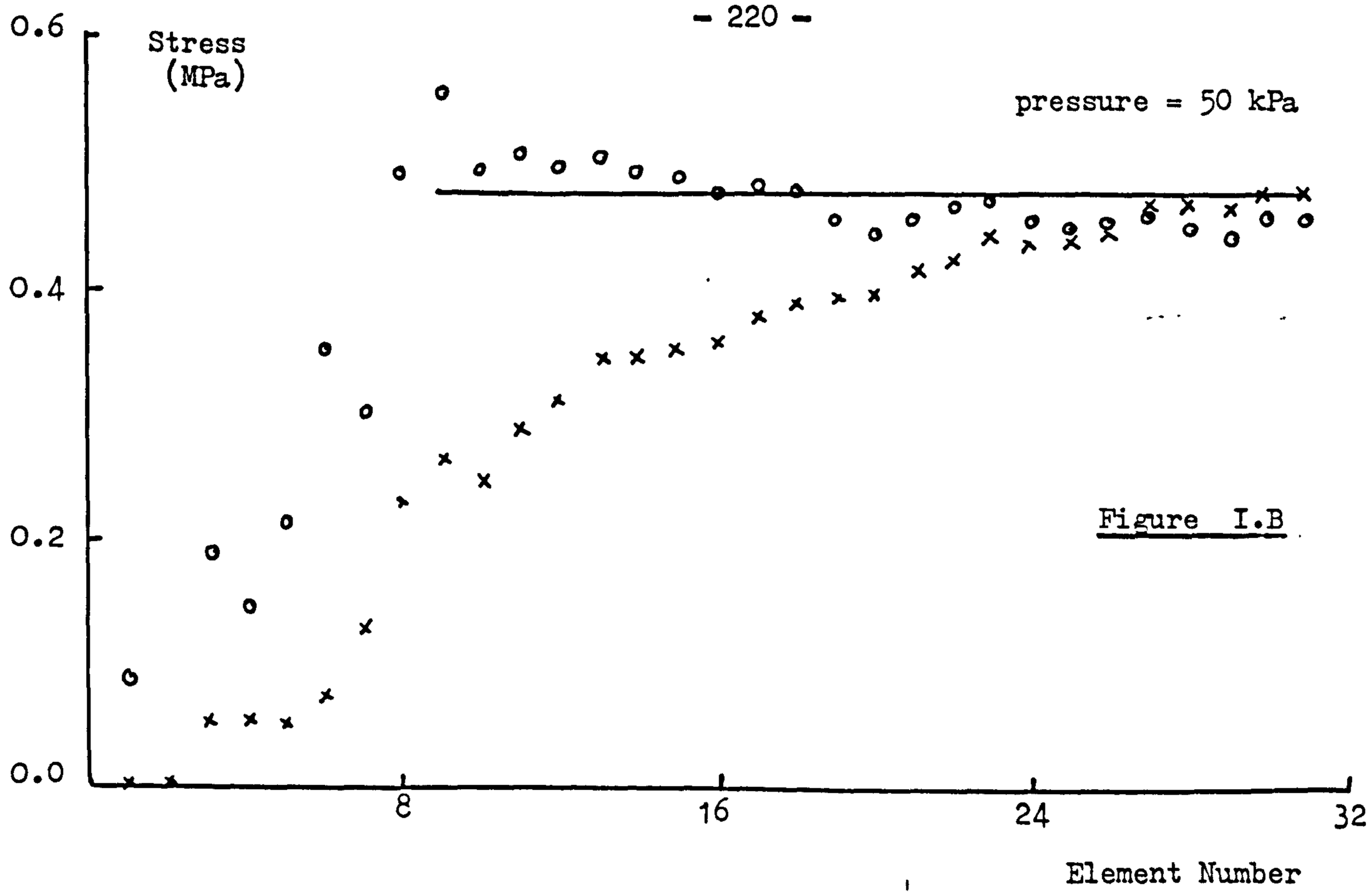

Figure I.B

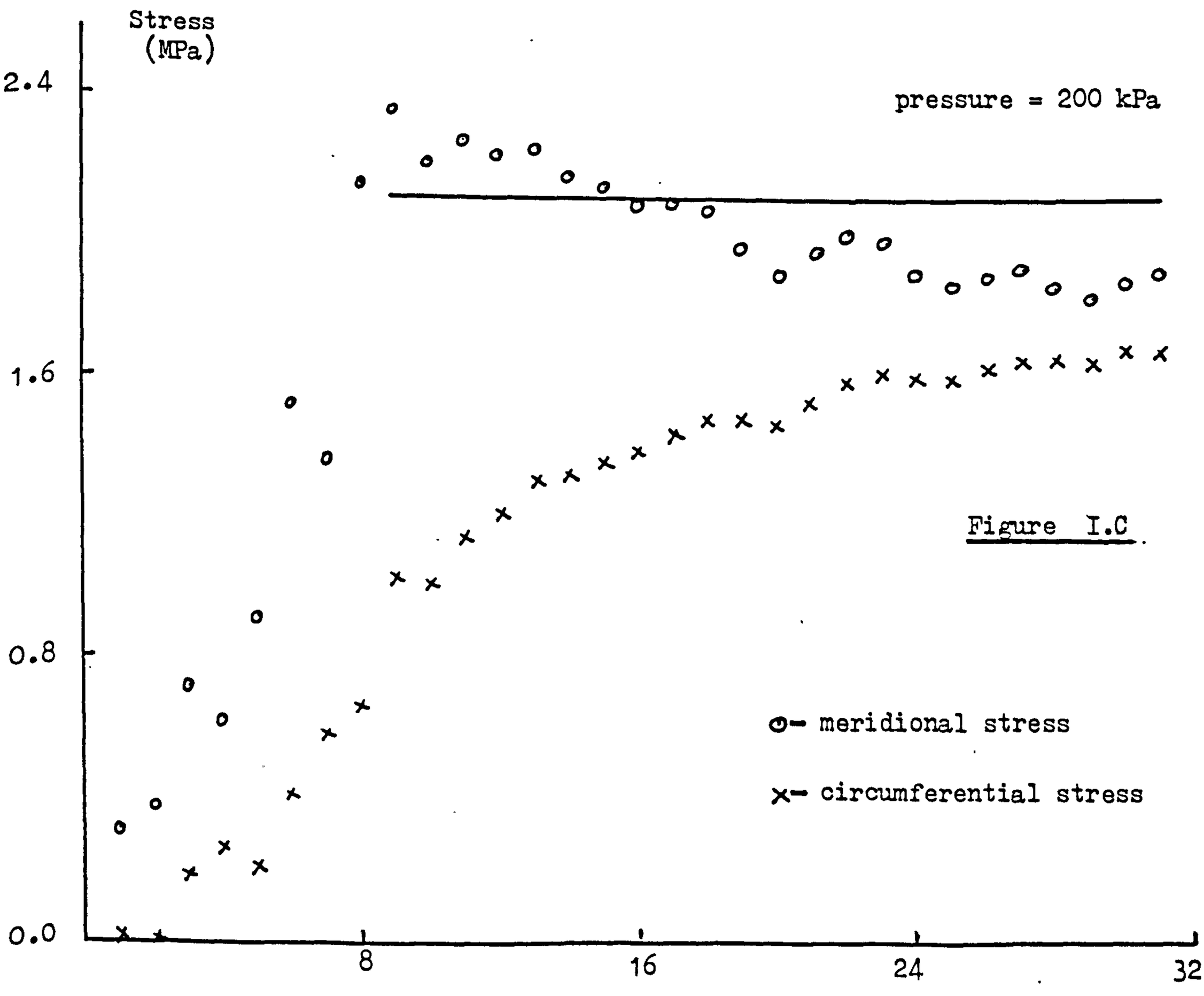

Figure I.C

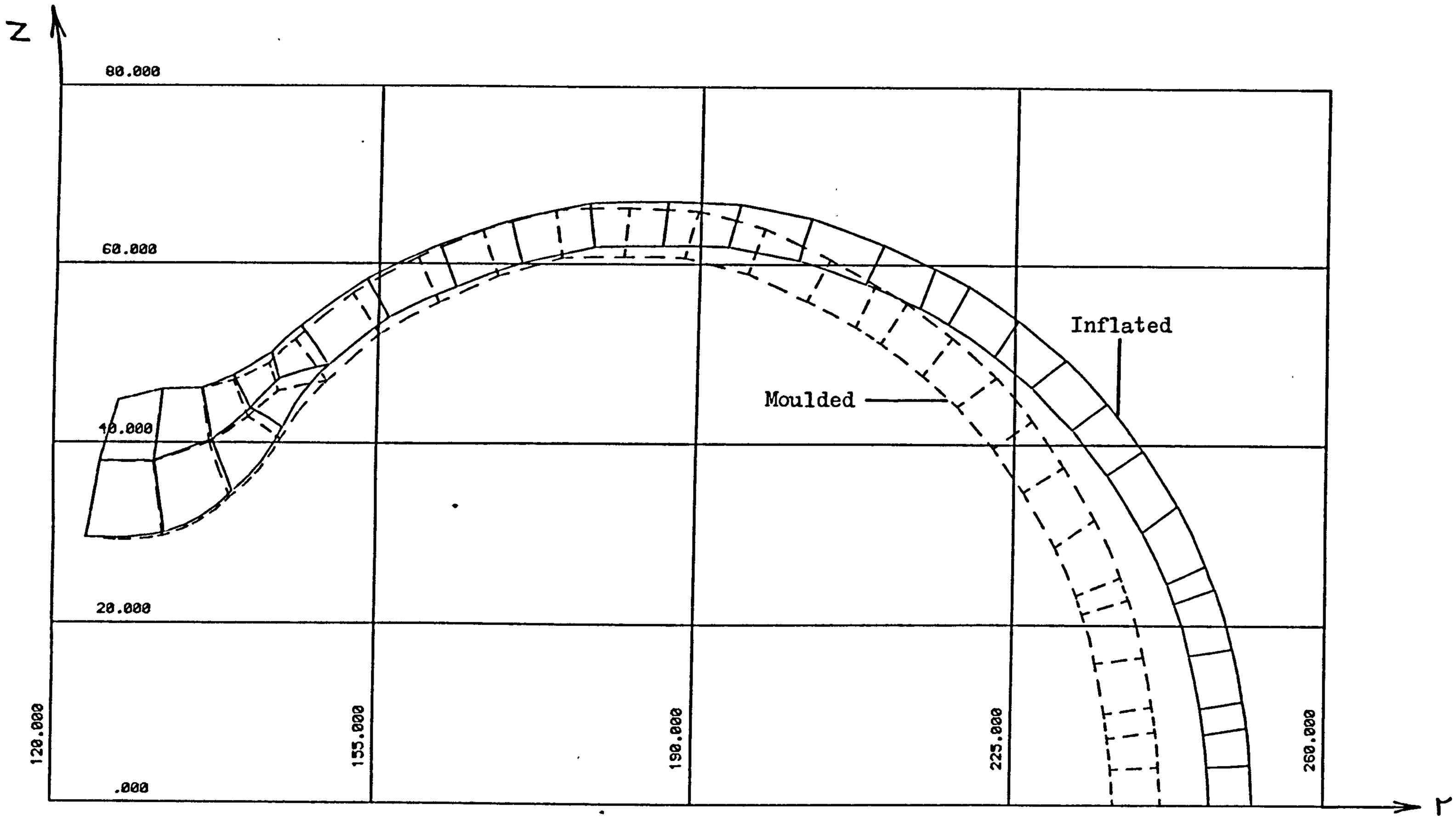

TITLE.

TYRE CARCASS MESH 31 ELEMENTS.
INTERNAL PRESSURE = 200.0kPa.

Units - mm	Figure I.D
SCALE. 1.5/1.0	

Figure I.B shows the comparison between the stresses calculated by the two methods, the solid line indicating the level of stress, meridional and circumferential, given by membrane theory. The results from the finite element analysis are plotted against element number which, because the elements are similar in size, approximates to the change in meridional angle. It may be seen that in the bead and clinch regions, elements 1 to 9 where the membrane theory does not apply, the stresses are low. However, in the main body of the tyre, the meridional stresses are scattered about the value predicted by membrane theory. The circumferential stresses, on the other hand, only reach the predicted level in the upper half of the tyre, elements 16 to 31.

With the analysis performed at a pressure of 200 kPa when $N_m = N_c = 10.4$ kN/m, figure I.C, the agreement is less close although the same pattern is observed in the comparison. At this pressure, a very significant change in geometry has occured, figure I.D, and consequently divergence of the results would be expected. Nevertheless, at 200 kPa, the principal stresses are still approximately equibiaxial in the critical, upper half of the tyre where the greatest stresses and strains due to radial loading on to a road surface will be experienced.

From this examination of the 126-10 'A2' tyre by finite element stress analysis, it may be concluded that the simpler membrane theory is sufficient for defining the meridional profile of a tyre. In this particular case, it is confirmed that the stresses due to inflation are approximately equibiaxial. For future work, there can be no doubt that finite element methods will have an important role, particularly as they are developed to handle general three-dimensional problems. However they can only be used to assess designs and, unlike the approaches using membrane theory described in chapter IV, cannot define a profile.

References

1) P.S. Oubridge, B.J. Hinton, C.M. Handley, Plas. & Rub. Proc. & Appl. 2, p 151 (1982).
2) H.J. Anderson, Univ. Coll. of Swansea and Dunlop Tech. Div., private communcation.
3) G.D. Hubbard, Dunlop Tech. Div., private communication.

4) A.G. James, A. Green, G.M. Simpson, J. of App. Pol. Sc., 19, p.2033 (1975).

5) A.G. James, A. Green, J. of App. Pol. Sc., 19, p.2319 (1975).

APPENDIX II

Meridional Profile from Combined Arcs

Equation for the Elliptical Arc

Referring to figure II.A, the elliptical arc EM is required to meet the following criteria:

1. it passes through the point E;
2. its slope at E equals that of the circular arc CE at E;
3. its radius of curvature at E is equal to r_1;
4. its tangent at M, when $\rho = \rho_m$, is normal to the axis.

Now the general equation of an ellipse whose semi-axes are parallel to Cartesian axes is:

$$ay^2 + bx^2 + cy + dx = 1 \qquad (1)$$

where, for the case of the tyre profile, the abscissa Ox is parallel to its axis and the ordinate Oy lies along a radial line in the plane of the meridian.

Differentiating equation (1) with respect to y:

$$2ay + 2bx \frac{dx}{dy} + c + d \frac{dx}{dy} = 0 \qquad (2)$$

But at M, $\frac{dx}{dy} = 0$ when $y = \rho_m$, thus:

$$c = -2a\rho_m \qquad (3)$$

Differentiating again with respect to y:

$$2a + 2b \left(x \frac{d^2x}{dy^2} + (dx/dy)^2\right) + d \frac{d^2x}{dx^2} = 0 \qquad (4)$$

Figure II.A

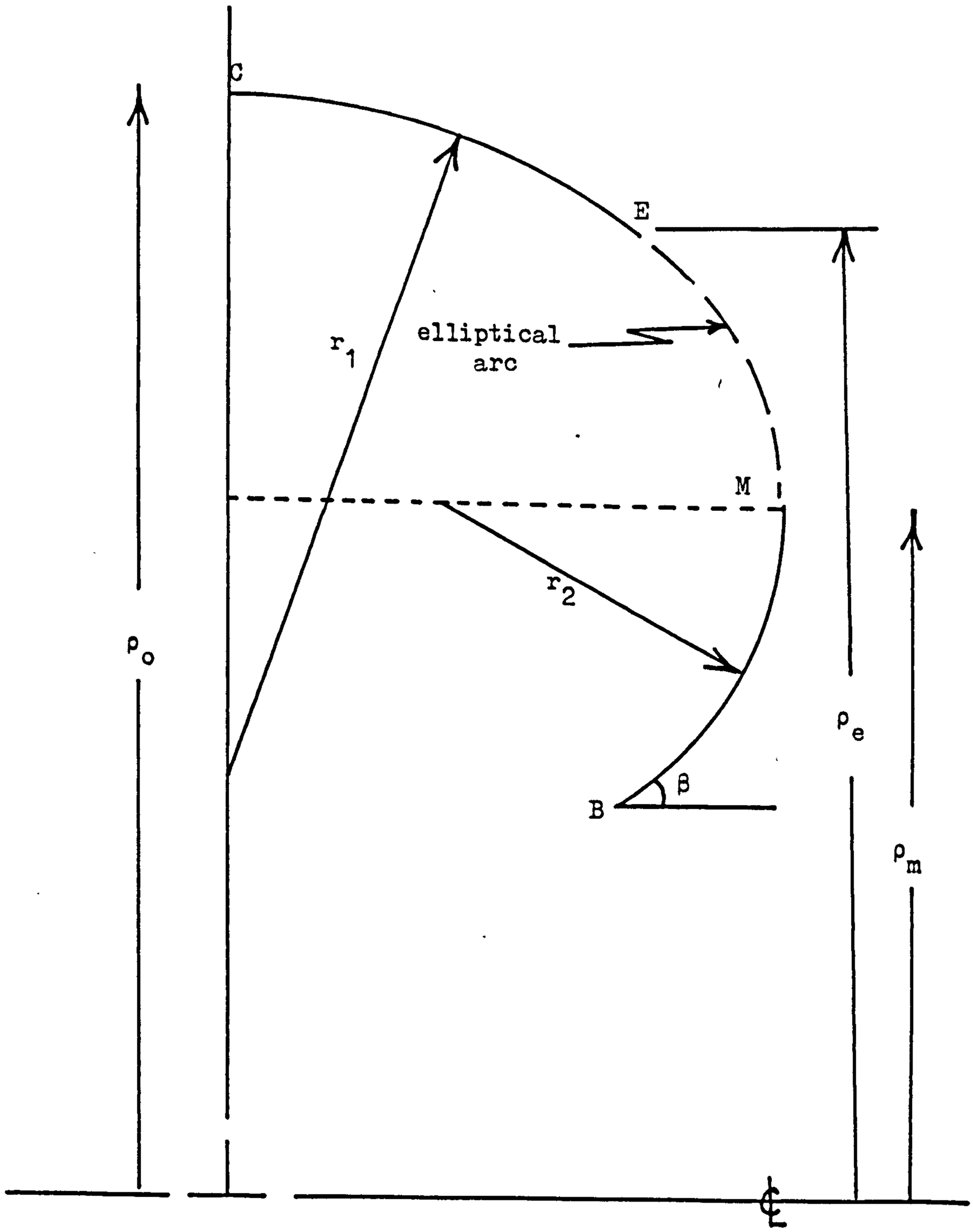

Now the radius of curvature of some function $x = f(y)$ may be expressed as:

$$r = \frac{(1 + x'^2)^{3/2}}{x''}$$

where x' and x'' are the first and second derivatives respectively.

Consequently if the elliptical arc is to have the same curvature at E as the circular arc, their first and second differentials must be equal when $y = \rho_e$. Suppose the equation of the circular arc CE is:

$$(y - g)^2 + (x - h)^2 = r_1^2$$

then $h = 0$ because its centre lies on the ordinate and:

$$x'_e = \frac{g - \rho_e}{x_e} \tag{5}$$

$$x''_e = -(x'^2 + 1)/x_e \tag{6}$$

Thus, by substituting from equations (5) and (6) into equations (1), (2) and (4) with $y = \rho_e$, and using the value for c from equation (3), the coefficients of the equation describing the ellipse can be determined. Also the meridional angles and radii of curvature at points between E and M may be calculated.

APPENDIX III

Computer Program FTGPR

This program calculates the profile of a tyre section defined by circular and elliptical arcs. The membrane tensions are also output.

```
      PROGRAM FTGPR
      REAL*8 H1,H2
      COMMON X(30),Y(30),A(30),RCM(30),RCC(30),SM(30),SC(30)
*
*     TYRE PROFILE DEFINED BY CIRCULAR AND ELLIPTICAL ARCS
*     RUN NAME: RUNFTG
*
      PI=4.0*ATAN(1.0)
      PRINT*,'TITLE, MAX.OF 16 CH.S'
      READ(3,1)H1,H2
    1 FORMAT(2A8)
      PRINT*,'RADIUS TO CROWN (MM)'
      READ(3,*)RC
      PRINT*,'MERIDIONAL RADIUS IN TREAD REGION (MM)'
      READ(3,*)RT
      PRINT*,'HALF WIDTH OF TREAD REGION (MM)'
      READ(3,*)WT
      PRINT*,'RADIUS TO MAXIMUM WIDTH (MM)'
      READ(3,*)RM
      PRINT*,'TERMINATING ANGLE (DEG)'
      READ(3,*)ABD
      PRINT*,'INFLATION PRESSURE (KPA)'
      READ(3,*)PS
      AB=ABD*PI/180.0
*
*     TREAD REGION
*
      AT=ATAN(WT/(RT*SQRT(1.0-WT*WT/(RT*RT))))
    2 DO 3 J=1,8
      X(J)=RT*SIN((J-1)*AT/7.0)
      Y(J)=RC-RT*(1.0-COS((J-1)*AT/7.0))
      A(J)=PI/2.0-(J-1)*AT/7.0
      RCM(J)=RT
    3 RCC(J)=Y(J)/SIN(A(J))
*
*     UPPER SIDEWALL
*
      YC=RC-RT
      DX=(YC-Y(8))/X(8)
      D2X=-(DX*DX+1.0)/X(8)
      CALL CONIC(X(8),Y(8),DX,D2X,RM,RS)
      WS=X(23)
*
*     LOWER SIDEWALL
*
      DO 4 J=24,30
      X(J)=WS-RS*(1.0-COS((J-23)*(PI/2.0-AB)/7.0))
      Y(J)=RM-RS*SIN((J-23)*(PI/2.0-AB)/7.0)
      A(J)=(J-23)*(PI/2.0-AB)/7.0
      RCM(J)=RS
    4 RCC(J)=-Y(J)/SIN(A(J))
*
*     CALCULATE MEMBRANE TENSIONS
*
      DO 9 J=1,30
      IF(J.EQ.23)GO TO 9
      SM(J)=(PS*ABS(Y(J)*Y(J)-RM*RM)/(2.0*Y(J)*SIN(A(J))))*1.0E-3
```

```
      SC(J)=(RCC(J)*(PS-SM(J)*1.0E3/RCM(J)))*1.0E-3
      A(J)=A(J)*180.0/PI
    9 CONTINUE
      SM(23)=(SM(22)+SM(24))/2.0
      SC(23)=(SC(22)+SC(24))/2.0
      WRITE(2,5)
    5 FORMAT(1H ,'TYPE PROFILE DEFINED BY CIRCULAR'/
     31H ,6X,'AND ELLIPTICAL ARCS')
      WRITE(2,13)H1,H2,RC,RT,WT,RM,Y(30),ABD,PS
   13 FORMAT(///1H ,2A3//1H ,'RADIUS TO CROWN = ',F7.2,' MM'
     2/1H ,'RADIUS OF CURVATURE IN TREAD = ',F7.2,' MM'
     3/1H ,'HALF WIDTH OF TREAD = ',F7.2,' MM'
     3//1H ,'RADIUS TO MAXIMUM WIDTH = ',F7.2,' MM'
     3//1H ,'TERMINATING RADIUS = ',F7.2,' MM'
     3/1H ,'TERMINATING ANGLE = ',F7.2,' DEG'
     3//1H ,'INFLATION PRESSURE = ',F7.2,' KPA')
      WRITE(2,10)((J,X(J),Y(J),A(J),RCM(J),RCC(J),SM(J),SC(J)
     3),J=1,30)
   10 FORMAT(//1H ,6X,1HX,6X,1HY,6X,1HA,6X,3HRCM,5X,3HRCC,7X,2HSM,
     311X,2HSC/(1H ,I2,3F7.2,2F8.2,2E12.3))
      WRITE(2,11)
   11 FORMAT(1H ,4X,'(MM)',3X,'(MM)',3X,'(DEG)',3X,'(MM)',
     34X,'(MM)',6X,'(KN/M)',6X,'(KN/M)')
      STOP
      END
```

```
      SUBROUTINE CONIC(X1,Y1,DX,D2X,Y2,RS)
      COMMON X(30),Y(30),A(30),RCM(30),RCC(30),SM(30),SC(30)
      DIMENSION AA(3,3),C(3),B(4)
*
*     TO FIT ELLIPTICAL ARC
*
      AA(1,1)=Y1*Y1-2.0*Y1*Y2
      AA(1,2)=X1*X1
      AA(1,3)=Y1
      AA(2,1)=2.0*(Y1-Y2)
      AA(2,2)=2.0*Y1*DX
      AA(2,3)=DX
      AA(3,1)=2.0
      AA(3,2)=2.0*(X1*D2X+DX*DX)
      AA(3,3)=D2X
      C(1)=1.0
      C(2)=0.0
      C(3)=0.0
      CALL SOLV(AA,C,B,3)
      B(4)=B(3)
      B(3)=-2.0*B(1)*Y2
      DO 3 J=9,23
      Y(J)=Y1-(Y1-Y2)*(J-8)/15.0
      X(J)=(-B(4)-SQRT(B(4)*B(4)-4.0*B(2)*
     2(B(1)*Y(J)*Y(J)+B(3)*Y(J)-1.0)))/(2.0*B(2))
      DX=(2.0*B(1)*Y(J)+B(3))/(2.0*B(2)*X(J)+B(4))
      A(J)=ATAN(ABS(DX))
      D2X=2.0*(B(1)+B(2)*DX*DX)/(2.0*B(2)*X(J)+B(4))
      RCM(J)=((1.0+DX*DX)**1.5)/D2X
      IF(J-23)1,2,2
    1 RCC(J)=Y(J)/SIN(A(J))
      GO TO 3
    2 RCC(J)=0
    3 CONTINUE
      RS=1.0/D2X
      RETURN
      END
```

```
      SUBROUTINE SOLV(A,C,B,N)
      DIMENSION A(3,3),C(3),B(4)
*
*     SOLUTION OF LINEAR SIMULTANEOUS EQUATIONS
*
      NN=N-1
      DO 7 K=1,NN
      L=K
      KK=K+1
      DO 1 I=KK,N
      IF(ABS(A(I,K))-ABS(A(L,K)))2,2,1
    1 L=I
    2 CONTINUE
      IF(L-K)3,5,3
    3 DO 4 J=K,N
      T=A(K,J)
      A(K,J)=A(L,J)
    4 A(L,J)=T
      T=C(K)
      C(K)=C(L)
      C(L)=T
    5 CONTINUE
C     FACTORS INTERCHANGED,NOW TRIANGULATION WITH BACK SUBSTITUTION
      DO 7 I=KK,N
      DO 6 J=KK,N
    6 A(I,J)=A(I,J)-A(K,J)*A(I,K)/A(K,K)
    7 C(I)=C(I)-C(K)*A(I,K)/A(K,K)
      B(N)=C(N)/A(N,N)
      DO 9 I1=1,NN
      I=N-I1
      SUM=0.0
      I2=I+1
      DO 8 J=I2,N
    8 SUM=SUM+A(I,J)*B(J)
    9 B(I)=(C(I)-SUM)/A(I,I)
      RETURN
      END
```

Output - Program FTGPR

TYRE PROFILE DEFINED BY CIRCULAR
AND ELLIPTICAL ARCS

PROFILE 2 (R=75)

RADIUS TO CROWN = 240.00 MM
RADIUS OF CURVATURE IN TREAD = 75.00 MM
HALF WIDTH OF TREAD = 50.00 MM

RADIUS TO MAXIMUM WIDTH = 175.00 MM

TERMINATING RADIUS = 132.25 MM
TERMINATING ANGLE = 40.00 DEG

INFLATION PRESSURE = 200.00 KPA

	X	Y	A	RCM	RCC	SM	SC
1	.00	240.00	90.00	75.00	240.00	.112E+02	.120E+02
2	7.80	239.59	84.03	75.00	240.90	.112E+02	.121E+02
3	15.52	238.38	78.05	75.00	243.65	.112E+02	.122E+02
4	23.08	236.36	72.08	75.00	248.41	.112E+02	.125E+02
5	30.38	233.57	66.11	75.00	255.46	.112E+02	.129E+02
6	37.35	230.04	60.14	75.00	265.27	.112E+02	.135E+02
7	43.91	225.80	54.16	75.00	278.53	.111E+02	.144E+02
8	50.00	220.90	48.19	75.00	296.37	.110E+02	.157E+02
9	55.22	217.34	44.74	72.42	309.51	.110E+02	.150E+02
10	56.08	214.78	41.37	70.05	325.01	.109E+02	.143E+02
11	58.62	211.72	38.06	67.87	343.44	.109E+02	.136E+02
12	60.88	208.66	34.80	65.89	365.62	.108E+02	.129E+02
13	62.88	205.60	31.57	64.10	392.66	.108E+02	.123E+02
14	64.65	202.54	28.33	62.50	426.13	.108E+02	.116E+02
15	66.20	199.48	25.20	61.07	468.59	.108E+02	.109E+02
16	67.53	196.42	22.03	59.82	523.70	.108E+02	.102E+02
17	68.67	193.36	18.87	58.75	597.84	.108E+02	.951E+01
18	69.63	190.30	15.72	57.84	702.41	.108E+02	.883E+01
19	70.40	187.24	12.57	57.11	860.21	.109E+02	.816E+01
20	70.99	184.18	9.43	56.53	1124.42	.109E+02	.750E+01
21	71.42	181.12	6.28	56.13	1654.63	.110E+02	.685E+01
22	71.67	178.06	3.14	55.93	3248.54	.111E+02	.623E+01
23	71.75	175.00	.00	55.80	.00	.112E+02	.590E+01
24	71.32	163.06	7.14	55.80	-1351.52	.114E+02	.553E+01
25	70.03	161.23	14.29	55.80	-653.39	.115E+02	.553E+01
26	67.89	154.61	21.43	55.80	-423.20	.119E+02	.553E+01
27	64.96	143.31	28.57	55.80	-310.11	.122E+02	.553E+01
28	61.26	142.42	35.71	55.80	-243.99	.124E+02	.553E+01
29	56.86	137.04	42.86	55.80	-201.43	.127E+02	.553E+01
30	51.82	132.25	50.00	55.80	-172.64	.130E+02	.558E+01
	(MM)	(MM)	(DEG)	(MM)	(MM)	(KN/M)	(KN/M)

APPENDIX IV

Computer Program BTFR

This program uses the analogue of a conventional cross-biassed construction to calculate the profile and membrane stresses of a tyre section.

```
      PROGRAM BTPR
*
*  TYRE PROFILE BASED ON CROSS-BIASSED CONSTRUCTION
*  PUN NAME: POBTP
*
      REAL*8 H1,H2
      COMMON X(36),Y(36),RCM(36),SM(36),SC(36),
     &PI,RC,RM,WR,W,CCP,PS
      DIMENSION A(3),B(3)
      PI=4.0*ATAN(1.0)
      PRINT*,'TITLE, MAX.OF 16 CH.S'
      READ(2,1)H1,H2
    1 FORMAT(2A8)
      PRINT*,'RADIUS TO CROWN (MM)'
      READ(3,*)RC
      PRINT*,'TYRE WIDTH (MM)'
      READ(3,*)WR
      PRINT*,'TERMINATING RADIUS (MM)'
      READ(3,*)BR
      PRINT*,'TERMINATING ANGLE, MULTIPLE OF 5 DEG'
      READ(3,*)TAB
      PRINT *,'LOWER LIMIT FOR BIAS ANGLE (DEG)'
      READ(3,*)BAD1
      PRINT*,'UPPER LIMIT FOR BIAS ANGLE (DEG)'
      READ(3,*)BAD2
      PRINT*,'ESTIMATE FOR RADIUS TO MAXIMUM WIDTH (MM)'
      READ (3,*)RM
      PRINT*,'INFLATION PRESSURE (KPA)'
      READ(3,*)PS
      WRITE(2,14)
   14 FORMAT(1H ,'TYRE PROFILE BASED ON CROSS-PLY'/
     &1H ,9X,'CONSTRUCTION')
      IAB=INT(TAB+0.5)
      NA=IAB/5
      A(1)=BAD1*PI/180.0
      A(2)=BAD2*PI/180.0
      NP=0
    2 DO 4 K=1,2
*
*  CALCULATE UPPER TYRE PROFILE
*
    3 CALL PROF(1,18,A(K),B(K))
      NP=NP+1
*
*  TEST AND ADJUST RM FOR TYRE WIDTH
*
      IF (ABS(W-WR).LE.0.1)GO TO 4
      RM=RC-WR*(RC-RM)/W
      GO TO 3
*
*  CALCULATE LOWER TYRE PROFILE
*
    4 CALL PROF(2,NA,A(K),B(K))
*
*  TEST IF TERMINATING RADIUS WITHIN RANGE
*
      IF(B(1).LT.BR.OR.B(2).GT.BR)GO TO 10
```

```
*
*  RECALCULATE TYRE PROFILE WITH WEIGHTED BIAS ANGLE
*
      A(3)=A(1)+(BR-B(1))*(A(2)-A(1))/(B(2)-B(1))
      CALL PROF(1,IB,A(3),B(3))
      CALL PROF(2,NA,A(3),B(3))
*
*  TEST AND REDEFINE BIAS ANGLE RANGE FOR TERMINATING RADIUS
*
      IF(ABS(P(3)-BP).LE.0.1)GO TO 7
      IF(B(3)-BR)5,6,6
    5 A(2)=A(3)
      GO TO 2
    6 A(1)=A(3)
      GO TO 2
    7 BAD=A(3)*180.0/PI
      WRITE(2,8)H1,H2,NP,BAD,RC,RM,W,B(3),TAB
    8 FORMAT(///1H ,2A8//1H ,'NO.OF ITERATIONS =',I3//1H ,4X,
     &'CROWN BIAS ANGLE =',F6.2,' DEG',5X,'RADIUS TO CROWN =',
     &F6.1,' MM'/1H ,' RADIUS TO MAX.WIDTH =',F6.1,' MM',6X,'WIDTH ='
     &F6.1,' MM'/1H ,'RADIUS TO TERM.POINT =',F6.1,' MM',4X,
     &'TERMINATING ANGLE =',F6.2,' DEG')
      II=0
      XC=0.0
      SMC=(PS*(RC*RC-RM*RM)/(2.0*RC))*1E-3
      SCC=((PS-SMC*1E3/CCR)*RC)*1E-3
      NA=NA+1S
      WRITE(2,9)II,XC,RC,CCR,SMC,SCC,
     &((I,X(I),Y(I),RCM(I),SM(I),SC(I)),I=1,NA)
    9 FORMAT(///1H ,8X,'X',9X,'Y',8X,'RCM',
     &11X,'SM',13X,'SC'/(1H ,I2,4X,3(F5.1,5X),2(E11.4,4X)))
      WRITE(2,13)
   13 FORMAT(1H ,7X,'(MM)',6X,'(MM)',6X,'(MM)',
     &9X,'(KN/M)',9X,'(KN/M)')
      GO TO 12
   10 WRITE(2,11)H1,H2
   11 FORMAT(1H ,2A8//1H ,'INITIAL BIAS ANGLE LIMITS TOO NARROW')
   12 STOP
      END
```

```
      SUBROUTINE PROF(NG,NA,BA,B)
      COMMON X(36),Y(36),RCM(36),SM(36),SC(36),
     &PI,RC,RM,WR,W,CCR,PS
      A=PI/36.0
      L=0
      IF(NG.EQ.2)L=18
      SXY1=SXY2=0.0
      DO 8 J=1,NA
      IF(J-1)1,1,4
    1 IF(NG-2)2,3,3
    2 CR=RAD(RC,RM,BA,RC)
      X(1)=CR*SIN(A)
      Y(1)=RC-CR*(1.0-COS(A))
      RCM(1)=CR
      CCR=CR
      GO TO 7
    3 CR=RAD(RC,RM,BA,RM)
      X(19)=W/2.0-CR*(1.0-COS(A))
      Y(19)=RM-CR*SIN(A)
      RCM(19)=CR
      WCR=CR
      GO TO 7
    4 CR=RAD(RC,RM,BA,RP)
      SXY1=SXY1+(PCR-CR)*SIN((J-1)*A)
      SXY2=SXY2+(PCR-CR)*COS((J-1)*A)
      IF(NG-2)5,5,6
    5 X(J)=CR*SIN(J*A)+SXY1
      Y(J)=RC-(CCR-(CR*COS(J*A)+SXY2))
      RCM(J)=CR
      GO TO 7
    6 X(L+J)=W/2.0-(WCR-(CR*COS(J*A)+SXY2))
      Y(L+J)=RM-(CR*SIN(J*A)+SXY1)
      RCM(L+J)=CR
    7 PCR=CR
      RP=Y(L+J)
    8 CONTINUE
      IF(NG.EQ.1)W=2.0*X(18)
      IF(NG.EQ.2)B=Y(L+NA)
      DO 9 J=1,NA
      T=PS*PI*RC*RC*SIN(BA)*(RC*RC-RM*RM)/
     &(RC*RC-Y(L+J)*Y(L+J)*COS(BA)*COS(BA))
      COSA=COS(BA)*Y(L+J)/RC
      SINA=SQRT(1.0-COSA*COSA)
      SM(L+J)=(T*SINA/(2.0*PI*Y(L+J)))*1E-3
    9 SC(L+J)=SM(L+J)*COSA*COSA/(SINA*SINA)
      RETURN
      END

      FUNCTION RAD(RC,RM,BA,RP)
      RAD=(RC*RC-RM*RM)*RC*SIN(BA)*
     &SQRT(RC*RC-RP*RP*COS(BA)*COS(BA))/
     &(RP*(2.0*RC*RC-(3.0*RP*RP-RM*RM)*
     &COS(BA)*COS(BA)))
      RETURN
      END
```

Output - Program BTPR

TYRE PROFILE BASED ON CROSS-PLY CONSTRUCTION

PROFILE 18

NO.OF ITERATIONS = 41

CROWN BIAS ANGLE = 45.01 DEG RADIUS TO CROWN = 240.0 MM
RADIUS TO MAX.WIDTH = 178.5 MM WIDTH = 130.0 MM
RADIUS TO TERM.POINT = 130.0 MM TERMINATING ANGLE = 50.00 DEG

	X	Y	RCM	SM	SC
0	.0	240.0	69.0	.1072E+02	.1071E+02
1	6.0	239.7	69.0	.1072E+02	.1067E+02
2	12.0	239.0	68.9	.1072E+02	.1053E+02
3	17.8	237.7	68.5	.1072E+02	.1031E+02
4	23.4	235.9	67.8	.1073E+02	.1001E+02
5	28.8	233.6	67.0	.1074E+02	.9663E+01
6	34.0	231.0	66.1	.1075E+02	.9268E+01
7	38.7	227.9	65.1	.1077E+02	.8844E+01
8	43.2	224.5	64.0	.1081E+02	.8404E+01
9	47.2	220.8	63.1	.1085E+02	.7958E+01
10	50.9	216.8	62.2	.1091E+02	.7516E+01
11	54.2	212.6	61.4	.1098E+02	.7083E+01
12	57.0	208.1	60.7	.1107E+02	.6664E+01
13	59.4	203.5	60.1	.1117E+02	.6263E+01
14	61.4	198.6	59.7	.1130E+02	.5883E+01
15	63.0	193.7	59.5	.1144E+02	.5522E+01
16	64.1	188.6	59.4	.1160E+02	.5184E+01
17	64.8	183.5	59.4	.1179E+02	.4866E+01
18	65.0	178.3	59.6	.1199E+02	.4570E+01
19	64.8	173.3	59.9	.1221E+02	.4304E+01
20	64.1	168.1	60.4	.1246E+02	.4046E+01
21	62.9	162.9	61.0	.1274E+02	.3808E+01
22	61.3	157.7	61.8	.1303E+02	.3587E+01
23	59.2	152.7	62.7	.1335E+02	.3384E+01
24	56.6	147.7	63.3	.1368E+02	.3197E+01
25	53.6	143.0	64.9	.1404E+02	.3025E+01
26	50.1	138.4	66.2	.1440E+02	.2870E+01
27	46.1	134.0	67.5	.1478E+02	.2729E+01
28	41.7	130.0	69.0	.1516E+02	.2603E+01
	(MM)	(MM)	(MM)	(KN/M)	(KN/M)

APPENDIX V

Computer Program FTCAPR

The analogue of a cross-biassed construction, with a constant bias angle around the meridian, is used to calculate the profile and membrane stresses of a tyre section.

```
      PROGRAM FTCAPR
      REAL*8 H1,H2
      DIMENSION X1(19),Y1(18),X2(19),Y2(18),
     *S41(19),SC1(18),SM2(18),SC2(19),R1(18),R2(18)
*
*  TYRE PROFILE DEFINED BY CONSTANT BIAS ANGLE CONSTRUCTION
*  RUN NAME: POFTC
*
      PI=4.0*ATAN(1.0)
      PRINT*,'TITLE, MAX.OF 16 CH.S'
      READ(3,1)H1,H2
    1 FORMAT(2A8)
      PRINT*,'BIAS ANGLE (DEG)'
      READ(3,*)BAD
      PRINT*,'TYRE WIDTH (MM)'
      READ(3,*)WP
      PRINT*,'TERMINATING RADIUS (MM)'
      READ(3,*)BR
      PRINT*,'ESTIMATED RADIUS TO CROWN (MM)'
      READ(3,*)RC
      PRINT*,'ESTIMATED RADIUS TO MAXIMUM WIDTH (MM)'
      READ(3,*)RM
      PRINT*,'TERMINATING ANGLE, MULTIPLE OF 5 DEG'
      READ(3,*)TAB
      PRINT*,'INFLATION PRESSURE (KPA)'
      READ(3,*)PS
      IAB=INT(TAB+0.5)
      BA=BAD*PI/180.0
      C=(COS(BA)/SIN(BA))**2
      NA=IAB/5
      NP=0
*
*  CALCULATE UPPER TYRE PROFILE
*
    4 CALL PROFX(1,13,X1,Y1,R1,C,RC,RM,W,B)
      NP=NP+1
*
*  TEST AND ADJUST RM FOR TYRE WIDTH
*
      IF(ABS(W-WP).LE.0.1)GO TO 5
      RM=RC-.R*(RC-RM)/W
      GO TO 4
*
*  CALCULATE LOWER TYRE PROFILE
*
    5 CALL PROFX(2,NA,X2,Y2,R2,C,RC,RM,W,B)
*
*  TEST AND ADJUST RC FOR TERMINATING RADIUS
*
      IF(ABS(B-BR).LE.0.1)GO TO 6
      RC=RC-(B-BR)
      GO TO 4
*
*  CALCULATE MEMBRANE TENSIONS
*
    6 DO 7 I=1,18
      Y1(I)=RC-Y1(I)
```

```
      SM1(I)=((RC*RC-RM*RM)/(2*Y1(I)*(RC/Y1(I))**C))*PS*1.0E-3
    7 SC1(I)=C*SM1(I)
      DO 10 I=1,NA
      Y2(I)=RC-Y2(I)
      SM2(I)=((RC*RC-RM*RM)/(2*Y2(I)*(RC/Y2(I))**C))*PS*1.0E-3
   10 SC2(I)=C*SM2(I)
      II=0
      XC=0.0
      YC=RC
      RCC=R1(1)
      SMC=((RC*RC-RM*RM)/(2.0*RC))*PS*1.0E-3
      SCC=C*SMC
      WRITE(2,8)
    8 FORMAT(1H ,'TYRE PROFILE WITH CONSTANT BIAS ANGLE'/
     &1H ,12X,'CONSTRUCTION')
      WRITE(2,11)H1,H2,NP,W,B,BAD,RC,RM,PS,
     &II,XC,YC,RCC,SMC,SCC,
     &((I,X1(I),Y1(I),R1(I),SM1(I),SC1(I)),I=1,19),
     &((I,X2(I),Y2(I),R2(I),SM2(I),SC2(I)),I=1,NA)
   11 FORMAT(///1H ,2A8,//1H ,'NO.OF ITERATIONS =',I3//1H ,6X,
     &'SECTION WIDTH =',F7.2,' MM'/
     &1H ,' TERMINATING RADIUS =',F7.2,' MM'/1H ,9X,'BIAS ANGLE =
     &F7.2,' DEG'/1H ,4X,'RADIUS TO CROWN =',F7.2,' MM'/1H ,
     &'RADIUS TO MAX.WIDTH =',F7.2,' MM'//1H ,1X,
     &'INFLATION PRESSURE =',F7.2,' KPA'///1H ,
     &7X,'X',7X,'Y',7X,'R',
     &11X,'SM',11X,'SC'/(1H ,I2,2F8.2,F9.3,2E13.3))
      WRITE(2,12)
   12 FORMAT(1H ,5X,'(MM)',4X,'(MM)',4X,'(MM)',8X,
     &'(KN/M)',7X,'(KN/M)')
      STOP
      END
```

```
      SUBROUTINE PROFX(NQ,NA,X,Y,R,C,RC,RM,W,B)
      DIMENSION X(18),Y(18),R(18)
      RAD(RC,RM,RP,C)=(RC*RC-RM*RM)/
     $(C*RM*RM*RC**C/RP**(C+1)+(2-C)*RC**C/RP**(C-1))
      PI=4.0*ATAN(1.0)
      A=PI/36.0
      SXY1=0
      SXY2=0
      DO 8 J=1,NA
      IF(J-1)1,1,4
    1 IF(NQ-2)2,3,3
    2 CR=RAD(RC,RM,PC,C)
      X(J)=CR*SIN(A)
      Y(J)=CR-CR*COS(A)
      CCR=CR
      GO TO 7
    3 CR=RAD(RC,RM,RM,C)
      X(J)=0.5*W-(CR-CR*COS(A))
      Y(J)=(RC-RM)+CR*SIN(A)
      WCR=CR
      GO TO 7
    4 CR=RAD(PC,RM,RP,C)
      SXY1=SXY1+(PCR-CR)*SIN((J-1)*A)
      SXY2=SXY2+(PCR-CR)*COS((J-1)*A)
      IF(NQ-2)5,6,6
    5 X(J)=CR*SIN(J*A)+SXY1
      Y(J)=CCR-(CR*COS(J*A)+SXY2)
      GO TO 7
    6 X(J)=0.5*W-(WCR-(CR*COS(J*A)+SXY2))
      Y(J)=(RC-RM)+CR*SIN(J*A)+SXY1
    7 PCR=CR
      RP=RC-Y(J)
      R(J)=CR
    8 CONTINUE
      IF(NQ.EQ.1)W=2*X(18)
      IF(NQ.EQ.2)B=RC-Y(NA)
      RETURN
      END
```

Output - Program FTCARR

TYRE PROFILE WITH CONSTANT BIAS ANGLE
CONSTRUCTION

PROFILE 2C

NO. OF ITERATIONS = 3

SECTION WIDTH = 130.05 MM
TERMINATING RADIUS = 129.97 MM
BIAS ANGLE = 45.00 DEG
RADIUS TO CROWN = 225.92 MM
RADIUS TO MAX. WIDTH = 165.64 MM

INFLATION PRESSURE = 200.00 KPA

	X	Y	R	SM	SC
0	.00	225.92	67.951	.104E+02	.104E+02
1	5.92	225.66	67.951	.104E+02	.104E+02
2	11.79	224.89	67.396	.104E+02	.104E+02
3	17.56	223.61	67.733	.104E+02	.104E+02
4	23.19	221.84	67.461	.104E+02	.104E+02
5	28.58	219.60	67.080	.104E+02	.104E+02
6	33.74	216.92	66.592	.104E+02	.104E+02
7	38.59	213.82	65.995	.104E+02	.104E+02
8	43.11	210.36	65.295	.104E+02	.104E+02
9	47.26	206.56	64.491	.104E+02	.104E+02
10	51.01	202.47	63.587	.104E+02	.104E+02
11	54.33	198.13	62.583	.104E+02	.104E+02
12	57.21	193.61	61.493	.104E+02	.104E+02
13	59.64	188.94	60.324	.104E+02	.104E+02
14	61.62	184.18	59.075	.104E+02	.104E+02
15	63.13	179.37	57.761	.104E+02	.104E+02
16	64.20	174.57	56.391	.104E+02	.104E+02
17	64.82	169.82	54.980	.104E+02	.104E+02
18	65.03	165.15	53.539	.104E+02	.104E+02
1	64.83	161.09	52.239	.104E+02	.104E+02
2	64.25	156.69	50.782	.104E+02	.104E+02
3	63.32	152.49	49.342	.104E+02	.104E+02
4	62.06	148.50	47.923	.104E+02	.104E+02
5	60.50	144.75	46.557	.104E+02	.104E+02
6	58.68	141.25	45.240	.104E+02	.104E+02
7	56.62	138.01	43.983	.104E+02	.104E+02
8	54.35	135.05	42.812	.104E+02	.104E+02
9	51.89	132.37	41.719	.104E+02	.104E+02
10	49.27	129.97	40.713	.104E+02	.104E+02
	(MM)	(MM)	(MM)	(KN/M)	(KN/M)

APPENDIX VI

Derivation of Equation for Radial Stiffness

Figure VI.A is a simplified representation of a tyre's sidewall from the bead to the shoulder. It is assumed to be inextensible but flexible and to form a circular arc of length s, radius r and height h. If γ is the angle subtended by half the sidewall, then:

$$s = 2r\gamma \qquad \text{and} \qquad h = 2r \sin \gamma$$

giving:

$$h = \frac{s \sin \gamma}{\gamma}$$

But $\sin \gamma \simeq \gamma - \gamma^3/6$ (by expansion)

thus $h = s(1 - \gamma^2/6)$

and $\gamma = \left[\frac{6(s - h)}{s}\right]^{\frac{1}{2}}$ (1)

Now if T is the tension per unit length in the sidewall when the tyre is freely inflated, the force δF exerted vertically by an element of circumferential length δx on the bead is:

$$\delta F = T \cos \gamma . \delta x$$

or $\delta F \simeq T(1 - \gamma^2/2)\delta x$ (by expansion)

Substituting for γ from equation (1):

$$\delta F = T[1 - 3(s - h)/s]\delta x \qquad (2)$$

Now consider the element of the sidewall when it is deflected radially by d', so that its height becomes:

$$h' = h - d'$$

The vertical component on the bead then becomes:

$$\delta F = T[1 - 3(s + d' - h)/s]\delta x$$

and the total vertical force on the bead in the zone of the contact patch is:

$$F = \int_{d' \text{ at } -a}^{d' \text{ at } a} T[1 - 3(s + d' - h)/s]dx$$

or $$F = \int T.dx - 3 \int T(s - h)/s.dx - 3 \int T\, d'/s.dx \qquad (3)$$

where $x = -a$ and $x = a$ are the limits of the distortion of the sidewall in the contact zone; not, in general, equal to the contact patch length.

Now in the undistorted sector of the tyre diametrically opposite to the contact zone, the equivalent integration of equation (2) yields the first two terms of equation (3). Thus the net upward force is:

$$3 \int T\, d'/s.dx = \frac{W_p}{2}$$

where $W_p/2$ is the load carried pneumatically by one sidewall of the tyre.

Consequently:

$$W_p = \frac{6T}{s} \int_{d' \text{ at } -a}^{d' \text{ at } a} d'.dx \qquad (4)$$

To solve this integral, consider the whole tyre and assume that the radial deflection, d, distorts it along a sector of length 2a, as shown in figure VI.B. The integral in equation (4) is the area ABC, so that:

$$\int_{-a}^{a} d'.dx = \frac{\alpha}{\pi} \pi R^2 - R^2 \cos \alpha.\sin \alpha$$

$$= \alpha R^2 - \tfrac{1}{2} R^2 \sin 2\alpha$$

where R is the free radius of the tyre, and α is the angle subtended at its axis by half the contact zone.

Expanding sin 2α gives:

$$\int_{-a}^{a} d'.dx \simeq R^2[\alpha - \tfrac{1}{2}(2\alpha - 8\alpha^3/6)]$$

$$= 2R^2\, \alpha^3/3$$

Substituting in equation (4):

$$W_p = \frac{4TR^2\ \alpha^3}{s} \qquad (5)$$

However, from figure VI.B:

$$d = R(1 - \cos\alpha) \simeq R(1 - 1 + \alpha^2/2)$$

$$\text{or} \qquad \alpha = \sqrt{\frac{2d}{R}}$$

so that:

$$W_p = \frac{4TR^{\frac{1}{2}}}{s}\ (2d)^{3/2} \qquad (6)$$

In a flexible membrane, the tension T is equal to the product of its radius of curvature, r, and the inflation pressure, p,

ie. $T = pr$

if the second principal curvature is ignored.

Also, if the two sidewalls lie on a common circle whose diameter is the width, w, of the tyre, then:

$$T = \frac{pw}{2}$$

and $s = 2r\gamma = w\gamma.$

Substituting in equation (6):

$$W_p = \frac{4pw}{2w\gamma}\ R^{\frac{1}{2}}\ (2d)^{3/2}$$

$$\text{or} \qquad W_p = 5.66p\ \frac{R^{\frac{1}{2}}d^{3/2}}{\gamma} \qquad (7)$$

and, from geometrical considerations, figure VI.C:

$$\gamma = \tan^{-1}\sqrt{(w/w')^2 - 1} \qquad (8)$$

where w' is the width of the rim upon which the tyre is mounted.

To describe the behaviour of a tyre which exhibits both pneumatic and structural stiffness, an expression for the latter must also be derived. For this simplified analysis, assume a sidewall has an effective spring

rate k per unit circumference. The force developed structurally by an element δx when deflected will then be:

$$\delta F = kd'.\delta x$$

so that:

$$W_s = 2k \int_{d' \text{ at } -a}^{d' \text{ at } a} d'.dx$$

Integrating as before, the total load carried structurally is:

$$W_s = 3.77k\ R^{\frac{1}{2}}d^{3/2} \qquad (9)$$

Summing equations (7) and (9), the total load carried by the tyre is:

$$W = W_p + W_s$$

or $$W = \left[3.77k + \frac{5.66p}{\gamma}\right] R^{\frac{1}{2}}d^{3/2} \qquad (10)$$

with γ given by equation (8).

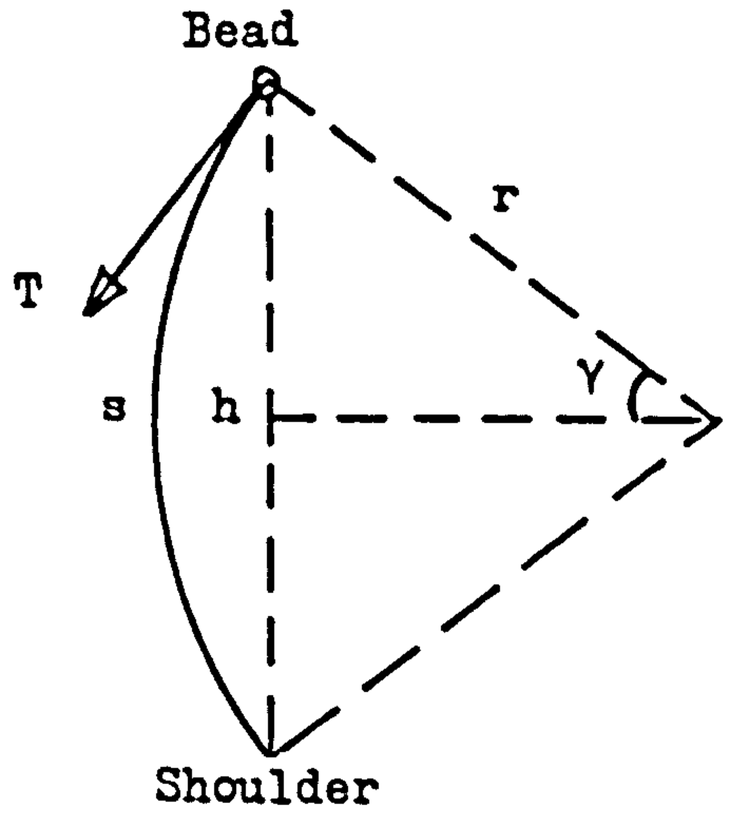

Figure VI.A

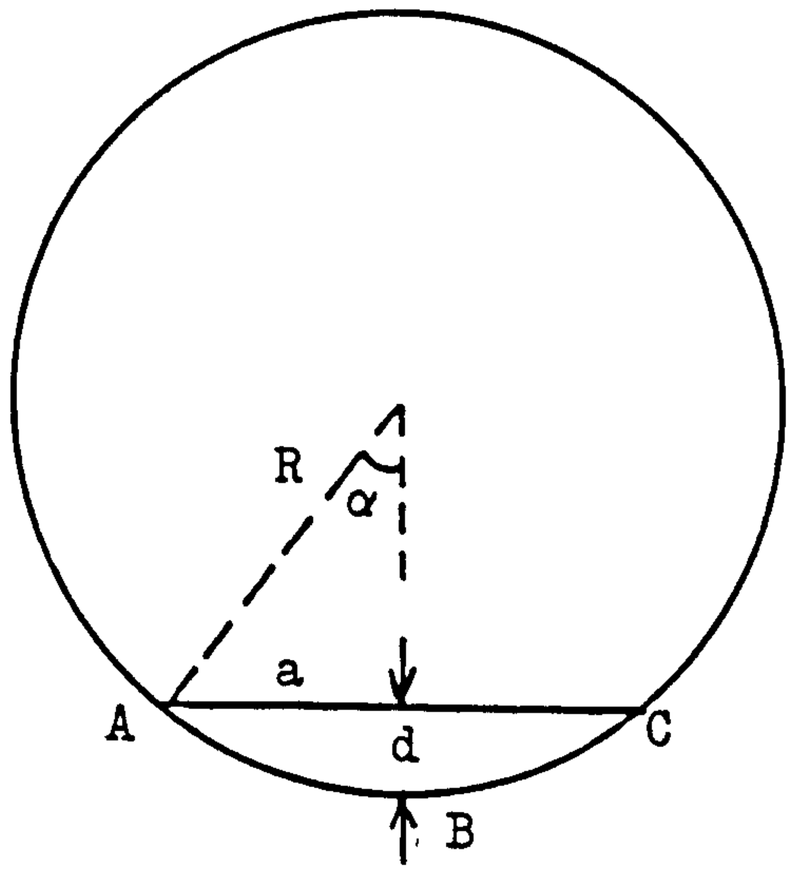

Figure VI.B

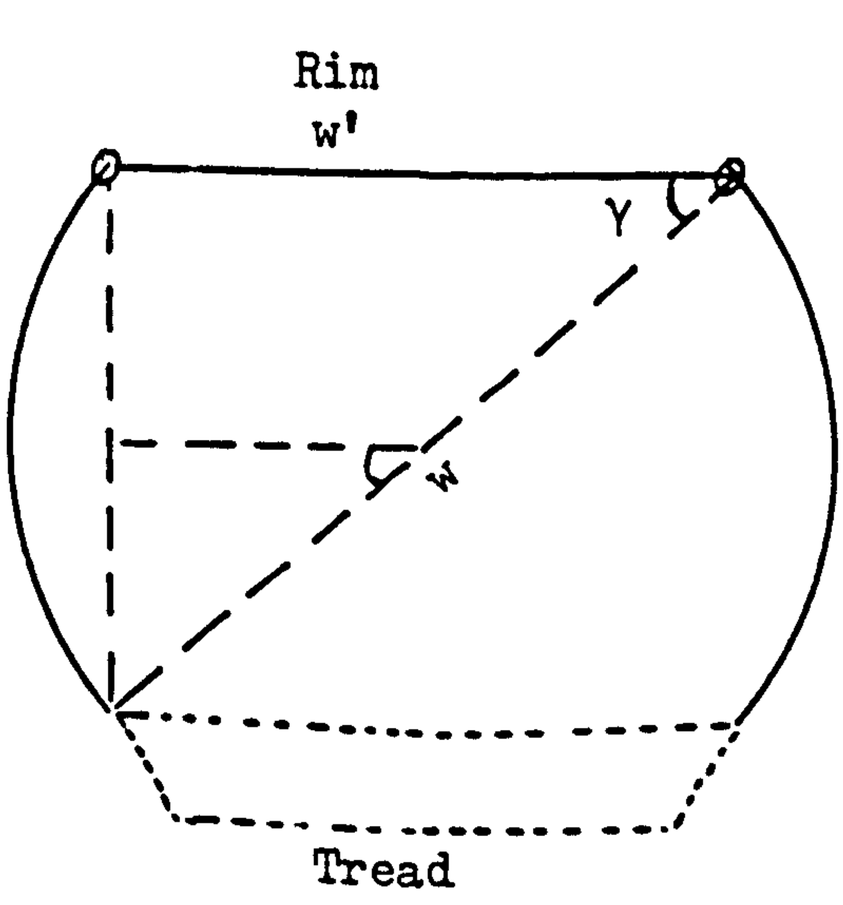

Figure VI.C

APPENDIX VII

Computer Program TWPD

This program analyses the radial behaviour of a tyre, as measured by load, pressure and deflection, into structural and pneumatic components.

```
      PROGRAM TWPD
      REAL*8 H1,H2
      DIMENSION W(100),D(100),P(100),WD(100),SD(3),AA(3),BB(3)
*
*  ANALYSIS OF TYRE LOAD-PRESSURE-DEFLECTION DATA
*  RUN NAME: POWPD (USE PUSTATS STAN FOR TAB.)
*
      PRINT*, 'TITLE, MAX.OF 16 CH.S'
      READ(3,1) H1,H2
1     FORMAT(2A8)
      K=0
2     PRINT*, 'INFLATION PRESSURE (KPA), PUT = -1. TO COMPLETE DATA'
      READ(3,*)PP
      IF(PP)6,3,3
3     PRINT*, 'LOAD (N) AND DEFLECTION (MM) - TAB.2'
      PRINT*, 'ENTER -1. -1.  FOR NEXT PRESSURE'
      READ(3,4)WW,DD
4     FORMAT(5F12.5)
      IF(DD)2,5,5
5     K=K+1
      W(K)=WW
      D(K)=DD
      P(K)=PP
      GO TO 3
6     CDN=1.0
      DDN=0.1
*
*  3 VALUES FOR POWER INDEX
*
7        DO 9 J=1,3
         DN=CDN+(J-2)*DDN
*
*  TRANSFORM LOAD/DEFLECTION TO GIVE LINEAR EQUATION
*
         DO 8 I=1,K
8        WD(I)=W(I)/D(I)**DN
9        CALL REG (P,WD,K,AA(J),BB(J),SD(J))
*
*  TERMINATE ANALYSIS IF POWER INDEX INCREMENT = 0.0125
*
         IF(DDN.LT.0.013)GO TO 16
         IF(SD(2)-SD(3))11,13,10
*
*  INCREASE POWER INDEX
*
10       CDN=CDN+DDN
         GO TO 7
11       IF(SD(2)-SD(1))15,14,12
*
*  DECREASE POWER INDEX
*
12       CDN=CDN-DDN
         GO TO 7
*
*  HALVE POWER INDEX INCREMENT AND INCREASE INDEX
*
13       DDN=DDN/2.0
```

```
            CDN=CDN+DDN
            GO TO 7
      *
      *  HALVE POWER INDEX INCREMENT AND DECREASE INDEX
      *
   14       DDN=DDN/2.0
            CDN=CDN-DDN
            GO TO 7
      *
      *  HALVE POWER INDEX INCREMENT BUT MAINTAIN INDEX
      *
   15       DDN=DDN/2.0
            GO TO 7
      *
      *  CHOOSE BEST FIT ON BASIS OF RMS
      *
   16       IF(SD(2)-SD(3))13,20,17
   17       DN=CDN+DDN
            SD1=SD(3)
            A=AA(3)
            B=BB(3)
            GO TO 21
   18       IF(SD(2)-SD(1))20,20,19
   19       DN=CDN-DDN
            SD1=SD(1)
            A=AA(1)
            B=BB(1)
            GO TO 21
   20       DN=CDN
            SD1=SD(2)
            A=AA(2)
            B=BB(2)
      *
      *  CALCULATE SUM OF SQUARES ABOUT FITTED EQUATION
      *
   21       SDA=0.0
            DO 22 I=1,K
   22       SDA=SDA+(W(I)-(A+B*P(I))*D(I)**DN)**2.0
      *
      *  ROOT MEAN SQUARE
      *
            SDA=SQRT(SDA/(K-3))
            PRINT*, 'NUM.OF PRESSURES FOR FITTED VALUES'
            READ(3,*)KP
            PRINT*, 'PRESSURES (KPA) - TAB.5'
            READ(3,4)(P(J),J=1,KP)
            PRINT*, 'NUM.OF DEFLECTIONS FOR FITTED VALUES'
            READ(3,*)KD
            PRINT*, 'DEFLECTIONS (MM) - TAB.5'
            READ(3,4)(D(J),J=1,KD)
      *
      *  CALCULATE FITTED VALUES
      *
            I=0
            DO 23 K=1,KP
            DO 23 J=1,KD
            I=I+1
```

```
      WD(I)=(A+B*P(K))*D(J)**DN
      WRITE(2,27)
27    FORMAT(1H ,'ANALYSIS OF LOAD-PRESSURE-DEFLECTION DATA')
      WRITE(2,24)H1,H2,A,B,DN,SDM,SDA
24    FORMAT(///1H ,15X,'W = (A + B.P) * D**N'///1H ,2A8//1H ,5X,
     -'A =',E11.4,5X,'B =',E11.4,5X,'N =',F7.4//1H ,10X,
     -'REG.N RMS =',E11.4/1H ,10X,'EQN.N RMS =',E11.4///1H ,
     -'FITTED VALUES'//1H ,7X,'P',9X,
     -'D',12X,'W')
      I=0
      DO 25 K=1,KP
      DO 25 J=1,KD
      I=I+1
25    WRITE(2,26)P(K),D(J),WD(I)
26    FORMAT(1H ,F10.1,F10.2,E15.4)
      WRITE(2,28)
28    FORMAT(1H ,5X,'(KPA)',5X,'(MM)',10X,'(N)')
      STOP
      END
```

```
      SUBROUTINE REG(X,Y,N,A,B,SD)
*
*  SUBROUTINE FOR LINEAR REGRESSION
*
      DIMENSION X(100),Y(100)
      SX=0.0
      SY=0.0
      SXY=0.0
      SXSQ=0.0
      SYSQ=0.0
      DO 1 J=1,N
      SX=SX+X(J)
      SY=SY+Y(J)
      SXY=SXY+X(J)*Y(J)
      SXSQ=SXSQ+X(J)*X(J)
1     SYSQ=SYSQ+Y(J)*Y(J)
      AN=FLOAT(N)
*
*  SLOPE
*
      B=(SXY-SX*SY/AN)/(SXSQ-SX*SX/AN)
*
*  INTERCEPT
*
      A=SY/AN-B*SX/AN
      E=(SYSQ-SY*SY/AN)-B*B*(SXSQ-SX*SX/AN)
*
*  ROOT MEAN SQUARE
*
      SD=SQRT(E/(AN-2.0))
      RETURN
      END
```